LONDON'S GLOBAL UNIVERSITY

Investigating small molecule therapeutics to improve regeneration and functional recovery following peripheral nerve damage.

Melissa Lucy Doreen Rayner

Thesis submitted in fulfilment of the requirements for the degree of

Doctor of Philosophy.

School of Pharmacy

University College London

September, 2018

Declaration

I, Melissa Rayner, confirm that the work presented in this thesis is my own. Where information has been derived from other sources, I confirm that this has been indicated in the thesis.

Signed: _____

Date: _____

Acknowledgements

I would like to express my sincere gratitude to my supervisors Dr Jess Healy and Dr James Phillips for their continuous support and guidance throughout the PhD. Thank you for all the time and encouragement you have given during the project but also towards the additional projects and activities I had the opportunity to get involved with.

I would particularly like to thank the biological services unit staff for all of their generous support during *in vivo* experiments and especially to Francesca Busuttil for her willingness to give her time so generously to assist during long surgery days. In addition, special thanks also go to Rachael Evans for her input and hard-work during the development of the *in vitro* screening tool, Alessandra Grillo for her great effort and contribution to the biomaterials work and to Essam Tawfik for providing the PLGA nanofibres. I am grateful to all of my colleagues and friends in the Healy and Phillips labs for all of their inspiration and making the lab a friendly and enjoyable place to work.

Furthermore, I am thankful to Professor Steve Brocchini and all of the CDT management team for giving me the opportunity to complete my PhD as a part of the CDT. Special thanks go to my CDT cohort for sharing this journey with me and all of our wonderful adventures.

Finally, and most importantly, I would like to thank all of my family and friends who have been there for me throughout this challenging journey. A special mention goes to Ahmed Jamel for his continuous encouragement and belief in me.

Publications

Papers

MLD Rayner, S Laranjeira, RE Evans, RJ Shipley, J Healy, JB Phillips (2018). Developing an *in vitro* model to screen drugs for nerve regeneration. *Anatomical record. (In press).*

MLD Rayner, JB Phillips, J Healy (2018) Repurposing small molecules to target the Rho/ROCK pathway as new therapies for peripheral nerve injuries. *(Submitted).*

MLD Rayner, T Quick, JB Phillips (2018) Quantifying regeneration in humans following peripheral nerve injury. *(Submitted).*

MLD Rayner, A Grillo, J Healy, JB Phillips (2018) Ibuprofen loaded ethylene vinyl acetate for controlled local delivery to treat peripheral nerve injuries. *(Paper in preparation).*

MLD Rayner, E Tawfik, C Vasiliki, D Craig , J Healy, JB Phillips (2018) Ibuprofen loaded electrospun PLGA nanofibres for controlled local delivery to treat peripheral nerve injuries. *(Paper in preparation).*

AGE Day, C Murray-Dunning, C Schuh, **MLD Rayner**, L Thanabalasundaram, L Stevanato, N Grace, G Cameron, RAL Drake, J Sinden, JB Phillips (2018) Optimisation of peripheral nerve repair constructs containing Engineered Neural Tissue made using CTX0E03 cells. (*Paper in preparation).*

MLD Rayner, A Grillo, J Healy, JB Phillips (2017) Developing biomaterials for the local delivery of drugs following peripheral nerve injury *Tissue and Cell Engineering Society, Manchester (UK).*

C O'Rourke, **MLD Rayner**, PJ Kingham, JB Phillips (2017) *Tuning collagen hydrogel stiffness to enhance the regenerative phenotype of adipose stem cells for peripheral nerve repair* European Cells and Materials Meeting abstracts, Collection 2, P277

MLD Rayner, R Evans, J Healy, JB Phillips (2016) Development of an advanced 3D neuronal cell culture as a screening tool for drugs promoting nerve regeneration. European Cells and Materials Meeting abstracts, Collection 1, page 177.

MLD Rayner, J Healy, JB Phillips (2016) Using advanced 3D engineered cell cultures to analyse the effect of drugs on peripheral nerve regeneration *in vitro*. European Cells and Materials Meeting abstracts, Collection 5, page 145.

A Finch, K Akpokavie, S Grieb, C Da Costa Mathews, and **M Rayner** (2015). Characterisation of a haze observed in reconstituted lyophile solutions. *Analytical Matters, Pfizer.*

Conference proceedings

MLD Rayner, A Grillo, J Healy, JB Phillips (2018) Ibuprofen-loaded biomaterials for controlled local delivery to treat peripheral nerve injuries*. TERMIS 5th World Congress, Kyoto (Japan).*

AGE Day**, MLD Rayner**, JB Phillips (2018) Development methods for delivering engineered neural tissue within peripheral nerve repair conduit. *TERMIS 5th World Congress, Kyoto (Japan).*

MLD Rayner, J Healy, JB Phillips (2018). Using advanced 3D engineered cell cultures to investigate drug synergy in promoting peripheral nerve regeneration. *Tissue and Cell Engineering Society. Keele (UK)*

MLD Rayner, J Healy, JB Phillips (2017). Investigating the effects of ibuprofen on axon regeneration and functional recovery following peripheral nerve injury *ISPNR, Barcelona (Spain).*

MLD Rayner, A Grillo, J Healy, JB Phillips (2017). Developing biomaterials for the local delivery of drugs following peripheral nerve injury *Tissue and Cell Engineering Society, Manchester (UK).*

MLD Rayner, J Healy, JB Phillips (2017). Investigating the effects Ibuprofen on axonal regeneration and functional recovery following peripheral nerve injury *6th Vienna Symposium on Surgery of Peripheral Nerves, Vienna (Austria).*

MLD Rayner, J Healy, JB Phillips (2017). Investigating the effects Ibuprofen on axonal regeneration and functional recovery following peripheral nerve injury *Neuroscience Symposium, UCL, London (UK).*

M Rayner, J Healy, JB Phillips (2016). Using advanced 3D engineered cell cultures to analyse the regenerating effect of drugs on neural cells in isolation. *Eastman Dental Institute PhD Research Symposium.*

M Rayner M, J Healy, JB Phillips (2016). Using advanced 3D engineered cell cultures to analyse the effect of drugs on peripheral nerve regeneration *in vitro*. *Tissue and Cell Engineering Society, University College London, London (UK).*

M Rayner, R Evans, J Healy, JB Phillips (2016). Development of an advanced 3D neuronal cell culture as a screening tool for drugs promoting nerve regeneration. *Tissue Engineering and Regenerative Medicine International Society, Uppsala (Sweden).*

M Rayner, C Da Costa Matthews C, B Cooper (2015). Dynamic Light Scattering as a tool to benchmark the submicron region in parenteral formulations. *Global Research & Development, Drug Product Design, Pfizer, Sandwich (UK).*

M Rayner, R Kendall, S Orubu, C Tuleu (2015) The milky way: Towards development of a formulation and process design space to ensure the development of innovative, safe, effective and natural drug delivery to young children. *UKICRS, University of Nottingham, Nottingham (UK).*

Abstract

Peripheral nerve injury (PNI) can be debilitating and results in loss of function, coupled with slow neuron regeneration. Microsurgical treatments remain the gold standard therapy, with no drug therapies currently available. Effective pharmacological treatments could potentially maintain neuronal viability, encourage axonal growth, improve axonal specificity to targets and reduce neuropathic pain. Some drugs and targets have been identified but challenges remain with clinical translation. Advancements in understanding the molecular and cellular events occurring following PNI identifies signalling pathways that could be targeted with drug therapies.

The failure in drug therapies reaching PNI clinical trials may be due to the lack of effective *in vitro* and *in vivo* pre-clinical models. This study developed and applied models to be used as effective screening tools to address this need. Many compounds demonstrated positive effects on neurite growth when screened in a 3D-engineered co-culture model. NSAIDs (ibuprofen and sulindac sulfide) demonstrated beneficial effects and were studied further in two injury models demonstrating increased axonal growth and improved function.

Local controlled-release drug delivery systems have become more attractive because of the drawbacks in conventional drug treatments. This study investigated drug release from various biomaterials in order to obtain an optimal material for implantation and sustained drug delivery. Suitable biomaterials were implanted *in vivo* to deliver ibuprofen or sulindac sulfide. Both drugs demonstrated beneficial effects on axonal regeneration and functional recovery. Embedding drugs into biocompatible and bio-degradable materials provides effective delivery systems for future translation.

Studying NSAIDs revealed a previously unreported relationship between PPAR-γ affinity and regeneration. A NSAID derivative demonstrated the greatest effects on neurite growth *in vitro* at lower doses than other compounds tested. In summary, this work has

identified therapeutic targets to aid the development of novel compounds, as well as, drug repurposing, and effective tools for the pre-clinical screening of these drugs.

Impact statement

This thesis contributes to translational research in peripheral nerve injury (PNI), specifically the identification of small molecule therapies to improve regeneration and functional recovery. The findings from aspects of this work have already started to enhance the clinical translation of drug therapies in this area through being used to underpin the development of a clinical trial in repurposing a drug for PNI.

PNI occurs in 2-5% of trauma cases affecting ~ 1 million patients in Europe and the US annually. 600,000 of these patients will undergo nerve surgery with only 50% of patients regaining function, which is usually still unsatisfactory. Achieving successful recovery following PNI remains a significant clinical issue due to the remarkably long time it takes for nerves to regenerate. The resulting delay in reinnervation causes atrophy of target organs reducing the extent to which motor and sensory function is restored, leaving patients with a poor quality of life.

This work has made progress towards addressing this important unmet clinical need in regenerative medicine through the development of potential future therapies to increase the rate of regeneration and improve outcomes for patients. Studying the molecular and cellular events following an injury has provided a valuable opportunity to develop new drugs as well as the identification of other drugs for repurposing. The development of *in vitro, in vivo* and *in silico* models has enabled higher through-put screening of potential candidates that hit targets of interest. The *in vitro* models have been disseminated to enable the wider research community to adopt them, contributing further to work in this field.

Overall this project has made advancements in drug development and delivery in the field of PNI to improve nerve regeneration and reduce the delay that leads to tissue atrophy, improving recovery of function. Potentially these therapies could also reduce the extent and duration of disability for patients, provide a minimally-invasive medicinal treatment where none are currently available, and local drug delivery will reduce the systemic side effects associated with long-term oral dosing.

Abbreviations

2D	Two dimensional
3D	Three dimensional
Aβ42	Amyloid beta peptide 1-42
Apo E	Apolipoprotein E
AF-2	Activation function-2
BSA	Bovine serum albumin
Bcl-2	B-cell lymphoma-2
bDNF	Brain derived neurotrophic factor
bFGF	Basic fibroblast growth factor
CAM	Cell adhesion molecules
cAMP	Cyclic adenosine monophosphate
CMAP	Compound muscle action potential
CNS	Central nervous system
COX	Cyclooxygenase
CRD	Cysteine rich domain
CREB	cAMP response element binding protein
CRMP2	Collapsin response mediator protein-2
CSPG	Chondroitin sulphate peptidoglycans
DRG	Dorsal root ganglion
ECM	Extracellular matrix
EngNT	Engineered neural tissue
EPO	Erythropoietin
Eq	Equivalence
ERK	Extracellular signal-regulated kinase
EVA	Ethylene vinyl acetate
FBS	Fetal bovine serum
FDA	US Food and Drug Administration
FT-IR	Fourier transform infrared spectroscopy
GAPs	GTPase activating proteins

GDIs	Guanine nucleotide dissociation inhibitors
GDP	Guanosine diphosphate
GEFs	Guanine nucleotide exchange factors
GDNF	Glial cell derived neurotrophic factor
GFAP	Glial fibrillary acidic protein
Grb2	Growth factor receptor bound protein 2
GTP	Guanosine triphosphate
HPLC	High performance liquid chromatography
IL-6	Interleukin 6
iPSC	Induced pluripotent stem cell
IP	Inositol triphosphate
LBP	Ligand binding pocket
LCMS	Liquid chromatography mass spectrometry
LM	Light microscopy
MAG	Myelin-associated glycoprotein
MAPK	Mitogen associated protein kinase protein
MCNV	Motor conduction nerve velocity
MHRA	UK Medicines and Healthcare Products Regulatory Agency
MLC	Myosin light chain
MRC	Medical research council
MUNE	Motor unit number estimation
NCAM	Neural cell adhesion molecules
Nck	Cytoplasmic protein
NF-H	Neurofilament heavy
NF-L	Neurofilament light
NF-M	Neurofilament medium
NGF	Nerve growth factor
NMR	Nuclear magnetic resonance spectroscopy
NSAID	Non-steroidal anti-inflammatory drug
P0	Protein zero
p75NTR	p75 neurotrophin receptor

PBS	Phosphate buffer solution
PCL	Polycaprolactone
PKA	Protein kinase A
PGA	Poly(glycolic acid)
PH	Pleckstrin-homology domain
PLA	Poly(lactic acid)
PLGA	Poly(Lactic-co-Glycolic) acid
PNI	Peripheral nerve injury
PNS	Peripheral nervous system
PPAR-γ	Peroxisome proliferator associated receptor gamma
PTEN	Phosphatase and tensin homolog
PTP	Protein tyrosine phosphatase
qPCR	Quantitative polymerase chain reaction
RAGs	Regenerating associated genes
RBD	Rho-binding domain
ROCK	Rho associated protein kinase
SEM	Scanning electron microscopy
SFI	Static functional index
SHP-2	Protein tyrosine phosphatase-2
SSI	Static sciatic index
TCL	Thin layer chromatography
TEM	Transmission electron microscopy
TFI	Tibial functional index
Trk	Tyrosine kinase receptor
TZD	Thiazolidinedione
US	United states
UV	Ultra violet
VAS	Visual analogue score
VEGF-A	Vascular endothelial growth factor - A

Contents

Index of figures

CHAPTER 3

CHAPTER 4

CHAPTER 6

Index of tables

Index of schemes

Chapter 1: Introduction

1.1 The nervous system

The nervous system consists of two parts, the central nervous system (CNS) and the peripheral nervous system (PNS), and its role is to transmit signals responsible for the control of the body and communication among its parts. The CNS consists of the brain and spinal cord and the PNS consists of nerves containing bundles of fibres or axons that connect the CNS to the rest of the body (Figure 1.1). Efferent (motor) nerves transmit signals from the brain and the afferent (sensory) nerves transmit information from the body to the CNS *(Michael-Titus et al., 2007)*.

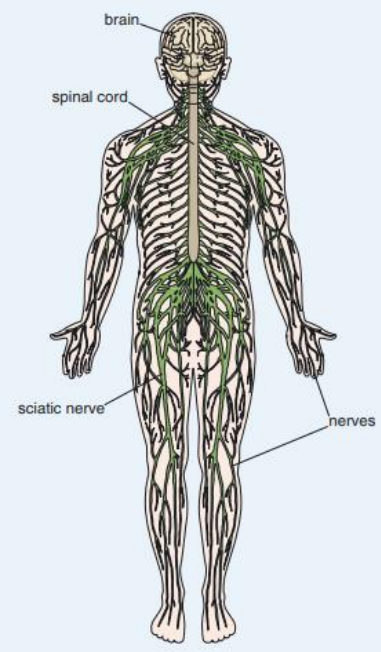

Figure 1.1: Anatomy of the nervous system. *The central nervous system consists of the brain and spinal cord and the peripheral nervous system consists of the nerves that extend out to the rest of the body (Phillips, 2008).*

The nervous system is a complex structure consisting of specialised cells named neurons which possess functional structures that allow them to send signals to other cells. These signals are sent in the form of electrochemical waves along thin fibres or axons to excite or inhibit the end target cell (Figure 1.2) *(Michael-Titus et al., 2007)*. The neurons are supported by other specialised cells named glia which provide structural and metabolic support. Any interruption within this system can result in loss of transmission of signals and subsequent reduction in function.

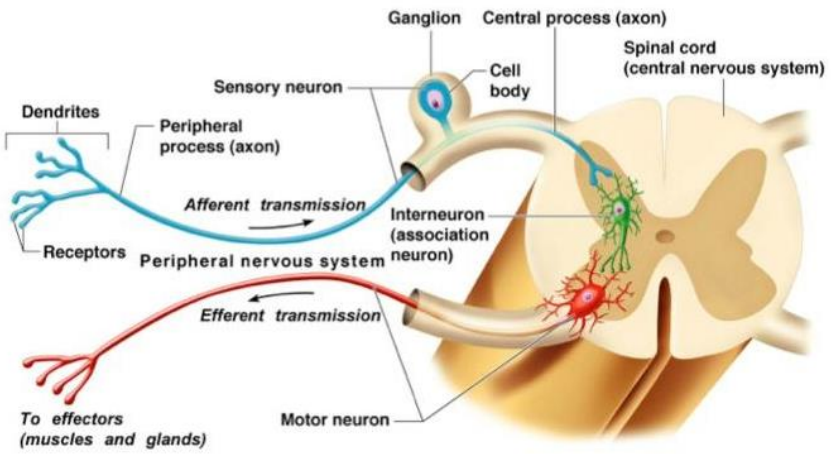

Figure 1.2: Connectivity of neurons between the CNS and PNS *(Marieb, 2009).*

Peripheral nerves act as conduits for axons which extend between the CNS and peripheral receptors or effectors. The cell bodies are adjacent to the CNS (Figure 1.2). The axons can be unmyelinated or myelinated by Schwann cells and are bound together into fascicles by connective tissue to form the endoneurium, which is enclosed in the perineurium sheath. This whole structure is encased inside a tough outer layer called the epineurium (Figure 1.3) *(Michael-Titus et al., 2007)*.

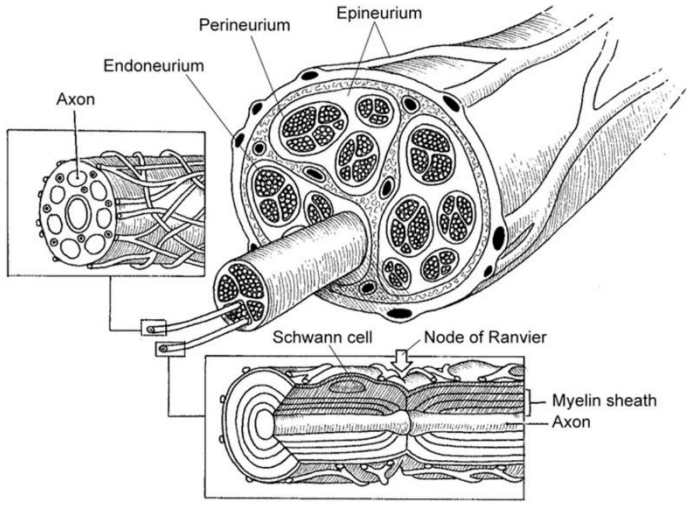

Figure 1.3: Structure of a peripheral nerve and its fundamental layers *(Biazar et al., 2010).*

Injury to the nervous system can have devastating consequences especially within the CNS, as it usually results in irreversible damage. However, unlike the CNS, the PNS has the capacity to spontaneously regenerate and there is opportunity to regain function

(Chen et al., 2007, Schmitt et al., 2003). This difference between the two systems is dependent on the different molecular programs within the neuronal cell bodies following injury *(Schmitt et al., 2003)*, and the flexibility of the neural cells at the injury site. Within the PNS, neurons and Schwann cells differentiate into cells with regenerative potential, which is absent in the CNS *(Jessen and Mirsky, 2016*). Despite this, damage to the PNS can still be debilitating and result in loss of motor and sensory function. This could be attributed to poor neuron regeneration capacity and the lack of effective therapies to improve this regenerative rate *(Hoke and Brushart, 2010)*. Therefore, there is a clear unmet clinical need to improve outcomes in this field *(Martinez de Albornoz et al., 2011)*.

1.2 Peripheral nerve injury (PNI)

Peripheral nerve injury (PNI) has a high prevalence and affects all patient populations *(Chan et al., 2014).* There are approximately 20 million patients in the US alone living with peripheral nerve damage through trauma and medical disorders *(Lundborg, 2003, Taylor et al., 2008)*. There are many causes of injury to the PNS, all of which can result in lasting morbidity, disability and high economic costs *(Jones et al., 2016).* Surgery is performed in ~600,000 patients in the US and Europe per year resulting in an annual cost of ~$150 billion *(Panagopoulos et al., 2017).*

PNI can be attributed to direct mechanical trauma *(Faroni et al., 2015),* diseases such as diabetic neuropathy, and drug therapies such as chemotherapy or radiotherapy in head, neck and breast cancers *(Jones et al., 2016)*. However, the most common cause of PNI is trauma which results from motor vehicle accidents, surgery, and births (obstetrical brachial plexus injury accounts for 1.24 per 1000 population) *(Jones et al., 2016).* The most common PNI occurring in trauma patients that requires surgical repair are digital nerve injuries and affect 6.2/100000 population per year *(Jones et al., 2016)*. Injury commonly results in life-long loss or disturbance in end-organ function, which compromises the patient's quality of life, but is highly dependent upon the severity and location of the injury *(Deumens et al., 2010)*. Neurapraxia and axonotmesis have a much better prognosis compared to neurotmesis, which results in damage of the axon and

surrounding tissue and is severely debilitating *(Deumens et al., 2010)*. Nerve injury severity is specified using Sunderland's five degree grading system (Figure 1.4).

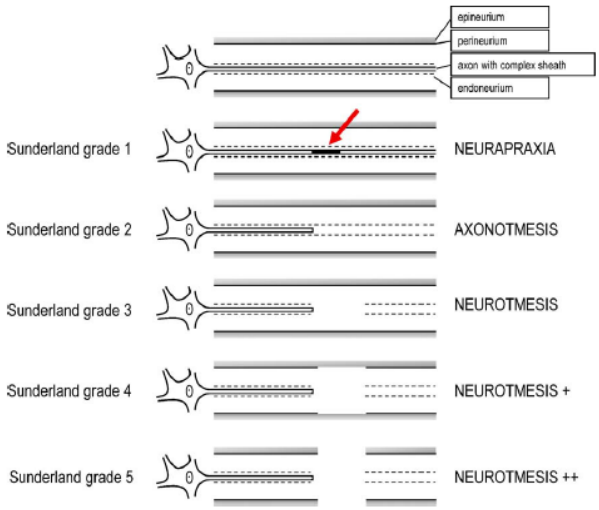

Figure 1.4: Sunderland's five degree grading of nerve injury *(Sunderland, 1951). Sunderland grades 2-5 (axonotmesis and neurotmesis) result in damage to the axon causing loss of function, however, grade 1 (neurapraxia) (shown by red arrow) results in a temporary loss of function due to the short term (maximum 6-8 weeks) blockage of nerve conduction.*

In injuries with a Sunderland grade of 2 and above sprouting at the proximal stump usually occurs within hours of injury and acts as the first step of the regeneration process in neurons, these sprouts develop into cellular outgrowths after several days *(Hall, 2005).* However, the regenerative ability of the neuron is poor, with a growth rate of ~1-3mm/day *(Chan et al., 2014).* Regeneration is slow and is delayed in older patients with a linear decline with age. Successful regeneration is highly dependent on both efficient axon regrowth and myelination of those axons by Schwann cells *(Chen et al., 2007).* Poor regeneration will delay the connection between these two cell types resulting in the loss of Schwann cells in the distal stump, which in turn will cause them to lose their supportive role in guiding axon growth. Axon regeneration is also promoted by up-regulation of neurotrophic factors, cytokines and axon adhesion molecules produced by these Schwann cells. These factors support the intrinsic growth capacity in the neuronal cell body, which encourages axon regrowth *(Chen et al., 2007)*.

Furthermore, a lack of connection between the axons and target organ results in poor outcomes due to atrophy of the target organ with a consequential loss of functional recovery *(Hoke and Brushart, 2010)*. Axonal specificity is also required for successful

functional recovery. To ensure sensory and motor axons are guided to their correct end-organ target, target pathway and target-derived factors are released *(Wood and Mackinnon, 2015)*.

On the contrary, there may be abnormal regeneration which results in nerve swelling at the proximal end, known as a neuroma (Figure 1.5 (E)). A neuroma is the product of random proliferating axonal sprouts and scar tissue deposited by fibroblasts. It is thought to be due to neurites that have escaped from the damaged perineurium *(Lee and Guyuron, 2015)*.

Therefore, the capacity for functional regeneration is directly dependent upon the type of injury, degree of axonal guidance and the proximity of the injury to the nerve cell body *(Faroni et al., 2015).* Following peripheral nerve crush or axotomy it is evident that many molecular and cellular changes occur at three main sites; the neuronal cell body, site of injury and end-organ target.

1.2.1 Neuronal cell body

Large numbers of neurons are at risk of death following PNI but the exact loss is unknown, as it is highly dependent on the experimental model and analytical method for quantification used *(Hart et al., 2008)*.There are various other factors that can affect the extent of neuronal cell death including the grade of injury and the proximity of the nerve injury to the cell body. Cell death is more likely to occur in proximal injuries, especially in motor neurons. A study demonstrated that 27% of L4-6 neurons were lost in a sciatic nerve transection in the thigh in comparison to 7% loss with the same injury in the calf *(Ygge, 1989)*. However, in general motor neurons are more resistant than sensory neurons, as a third of sensory neurons will be lost following a distal injury *(Hart et al., 2008)*.

Neuron cell survival is vital for initial axon sprouting within the proximal segment and the subsequent regeneration to the distal segment and reinnervation of the end-organ. The withdrawal of target-derived neurotrophic factors determines gene and protein expression for either regeneration or cell apoptosis. Following an injury both the

regenerative and cell death pathways are triggered and the cell's fate highly depends on the later balance of the two *(Nunez and del Peso, 1998)*. Neuronal cell death is relatively slow (15-20 hours) which provides an opportunistic time-frame for pharmacological intervention to provide neuro-protection and promote regeneration *(Faroni et al., 2015).* A study found that the administration of N-Acetyl cysteine provided neuroprotection with no significant loss of neurons at 2 weeks post-injury with a dose of 150-300 mg/kg/day in a rat sciatic nerve transection model *(West et al., 2007)*.

Furthermore, following PNI the cell body receives a primary signal of a high frequency burst of action potentials which causes the opening of calcium channels and subsequent initiation of the Jun-kinase cascade *(Faroni et al., 2015)*. The resulting influence on transcription causes an upregulation of specific axonal proteins, such as GAP43, which aid regeneration, but also a change in the expression of regeneration-associated genes (RAGs) *(Ma and Willis, 2015, Schmitt et al., 2003)*.

1.2.2 Site of Injury

Following an injury the proximal segment undergoes regeneration and the distal segment degeneration. The activity in the distal part of a damaged nerve is referred to as Wallerian degeneration (Figure 1.5 (B)) and occurs within 24-48 h of the injury *(Yang et al., 2008)*. It involves the activation and recruitment of "clean-up" cells such as Schwann cells and macrophages to remove and recycle axonal and myelin derived factors, thus creating a permissive environment that can support axonal regeneration *(Chen et al., 2007)*. After sufficient debris has been removed, the Schwann cells align into columns to form bands of Büngner (Figure 1.5 (C)) *(Deumens et al., 2010)*. The result is the production of a permissive environment rich in neurotrophic factors to aid regeneration.

Recent studies have advanced our understanding of how Schwann cells assist macrophages in removing myelin debris during later stages of an injury. Gomez-Sanchez *et al.* (2015) showed that the Schwann cells initiate the degradation of myelin proteins and lipids after nerve injury through a mechanism called autophagy, whereby cells break down their own intrinsic cellular components *(Gomez-Sanchez et al., 2015)*.

After 24 hours Schwann cells proliferate and undergo re-programming and proliferation which enables them to switch between phenotypes. Principally from a mature myelinating or Remak phenotype to a regenerating phenotype which results in the up-regulation of several growth factors such as nerve growth factor (NGF), brain derived neurotrophic factor (BDNF), glial cell line-derived neurotrophic factor (GDNF), basic fibroblast growth factor (bFGF) *etc*. and cell adhesion molecules (CAM) including L1 and neural cell adhesion molecule (NCAM) and the downregulation of structural proteins such as protein 0 (P0), myelin-associate glycoprotein (MAG) and myelin basic protein *(Jessen and Mirsky, 2016).*

1.2.3 End-organ target

For an effective functional outcome the regenerating axon needs to re-innervate the specific target organ, however, for this to be successful there are obstructions in the distal site to overcome. These include minimising misdirection by pruning growth cones that do not reach the target organ. In addition, Schwann cells distal to the injury become chronically denervated and dormant due to reduced contact with neural cells. This denervation is time-dependent and correlates with how proximal the injury occurs. A decrease in contact time reduces the ability of Schwann cells to support axonal progression and to provide essential trophic factors. As a result this leads to apoptosis of the surrounding Schwann cells and tissue atrophy *(Faroni et al., 2015).*

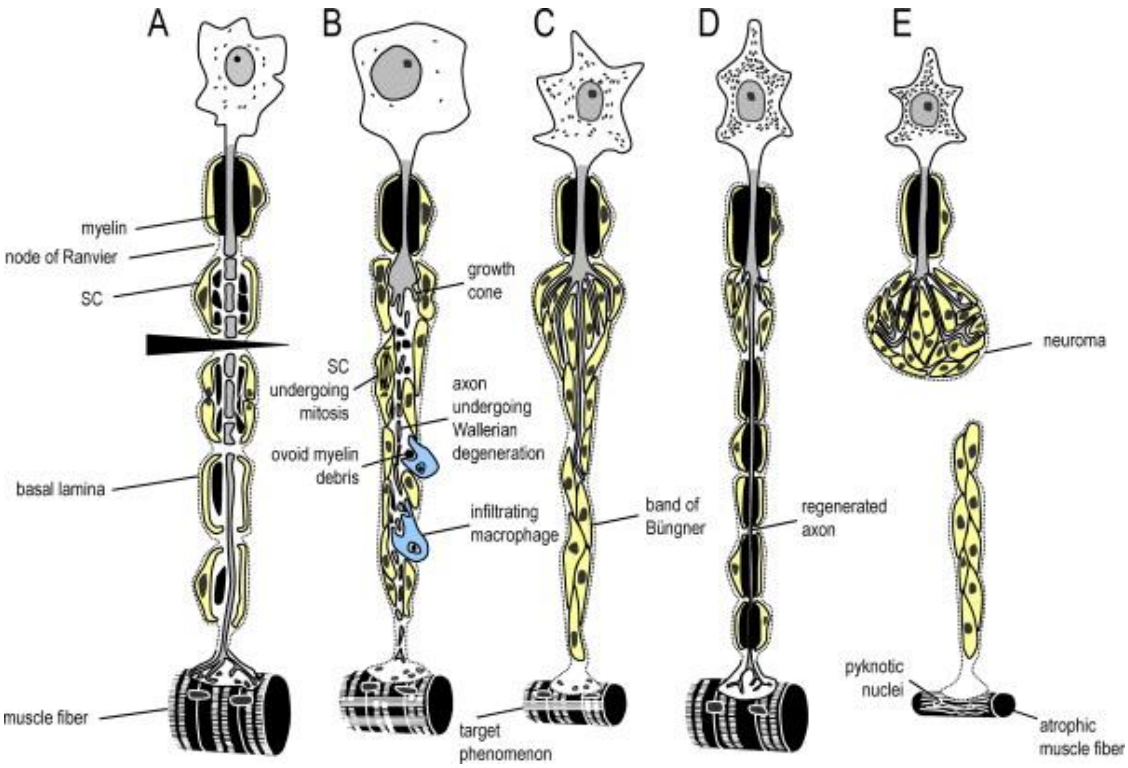

Figure 1.5: Sequence of cellular events triggered by peripheral nerve injury. *(A) - Neurotmesis. (B) - Nerve undergoing the process of Wallerian degeneration. (C) - Alignment of Schwann cells forming Bands of Büngner several days into regeneration. (D) - Successful regeneration of an axon. (E) - Development of a neuroma resulting in the loss of nerve regeneration (Deumens et al., 2010).*

1.3 Main cell mediators in PNI

In previous preclinical studies two key mediators, namely Schwann cells and macrophages, have been identified as potential targets associated with improved regeneration *(Gomez-Sanchez et al., 2015, Mokarram et al., 2012)*. The significant interactions between these two cell types and the nerve environment has classified them as having a major role in promoting neurite growth *(Jessen et al., 2008)*. Enhanced understanding of the role of these cell types in regeneration will aid the identification of possible pharmacological targets.

1.3.1 Schwann Cells

Schwann cells are key mediators in nerve regeneration and exert control over molecular mechanisms and pathways to aid development, myelination and myelin maintenance *(Jessen et al., 2008)*. Hall, (1986) demonstrated the vital role Schwann cells play in the regeneration process using a mouse sciatic nerve gap (0.5 mm) model repaired with an autograft. A reduction in the quality and extent of regeneration in the absence of

Schwann cells was shown *(Hall, 1986)*. Schwann cells have the ability to differentiate or transdifferentiate between phenotypes, essentially to a repair (Büngner) cell shortly after injury, thus switching from a role in maintenance of axonal ensheathment to that of regeneration (Figure 1.6). Therefore, these cells are specialised and differ from other Schwann cell lineage *(Jessen and Mirsky, 2016).* Transdifferentiation changes the expression of thousands of genes with the downregulation of myelin transcription factor (Krox-20), structural proteins and membrane associated proteins characteristic of myelinating Schwann cells *(Jessen and Mirsky, 2016, Wood and Mackinnon, 2015)*. In parallel there is upregulation of genes associated with immature Schwann cells such as p75 neurotrophin receptor (p75NTR) and glial fibrillary acidic protein (GFAP) in addition to neurotrophic factors and surface proteins that are not involved in either healthy or developing nerves, indicating there is a novel repair phenotype following injury *(Jessen and Mirsky, 2016)*. These "repair" Schwann cells also have the capacity to activate an immune response and recruit immune cells, particularly macrophages, to the distal stump *(Yang et al., 2008)*.

Following Wallerian degeneration the Schwann cells adopt an elongated bipolar morphology and form bands of Büngner which act as a conduit to guide the regeneration of the axon *(Deumens et al., 2010, Gaudet et al., 2011, Hall, 2005, Jessen and Mirsky, 2016)*. During regeneration Schwann cells are in a transient state but can differentiate back to myelinating cells succeeding regeneration *(Jessen and Mirsky, 2016)*.

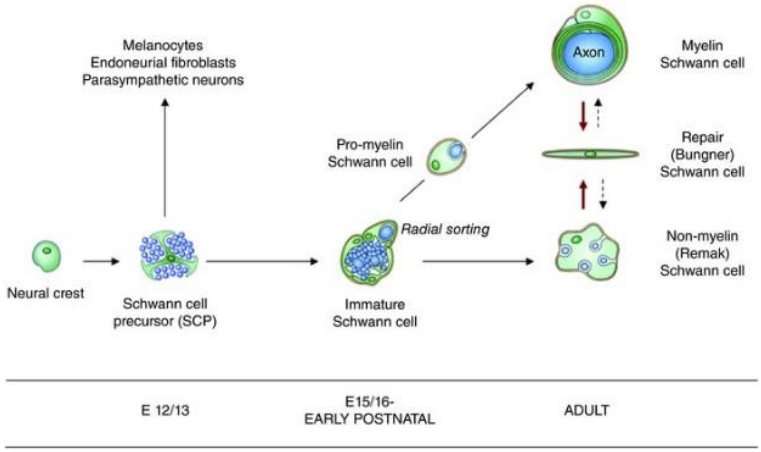

Figure 1.6: Lineage of Schwann cell development. *In healthy nerves the Schwann cells develop into either a myelin or non-myelin (Remak) cell, however, following PNI there is suggested to be a novel phenotype known as a repair (Büngner) cell which performs different functions to aid regeneration (Jessen and Mirsky, 2016).*

1.3.2 Macrophages

The primary role of macrophages in peripheral nerve regeneration is demyelination in the process of Wallerian degeneration during which they penetrate Schwann cell tubes to degrade the myelin sheaths *(Hall, 2005)*. They have proven to be difficult targets for therapy due to their 'double-edged' characteristics of scavenging debris and stimulating trophic factors to help to remodel the extracellular matrix *(Mokarram et al., 2012).*

There are two populations of macrophages during peripheral nervous system injury; resident and recruited. The resident endoneurial macrophages account for 4% of the cellular population and respond rapidly to injury. Recruited macrophages are attracted to the site of injury by chemokines expressed by denervated Schwann cells *(Hall, 2005).* Macrophages present two phenotypes; pro-inflammatory M1 cells and pro-regenerative M2 cells *(Mokarram et al., 2012, Martinez and Gordon, 2014).* M2 macrophage cells result in an increased rate of Schwann cell migration relative to M1 phenotype (Figure 1.7). The pro-regenerative M2 cells are split further into three sub-phenotypes M2a, M2b and M2c. M2a and M2c act to enhance tissue repair and promote healing, whereas M2b plays a regulatory role *(Mokarram et al., 2012).*

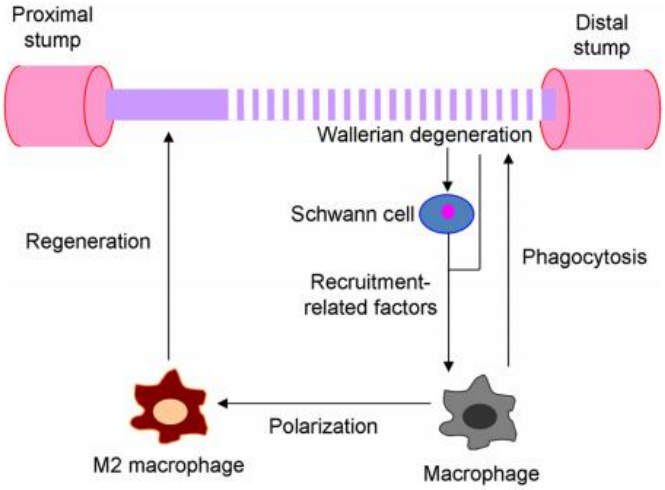

Figure 1.7: Macrophage activity during peripheral nerve injury *(Chen et al., 2015).*

Recruited macrophages promote regeneration by secreting apolipoprotein E (Apo E) as they scavenge lipids to deliver to Schwann cells for re-use in axon re-growth *(Hall, 2005)*. They also act as a source of axonal regeneration-related factors such as extracellular matrix (ECM), growth factors, cytokines and chemokines and promote vascularisation in

the distal stump *(Jessen and Mirsky, 2016, Chen et al., 2015)*. A recent study demonstrated how macrophages exert an additional process to direct the Schwann cells using increased vascularisation. The macrophages stimulate the movement of Schwann cells across the bridge between the proximal and distal stump by secreting vascular endothelial growth factor (VEGF-A) in response to a hypoxic environment. The hypoxic conditions stimulate the formation of blood vessels which direct the Schwann cells *(Cattin et al., 2015).*

Finding ways to manipulate macrophage or Schwann cell phenotype may provide a route to identify novel drug targets for nerve regeneration. Aside from these cell types, there is also potential to target the neurons directly with pharmaceutical agents that have neuroprotective properties. Hiraga *et al. (2006)* used a mouse sciatic nerve injury model to determine that the drug fasudil acted directly on motor neurons to promote nerve regeneration through the inactivation of the Rho/ROCK pathway.

Following an injury, changes in the neuronal cell body result in neurons switching from a resting to a regenerating mode. The associated molecular pathways have a substantial effect on axonal growth and they have provided potential targets for pharmaceutical treatments.

1.4 Molecular signalling pathways

Recent studies have demonstrated the effect of signalling pathway activation and the consequent changes in gene expression on nerve regeneration (Figure 1.8) *(Tedeschi, 2011, Hiraga et al., 2006).* Most studies have focused on excitatory pathways that act to enhance regeneration, however the location, whether it be within the neurons, Schwann cells or other neural cells is still under investigation *(Wood and Mackinnon, 2015)*.

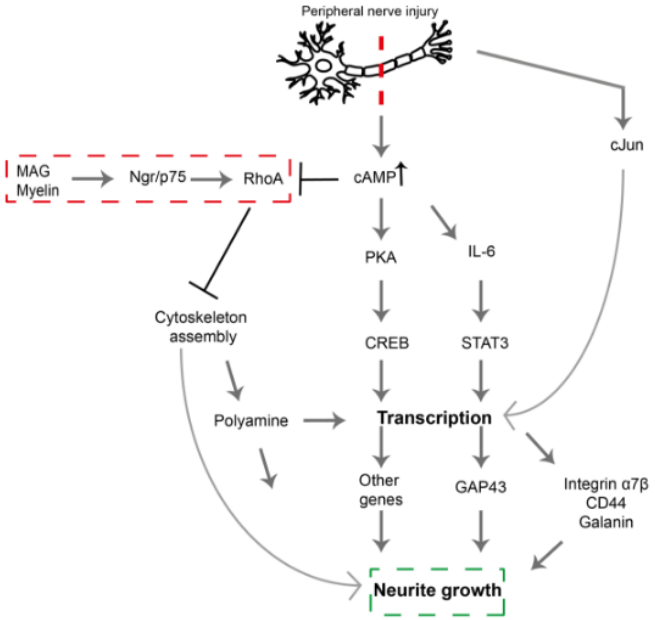

Figure 1.8: Signalling pathways following peripheral nerve injury. *All pathways are excitatory acting to enhance axonal growth except the Rho/ROCK inhibitory pathway indicated in red. Modified from (Chen et al., 2007).*

An example of a commonly studied excitatory intracellular messenger is cyclic adenosine monophosphate (cAMP) which increases in Schwann cells following a PNI and acts as an inducer for regeneration *(Raff et al., 1978, Knott et al., 2014, Stewart et al., 1991).* The promotion of regeneration on the up-regulation of cAMP is clearly evident as it significantly increases neurite growth and the release of growth associated proteins, whereas its inhibition reduces growth *(Chen et al., 2007).* This observation has implications for neuronal guidance, cell differentiation and neurite growth. The assembly of cytoskeleton proteins is essential for axon elongation. In the neuron cAMP activates protein kinase A (PKA), a kinase that blocks the activity of myelin-associated glycoprotein (MAG) in the Rho A GTPase inhibitory pathway (Figure 1.8). The upregulated PKA and cAMP induce arginase-1 activity via the phosphorylation of cAMP response element binding protein (CREB), which act synergistically to overcome the growth inhibitory effects of MAG *(Chan et al., 2014).*

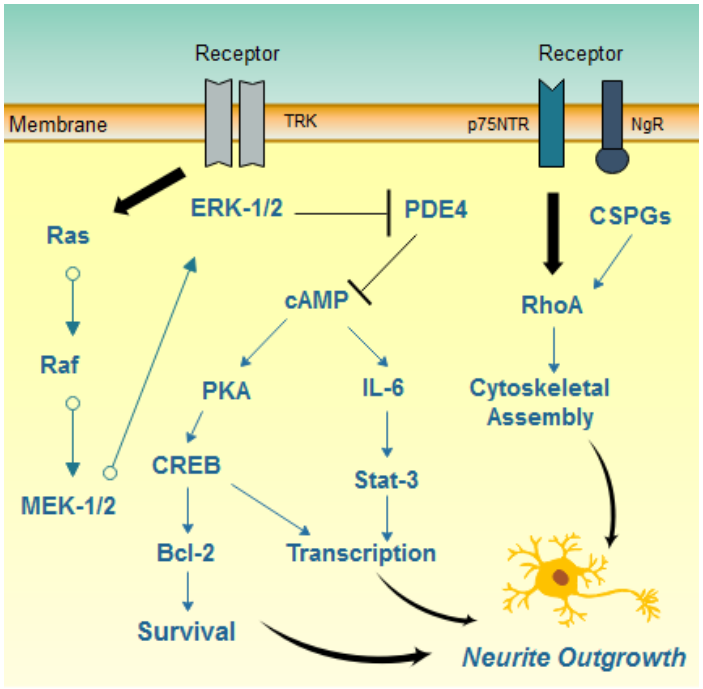

Figure 1.9: The Ras-ERK and cAMP – PKA signalling pathways in peripheral nerve.

cAMP also plays an apparent role in the plasticity of Schwann cells; but its mechanism is unknown. It appears to drive myelinating cells back to their immature state and, therefore, negatively regulates the myelinating Schwann cell phenotype. This is likely to impact Schwann cell biology in three significant ways plasticity, demyelination pathologies and regeneration response *(Chen et al., 2007).*

Another commonly studied excitatory pathway is the Ras-ERK signalling pathway. The extracellular signal-regulated kinase (ERK) is a member of the mitogen associated protein kinase family (MAPK) and plays a role in neurite outgrowth and axon survival by activating anti-apoptotic proteins including B-cell lymphoma 2 (Bcl-2) *(Chan et al., 2014)*. The ERK pathway is activated through the binding of the growth factor neurotrophin to the tyrosine kinase (TrK) receptor. This leads to subsequent Ras activation which initiates the serine-threonine kinase Raf, tyrosine-threonine kinase MAP/ERK kinase (MEK) and ERK cascade, which encourages neurite growth (Figure 1.9) *(Klesse et al., 1999)*.

Within the complex network of signalling pathways, the majority are excitatory acting to promote neurite growth; however, one inhibitory pathway has been identified. The Rho A pathway suppresses axonal growth by causing growth cone collapse, as it regulates

the actin cytoskeleton through the downstream effector Rho associated protein kinase (ROCK) (Figure 1.8) *(Roloff et al., 2015).* In recent years studies have demonstrated that targets within the Rho/ROCK pathway may be promising for the development of pharmaceutical therapies as neurons, particularly motor neurons, have an increased responsiveness to the pathway following PNI *(Joshi et al., 2015, Wood and Mackinnon, 2015).* Blocking the inhibitory pathway, which prevents growth cone collapse, has shown promising results in *in vitro* and *in vivo* studies *(Tang, 2003, Wood and Mackinnon, 2015)*.

1.4.1 Rho/ROCK signalling pathway

In brief, activation of the GTPase Rho (or Rho A) to its GTP-bound form with the help of downstream effector kinase ROCK leads to stiffening of the actin cytoskeleton. This initialises changes in the signalling of many downstream effectors, inhibiting axonal elongation and mediating growth cone collapse (Figure 1.10) *(Chan et al., 2014, Hiraga et al., 2006, Madura et al., 2004).* This underlines the potential usefulness of developing treatments that act directly upon the Rho/ROCK pathway.

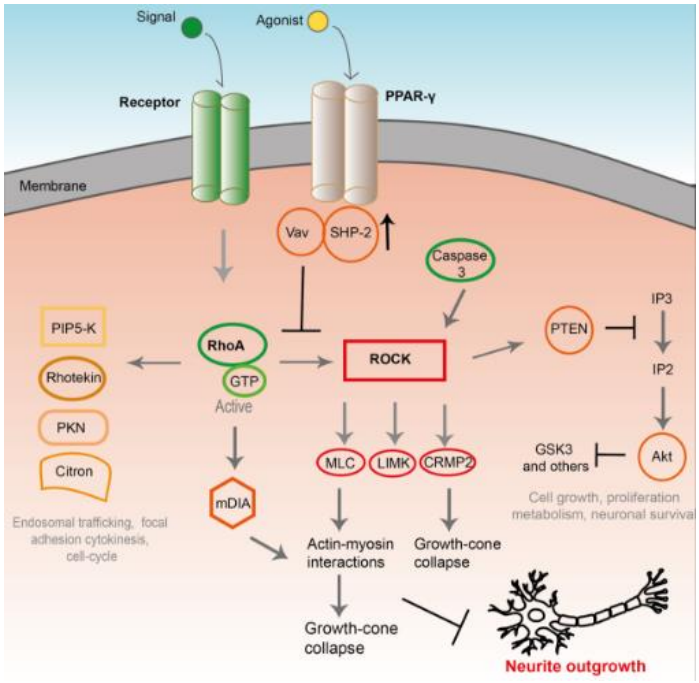

Figure 1.10: Overview of the Rho/ROCK inhibitory pathway and its potential targets for drug treatments. *(Peroxisome proliferator associated receptor gamma (PPAR-γ), protein tyrosine phosphatase-2 (SHP-2), myosin light chain (MLC), LIM kinase (LIMK), collapsin response mediator protein-2 (CRMP2), protein kinase B (Akt), phosphatase and tensin homolog (PTEN), inositol trisphosphate (IP)).*

The Rho/ROCK pathway (Figure 1.10) can also be modulated through activation of upstream receptors, such as the receptor tyrosine kinases; Eph, G-protein coupled receptors, plexins, ApoER2 *(Schmandke et al., 2007)* and the peroxisome proliferator-activated receptor gamma (PPAR-γ) *(Wakino et al., 2004)*, and through the action of neurogenic inhibitors such as MAG, Nogo-A and chondroitin sulphate proteoglycans (CSPG). These inhibitory signals appear to converge on the Rho GTPase pathway ultimately blocking effective regeneration *(Tang, 2003, Wood and Mackinnon, 2015)* and provide additional targets for the inhibition of this signalling pathway. As the Rho/ROCK signalling pathway appears to act as a nexus for opposing nerve regeneration it has attracted considerable interest and several potential targets for drug therapies have been identified. The success of such treatments will be dependent on their ability to inhibit the downstream activity of Rho on actin cytoskeleton remodelling in the growth cones which is essential for axonal regrowth *(Joshi et al., 2015, Tang, 2003)*. The main targets which have been explored are discussed below.

1.4.1.1 Rho GTPases and Rho GEFs

Rho, together with Rac and Cdc42, belongs to the family of small GTPases, which have a role in cellular motility and cytokinesis *(Kubo et al., 2008, Lu et al., 2009).* Modulation of Rho, Rac1, and Cdc42 GTPase activity has been demonstrated to affect various aspects of dendritic development and influences neuronal information processing *(Van Aelst and Cline, 2004)*.

Due to their role in the rapid and dynamic reorganisation of the actin cytoskeleton Rho GTPases have been implicated as targets in a number of therapeutic areas including; cardiovascular, pulmonary, retinal and neurological disorders as well as cancer *(Amano et al., 2010, Lu et al., 2009).* In recent years evidence has also been accumulating to support the essential role played by Rho GTPases in nerve cell function and survival and axonal growth through the orchestration of growth cones *(DeGeer and Lamarche-Vane, 2013)*.

The signalling pathway is complex and there are over 60 known downstream effectors for Rho proteins which determine the subsequent output such as changes in cell morphology, polarity, vesicular trafficking or cell cycle control *(Hodge and Ridley, 2016).* One of the primary outcomes of Rho activation is the reorganisation of the actin cytoskeleton (Figure 1.10) *(Hodge and Ridley, 2016, Lu et al., 2009, Shang et al., 2012, Amin et al., 2013)*. The stiffening of the cytoskeleton induces downstream effectors, which inhibits axonal elongation and mediates growth cone collapse, thus inhibiting nerve regeneration *(Chan et al., 2014, Hiraga et al., 2006, Madura et al., 2004).*

Rho GTPases can be viewed as molecular switches whose activity depends upon regulatory proteins which are specific to each family member, these include guanine nucleotide exchange factors (GEFs), GTPase activating proteins (GAPs) and guanine nucleotide dissociation inhibitors (GDIs). GAPs maintain a basal level of GTPase activity via hydrolysis of active GTP-bound Rho to inactive GDP-bound Rho, whereas GEFs such as LARG, PDZ-RhoGEF and p115-RhoGEF activate GTPases and enhance exchange to the GTP-bound form *(Schmandke et al., 2007, DerMardirossian and Bokoch, 2005)*. GDIs, mainly RhoGDI-1(α), on the other hand inactivate GTPases by binding to the GDP-bound form preventing the exchange to the active GTP-bound form *(DeGeer and Lamarche-Vane, 2013).* Post translational modification of Rho (e.g. prenylation, farnesylation *etc*.) has been shown to be crucial for the interaction between Rho GTPases, GDIs and GAPs where GTP hydrolysis can only occur on Rho which has been post translationally modified, therefore inhibition of this process will also affect cell growth and cytoskeletal organisation *(Hancock and Hall, 1993, Molnar et al., 2001)*.

Inhibitors targeting these proteins would provide a basis to control neuronal growth following PNI, however, a lack of specific tool compounds has hampered progress *(Lu et al., 2009, Tang, 2003).* Increased understanding of the structural basis for the interaction between Rho and its regulatory proteins may help to plug this gap, and some progress has been made towards this goal.

GEFs that have been investigated as drug targets in nerve regeneration include Vav2, Vav3 and LARG which play a role in modulating the cycle between GTP-bound and

GDP-bound Rho *(Keilhoff et al., 2012, Shang et al., 2012).* The GEFs Vav2/3 role in peripheral nerve regeneration was studied using a sciatic nerve transection model in double knockout mice (Vav2/3). The results demonstrated delayed Wallerian degeneration and revascularisation in the knockout mice compared to the wild-type, suggesting that Vav is required for normal degeneration, regeneration, revascularisation and improved functional recovery following injury *(Keilhoff et al., 2012).* However, to the best of our knowledge no small molecule inhibitors targeting this interaction have been reported to date.

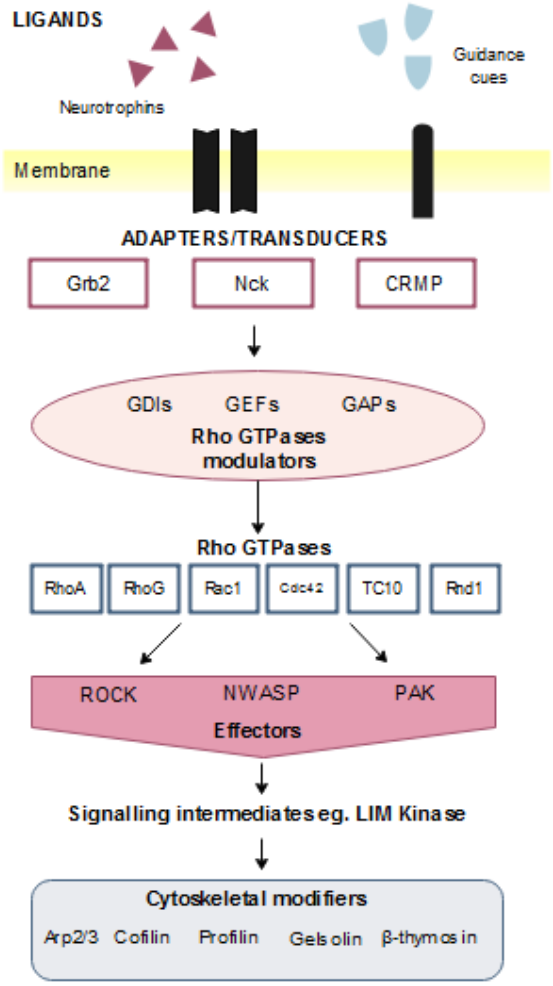

Figure 1.11: Overview of potential pharmacological targets within the Rho/ROCK pathway. (Growth factor receptor-bound protein 2 (Grb2), Cytoplasmic *protein (NcK),* collapsin response mediator protein-2 (CRMP2), guanine nucleotide dissociation inhibitors (GDIs), guanine nucleotide exchange factors (GEFs), GTPase activating proteins (GAPs)).

1.4.1.2 Rho Kinase (ROCK)

ROCK, the Rho-associated coiled-coil-containing protein kinase, is the most extensively studied downstream effector in the Rho pathway. ROCK is a serine/threonine protein

kinase belonging to the AGC family with MW of ~160 kDa *(Amano et al., 2010, Lu et al., 2009).* Two isoforms of ROCK exist and are characterised by their spatially differential expression; ROCK I is found in non-neuronal tissues and ROCK II is predominantly in the brain and muscle tissues *(Kubo et al., 2008, Lu et al., 2009, Amin et al., 2013).* The two isoforms have 65% overall sequence similarity and 92% similarity in their kinase domains. ROCK consists of a kinase domain, a Rho-binding site and a pleckstrin-homology domain with an internal cysteine rich domain at the carboxyl terminus (Figure 1.12) *(Amano et al., 2010, Kubo et al., 2008).* ROCK kinase activity is auto inhibited by the C-terminal domain that folds back onto the catalytic domain. The GTP-bound form of Rho is thought to activate ROCK by binding to its Rho binding domain and blocking the auto inhibitory loop on the catalytic domain *(Kubo et al., 2008).* Independent of Rho, ROCK can also be activated by caspases, which cleave the auto inhibitory C-terminal domain and by arachidonic acid and sphingosylphosphorylcholine *(Schmandke et al., 2007, Lu et al., 2009)*. Activation of ROCK leads to phosphorylation of downstream proteins such as myosin light chain (MLC), LIM kinase and collapsin response mediator protein-2 (CRMP2), which results in stiffening of the cytoskeleton and growth cone collapse.

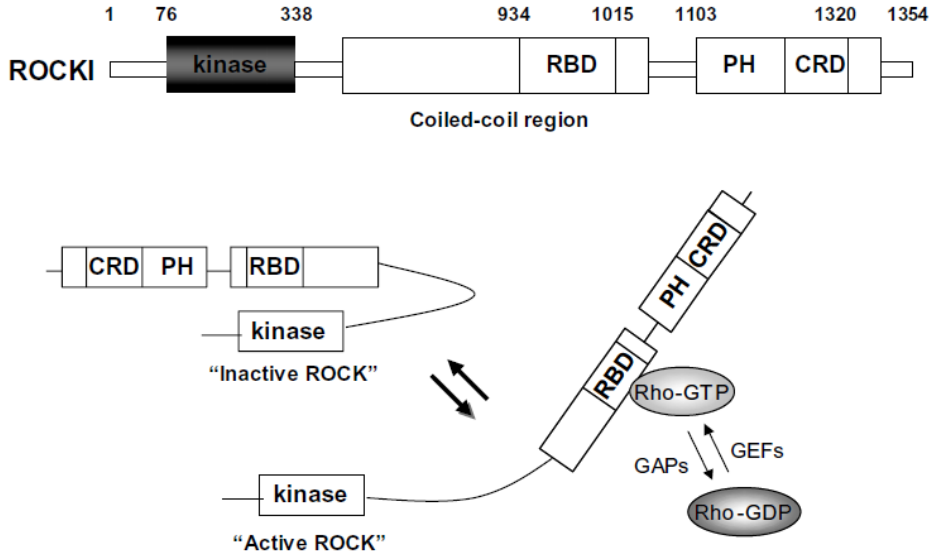

Figure 1.12: Mechanism of ROCK activation *(Kubo et al., 2008). (Rho-binding site (RBD), pleckstrin-homology domain (PH), cysteine rich domain (CRD), guanosine-5'-triphosphate (GTP), guanosine diphosphate (GDP), guanine nucleotide exchange factors (GEFs), GTPase activating proteins (GAPs)).*

1.4.1.3 Peroxisome proliferator-activated receptor gamma (PPAR-γ)

PPAR-γ is a member of the nuclear receptor family that heterodimerizes with retinoic acid-X receptors and is rendered transcriptionally active by binding to a specific DNA sequence element termed the PPAR response element *(Wakino et al., 2004, Quintanilla et al., 2014)*. Activation of PPAR-γ subsequently leads to inhibition of the Rho/ROCK pathway via upregulation of the protein tyrosine phosphatase, Src homology region 2–containing protein tyrosine phosphatase-2 (SHP-2). This cytosolic protein tyrosine phosphatase (PTP) dephosphorylates the Rho-GEF Vav, inactivating it thus suppressing the conversion of inactive GDP-Rho to active GTP-Rho and ultimately resulting in the suppression of Rho/ROCK activity *(Wakino et al., 2004)*.

This is supported by an *in vivo* study in adult rats, which demonstrated suppression of Rho/ROCK activity was consistent with upregulated SHP-2 expression and inactivation of Vav following 4 weeks treatment with the PPAR-γ agonist, pioglitazone *(Wakino et al., 2004)*. Of particular relevance to PNI, Lezana *et al. (2016)* also demonstrated the presence of PPAR-γ in axons within a rat sciatic nerve and that PPAR-γ activation increased at 2, 4, and 6 h after a nerve ligation or crush injury.

Ligands bind to the ligand-binding pocket (LBP) of PPAR-γ modulating the activation function 2 (AF-2). AF-2 is a coactivator binding surface comprised of residues from the C-terminal helices (H) 12, H3 and H5 *(Puhl et al., 2015, Nolte et al., 1998)*. Agonist binding results in increased conformational rigidity of H12, locking the protein into an active conformation, this enables co-activator binding (via the conserved LXXLL motif) and results in formation of a transcriptionally active form of the receptor. The binding mode of the respective ligands and the associated extent of stabilisation of H12 in the active conformation correlates with the magnitude of the transcriptional response. Full agonists, for example, occupy both sub-pockets of the Y-shaped LBP, forming strong contacts with a tyrosine residue (Tyr473) on the inner surface of H12. This results in H12 maintaining a rigid active position, promoting AF-2 activity *(Puhl et al., 2015).* Partial agonists, on the other hand, can adopt multiple conformations, with multiple copies of

the ligand occupying 1 or both sub pockets, and may or may not directly interact with key residue Tyr473.

1.5 Therapeutic approaches

Despite advancements made in PNI research, effective pharmacological treatment still remains challenging *(Isaacs, 2013).* Drug discovery and development is expensive and time-consuming with a high risk of failure, therefore, more companies are adopting drug repurposing as an alternative *(Padhy and Gupta, 2011)*. This technique employs data mining, bioinformatics and other screening platforms to identify drugs that are already used in other clinical indications and to reposition them for new applications *(Padhy and Gupta, 2011)*. Many drugs identified for nerve regeneration have been the result of this repurposing approach and in particular, Rho inhibitors and PPAR-γ agonists that are used for treating other clinical conditions have been identified in this way.

1.6 Drugs targeting Rho/ROCK pathway that have been investigated in PNI models.

In recent years many agents that target the Rho/ROCK pathway have been identified and tested within PNI models and have demonstrated promising benefits, through effects on axonal outgrowth and improved functional recovery. These are summarised in table 1.1.

Compound	Chemical structure	Model	Mechanism of action	Effect on nerve regeneration	Reference
Fasudil (HA-1077)	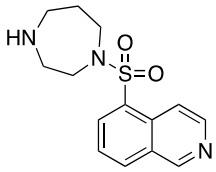	*In vitro* Dorsal root ganglion (DRG). *In vivo*: Sciatic nerve transection in rats. Silastic chamber 3-5mm gap. *In vivo:* Interpositional graft in the peroneal nerve in rats. Treated intraperitoneally or directly into the graft by microinjection. *In vitro:* N2a cell line induced by ischemia and ischemia – reperfusion.	ROCK inhibitor	*In vitro:* Increased neurite outgrowth *In vivo*: Increased number of axons and associated SCs. Accelerated functional regeneration. Improvement in the survival rate of N2a cells of ischemia group and reperfusion group after 24 h.	*(Cheng et al., 2008)* *(Madura et al., 2007)* *(Xiao et al., 2014)*
Ibuprofen	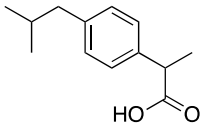	*In vivo*: Interpositional graft on adult rat tibial nerve; treated through osmotic pumps. *In vitro:* NG108-15, DRG and 3D co-culture. *In vivo:* Transection with primary repair in sciatic nerve treated through osmotic pump.	Strong partial PPAR-γ agonist	Recovery of TFI and increase of area of axon and myelin. *In vitro:* Elongation of neurites *In vivo:* Increase in axon number.	*(Madura et al., 2011)* *(Rayner et al., 2018)*
Diclofenac	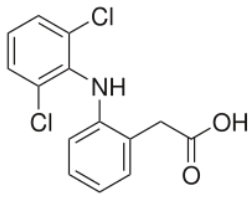	*In vivo:* Sciatic nerve transection with artery graft filled with diclofenac.	Partial PPAR-γ agonist	Improved functional recovery and faster recovery of regenerated axons.	*(Mohammadi et al., 2013b)*
Pioglitazone	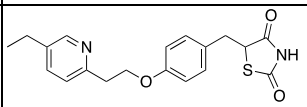	*In vivo*: Crush injury on sciatic nerve in CD36-deficient mice.	Highly selective PPAR-γ agonist	Improved re-myelination.	*(Eto et al., 2008)*
Rosiglitazone	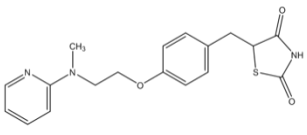	*In vitro:* N2A cell culture.	Highly selective PPAR-γ agonist	Promoted neurite outgrowth and increased population of neurite-bearing cells.	*(Chiang et al., 2014)*

Y-27632	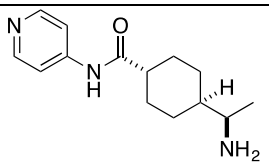	*In vitro*: Rat motor and sensory neurons. *In vivo:* Mouse femoral nerve crush model. *In vitro:* Co-culture rat primary Schwann cells and DRG.	ROCK Inhibitor	*In vitro*: Enhanced axonal growth. Motor and sensory neurons express different levels of Rho A. *In vivo:* Increased motor function *in vivo.* Increased neurite length.	*(Joshi et al., 2015)* *(Fuentes et al., 2008)*
Dimethyl-Fasudil (HA-1152)	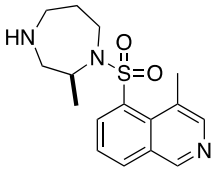	*In vitro:* Co-culture rat primary Schwann cells and DRG. *In vitro:* Postnatal mouse spiral ganglion.	ROCK Inhibitor	Increased neurite length. Increased neurite growth.	*(Fuentes et al., 2008)* *(Lie et al., 2010)*

Table 1.1: Studies that have explored the regenerative capacity of drugs that target the Rho/ROCK pathway directly or indirectly. *Inclusion criteria included studies that have used drugs targeting Rho, ROCK, PPAR-gamma, SHP-2 or VAV directly in the peripheral nervous system. Studies exploring outcome measures such as neuropathic pain or regeneration in spinal cord injuries were excluded.*

At present no small molecules directly targeting Rho have been studied in PNI, however, a number of promising inhibitors of the Rho effector, ROCK have been developed *(Mueller et al., 2005).* Fasudil (Table 1.1) is a ROCK inhibitor which is approved for use in the clinic; it is marketed in Japan as a treatment for cerebral vasospasm after subarachnoid haemorrhage and it was also evaluated for use in patients with stable angina pectoris *(Nishio et al., 2006).* It has also demonstrated beneficial effects in other clinical applications such as CNS injury, oncology, bronchial asthma, pulmonary hypertension, glaucoma, pre-term labour, erectile dysfunction and renal disease *(Mueller et al., 2005, Olson, 2008)* (Table 9.1, Appendix 1). Fasudil is a moderate inhibitor of ROCK *(Mueller et al., 2005)*, K_i = 330 nM, and has shown potential in promoting axonal growth *(Cheng et al., 2008, Lingor et al., 2007)* and improving functional outcomes in models of peripheral nerve injury *(Madura et al., 2007).*

It was found that the active metabolite of fasudil, hydroxy-fasudil, had a greater affinity for ROCK (K_i = 170 nM), which also led to the development of dimethyl-fasudil (H-1152), which has an increased affinity for ROCK (K_i = 1.6 nM) *(Mueller et al., 2005)*. Despite being the most potent ROCK inhibitor developed to date, dimethyl-fasudil has only been

studied *in vitro* for PNI using neuronal cell cultures. The studies resulted in an increase in neurite outgrowth and demonstrated the potential for dimethyl-fasudil to be taken forward in animal studies to determine functional recovery as well as regeneration *(Fuentes et al., 2008, Lie et al., 2010) .*

Another ROCK inhibitor, Y-27632 (Table 1.1), has also been extensively studied (K_i = 220/300 nM ROCKI/ROCKII) and was suggested to enhance neurite outgrowth *in vitro* and to improve motor function following treatment *in vivo (Joshi et al., 2015)*. Later generations of the ROCK inhibitors, including Y-39983 resulted in improved affinity for ROCK but have yet to be evaluated for regenerative capacity in PNI.

ROCK has been shown to regulate the force and velocity of actomyosin in smooth muscle and non-muscle cells through the inhibition of myosin phosphatase-mediated dephosphorylation of myosin II and this forms the basis as to why ROCK is a good target for diseases such as hypertension and bronchial asthma *(Wettschureck and Offermanns, 2002).* The compounds demonstrating these effects haven't been tested in PNI despite their proven effect on the Rho/ROCK pathway. This may be due to their pharmacological activity in other tissues which may raise concerns about toxicity and off-site effects. This problem could be addressed by the local delivery of drugs, which is an area that has grown in interest for nerve injuries. A recent study demonstrated the use of conduits made from a biocompatible material, polytetrafluoroethylene (PTFE), to deliver FK506 locally for PNI to reduce the systemic side effects *(Labroo et al., 2017)*.

Small molecules that target the PPAR-γ receptor have also been studied for peripheral nerve regeneration. Agonists for this receptor usually contain a lipophilic backbone and an acidic moiety, usually a carboxylate *(Puhl et al., 2015)* and many non-steroidal anti-inflammatory drugs (NSAIDs) such as ibuprofen (Table 1.1) fulfil these structural characteristics and have demonstrated different degrees of partial agonism for PPAR-γ *(Puhl et al., 2015)*. To date promising results have been reported for treatment with ibuprofen and diclofenac following PNI, for example Madura *et al.* (2011) demonstrated an improvement in functional recovery and remyelination of axons after 3 months following 3 weeks ibuprofen treatment in a rat tibial nerve transection model.

Furthermore, treatment with diclofenac delivered to a transection of a rat sciatic nerve via an artery graft elicited improvement in functional recovery and axon regeneration *(Mohammadi et al., 2013b)*.

To the best of our knowledge other NSAIDs have yet to be investigated in PNI models, despite demonstrating affinity for PPAR-γ *(Puhl et al., 2015)*. Given the promising results obtained with ibuprofen and diclofenac, further investigation of NSAIDs as promising agents to promote regeneration may prove fruitful. It is likely that greater understanding of how NSAIDs interact with PPAR-γ will help the development of more effective drugs targeting this receptor for the treatment of PNI *(Lezana et al., 2016)*.

Another class of drugs that act upon PPAR-γ is the glitazones which are used clinically as anti-diabetics. Pioglitazone and rosiglitazone have been studied for use in PNI. Pioglitazone demonstrated improved myelination following 3 weeks treatment in a crush injury model in the sciatic nerve in mice *(Eto et al., 2008)*, further supporting the proposal of PPAR-γ as a promising target for PNI.

In contrast to PNI, many compounds have been tested in the CNS and demonstrated beneficial effects on neuronal regeneration or neuroprotection with limited side effects when tested in animal models (Table 9.1, Appendix 1). Compounds inhibiting the Rho/ROCK pathway in the CNS have been found to result in improved axon regeneration and functional recovery, which is supported by studies demonstrating the opposite is true with agents activating the Rho/ROCK pathway blocking neurite outgrowth *(Fujita and Yamashita, 2014, Kubo and Yamashita, 2007).*

It has been suggested that Rho/ROCK inhibitors are effective in neurological diseases due to their action on inflammatory pathways *(Lu et al., 2009)*; however, Rho GTPases are also involved in other intracellular signalling processes following injury. Their blockade has been shown to aid functional neurological recovery in Basso Mouse Scale (BMS) and Basso, Beattie, Bresnahan (BBB) locomotor assessments in a spinal cord hemi-section, contusion or transection *(Watzlawick et al., 2014)*, indicating they have a significant role during regeneration. Rho has been shown to be present in neuronal and non-neuronal cells *in vivo (Dubreuil et al., 2003, McKerracher and Winton, 2002)* with an

increase in the active GTP-bound Rho following injury *(Fournier et al., 2003).* In turn Rho activation modulates non-neuronal cell activation and morphology, neuronal cell death and inflammatory responses *(Dubreuil et al., 2003).*

Drugs are beginning to reach clinical trials for the treatment of CNS injuries, underpinning that this is a clinical area with significant potential and, as of yet, unmet need. BA-210 (trademarked as Cethrin ®) that blocks the activity of Rho has been tested in a Phase I/IIa clinical trial for spinal cord injury *(Fehlings et al., 2011)*. Improvement in function was observed with treatment and the drug has now moved into Phase 2b/3 clinical trials under the name VX-210 *(Fehlings et al., 2018, McKerracher and Anderson, 2013)*.

Increased understanding of the mechanism through which molecules inhibit the Rho/ROCK pathway in other pathologies not associated with the PNS may aid the optimisation of drug therapies for use in PNI. From the studies implemented for other clinical indications, it is evident there are a host of small molecules available that act upon the targets of interest within the Rho/ROCK pathway and their repositioning is likely to be valuable in moving therapies rapidly towards the clinic for PNI.

1.7 Drug screening

Pre-clinical model systems including *in vitro* cell cultures and animal studies are fundamental in the discovery and development of new pharmaceutical therapies *(Breyer et al., 2015)*. Primary compound screening in humans raises obvious ethical and regulatory concerns and so model systems are paramount to establish efficacy and safety before they are taken forward into clinical trials *(Breyer et al., 2015)*. However, there are drawbacks in using different species, as studies have demonstrated that there is still difficulty in correlating the effects seen between animals and humans. This means that animal models are inefficient in predicting therapeutic effects which in turn results in the failure of new drugs reaching the market *(Seok et al., 2013, Suckling, 2008)*. Therefore, there is a clear need for the development and validation of cellular and animal models that can harmonise with the behaviour seen with human disease. This is

becoming easier as the molecular basis of disease pathogenesis is understood *(Breyer et al., 2015)*.

To date there are no effective cell culture models to screen new potential drugs for PNI. In PNI the synergistic activity of neurons and Schwann cells plays a key role in nerve regeneration, therefore it is desirable to recreate this key cell-to-cell interaction in a model when screening the effects of drug therapies. Using a tool that is more biologically comparable than a monolayer culture of isolated cells may provide pertinent data on drug safety and efficacy to inform subsequent animal and clinical studies *(Denayer et al., 2014)*. A 3-dimensional (3D) co-culture model system would allow the exploration of key regenerative events such as neurite formation and optimal dosing regimens and could also be used in understanding the mechanism of action of drug candidates. Moreover, cell cultures enable the use of primary human cells which align studies even closer to the human environment. There can be a greater degree of control and monitoring supporting the continuous study of isolated and detailed cellular responses.

Having an effective *in vitro* screening tool could reduce the number of ineffective compounds taken forward in animal studies and future clinical trials. This means animal models can be used more effectively to screen drugs that have a high potential for use in PNI and help reduce, refine and replace the use of animals in parallel.

1.8 Drug delivery

Most advancements made in the development of targeted therapeutics for peripheral nerve regeneration have been in the delivery of cells types, proteins, platelet-rich plasma or gene therapy *(Federici at al., 2007, Kuffler 2014).* These clinical interventions have proven beneficial in promoting nerve regeneration via the induction of axon outgrowth and neurological recovery *(Kuffler, 2014).* The usual method of delivery for these therapies is through the use of conduits which are surgically implanted into the site of injury. The conduits are usually made from biocompatible materials found naturally within the body such as collagen and fibrin as well as many synthetic polymers. As these materials have shown to be successful in delivering other therapies, this platform could

be viable for drug therapies as well *(Daly et al., 2012, Liu et al., 2011, Madduri et al., 2010, McGrath et al., 2010)*.

Despite the growing interest for drug therapies for PNI the research in using delivery systems to deliver these drugs is lacking. Furthermore, there has been no development in identifying a suitable treatment duration for any agent, however, as regeneration of nerves in humans takes a remarkable time (months-years) it can be assumed that the treatment durations may need to extend to this amount of time. Long term oral treatment can lead to side effects, reduced therapeutic efficiency due to minimal levels of drug reaching the target tissue and problems with patient compliance. Therefore, a device that can deliver drugs locally to the nerve injury site at a sustained rate over a long period of time would be advantageous in overcoming these matters. Extensive work has been conducted to develop biomaterials to deliver drugs to other tissues for various clinical conditions *(Fenton et al., 2018, Langer, 2004)*, therefore, it would be beneficial to apply these methods to PNI.

Project aims

The overall goal of the PhD project was to further the development of small molecule therapeutics in the field of peripheral nerve injury.

This led to five main aims:

1.) Development of an *in vitro* model as a screening tool in the discovery of drug therapies including novel compounds and repurposed drugs.
2.) Determining an *in vivo* model to screen the regenerative effects of drug agents in pre-clinical studies and investigating the various regenerative and functional outcome measures available.
3.) Manufacturing and testing drug-loaded biomaterials for use as drug delivery systems.
4.) Determining the correlation between drug affinity for PPAR-γ and its regenerative capacity.
5.) Synthesising a compound derivative that targets the Rho/ROCK pathway.

Chapter 2: Materials and methods

2.1 Cell cultures

2.1.1 SCL4.1/F7 Schwann cell line

Schwann cell line SCL4.1/F7 (Health Protection Agency) rat cells were grown in culture medium (DMEM; Sigma-Aldrich) supplemented with 10% v/v heat inactivated fetal bovine serum (FBS) (Thermo fisher scientific) and 100 U/mL of Penicillin, 100 µg/mL of Streptomycin (Sigma-Aldrich), in standard cell culture flasks. The cultures were maintained at sub-confluency at 37 ºC with 5% CO_2 and passaged when required.

2.1.2 PC12 Neuronal cell line

PC12 cells (rat neuronal cell line Pheochromocytoma cells from rat adrenal medulla used as a neuronal cell line, 88022401; Sigma-Aldrich) were grown in suspension in culture medium (RPMI 1640; Sigma-Aldrich) supplemented with 100 U/mL of Penicillin, 100 µg/mL of Streptomycin, 2 mM l-glutamine, 10% v/v heat-inactivated horse serum (Sigma-Aldrich) and 5% v/v FBS in standard cell culture flasks. The cultures were maintained at sub-confluency at 37 ºC with 5% CO_2 and passaged when required.

2.1.3 NG108-15 Neuronal cell line

NG108-15 cells (rat neuronal cell line, Sigma-Aldrich) were grown in culture medium (DMEM, Sigma-Aldrich) in standard cell culture flasks. The cultures were maintained at sub-confluency at 37 ºC with 5% CO_2 and passaged when required.

2.1.4 Dorsal Root Ganglion (DRG) harvest and culture

Dorsal root ganglion (DRG) neurons were obtained from adult Sprague Dawley rats. The spinal column was excised from rats that were culled using a Schedule 1 method (CO2 asphyxiation) according to local regulations. Using an Olympus SZ40 dissecting microscope the DRGs were removed and incubated with 0.125% w/v collagenase type IV (Sigma-Aldrich) at 37 ºC for 90 mins, then dissociated by trituration. Collagenase was removed with two consecutive 20 mL washes using culture medium (DMEM; Sigma-

Aldrich) supplemented with 10% v/v heat inactivated FBS (Biosera) and 100 U/mL of Penicillin, 100 µg/mL of Streptomycin by centrifugation at 400 g for 5 mins.

Crude DRG cell suspension was incubated in DMEM culture medium supplemented with 0.01 mM cytosine arabinoside (Sigma-Aldrich) in a poly-D-lysine (Sigma-Aldrich) coated flask at 37 ºC, 5% CO2 for 24 h. Cells were detached using 0.25% trypsin-EDTA solution and centrifuged at 400 x g for 5 mins. The supernatant was discarded and the cell suspension derived from the DRGs was re-suspended in the appropriate volume of DMEM culture medium for use in experimental studies.

2.1.5 Monolayer cell cultures

Neuronal cells (PC12, NG108-15 and DRGs) were seeded at a density of 10,000 cells in 100 µL for cell lines, or cells from 1 DRG per coverslip, onto poly-D-lysine (Sigma-Aldrich) coated circular coverslips (13 mm) for analysis (13,000 cells/cm^2).

2.2 Fabrication of 3D EngNT co-cultures

Anisotropic cellular gels were prepared as described previously *(Phillips and Brown, 2011)*. Briefly, 1 mL of solution containing; 80% v/v Type I rat tail collagen (2 mg/mL in 0.6% acetic acid; First Link), 10% v/v minimum essential medium (Sigma-Aldrich), 5.8% v/v neutralising solution (TAP Biosystems) and 4.2% Schwann cell suspension (4x10^6 SCL4.1/F7 cells per 1 mL gel) was integrated with tethering mesh at opposite ends of a rectangular mould (Dimensions 16.4 mm x 6.5 mm x 5 mm) *(East et al., 2010)* (Figure 2.1). Cellular gels were immersed in 10 mL DMEM medium and incubated at 37 ºC with 5% CO_2 for 24 h to enable cellular self-alignment, then stabilised using plastic compression.

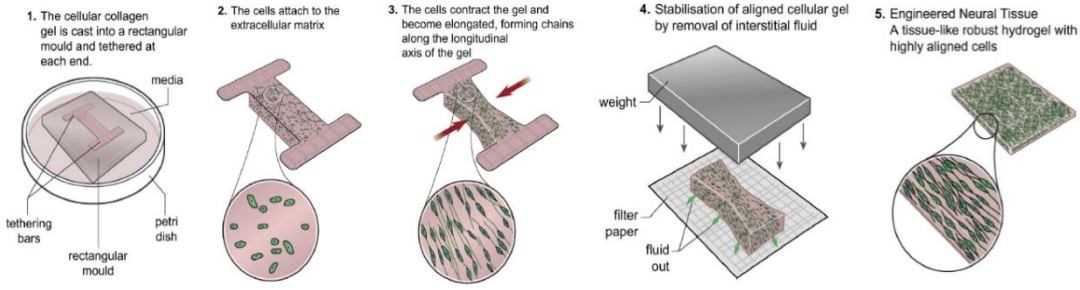

Figure 2.1: Fabrication of 3D EngNT co-cultures *(Georgiou et al., 2013).*

Plastic compression was conducted by transferring the gel to a standard blotting element, which comprised of a layer of stainless-steel support mesh covered by a layer of nylon mesh placed on top of three layers of circular Grade 1 Whatman filter paper *(Phillips and Brown, 2011)*. The gel was then covered with a second layer of nylon mesh and a glass sheet. Compression was then completed by placing a 120 g stainless steel weight on top of the blotting element (stress equivalent to approximately 1.8 kN/m^2) for 1 min (Figure 2.2).

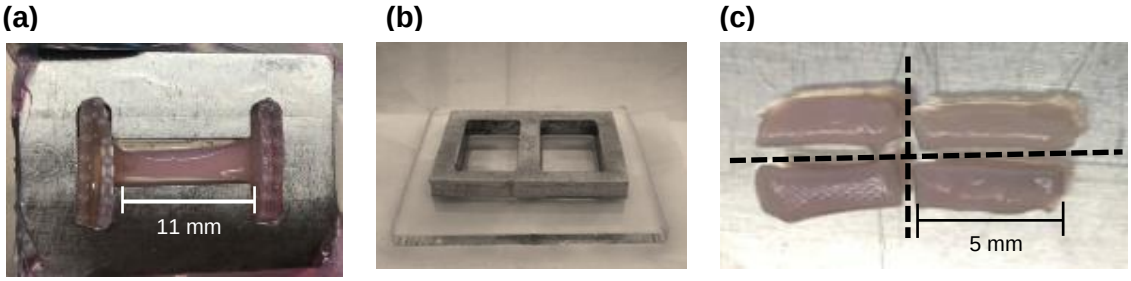

Figure 2.2 EngNT co-culture gel preparation. *Collagen containing SCL4.1/F7 Schwann cell line integrated with tethering mesh at opposite ends of a rectangular mould (a). Plastic compression set up with 120 g weight (b). Stabilised gels cut into 4 segments (c).*

Each stabilised aligned cellular gel was cut into 4 equal segments to obtain a control and three test regions from each gel. Each gel segment was transferred to a separate well in a 24-well plate, then 100,000 PC12 or NG108-15 cells, or DRGs in 50 µL medium (~2 DRG bulbs per gel segment) were seeded on top of each segment for co-cultures. The gels were incubated for 1 h at 37 ºC to allow attachment of neuronal cells to the collagen gel, then 1 mL of culture medium (DMEM; Sigma-Aldrich), supplemented with 10% heat inactivated fetal bovine serum (FBS) (Biosera) and 100 U/mL of Penicillin and 100 µg/mL of Streptomycin, was added to each well. The neurons were seeded onto the top surface of the gels and neurites extended across the horizontal plane following the aligned Schwann gels (Figure 2.3).

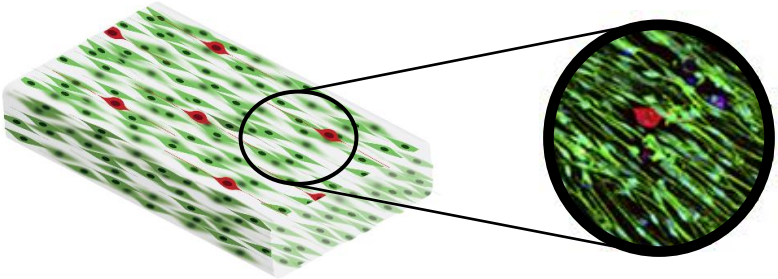

Figure 2.3 Neuronal cells seeded on top of fabricated EngNT. *Adapted from (Georgiou et al., 2013, Rayner et al., 2018)*

2.3 Drug Treatments

Monolayer cell cultures or 3D EngNT co-cultures were subjected to treatments of drugs or GW9662 (Generon), a potent PPAR-γ antagonist *(Lezana et al., 2016)*, for 72 h before being fixed with 4% w/v paraformaldehyde (PFA) in PBS at 4 ºC for subsequent immunostaining and microscopy analysis. Drug stock solutions (10 mM) made up in water or DMSO were added directly to the media in the appropriate volume to provide the required drug concentration (drug concentration details given in chapters).

2.4 Surgical nerve injury models *in vivo*

All surgical procedures were performed in accordance with the UK Animals (Scientific Procedures) Act (1986), the European Communities Council Directives (86/609/EEC) and approved by the UCL Animal Welfare and Ethics Review Board. Adult male Wister rats (250-300 g) (Charles River). The rats were housed randomly into groups in clear plastic cages with soft bedding with free access to food and water. If autotomy occurred additional environmental enhancements (e.g. wood blocks) were provided and additional monitoring was conducted on all animals. The rate of autotomy was low at 3%. The animals were deeply anaesthetised by inhalation of isoflurane, and the left sciatic nerve was exposed at mid-thigh level. This was done by making an incision (~3 cm) parallel to the femur between the knee and hip then separating muscle layers to expose the nerve. Under the microscope (Zeiss CL 1500 ECO) the sciatic nerve was released from the surrounding tissue.

Two injury types were conducted at this stage either a crush (axonotmesis) or a transection (neurotmesis). The crush was achieved by applying a consistent pressure with a pair of sterile TAAB tweezers type 4 closed fully on the same point of the nerve (1.5 cm distal of the femur) for 15 s. This was repeated twice more in the same location with the tweezers positioned perpendicular to the nerve and rotated through 45° between each crush application (Figure 2.4 (b) and (c)). A 10/0 epineurial suture (Ethicon) was used to mark the injury site. The alternative injury model used was a nerve transection with a primary repair. This was conducted by making a cut through the whole sciatic

nerve using sharp scissors (1.5 cm distal of the femur) (Figure 2.4 (a)). The proximal and distal stumps were re-connected using two 10/0 epineurial sutures, one on each side of the sciatic nerve.

Following the injury either an osmotic pump (Alzet, model 1004) (Figure 2.4 (d)) or a biomaterial (Figure 2.4 (e) and (f)) delivery platform pre-loaded with vehicle control or drug treatment was implanted locally parallel to the sciatic nerve or wrapped around the injury site like a cuff. The overlying muscle layers were closed using two 4/0 sutures (Ethicon) and the skin was closed using stainless steel wound clips. The animals were allowed to recover and were maintained for 21 – 28 days.

All animals received the same level of interaction throughout the study. They were handled prior to surgery and repeatedly throughout the study for training and completion of functional testing. All animals were left to settle (~ 5 mins) before conducting any functional tests.

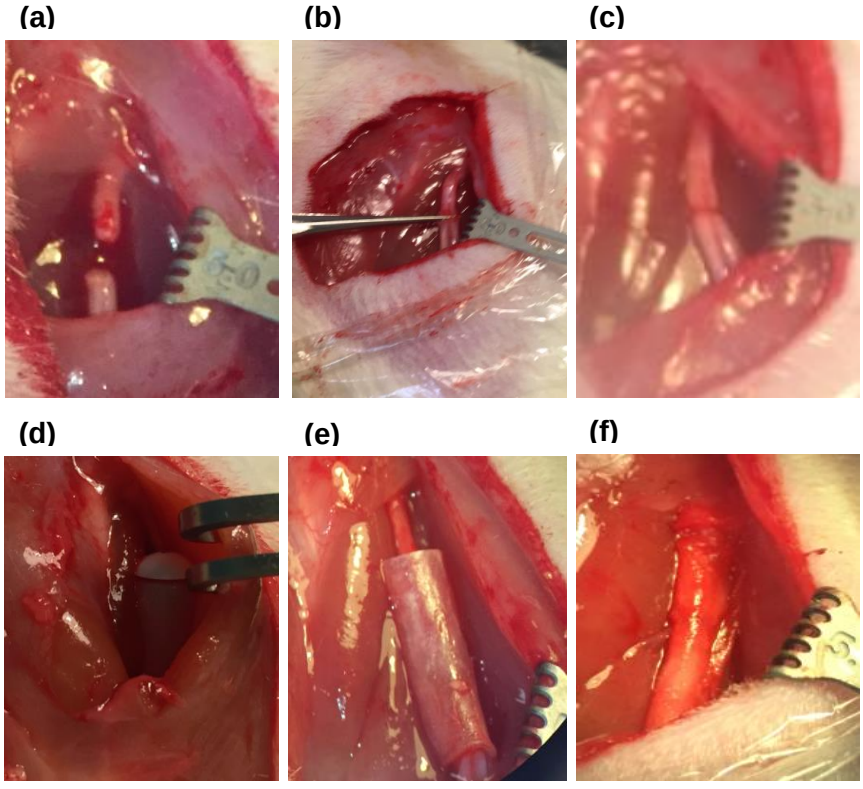

Figure 2.4: In vivo nerve injury models and drug delivery platforms. *Two injury types were conducted; a transection (neurotmesis) (a) or a crush (axonotmesis) (b, c). Drug delivery platforms used included osmotic pumps implanted alongside the sciatic nerve (d), drug loaded into biomaterials including ethylene vinyl acetate (EVA) (e) or electrospun poly(lactic-co-glycolic acid) (PLGA) nanofibers (f) which were both wrapped around the nerve injury site.*

2.5 Nerve tissue harvest

Animals were culled using CO_2 asphyxiation, according to local regulations, and the repaired nerves (~1.5 cm) were excised under an operating microscope and cut as required for analysis. The nerve tissue was either immersion-fixed in 4% (w/v) PFA in PBS at 4 ºC or placed into TRIzol® with subsequent snap freezing in liquid N_2.

2.6 Gastrocnemius muscle harvest and analysis

An incision was made in both hind legs between the hip down to the bottom of the paw. The gastrocnemius muscle was exposed by an incision made in the muscle plane. The gastrocnemius muscle was then separated from the soleus muscle by peeling back the muscle and gently freeing the plane (Figure 2.5). The harvested muscle from each leg was stored in 4% PFA on ice and weighed immediately.

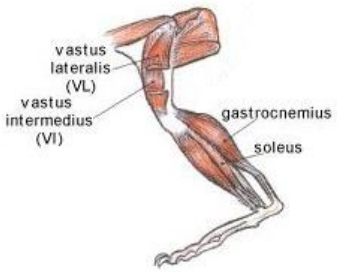

***Figure 2.5: Anatomy of the gastrocnemius muscle in a rat's hind leg**. (Adapted from Bender, 2015).*

2.7 Nerve tissue analysis

2.7.1 Cryo-sectioning

Following fixation the nerve samples were dissected into pieces for multiple analyses (Figure 2.6). The segments for cryo-sectioning were incubated in 30% sucrose overnight and underwent subsequent snap freezing in 1:1 FSC 22 Frozen Section Media (Leica) and 30% sucrose. Transverse sections (10 µm thick) were prepared from the proximal and distal stumps, at defined distances into the nerve stumps from the injury site, using a cryostat (Leica CM1860). The sections were adhered to glass slides (Superfrost™ Plus, Thermo Fisher Scientific) for histological analysis.

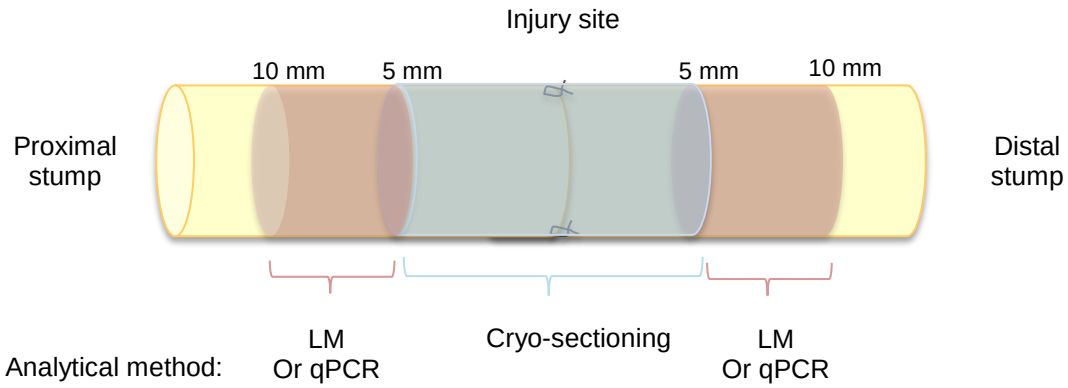

Figure 2.6: Nerve tissue preparation for multiple analytical methods. *(Light microscopy (LM) and quantitative Polymerase Chain Reaction (qPCR)).*

2.7.2 Immunohistochemistry

Nerve sections were washed in immunostaining buffer (PBS together with 0.2% Triton-X (Sigma-Aldrich)), 0.002% sodium azide (Sigma-Aldrich) and 0.25% Bovine Serum Albumin (Sigma-Aldrich) before the addition of serum to block non-specific binding (1/20 in immunostaining buffer) (horse serum (Vector laboratories) or goat serum (Dako) for 45 mins. The blocking serum was removed and sections were incubated with primary antibody diluted in immunostaining buffer overnight at 4 ºC. The sections were washed with immunostaining buffer before addition of the secondary antibody and incubation at room temperature for 45 mins. Sections underwent a final wash with immunostaining buffer before mounting with Vectashield Hardset mounting medium with DAPI (Vector Laboratories). Antibodies and their corresponding dilutions used are listed in table 2.1.

2.7.3 Haematoxylin and Eosin

Nerve sections (10 µm thick) were dried on a heater plate overnight. The sections were stained with 0.1% Mayer's Haematoxylin for 20 mins and washed with water in a Coplin jar. They were then differentiated in 0.3% ammonia and washed before staining with 1% Eosin for 5 seconds. Washes were repeated and the sections were dehydrated through an ethanol series (50%, 70%, 90% and 100%) for 10 seconds each. The sections were immersed in Xylol for 10 seconds before mounting with DPX.

2.7.4 Quantitative polymerase chain reaction (qPCR)

Total RNA was isolated following the protocol provided by Ambion life technologies using TRIzol as the homogenisation reagent. Once the total RNA is extracted this was transcribed into complementary DNA (cDNA) using a high capacity RNA-to-cDNA kit (Applied Biosystems). 10 µL of Master Mix was added to 10 µL of RNA (100-500 ng of RNA per reaction) suspended in nuclease-free water. The cDNA produced was used as the template to complete the qPCR reaction. 5 µL of cDNA was added to 20 µL of Master Mix (including 1.25 µL of the primer of interest) in each well of a 96-well optical plate. The plate was run on a PTC-100 Thermal controller on a cycle at 25 °C for 10 mins increasing to 37 °C for 120 mins followed by a final step at 95 °C for 5 mins. Data analysis was completed manually using the relative ΔΔcT method to determine a fold change in gene expression. Primers of interest are listed in table 2.2.

2.7.5 Light Microscopy

The relevant dissected segments of nerve samples were transferred to 3% glutaraldehyde (Agar Scientific) in 0.1 M cacodylate buffer. The samples were then post-fixed in 1% (w/v) osmium tetroxide in PBS, dehydrated using a graded series of ethanol incubations, flat-embedded in TAAB embedding resin and polymerized at 60 °C for 48 h. Semi-thin sections of 0.5 µm were cut using a diamond knife on an Ultracut E microtome (Leica) then dried onto microscope slides. They were then stained with 1% (w/v) toluidine blue with added 5% (w/v) sodium borate and imaged using light microscopy with oil immersion using a x100 lens. Axon and fibre diameter were measured using ImageJ software from three predetermined fields through the middle of sections where the tissue density was greatest. These values were then used to calculate myelin thickness and G-ratios. G-ratio assesses axonal myelination by calculating the ratio of the inner axonal diameter to the total outer dimeter. Coding was used to blind the operator from the drug treatments.

2.8 Immunocytochemistry

Following fixation with 4% (w/v) PFA in PBS monolayer cells or gels were washed 3 times with PBS and permeabilised using 0.5% (v/v) Triton-X-100 (Sigma-Aldrich) in PBS. Washes were repeated before blocking (blocking serum 1/20 in PBS) (Vector Laboratories). Gels were washed before the addition of primary antibody of interest diluted in PBS. The antibody and gel/cells were incubated overnight at 4 °C. Washes were repeated before adding the corresponding secondary antibody (Dylight anti-mouse IgG 488 1:400, (Vector Laboratories) diluted in PBS). The secondary antibody was washed and the sample was stored at 4 ºC before viewing. Omission of primary or secondary antibody was routinely used as a control. When required Hoechst was used to stain nuclei by incubating the gel or cells on coverslips for 15 mins and then washed thrice with PBS.

2.9 Image analysis and quantification

Fluorescence microscopy (Zeiss Axiolab A1, Axiocam Cm1) was used to capture images of neurites from five pre-determined fields of each gel or coverslip using a x20 lens. The neurite number in the determined fields depended on the cell type and model used (~1-12 neurites). Briefly, the positions of the pre-determined fields on coverslips were equally spaced (625 µm apart) in a line across the diameter at the centre of the coverslip, for the gels the same method was used but the line of fields was along the edge of the construct where alignment was greatest *(East et al., 2010)*. The length of each neurite in each field was measured using ImageJ. Following stabilisation the gel acquired a thickness of 100 µm and the neurons extended predominantly in a single horizontal plane along the top surface, following the aligned Schwann cells *(Phillips, 2014)*. This allowed analysis of neurite growth to be compared in the monolayer and 3D co-cultures.

Tile scans were used to capture high-magnification (x20) micrographs from the entire nerve cross-section using a Zeiss LSM 710 confocal microscope and images were analysed using Volocity™ 6.4 (PerkinElmer) running automated image analysis protocols to determine the number of neurofilament-immunoreactive neurites in each

transverse nerve section. This was also used to determine the diameter of each axon. Blood vessel, macrophage and Schwann cell analysis was conducted from entire nerve sections using fluorescence microscopy (Zeiss Axiolab A1, Axiocam Cm1) and blood vessel diameter was measured using ImageJ software.

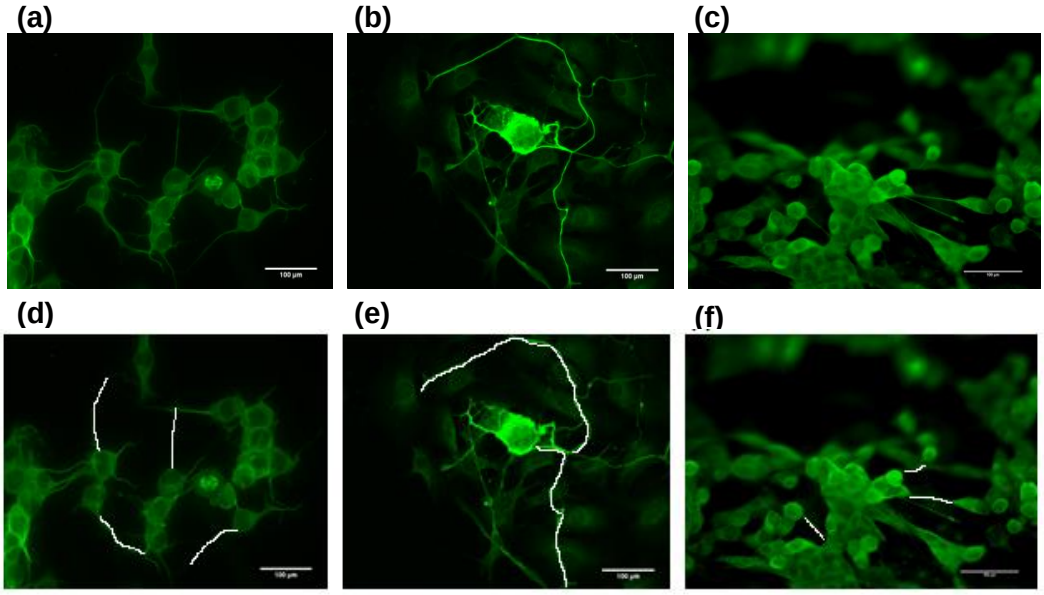

Figure 2.7: Neurite identification and measurement in cell cultures. *Neurons were detected by immunostaining with β-III tubulin (green) and neurite length was measured using ImageJ, examples shown on the images with traces of the neurites in white. Monolayer NG108-15s (a, d), monolayer DRGs (b, e) and PC12s when in the EngNT co-culture (c, f), scale bar = 100 µm.*

2.10 Functional outcomes *in vivo*

2.10.1 Electrophysiology

After 21 – 28 days animals were anaesthetised using isoflurane and nerve function was assessed by electrophysiology (Sapphire 4ME system) by comparing the repaired nerve to the contralateral undamaged nerve in each animal. A 21 day end point was used for the transection injury as this is the end of the inflammatory phase following injury and 28 days were used for the crush model as this is a sufficient time period to observe functional recovery. Electrodes (Natus) were attached to the animal; a grounding electrode was placed onto the tail of the animal and a reference electrode was placed above the hip bone. A stimulating electrode (Neurosign Bipolar Probe 2 × 100 mm × 0.75 mm electrode) was placed against the proximal nerve 2 mm above the injury site and a monopolar recording needle (Ambu® Neuroline concentric) was placed into the gastrocnemius muscle. The distance between the stimulating and

recording electrodes was standardised. The nerve was stimulated using a bipolar stimulation constant voltage configuration and the muscle response recorded. The stimulation threshold was determined by increasing the stimulus amplitude in 0.1 V steps (200 µs pulse), until both a reproducible, stimulus-correlated compound muscle action potential (CMAP) was recorded and a significant twitch of the animal's hind paw could be seen. The CMAP was used to determine the amplitude (mV) which was measured from baseline to the greatest peak and the latency which was measured from the time of stimulus to the first deviation from the baseline. CMAPs were conducted in triplicate for both the injured nerve and contralateral control nerve in each animal.

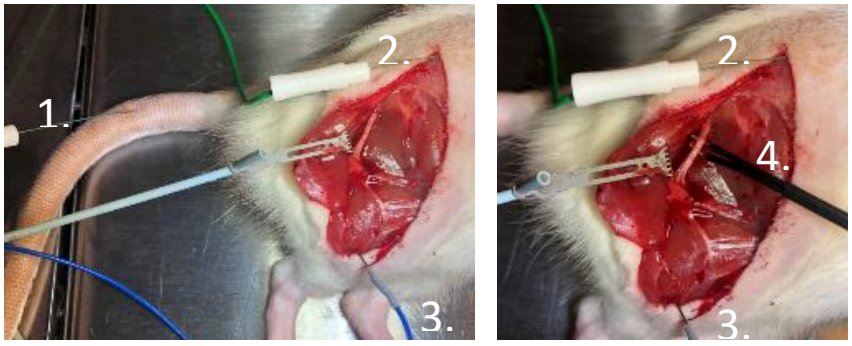

Figure 2.8: Placement of electrodes for electrophysiological assessment. *1- Grounding electrode, 2- Reference electrode, 3- Recording electrode, 4-Stimulating electrode.*

2.10.2 Von Frey

The animals were placed on a grid and von Frey filaments made of nylon, which all have the same length but vary in diameter to provide a range of forces (0.008 g - 300 g), were applied through the underside of the grid to stimulate the centre of the animal's hind paws. A response is measured by the retraction of the animal's paw in response to the filament stimulus. The threshold response was recorded by decreasing the stimulus until no response was detected.

2.10.3 Static sciatic index (SSI)

Functional recovery was analysed using the static sciatic index (SSI). The animal's hind paws were imaged and the toe spread factor (TSF), between the 1st and 5th toe, and the intermediary toe spread factor (ITSF), between the 2nd and 4th toe, were measured and equation 2.1 was used to calculate SSI *(Bervar, 2000)*.

Equation 2.1: SSI = (108.44 x TSF) + (31.85 x ITSF) – 5.49

$TSF = TS_{control} - TS_{injury}$, $ITSF = ITS_{control} - ITS_{injury}$

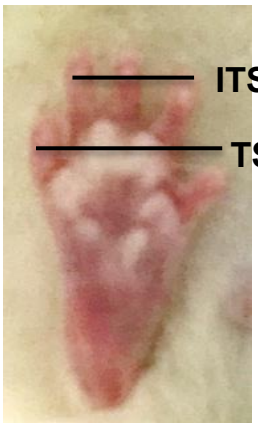

Figure 2.9: Toe spread measurements to calculate static sciatic index.

2.11 Drug loading into biomaterials

2.11.1 Ethylene vinyl acetate (EVA)

Drug embedded ethylene vinyl acetate (EVA) membranes were manufactured by combining EVA co-polymer beads (Sigma-Aldrich) with ibuprofen (Sigma-Aldrich) in chloroform (Sigma-Aldrich). Firstly, ibuprofen powder was dissolved in 20 mL chloroform and mixed homogenously. Different quantities of ibuprofen, 200 mg (1% w/v) 400 mg (2% w/v) and 800 mg (4% w/v) were used to test drug encapsulation. Once the drug had fully dispersed, 2 g of EVA beads were added into to the solution and continuously stirred overnight at room temperature. The obtained homogenous solution was added to a rectangular glass mould (83 mm x 63 mm x 2 mm) and dried at room temperature until all the solvent had evaporated (~24 hrs). The membrane was then cut into smaller flat sheets (5 mm x 5 mm x 0.5 mm, 10 mm x 10 mm x 0.5 mm and 7 mm x 12 mm x 0.5 mm) for characterisation and implantation studies. EVA sheets with no embedded drug were manufactured using the same procedure and used as control samples.

2.11.2 EVA constructs

EVA polymer membranes were manufactured into tubular-shaped constructs for implantation *in vivo*. This was done by wrapping the flat EVA sheet (7 mm x 12 mm x 0.5 mm) around a 19G needle and fusing the edge together with a few drops of chloroform.

The tubes were dried at room temperature and removed from the needle furnishing a tube with dimensions 5 mm x 12 mm and 1.5 mm inner diameter.

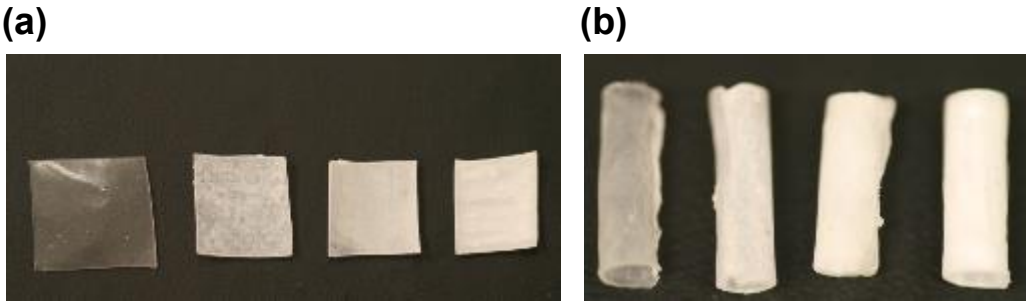

Figure 2.10: Ibuprofen-loaded ethylene vinyl acetate*. No drug loading, 1%, 2% and 4% ibuprofen loading into flat sheet membranes (a) and manufactured tube constructs (b).*

2.11.3 Polycaprolactone (PCL)

The polycaprolactone (PCL) (Sigma-Aldrich) polymer membranes were manufactured by dissolving 100 mg ibuprofen into 5 mL chloroform. Once the drug had fully dissolved the PCL beads were added to the solution and stirred overnight at room temperature. The homogenous polymer solution was poured into a circular Teflon mould (Ø 77 mm) and dried for 2-3 h at room temperature to allow the solvent to evaporate. Once the solvent was removed the membrane was cut into smaller sheets (7 mm x 12 mm x 0.4 mm) for characterisation. PCL membranes without drug were prepared using the same procedure and used as control samples.

2.11.4 Collagen

Collagen gels were manufactured as previously described in section 2.2 but the cell suspension was substituted with the drug solution. 20 mg of ibuprofen was added to 1 mL gel solution to produce a membrane with 2% (w/v). Gels were left to set at 37 °C for 24 hrs and then fully stabilised. The stabilisation method resulted in the loss of drug as water was removed (data not shown), so this method was discontinued.

2.11.5 Fibrin

Tisseel Lyo two-component fibrin sealant (Baxter) was used to prepare drug-loaded fibrin gels. All components were warmed to 37 °C before use. To prepare the first component

the drug was added to the lyophilized sealer protein (fibrinogen). This was then added to the aprotinin solution ensuring complete reconstitution. The second component required the preparation of lyophilized human thrombin (4 units / mL) stock solution in calcium chloride. The thrombin was transferred to a plastic mould to act as the base layer. The sealer protein solution was placed on top. 20 mg of ibuprofen was added to 1 mL fibrin solution to produce a membrane with 2% (w/v). The drug prevented the fibrin from setting correctly so this biomaterial was discarded from further analysis.

2.11.6 Poly (lactic-co-glycolic acid) (PLGA)

Poly (lactic-co-glycolic acid) (PLGA) (Corbion Purac with molecular weight (MW) of 96,000) nanofibers were fabricated by electrospinning using a Spraybase® electrospinning instrument (Spraybase®). The PLGA 17.5% w/v was dissolved in dichloromethane (DCM) (Sigma-Aldrich) and stirred gently for 45 min. Then 2.5% w/v ibuprofen or sulindac sulfide was added and stirred for another 45 min to achieve a drug to polymer ratio of 1:7, or 1:17 respectively. The ratios were selected based on complete encapsulation of the drug within the polymer. The solution was loaded into a 10 mL syringe with a diameter of 14.43 mm to be ejected through a 0.7mm needle. The flow rate and voltage used to stabilize the jet were 1 mL/h and 10-11 kV, respectively. The fibres were collected in aluminium foil at a distance of 12.5 cm. Similar parameters were used to prepare blank fibres with no drug embedded. The drug encapsulation efficiency and drug loading was determined by dissolving the fibres in 20 ml of acetonitrile for 4 h. The resulting solutions were analysed using UV-Vis spectroscopy. The PLGA nanofibre manufacture and characterisation was kindly completed by Prof Duncan Craig's lab, UCL School of Pharmacy.

2.11.7 Mesoporous Silica Nanoparticles

100 mg of mesoporous silica nanoparticles (MSN) (kindly donated by Ahmed El-Fiqi, UCL Eastman Dental Institute) were dispersed in 10 mL of an ibuprofen stock solution (2% w/v) prepared in distilled water and incubated for 6 hours at 37 °C to allow drug loading. The resulting solution was centrifuged at 400 g for 5 minutes to obtain a pellet

of MSN. They were then left to dry at 37 °C overnight. During this time the MSN aggregated and formed clumps so the pellet was triturated to re-obtain a powder. Drug loading into the MSN was determined by measuring the quantity of ibuprofen remaining in the stock solution and using UV-Vis spectrophotometry (Unicam UV500) and a standard curve (Figure 2.11)

2.11.8 MSN loaded into PCL

A PCL membrane with ibuprofen-loaded MSN was made by dispersing the MSN in 5 mL chloroform (10% or 20% of ibuprofen-loaded MSN, which corresponded to 50 mg and 100 mg of MSN, respectively). 500 mg of PCL beads were added to this solution and the mixture was stirred overnight at room temperature. The MSN loaded PCL was manufactured using the same method in 2.11.3. A PCL membrane with empty MSN was prepared in a similar manner.

2.12 Material characterisation

2.12.1 Scanning Electron Microscopy (SEM) and Transmission Electron Microscopy (TEM)

The morphology and particle size of the polymeric samples were characterised using SEM (Philips XL30 FEG or FEI Quanta 200F) at 5 kV. Samples were mounted onto metal specimen stubs, using double-sided adhesive tape, vacuum coated with a platinum film and then viewed and imaged. The particle size and porous structure of MSN was characterised using TEM (Philips CM12) operated at 80 kV.

2.12.2 Fourier Transform Infrared Spectroscopy (FTIR)

FTIR spectra were acquired using System 2000 FT-IR (Perkin Elmer) and the samples were scanned over the range of 4000-500 cm^{-1}. Each spectrum acquired was the mean of four consecutive scans of a single sample.

2.13 Drug release

For all materials the drug release was determined by incubating the material in 1 mL distilled water at 37 °C. The 1 mL solution was collected at fixed time points (1 h, 2 h, 3

h, 4 h and then every 24 h) and replaced with 1 mL of fresh distilled water. The solution collected was analysed with a UV-Vis spectrophotometer (Unicam UV500) at a wavelength of 263 nm (Sigma-Aldrich). The concentrations of ibuprofen and sulindac sulfide were determined using a standard curve with linear range (Figure 2.11). The absolute release of drug at each time point was calculated using the standard curve. The cumulative release of drug (CR_t) was determined using the equation (2.2), where AR_t is the amount of drug released at the sampling time t and CR_{t-1} is the total amount of drug released in all previous sampling times.

Equation 2.2: $CR_t = AR_t + CR_{t-1}$

The mass of drug contained in each sample was estimated as a proportion from the total mass of drug in the initial membrane. Both the initial membrane and samples were weighed and correlated to the initial drug loading.

Equation 2.3: Mass of drug in sample = $\frac{\text{Initial mass of drug x weight of sample}}{\text{Weight of initial membrane}}$

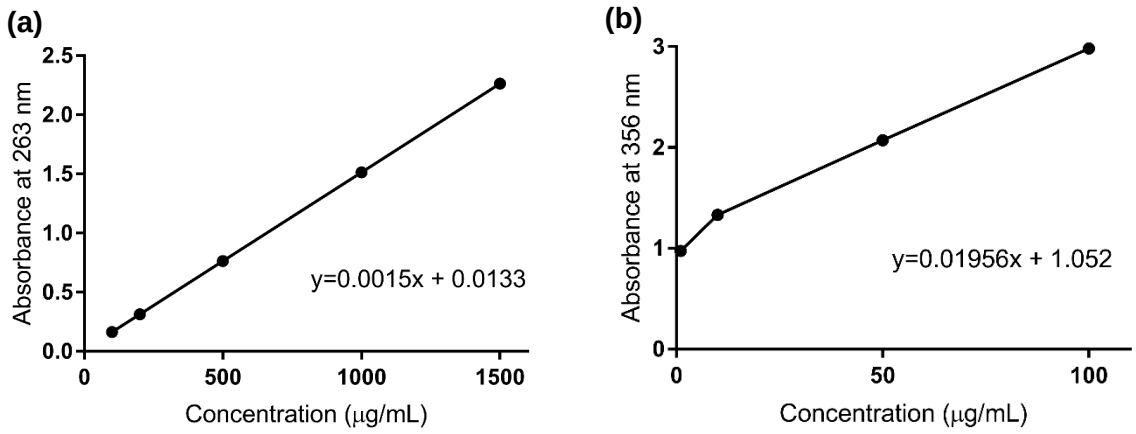

Figure 2.11: Standard curves for UV-Vis spectrophotometry analysis*. Ibuprofen in water (a) and sulindac sulfide in DMSO (b).*

2.14 Residual drug test

At the end of the *in vivo* release experiments the residual drug content of the conduits was measured. Briefly, the conduits were dissolved in 5 mL of chloroform and once the polymer had completely dissolved it was separated from the drug by adding 3 mL of distilled water. The solution was incubated at room temperature for 24 h in order to allow

the phases to separate. The amount of ibuprofen was determined using a UV-Vis spectrophotometer at a wavelength of 263 nm, as previously described.

2.15 Statistical analysis

A normality test was conducted on all data to determine appropriate statistical tests, and analysis of variance (ANOVA) or t-tests were performed where data followed a normal distribution. For all tests a one-way ANOVA was followed the appropriate post hoc test. For all tests, *p<0.05, **p<0.01, ***p<0.001 and ****p<0.0001 were considered to be significant. For data that didn't follow normal distribution, non-parametric tests were conducted.

2.16 Compound synthesis and characterisation

The sulindac sulfide derivative, (E)-2-(5-Fluoro-1-(napththalen-1-ylmethylene)-1H-inden-3-yl)-ethanoic acid (compound 3) was synthesised using scheme 1 *(Felts et al., 2007, Felts et al., 2008).* Characterisation was conducted at each stage of the synthetic route before proceeding to the next step to ensure the correct compound had been synthesised. This included standard analytical methods in chemical synthesis such as nuclear magnetic resonance (NMR) and mass spectroscopy

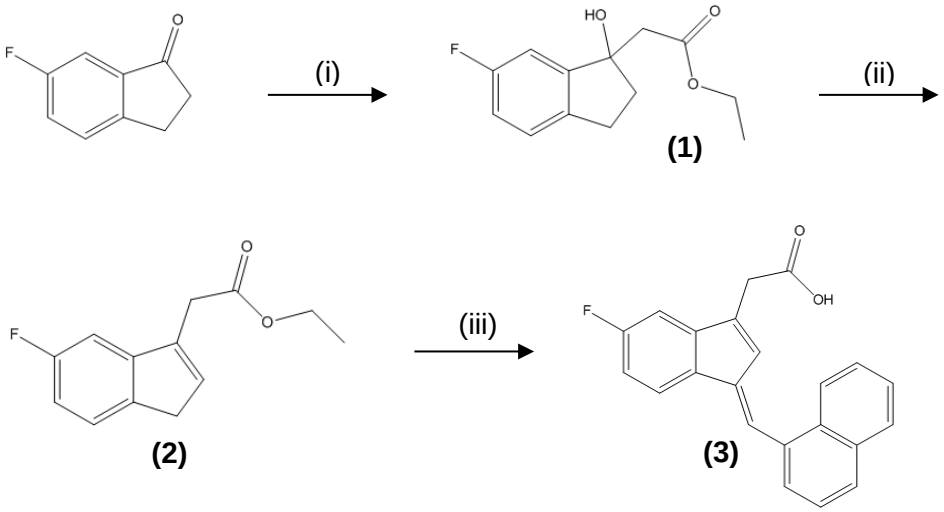

Scheme 1: Synthetic route to compound (3). *Reagents and conditions: (i) Ethyl bromoacetate, activated zinc, Benzene/Ether, reflux 16h; (ii) TsOH.H_2O, $CaCl_2$, Toluene, reflux 16h; (iii) 1-naphthylaldehyde, 1N NaOH, MeOH, reflux, 16h.*

All solvents were analytical or HPLC grade and used as supplied without further purification.

2.16.1 Nuclear magnetic resonance (NMR) spectroscopy

^{1}H spectra were obtained from a Bruker Avance 400 MHz (broadband probe) NMR spectrometer or a Bruker Avance 500 MHz (cryo-probe) NMR spectrometer. Deuterated solvents were used to dissolve the solvents (most commonly $CDCl_3$-d^6). The chemical shifts (δ) are reported in parts per million (ppm) and referenced against $CDCl_3$-d^6. Results were analysed using Bruker Topspin 3.2 and are shown as: chemical shift (integration, multiplicity, coupling constant, assignment). The following abbreviations were used to indicate the signal multiplicity: s (singlet), d (doublet), t (triplet), m (multiplet), dd (doublet of doublet), ddd (doublet of doublet of doublet), br s (broad singlet), br d (broad doublet), br m (broad multiplet). Coupling constants (J) are quoted in Hz and recorded to the nearest 0.1 Hz. Assignments were confirmed using 2D techniques such as COSY, HMQC and HSQC.

2.16.2 Mass spectrometry

Mass spectra were measured on Shimadzu LCMS-2020 which operated in positive or negative mode. Samples were dissolved in acetonitrile for analysis.

2.16.3 Column chromatography

All column chromatography was performed using Merck silica gel in a glass column. Elution was performed with specified analytical or HPLC grade solvents under a positive pressure of compressed air.

2.16.4 Thin layer chromatography

Thin layer chromatography (TLC) was performed using Merck silica gel 60 F254 aluminium-supported plates. The samples were visualised using UV light (254 nm).

2.16.5 High performance liquid chromatography (HPLC)

HPLC was performed using an Agilent technologies 1200 series HPLC system using a Waters XSelect® CSH C18 Column 50 x 6 mm (particle size: 2.5 µm) at a flow rate of 1 mL/min. The eluent system consisted of H_20 + 0.1% formic acid and acetonitrile + 0.1% formic acid. The initial composition was 5% acetonitrile with 95% H_2O and the final

composition was 95% acetonitrile and 5% H_2O over 20 min, held at 95% acetonitrile and returned to 5% over 1 min.

2.16.6 Rotary evaporator

All solvents were removed *in vacuo* using Buchi rotary evaporators under reduced pressure.

2.17 Synthesis of (6-Fluoro-1-hydroxy-indan-1-yl)-acetic acid ethyl ester (1)

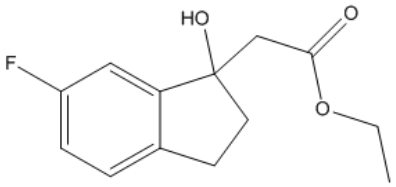

A solution of 5-Fluoroindan-1-one (Apollo Scientific) (2.06 g, 13.7 mmol) and ethyl bromoacetate (Sigma-Aldrich) (3.44 g, 20.6 mmol, 1.5 eq) in 10 mL benzene was added to a solution of activated zinc (Sigma–Aldrich) (3.77 g, 57.7 mmol, 4 eq) in 21 mL benzene and 10 mL ether over a 5 min period. A few crystals of iodine (Sigma–Aldrich) were added to initiate the reaction. The mixture was stirred at reflux at 80 °C and at 3 h intervals 2 batches of activated zinc (1.8 g, 27.5 mmol, 2 eq) and ethyl bromoacetate (1.8 g, 10.8 mmol) were added. The mixture was then held at reflux overnight (~16 h), after which time the solution was cooled to room temperature and 5 mL of ethanol and 23 mL acetic acid was added. The organic layer was separated by pouring this solution into 100 mL of a 1:1 aqueous acetic acid. The aqueous phase was extracted with ether. The organic phase was then washed repeatedly with water, sodium bicarbonate, water. The solution was then dried with magnesium sulphate for 15 mins before being filtered and concentrated *in vacuo* furnishing the crude product as an orange oil (2.06 g).

2.18 Synthesis of (6-Fluoro-3*H*-inden-1-yl)-acetic acid ethyl ester (2)

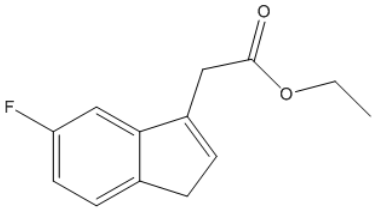

The crude product **(1)** (1.869 g, 7.84 mmol) was added to p-Toluenesulfonic acid monohydrate (Sigma-Aldrich) (2.986 g, 15.7 mmol, 2 eq) and calcium chloride (Sigma-Aldrich) (2.175g, 19.6 mmol, 2.5 eq) in 34 mL Toluene. The solution was stirred at reflux overnight (~16 h) then filtered and washed with benzene. The organic phase was separated and washed repeatedly with water, sodium bicarbonate, water. The solution was then dried with magnesium sulphate for 15 mins before being filtered and concentrated *in vacuo.* The product was then purified by silica gel column chromatography (13:1 hexane: ethyl acetate) furnishing a yellow oil (240 mg).

2.19 Synthesis of (E)-2-(5-Fluoro-1-(naphthalene-1-ylmethylene)-1H-inden-3-yl)-ethanoic acid (3)

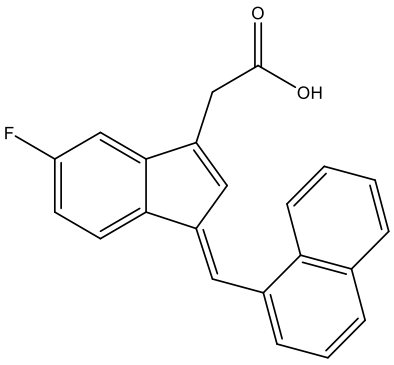

(6-Fluoro-3*H*-inden-1-yl)-acetic acid ethyl ester **(2)** (100mg, 0.154 mmol) and 1-naphthaldehyde (Sigma-Aldrich) (70.9 mg, 0.454 mmol, 1.2eq) were added in 0.22 mL 1 N sodium hydroxide and 0.44 mL ethanol and stirred at reflux for 16 h. The solution was cooled to room temperature and neutralised with 15% hydrochloric acid. The organic phase was separated and washed repeatedly with water, sodium bicarbonate, water. The solution was then dried with magnesium sulphate for 15 mins before being filtered and concentrated *in vacuo.* The compound was then extracted and purified using HPLC furnishing a yellow oil (10 mg).

Antibodies:

Antibody	Target	Dilution	Species	Source	Secondary
βIII-Tubulin	Neurons	1/400	Mouse	Sigma-Aldrich T8660	Anti-mouse 488
S100	Schwann cells	1/400	Rabbit	Dako Z0311	Anti-rabbit 549
p75 (NTR)	Schwann cells		Mouse	Merck (Millipore) MAB365	Anti-mouse 549
Neurofilament-H	Axons	1/1000	Mouse	Eurogentec SMI-35-050	Anti-mouse 549
CD68 (ED1)	Macrophages	1/100	Mouse	Millipore MAB1435	Anti-mouse 488
Arginase-1	M2 Macrophages	1/200	Goat	Santa Cruz Sc-18354	Anti-goat 594
RECA-1	Endothelial cells	1/100	Mouse	Bio-Rad MCA970R	Anti-mouse 488
c-Jun	Repair Schwann cells	1/300	Rabbit	Cell Signalling Technology 9165S	Anti-mouse 488

Table 2.1: List of antibodies used for histological analysis.

qPCR primers:

Primer	Target	Source	Forward primer 5'-3'	Reverse primer 5'-3'
Ankrd27	Housekeeping gene	Thermofisher Scientific	*CCCAGGATCCGAGAGGTGCTGTC*	*CAGAGCCATATGGACTTCAGGGGG*
RICTOR	Housekeeping gene	Thermofisher Scientific	*GAGGTGGAGAGGACACAAGCCC*	*GGCCACAGAACTCGGAAACAAGG*
GFAP	Schwann cells	Thermofisher Scientific	*GTACCAGGACCTGCTCAAT*	*CAACTATCCTGCTTCTGCTC*
Olig 1	Myelinating Schwann cells	Thermofisher Scientific	*ACCAAGTACCTGTCTCTAGCG*	*GGGACCAGATGCGGGAAC*
Krox 20 (EGR2)	Myelinating Schwann cells	Thermofisher Scientific	*GCGATTTAGCAACAACCC*	*CAATTTCTGGCAGTTCTCC*
p75^{NTR}	Repair Schwann cells	Thermofisher Scientific	*GAGCCGTGCAAGCCGTGCAAC*	*CTCAGGCTCCTGGGTGCTGGG*

Table 2.2: List of primers used for qPCR analysis

Chapter 3: Development and application of *in vitro* models to screen drugs for PNI.

3.1 Introduction

The rate of attrition in drug discovery is high with 90% of compounds entering clinical trials failing to gain regulatory approval and only 12% of compounds tested in humans making it onto the market *(Chuang-Stein et al., 2004, Huang et al., 2011, Langley et al., 2017)*. Pre-clinical studies determining the efficacy and safety of compounds are required by regulatory bodies, for example the UK Medicines and Healthcare Products Regulatory Agency (MHRA) or the US Food and Drug Administration (FDA) before any clinical trial application *(FDA, 2015, Steinmetz and Spack, 2009)*. One reason drug therapies fail to reach the market is the lack of effective pre-clinical models, that mimic the pathophysiology and disease states in humans, to test potential compounds *(Huang et al., 2011)*. In addition, gaps in the understanding of cellular and molecular mechanisms can make it challenging to correlate the relationship between therapeutic targets and pathophysiological conditions, making it difficult to predict therapeutic outcomes *(Huang et al., 2011)*.

The pre-clinical stages of the drug discovery pipeline can be divided into 2 parts 1.) *In vitro* cell culture based studies and 2.) Animal studies. These are vital steps and provide raw data that are required to inform future clinical trials *(FDA, 2015, Steinmetz and Spack, 2009)*. Robust and reliable models are required to ensure safety and efficacy before new drugs reach human subjects. In nerve repair as in other fields, numerous models have been established to test the efficacy of compounds pre-clinically, and increasingly a range of *in vitro* approaches are used prior to animal testing. However, most tend to employ monolayer cell cultures which have limitations that may reduce their usefulness.

3.1.1 Monolayer cell cultures

Monolayer cell cultures do have benefits in providing high throughput screening tools to study drug efficacy and toxicity, disease states and other biological responses through measuring cell responses to environmental factors *(Hopkins et al., 2015)*. However, despite advantages in providing simplistic models and low costs, monolayer cell culture models often fail to represent the complex 3D characteristics of living tissues *(Hopkins et al., 2015, Ko and Frampton, 2016)*. This is due to the cells being forced to adhere to a flat, stiff plastic or glass surface during monolayer culturing meaning they will respond to spatial and mechanical cues that are not present in their natural environment, which can impact their behaviour, function, growth and morphology considerably. These changes can significantly skew the results due to the complexities of the nervous system *(Ko and Frampton, 2016).*

In addition, monolayer cultures commonly incorporate single cell types and do not consider the synergistic effect of the other cells present in nerve tissue, resulting in an unrealistic representation of the physiological environment *(Ahmed et al., 2006, Ko and Frampton, 2016, Kofron et al., 2009, Kraus et al., 2015).* This is a particularly important concept in PNI due to the success of regeneration being highly dependent upon the synergistic functions of key cell mediators *(Chan et al., 2014)*. Armstrong *et al.* (2007) demonstrated that neurons in a monolayer co-culture with Schwann cells extended neurites in response to the secretion of neurotrophic factors but also through direct cell-to-cell contact between the two cell types. Therefore, this 3D cell-to-cell interaction of Schwann cells providing essential support to the neurons is a key feature that can be recreated in order to build more representative *in vitro* models.

3.1.2 Cell origin

The 3D tissue environment of the nervous system is complex and has a substantial impact on cellular functions *(Geuna et al., 2016)*. It is important to take care when selecting cells for use within *in vitro* PNI models. The use of cell lines in pre-clinical models have great advantages as they provide an abundant source of cells which are

originally derived from animal or human tissue. However, their biological properties can still differ greatly from normal tissue conditions, as the cells have usually been derived from neoplastic tissue or undergone immortalisation through genetic manipulation. Therefore, they can't fully predict what we expect to see *in vivo (Geuna et al., 2016).* Within these limitations, cell lines can be used but should be done so with selective criteria based on experience and their assessed reliability.

Primary cells can act to overcome some of these limitations as they often reproduce *in vivo* events more closely than cell lines, however, they have an ethical disadvantage as they rely on animals as a regular source of cells. Furthermore, a harvest of primary cell cultures will destroy the natural 3D tissue network and results in variable cultures which comprise of an impure mixture of neurons, glial cells, fibroblasts, endothelial cells etc. The changes made to the nerve environment will have a profound effect on the function of the harvested cells *(Geuna et al., 2016)*. Moreover, harvesting neurons or Schwann cells not only damages the permissible environment, but also results in the loss of contact between the two cell types. This reproduces a PNI event meaning that it is impossible to set up cultures with uninjured neurons *(Geuna et al., 2016)*.

Primary Schwann cells can be successfully harvested from animals and humans which retain features similar to those seen *in vivo (Haastert-Talini, 2012, Tao, 2013)*. However, their use is limited due to their short life span with resulting morphological changes and senescence, and fibroblast contaminated cultures. When studying PNI, one of the most important characteristics of Schwann cells is their proliferation *(Geuna et al., 2016)*. As this is a simple feature to model, most assays use immortalised cell lines obtained from tumours or genetically modified glial precursors such as RT4-D6P2T, JS-1, RSC96, R3 and S16Y cells *(Badache and De Vries, 1998, Imada and Sueoka, 1978, Kimura et al., 1990, Ridley et al., 1988, Toda et al., 1994)*. Immortalised cell lines are homogenous, standardised cells with identical genetics and so are well characterised. This aids the collection of consistent and reproducible results *(Carter and Shieh, 2015).* However, their main disadvantage is that they cannot be considered normal as they express unique gene patterns and so may not have the same properties and functions of normal cells.

They also divide indefinitely and the characteristics change over several passages *(Carter and Shieh, 2015)*. Despite this, immortalised cell lines of neuronal origin have been used to investigate processes that occur during neuronal differentiation such as axon guidance and growth *(Carter and Shieh, 2015)*.

Another alternative source of cells that could be used for *in vitro* models for PNI are stem cells. In particular, induced pluripotent stem cells (iPSCs), which can be generated directly from adult cells and give rise to every type of cell found in the body. Since their discovery in 2006, there has been a growing interest in the use of iPSCs as a cell-based therapy for peripheral nerve regeneration *(Xu et al., 2011)*. However, they have the potential to be used in research for peripheral nerve regeneration as they can be differentiated into both neurons *(Chambers et al., 2012)* and Schwann cells *(Liu et al., 2014).* Once the differentiation technology has been optimised, the iPSCs can be utilised as a primary cell culture for both monolayer and co-culture *in vitro* models to screen therapies for PNI *(Geuna et al., 2016)*.

3.1.2.1 Cell sources for this study

In PNI neuronal survival, differentiation, elongation, orientation and branching are the characteristics of interest in order to gain an understanding of what happens to the neurons following injury *(Geuna et al., 2016)*. Dorsal root ganglia (DRG) neurons located in the intervertebral foramina of the spinal column can be used to test the behaviour of sensory and motor neurons *(de Luca et al., 2015)*. As the neurons can be isolated, factors that modulate neuronal behaviour can be studied more closely. Furthermore, they mimic the nerve environment at the injury site and provide *in vitro* models to study nerve regeneration and myelination *(de Luca et al., 2015).* DRGs can also be co-cultured with the Schwann cells, however, these cells will continue to proliferate and this makes it difficult to discriminate neuronal responses to any given stimulus *(Geuna et al., 2016)*.

Primary neuron cultures have a short life span due to the absence of a permissible environment containing supporting glial cells, therefore, for simpler assays such as drug screening or biomaterial compatibility studies, cell lines are used. One cell line is that is

commonly used is PC12 cells, which are derived from rat phaeochromocytoma cells of sympathoadrenal origin. These cells have been used successfully to assess the pro-regenerative effect of compounds and biomaterials on neurite growth *(Greene and Tischler, 1976, Morano et al., 2014, Pittier et al., 2005).* Another cell line that has been used to study peripheral nerve regeneration is NG108-15 cells, a rat neuroblastoma–glioma hybrid cell line. NG108-15 cells were used in a 3D spheroidal co-culture with Schwann cells to study neurite development *(Kraus et al., 2015)*.

The neurons discussed will be studied in isolation but also in co-cultures with Schwann cells. The rat Schwann cell line SCL4.1/F7 was the first clonally derived immortal Schwann cell line and has established properties up to passage 40. The cell line was found to retain two characteristics seen in the parent Schwann cells; autocrine growth inhibition and calcium-dependent cell-substratum adhesion *(Haynes et al., 1994)*. SCL4.1/F7 cells provide a suitable tool to investigate the biochemical and cellular basis of Schwann cell-neuron interactions, myelin stabilisation and Schwann cell growth autoregulation *(Haynes et al., 1994)*. In conclusion, it is evident that the selection of the cell source for use in *in vitro* models is highly important and the decision should be based upon the specific research question of interest. Furthermore, combining neurons and glia in the co-cultures recreates key features of PNI repair.

3.1.3 3D models of peripheral nerve injury (PNI)

In the PNI field, monolayer culture and animal models have insurmountable limitations and, therefore, more 3D *in vitro* models are being developed as an alternative, for example explant cultures, self-assembling aggregate cultures and scaffold-based cell cultures *(Ko and Frampton, 2016)*. Various 3D culture model systems have been adopted by the biomaterials and tissue engineering communities to study the influence of extracellular matrices in neurite formation and growth, but these tend not to have been developed specifically for compound screening to identify new drugs *(Ahmed et al., 2006, Baldwin et al., 1996, Bozkurt et al., 2007, Herbert et al., 1998, Kofron et al., 2009, Kraus et al., 2015, Pittier et al., 2005).* The development of effective 3D *in vitro* models

potentially enables researchers to bridge between monolayer *in vitro* models and *in vivo* studies more successfully *(Hopkins et al., 2015)*. Consequently, as 3D cell cultures advance they could help improve the pre-clinical development process and the success of clinical trials *(Ko and Frampton, 2016).*

In order to maximise benefit to PNI research, new *in vitro* models need to build upon and complement existing approaches whilst overcoming particular limitations. Animal models of PNI repair such as crush or transection and repair of a nerve in rodents are widely used to test potential treatments *(Angius et al., 2012)*. However, while the complexity of such models echoes that of the human clinical situation and provides useful systems-level information, this complexity can be a hindrance to understanding fundamental cellular processes and mechanisms. Cell culture models on the other hand permit a much greater degree of control and monitoring, enabling specific variables to be isolated and detailed cellular responses to be measured. Furthermore, cell cultures are amenable to continuous monitoring, whereas cell and molecular information from animal experiments tends to be available only as a snapshot at the end-point. The potential for use of human cells in culture models may also help to circumvent some of the concerns about differences in responses to drug treatments between species. Finally, the increased use of more sophisticated non-animal models can help reduce, refine and replace the use of animals in many experiments, in line with the requirements of the 3Rs in research *(Russel and Burch, 1959).*

Hydrogels have been highly utilised for 3D neural co-cultures due to their low stiffness, high water content, and ability to be functionalised with cells. They can be made from natural or synthetic biomaterials such as; agarose, collagen type I, hyaluronic acid, *N*-(2-hydroxypropyl) methacrylamide, poly(ethylene glycol), alginate and silk fibroin *(Hopkins et al., 2015)*.

Engineered neural tissue (EngNT) refers to the anisotropic cellular hydrogels that have been developed for use in nerve repair *(Georgiou et al., 2013)*. This approach, however, also has the potential to be used as a model for pre-clinical *in vitro* drug screening as it enables quantification of the regeneration of neurons within an aligned 3D Schwann cell-

seeded collagen gel environment *(Rayner et al., 2018)*. EngNT is formed by cellular self-alignment in tethered collagen gels, followed by stabilisation using plastic compression to remove most of the interstitial fluid (Section 2.2). Sheets of EngNT have been used in peripheral nerve repair to deliver Schwann cells or Schwann cell-like therapeutic cells to mimic the autograft *(Georgiou et al., 2015, Martens et al., 2014, Sanen et al., 2017)*, and have also been used as *in vitro* models to explore neurodegenerative diseases *(O'Rourke et al., 2017).* When neurons are co-cultured with EngNT, neurite growth is supported and guided by aligned glial cells in a soft 3D extracellular matrix environment. This neurite growth therefore mimics some of the key features of the peripheral nerve environment distal to a PNI repair *in vitro*. By standardising a scalable co-culture methodology and developing robust quantitation protocols, this approach, therefore has the potential to be used as a model for drug screening.

3.1.4 Drugs to test the effectiveness of in vitro models

Some pharmacological agents have already been tested and have shown to promote regeneration following PNI, in particular through targeting the Rho/ROCK pathway, these include ibuprofen, pioglitazone, GW1929 and fasudil (Figure 3.1). Therefore, it is appropriate to use these agents to test the suitability of new potential PNI models.

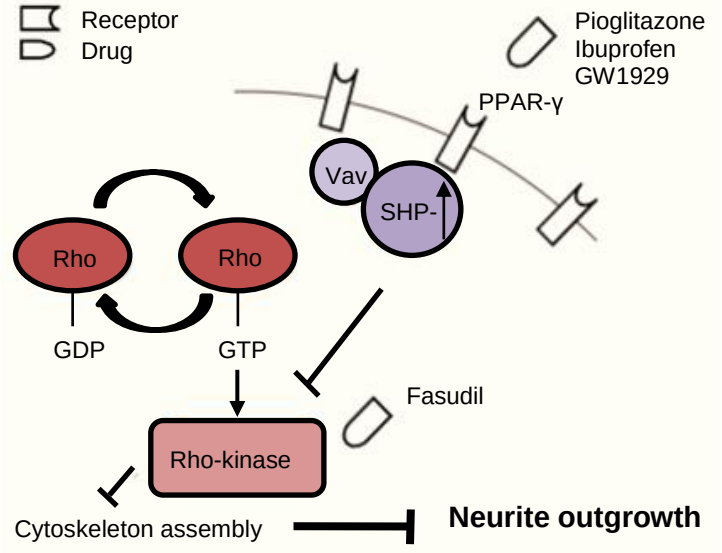

Figure 3.1: Agents that target the Rho/ROCK pathway and have demonstrated beneficial effects on peripheral nerve regeneration.

3.1.4.1 Ibuprofen

Ibuprofen is a non-steroidal anti-inflammatory drug (NSAID) widely used for analgesia and inflammation via cyclooxygenase (COX) 1 and 2 inhibition *(Rockwell and Ehrlich, 1990)*. Ibuprofen has demonstrated positive results on nerve regeneration *in vitro* and *in vivo (Fu et al., 2007, Madura et al., 2011)*, which is suggested to be through reducing secondary damage during the post-injury inflammatory phase and reducing neuropathic pain through its primary mechanism of action on COX. However, more recently it has been suggested that ibuprofen works through an alternative mechanism of action targeting PPAR-γ and consequently the Rho/ROCK pathway for PNI (Figure 3.1) *(Dill et al., 2010, Fu et al., 2007, Madura et al., 2011)*.

Studies have shown treating spinal cord injuries with ibuprofen resulted in some recovery *(Chan et al., 2014, Wang et al., 2009)*, but also that the drug had an effect on the Rho/ROCK pathway by reducing Rho A activity and levels of GTP-bound Rho *(Fu et al., 2007, Zhou et al., 2003)*. The correlation between PPAR-γ activation and Rho A suppression remains unclear, however, Dill *et al.* (2010) suggested that the protein tyrosine phosphatase-2 (SHP-2) couples PPAR-γ and Rho A to promote nerve regeneration. The activation of SHP-2 may suppress the conversion of Rho-GDP to the active Rho-GTP by restricting Rho A activation through the dephosphorylation of tyrosine residue of guanine nucleotide exchange factors *(Dill et al., 2010)*. PPAR-γ activation has shown to increase SHP-2 levels, however, further characterisation of the mechanism in PNI is needed *(Wakino et al., 2004)*. Ibuprofen is a promising therapeutically beneficial molecule for PNI; however it requires optimisation of dose timing, duration and route of administration before clinical adoption for this indication *(Chan et al., 2014)*.

3.1.4.2 Pioglitazone

Pioglitazone is known as a thiazolidinedione (TZD) approved by the FDA for treatment in Type II diabetes and is a PPAR-γ agonist *(Dill et al., 2010)*. Other TZDs include rosiglitazone, ciglitazone and troglitazone, of which only the former is FDA approved *(Quintanilla et al., 2013)*. In various models TZDs have demonstrated neuroprotection

by preventing inflammation and neuronal death *(Park et al., 2007, Lecca et al., 2015, Zhao et al., 2006, Dill et al., 2010),* increased neuronal elongation *(Quintanilla et al., 2013)* and improved re-myelination *(Eto et al., 2008)*. Dill *et al.* (2010) suggested that pioglitazone may also act to suppress COX-2 expression in response to oxidative stress, as shown using *in vitro* and *in vivo* CNS models. These features make pioglitazone a potentially beneficial therapy for PNI.

3.1.4.3 GW1929

GW1929 is a research compound and a highly potent PPAR-γ agonist, which has demonstrated greater effects on PPAR-γ than some of the TZDs *(Henke et al., 1998)*. GW1929 has been shown to increase neurite growth in neurons *(Dill et al., 2010)* and reduce inflammation providing neuroprotective effects following a cerebral ischemic-reperfusion injury *(Kaundal and Sharma, 2011)*. GW1929 has the potential to provide a novel pharmacological treatment for PNI.

3.1.4.4 Fasudil (HA-1077)

Fasudil also inhibits the Rho/ROCK pathway but by acting directly on ROCK (Figure 3.1). Its inhibitory action prevents growth cone collapse, ultimately promoting axon regeneration, but it also has a secondary action of preventing damage to the proximal stump due to the inflammatory response by preventing neutrophil migration *(Chan et al., 2014)*. Fasudil acts on both ROCKI and ROCKII by competitive association with the ATP binding site, however, this is not specific as it also inhibits PKA and protein kinase C *(Kubo et al., 2008)*. Fasudil has demonstrated benefits in PNI models by increasing neurite outgrowth *in vitro* and *in vivo (Cheng et al., 2008, Madura et al., 2007)*. Fasudil is a good candidate for treatment as it is already approved and used clinically to treat subarachnoid haemorrhage, however, a greater understanding of its mechanism and affinity for ROCK in PNI is needed *(Suzuki et al., 2007)*.

3.1.5 Aims of chapter 3

The aim of this chapter was to develop an *in vitro* model as a potential screening tool to enable progress towards the discovery of drug therapies. This was conducted through the comparison of monolayer culture and 3D EngNT co-culture nerve tissue models. Here the models were compared using small molecules that had already demonstrated positive effects on neurite growth in previous studies. A second part of the study was to use the optimal model to test novel small molecules for their regenerative capacity that were selected using cheminformatics screening.

3.2 Results

3.2.1 Effect of small molecules on monolayer neuronal cell cultures

3.2.1.1 NG108-15 cell line

To investigate the regenerative effect of various compounds on the NG108-15 neuron-like cell line, the cells were seeded onto coverslips and incubated for 72 h with varying concentrations of the compounds (listed in Table 3.1) or 100 μM or the PPAR-γ antagonist GW9662 *(Lezana et al., 2016)*. All the compounds tested increased neurite growth following treatment of NG108-15 neurons except the antagonist, GW9662. Significant neurite growth was observed with 100 μM and 200 μM ibuprofen, 30 μM fasudil, 20 μM GW1929, and 10 μM pioglitazone, in comparison with the no-drug control and antagonist GW9662 (Figures 3.2 and 3.3). In some cases the higher doses tested elicited a similar effect on neurite growth to the lower dose or gave no effect at all. From the selected compounds tested, ibuprofen demonstrated the greatest effect on neurite growth by 55.2%, whereas fasudil, pioglitazone, GW1929 increased the neurite length by 27.2%, 40.3%, 51.9% respectively (Figures 3.2 and 3.3).

Drug/Compound	Drug target	Doses tested	Reference
Ibuprofen	PPAR-γ agonist	10 μM, 100 μM, 200 μM	*(Dill et al., 2010)*
Fasudil	ROCK inhibitor	10 μM, 30 μM, 50 μM	*(Cheng et al., 2008)*
Pioglitazone	PPAR-γ agonist	1 μM, 5 μM, 10 μM	*(Quintanilla et al., 2013)*
GW1929	PPAR-γ agonist	5 μM, 10 μM, 20 μM	*(Dill et al., 2010)*
GW9662	PPAR-γ antagonist	100 μM	*(Lezana et al., 2016)*

Table 3.1: List of drugs/compounds and their corresponding doses tested using in vitro models. *The doses used were based upon those that elicited beneficial effects in previous literature.*

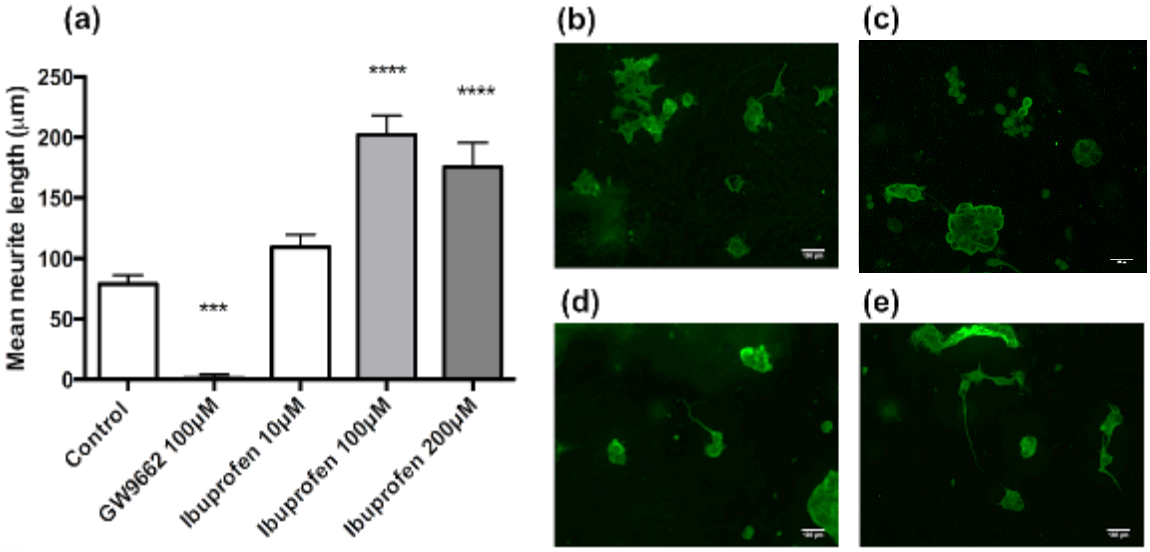

Figure 3.2: Ibuprofen increases neurite growth in monolayer NG108-15 neurons. *Significant increases in neurite length were seen in the presence of 100 µM and 200 µM ibuprofen when compared to the no-drug control, after 72 h exposure. No neurite growth was seen with the growth inhibitor GW9662 (a). Fluorescence micrographs of the monolayer cultures show neurite length with (b) no drug treatment, (c) 100 µM GW9662 (d) 10 µM ibuprofen and (e) 100 µM ibuprofen. Cultures were immunostained to detect β-III tubulin (green). Scale bar = 100µm. N=6, mean ± SEM for each condition. One-way ANOVA with Dunnett's post hoc test, ***p < 0.001 and ****p < 0.0001.*

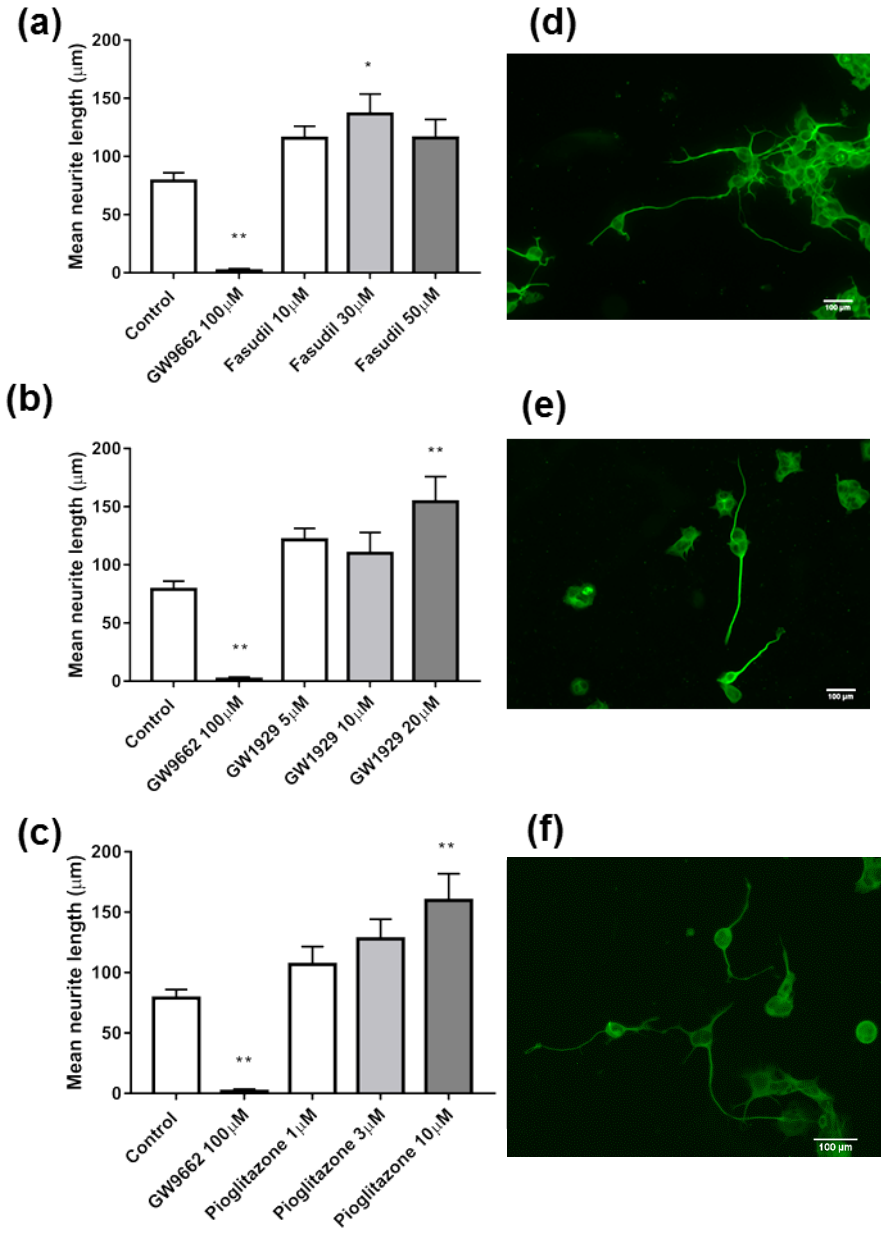

Figure 3.3: Fasudil, GW1929 and pioglitazone increase neurite growth in monolayer NG108-15 neurons. *Significant increases in neurite length were seen in the presence of 30 μM fasudil (a), 20 μM GW1929 (b), and 10 μM pioglitazone (c) when compared with the no-drug treatment control, after 72 h exposure. No neurite growth was seen with the PPAR-γ agonist GW9662 (a), (b), (c). Fluorescence micrographs of the monolayer cultures show neurite length with (d) 30 μM fasudil, (e) 20 μM GW1929 and (f) 10 μM pioglitazone. Cultures were immunostained to detect β-III tubulin (green). Scale bar = 100μm. N=6, mean ± SEM for each condition. One-way ANOVA with Dunnett's post hoc test, *p < 0.05 and **p < 0.01.*

3.2.1.2 PC12 cell line

The same methods were then used to investigate the effect of drug treatments on the PC12 neuron-like cell line. However no neurite growth occurred in any cultures of monolayer PC12 cells without additional growth factors, therefore drugs agents were not tested further in this model (Figure 3.4).

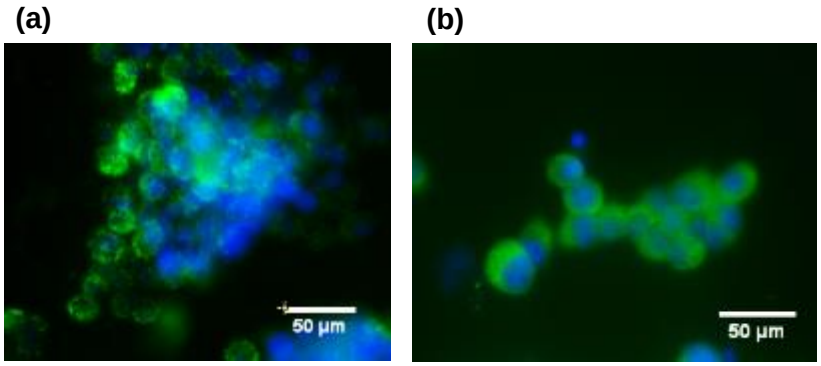

Figure 3.4: Fasudil elicited no neurite growth in monolayer PC12 neurons. *Representative fluorescence micrographs showing βIII-Tubulin (green) and DAPI (blue) on a monolayer of PC12 cells with no drug treatment (a) or 30 µM fasudil (b).*

3.2.1.3 Dorsal root ganglion (DRG) cultures

Dissociated DRG cultures were used to determine the pro-regenerative effects of ibuprofen and fasudil on primary neurons. The monolayer neural cell cultures were coated on glass coverslips and subjected to ibuprofen (Figure 3.5) or fasudil (Figure 3.6) treatments ranging from 0.1 to 100 µM, or 100 µM GW9662, for 72 h. Both drug treatments led to an increase in neurite length in a dose dependent manner in comparison to the no-drug control or GW9662 treatment (Figures 3.5 and 3.6).

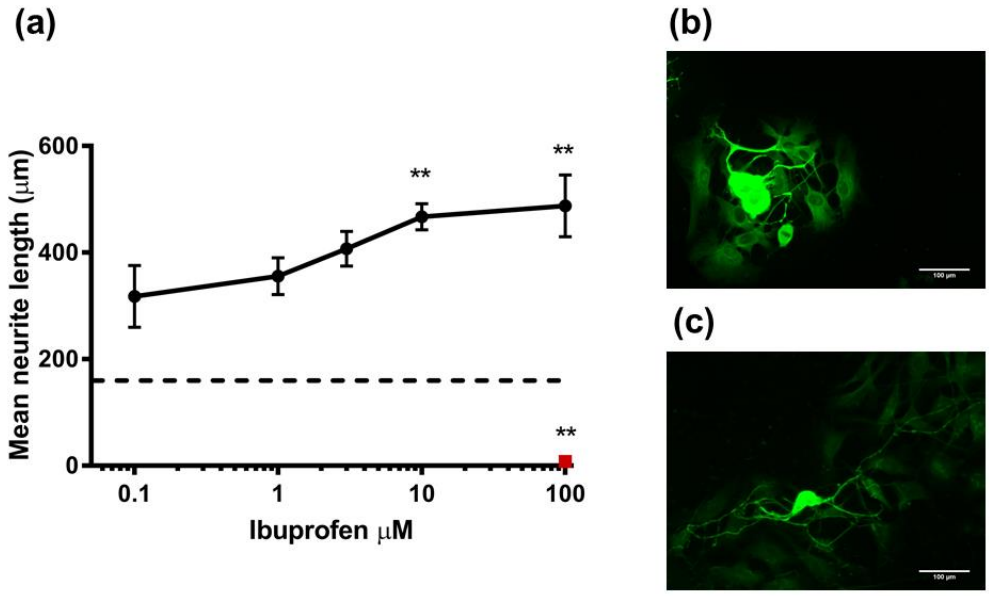

Figure 3.5: Ibuprofen increases neurite growth in monolayer crude prep DRG neurons. *Significant increases in neurite length were seen with 10 μM and 100 μM doses of ibuprofen, however, all doses increased neurite growth when compared with the no drug control (shown by dotted line) and 100 μM GW9662 (shown in red) after 72 h exposure (a). Fluorescence micrographs of the cultures show neurite length with no drug control (b), and 100 μM ibuprofen (c). Cultures were immunostained to detect β-III tubulin (green). Scale bar = 100μm. N=6, mean ± SEM for each condition One-way ANOVA with Dunnett's post hoc test, **p < 0.01.*

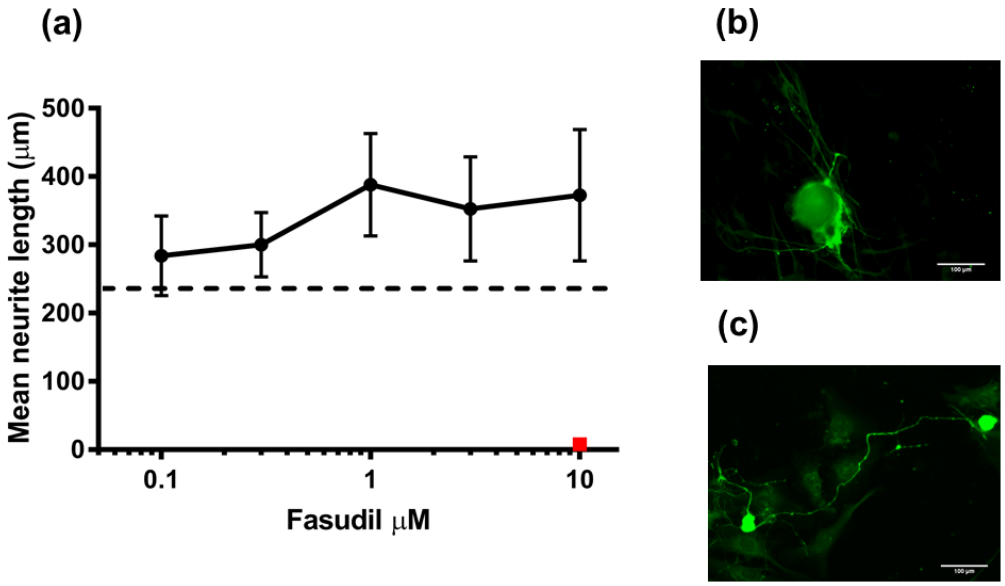

Figure 3.6: Fasudil increases neurite growth in monolayer crude prep DRG neurons. *No significant increases in neurite length were seen with fasudil treatment, however, all doses increased neurite growth when compared with the no drug control (shown by dotted line) and 100 μM GW9662 (shown in red) after 72 h exposure (a). Fluorescence micrographs of the cultures show neurite length with no drug treatment (b), and 100 μM fasudil (c). Cultures were immunostained to detect β-III tubulin (green). Scale bar = 100μm. N=6, mean ± SEM for each condition One-way ANOVA with Dunnett's post hoc test, no significance.*

3.2.2 Effect of small molecules on 3D EngNT co-cultures

3.2.2.1 Co-culture with SCL4.1/F7 and PC12 cell lines

3D EngNT co-culture models containing SCL4.1/F7 and PC12 cell lines, were used to investigate the capacity of ibuprofen, fasudil, GW1929 and pioglitazone in modulating neurite outgrowth. All four compounds were found to increase neurite growth at all treatment doses in comparison to the no drug control and antagonist, GW9662. A significant increase in neurite length was seen at a concentration of 10 μM and 100 μM ibuprofen and 10 μM GW1929 (Figure 3.7).

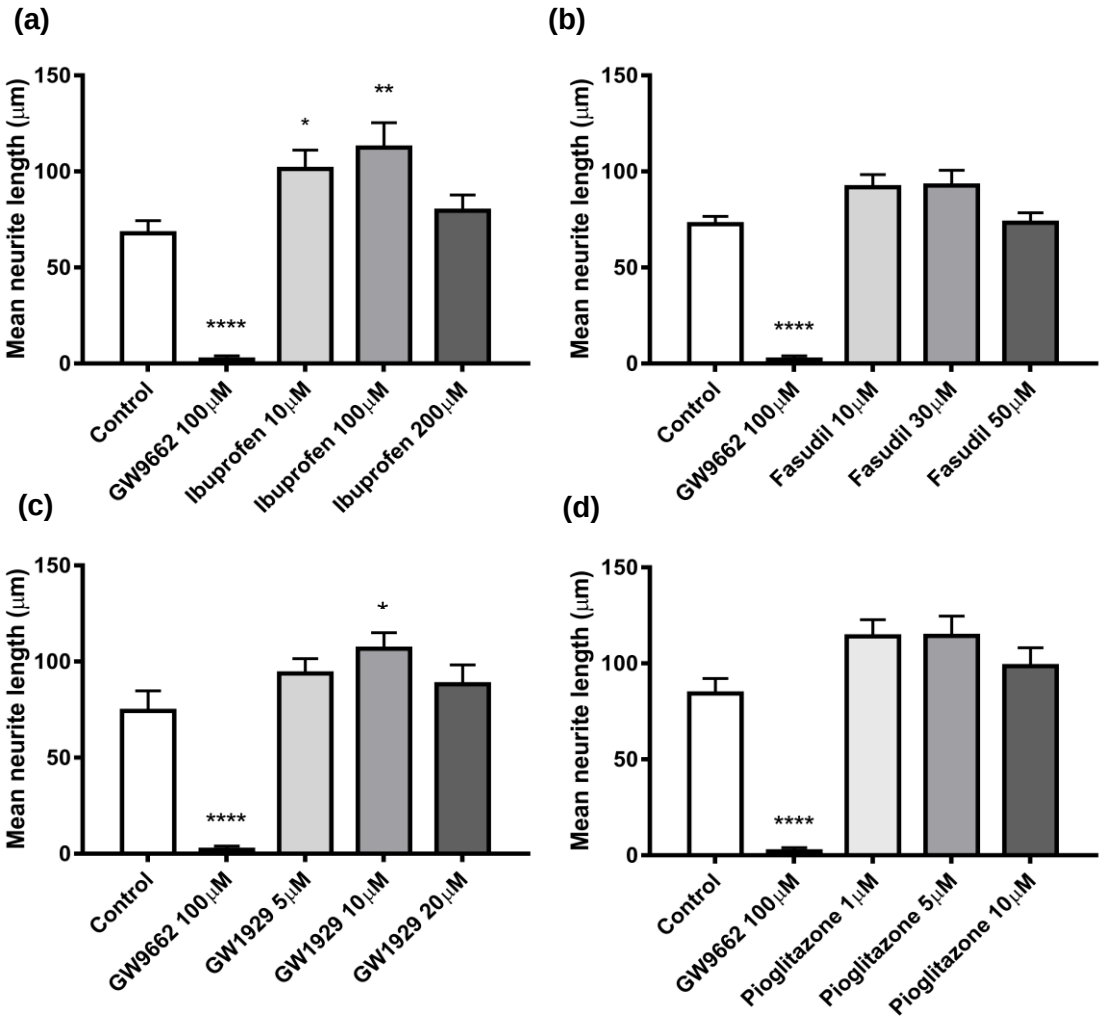

Figure 3.7: Ibuprofen, fasudil, GW1929 and pioglitazone increased neurite growth in the 3D EngNT co-culture consisting of SCL4.1/F7 and PC12 cell lines. *A significant increase in growth was seen with 10 μM and 100 μM ibuprofen and 10 μM GW1929. N=6 of EngNT co-culture gels, mean ± SEM for each compound tested. One-way ANOVA with Dunnetts post hoc test, *p < 0.05, **p< 0.01 and ****p < 0.0001.*

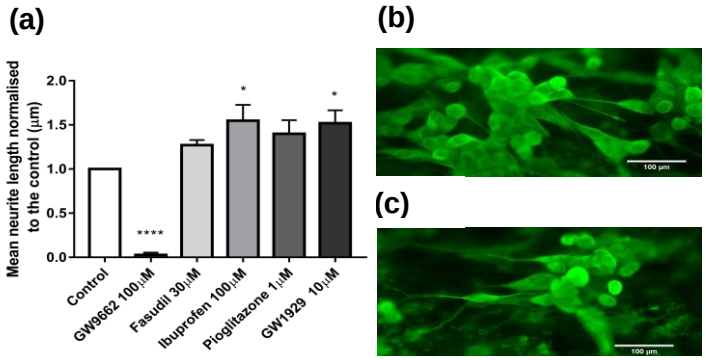

Figure 3.8: A summary of the optimal dose for each compound tested. *All compounds increased neurite growth in the 3D EngNT co-culture model except for the PPAR-γ antagonist, GW9662 (a). A significant increase in growth was seen with 100 µM ibuprofen and 10 µM GW1929 when normalised to their own no drug controls. Fluorescence micrographs of PC12 neuronal cells seeded on the gels without (b) and with (c) 100 µM ibuprofen drug treatment. Cultures were immunostained to detect β-III tubulin (green). Scale bar = 100µm. N=6 co-culture gels, mean ± SEM for each condition. One-way ANOVA with Dunnett's post hoc test, *p < 0.05, and ****p < 0.0001.*

As ibuprofen demonstrated the greatest effect on mean neurite growth in comparison to the other small molecules tested (Figure 3.8), further analysis was conducted to quantify other parameters (total neurite length in 5 fields and number of neurites per field). A significant increase was seen with the total neurite growth per 5 fields from 6 coverslips (Figure 3.9 (a)). The trend was similar to that seen with the mean neurite growth with a dose of 10 µM and 100 µM significantly increasing the total neurite length in comparison to no drug treatment. This effect was not seen with a dose of 200 µM with the total neurite growth decreasing in comparison to no drug treatment (Figure 3.9 (a)). Furthermore, ibuprofen had no significant effect of the number of neurites per field at any dose and a decrease in number was seen at a dose of 200 µM in comparison to the no drug control (Figure 3.9 (b)).

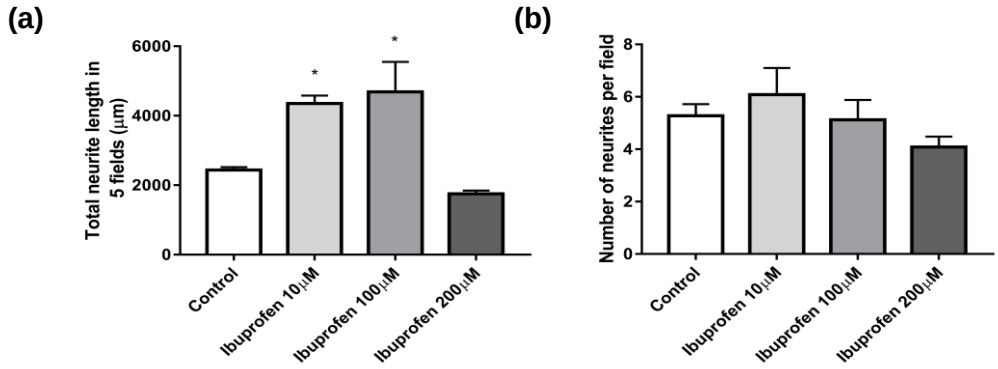

Figure 3.9: Ibuprofen increases total neurite growth per 5 fields (296 mm^2) in the 3D EngNT co-culture. *A significant increase in total growth was seen with 10 µM and 100 µM ibuprofen but not with 200 µM (a). No increase in the number of neurites was seen with ibuprofen treatment (b). N=6 of co-culture gels, mean ± SEM for each condition. One-way ANOVA with Dunnett's post hoc test, *p < 0.05.*

3.2.2.2 Co-culture with SCL4.1/F7 and NG108-15 cell lines

To validate the reproducibility of the effect of small molecules on neurite growth in the co-culture model a different cell line was also used, NG108-15. Ibuprofen was found to induce neurite extension in both cell lines in a similar dose-dependent manner at concentrations of 10 µM and 100 µM ibuprofen, however, no increase in neurite length was seen with a dose of 200 µM ibuprofen (Figure 3.10). An increase in comparison to the control was observed at concentrations of 10 µM and 100 µM.

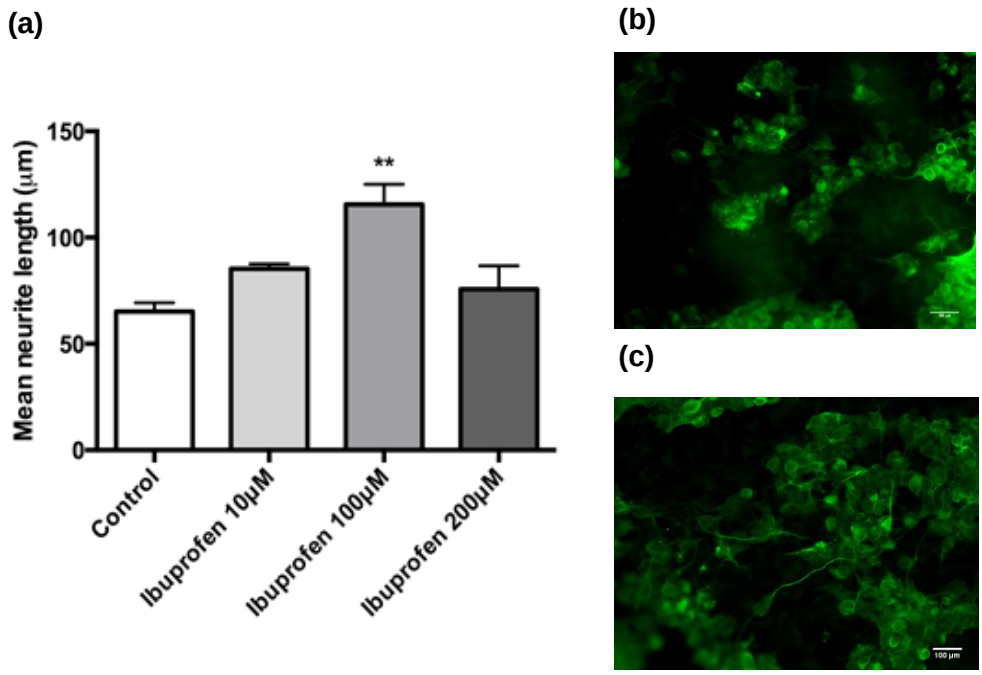

Figure 3.10: Ibuprofen increases neurite growth in the 3D EngNT co-culture with the NG108-15 cell line. *A significant increase in growth was seen with 100 µM ibuprofen in comparison with the no drug control (a). Fluorescence micrographs of NG108-15 neuronal cells seeded on the gels without (b) and with (c) 100 µM drug treatment. Cultures were immunostained to detect β-III tubulin (green). Scale bar = 100µm. N=3 of co-culture gels, mean ± SEM for each condition. One-way ANOVA with Dunnett's post hoc test, **p < 0.01.*

3.2.2.3 Co-culture with SCL4.1/F7 and DRG neurons

3D EngNT co-culture models were fabricated using adult rat DRG primary neuronal cells to determine the effect of ibuprofen on neurite outgrowth. A dose response similar to that with PC12 and NG108-15 cell lines was observed when treating the DRGs with ibuprofen, with a significant increase in neurite length in comparison with the control at a concentration of 100µM (Figure 3.11).

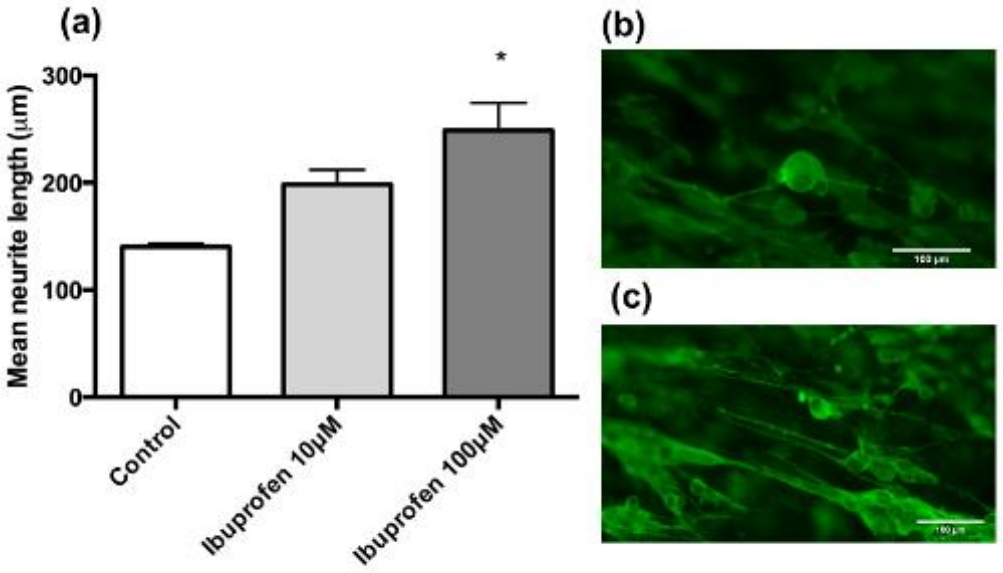

Figure 3.11: Ibuprofen increases neurite growth in the 3D EngNT co-culture with DRGs. *A significant increase was seen with a dose of 100 μM ibuprofen but not 10 μM (a). Fluorescence micrographs of DRG neurons on EngNT gels without (b) and with (c) 100 μM drug treatment. Cultures were immunostained to detect β-III tubulin (green). Scale bar = 100μm. N=6, mean ± SEM for each condition. One-way ANOVA with Dunnett's post hoc test, *p < 0.05.*

3.2.3 Cheminformatics

Cheminformatics was used to screen small molecules that act upon targets within the Rho/ROCK pathway (Figure 1.10). The targets were screened using Chembl software and included PPAR-γ (Table 3.2), Rho A (Table 3.3), ROCK (Table 3.4), and Caspase 3 (Table 3.5). The compounds were screened for their affinity for the associated target, their chemical structure and any effects they had previously shown on nerve regeneration. This included CNS, PNS and optic nerve regeneration but excluded effects on neuropathic pain, neuropathies or neural stem cell differentiation.

Target: PPAR-γ

Small molecule	Therapeutic indication	Affinity for target	Regenerative properties	Reference
Ibuprofen 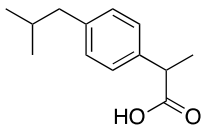	Anti-inflammatory (NSAID)	IC_{50}: 80.6 μM	Increased of area of axon and myelin. Improved motor function *in vivo*.	*(Madura et al., 2011)* *(Dill et al., 2010)* *(Fu et al., 2007)* *(Wang et al., 2009)* *(Xing et al., 2011)* *(Sharp et al., 2013)*
Diclofenac 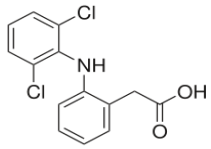	Anti-inflammatory (NSAID)	IC_{50}: 3.7 μM	Improved functional recovery and faster recovery of regenerated axons.	*(Mohammadi et al., 2013b)*
Sulindac sulfide 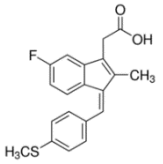	Anti-inflammatory (NSAID)	IC_{50}: 1.87 μM	Suppresses Rho A.	*(Zhou et al., 2003)*
Indomethacin 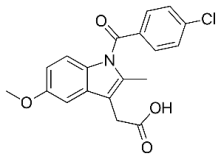	Anti-inflammatory (NSAID)	IC_{50}: 21.4 μM	Increased neurite growth and inactivation of Rho A.	*(Fu et al., 2007)* *(Xing et al., 2011)*
Pioglitazone 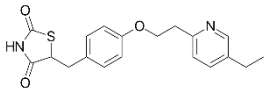	Anti-diabetic (Glitazone)	IC50: 720 nM	Improved re-myelination.	*(Eto et al., 2008)* *(Park et al., 2007)*
Rosiglitazone 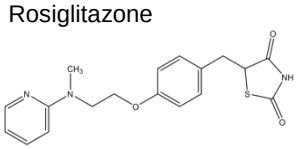	Anti-diabetic (Glitazone)	IC_{50}: 42 nM	Promoted neurite outgrowth and increased population of neurite-bearing cells.	*(Chiang et al., 2014)* *(Lezana et al., 2016)* *(Park et al., 2007)*
Troglitazone 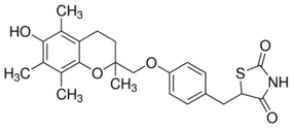	Anti-diabetic (Glitazone) Withdrawn	IC_{50}: 340 nM	Improved motor neuron survival.	*(Nishijima et al., 2001)*
GW1929 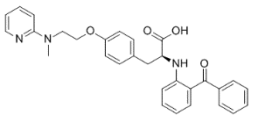	Research compound	IC_{50}: 1.4 nm	Increases neurite outgrowth	*(Dill et al., 2010)*

Mesalamine 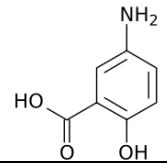	Anti-inflammatory (aminosalicylate)	-	Not explored	
Balsalazide 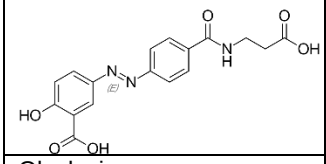	Anti-inflammatory (aminosalicylate)	-	Not explored.	
Olsalazine 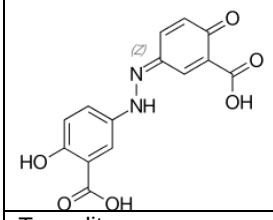	Anti-inflammatory (aminosalicylate)	-	Not explored.	
Tesaglitazar 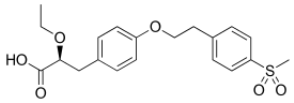	Proposed for Type II diabetes (Withdrawn)	-	Not explored.	
Muraglitazar 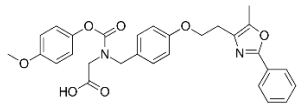	Proposed for Type II diabetes (Withdrawn)	-	Not explored.	
Aleglitazar 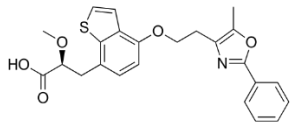	Proposed for Type II diabetes (Withdrawn)	-	Not explored.	

Table 3.2: Cheminformatics screen of small molecules that target PPAR- γ.

Target: Rho A

Small molecule	Therapeutic indication	Affinity for target	Regenerative properties	Reference
Rhosin 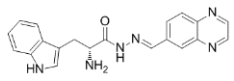	Research compound	Kd: 354 nM	Induces neurite growth.	*(Shang et al., 2012)*
CCG-1423 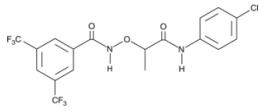	Research compound	IC_{50}: 1.5 µM	Not explored.	
Y16 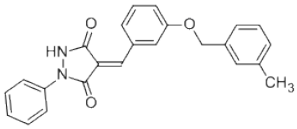	Research compound	-	Suppresses Rho A activity.	*(Shang et al., 2012)*
VX-210 Cethrin(®)	In clinical trials for acute spinal cord injury	-		*(Fehlings et al., 2011)* *(Fehlings et al., 2018)*

Table 3.3: Cheminformatics screen of small molecules that target Rho A.

Target: ROCK

Small molecule	Therapeutic indication	Affinity for target	Regenerative properties	Reference
Fasudil 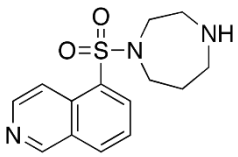	Cerebral Vasospasm	K_i: 330 nM	Increased neurite outgrowth and accelerated functional regeneration.	*(Cheng et al., 2008)* *(Madura et al., 2007)* *(Xiao et al., 2014)* *(Lingor et al., 2007)* *(Ding et al., 2010)* *(Nishio et al., 2006)* *(Sung et al., 2003)* *(Ichikawa et al., 2008)* *(Gopalakrishnan et al., 2008)*
Verosudil 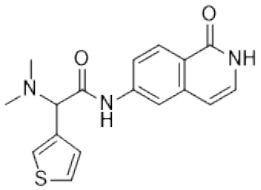	Clinical trials for glaucoma (Discontinued)	K_i: 0.2 nM	Not explored	
Ripasudil (K-115) (Glanatec) 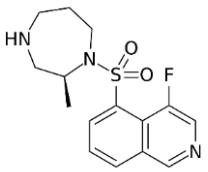	Glaucoma and ocular hypertension	IC_{50}: 19nM	Axonal protection.	*(Kitaoka et al., 2017)*
AMA0076 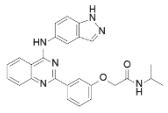	Clinical trials for glaucoma and ocular hypertension	IC_{50}: 2.3nM	Not explored.	
SAR-407899 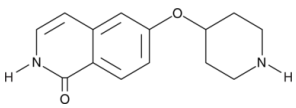	Clinical trials for pulmonary hypertension and	IC_{50}: 276nM	Not explored.	
Y-39983 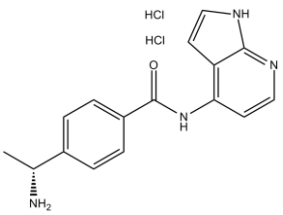	Research compound	IC_{50}: 3.6nM	Increased neurite length and number and downregulations of Rho A, ROCKI and ROCKII.	*(Yang et al., 2013)* *(Sagawa et al., 2007)* *(Tokushige et al., 2011)*

AT-13148 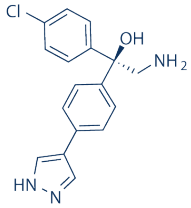	Research compound	IC_{50}: 4 nM	Not explored.	
Y-27632 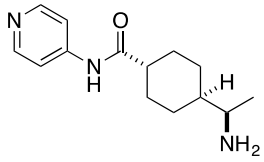	Research compound	K_i: 300 nM	Enhanced axonal growth and increased motor function *in vivo.*	*(Joshi et al., 2015)* *(Fuentes et al., 2008)* *(Gopalakrishnan et al., 2008)* *(Gunther et al., 2014)* *(Minase et al., 2010)* *(Fournier et al., 2003)* *(Zhang et al., 2006)* *(Dergham et al., 2002)* *(Chan et al., 2005)* *(Sung et al., 2003)* *(Sagawa et al., 2007)*
Dimethyl- Fasudil (H-1152) 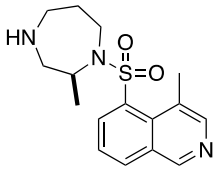	Research compound	K_i: 1.6 nM	Increases neurite length.	*(Fuentes et al., 2008)* *(Lie et al., 2010)* *(Lingor et al., 2007)* *(Minase et al., 2010)* *(Zhang et al., 2006)* *(Gopalakrishnan et al., 2008)*
Aminofurazan 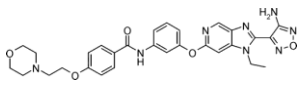	Research compound	IC_{50}: 19 nM	Not explored.	
AS 1892802 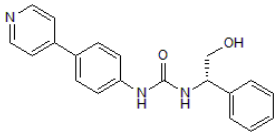	Research compound	IC_{50}: 52 nM	Not explored.	
GSK 269962 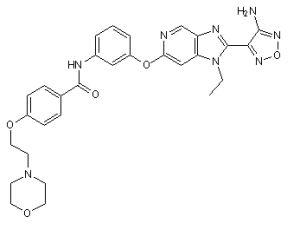	Research compound	IC_{50}: 4 nM	Not explored.	

GSK 429286 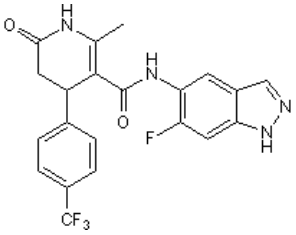	Research compound	IC_{50}: 14 nM	Not explored.	
Hydroxyfasudil (HA 1100) 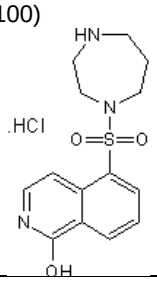	Research compound	K_i: 170 nM	Improved cognition and neuronal damage.	*(Huang et al., 2008)*
OXA 06 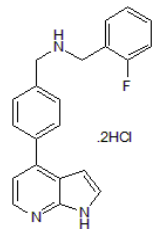	Research compound	IC_{50}: 10 nM	Not explored.	
RKI 1447 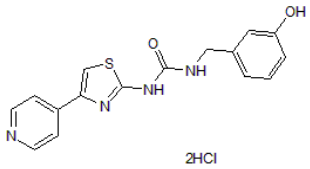	Research compound	IC_{50}: 6.2 nM	Not explored	
SB 772077B 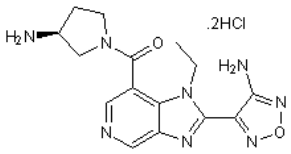	Research compound	IC_{50}: 5.6 nM	Not explored.	
SR 3677 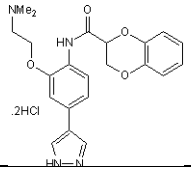	Research compound	IC_{50}: 3 nM	Not explored.	
TC-S 7001 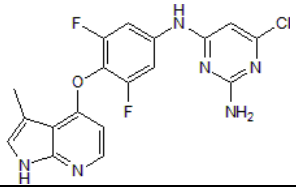	Research compound	IC_{50}: 1.1 nM	Not explored.	
Thiazovinin 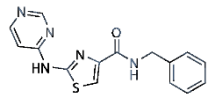	Research compound	IC_{50}: 0.5 µm	Not explored.	

SLx-2119 (KD025) 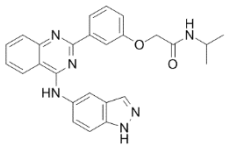	Research compound	IC_{50}: 105 nM	Not explored.	

Table 3.4: Cheminformatics screen of small molecules that target ROCK.

Target: Caspase-3

Small molecule	Therapeutic indication	Affinity for target	Regenerative properties	Reference
z-DEVD-fmk 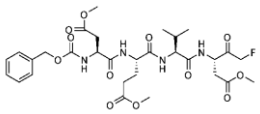	Research compound	K_i: <1 nM	Neuroprotective effects.	*(Barut et al., 2005)* *(Knoblach et al., 2004)*
Q-VD-OPh 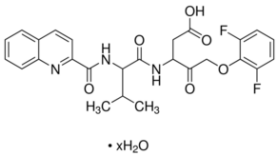	Research compound	IC_{50}: >25 nM	Reduced trauma-induced apoptosis and improved function *in vivo*.	*(Colak et al., 2009)*
Ivachtin 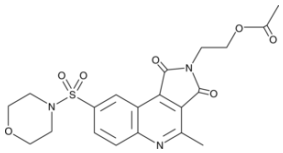	Research compound	IC_{50}: 23 nM	Not explored.	
Ac-DEVD-CMK 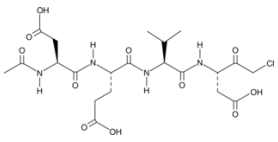	Research compound	-	Not explored.	
Ac-DEVD-CHO 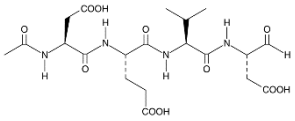	Research compound	K_i: 0.23 nM	Not explored.	

Table 3.5: Cheminformatics screen of small molecules that target Caspase 3.

3.2.4 Effect of identified compounds on 3D EngNT co-cultures

Following cheminformatics to screen for compounds that hit particular targets, some of the ideal compounds were then tested using the EngNT co-culture *in vitro* model. This allowed the robustness of the model to be tested as well as the identification of new agents that could be used in developing drug therapies for peripheral nerve injury. These compounds were selected based upon their affinity for particular targets within the Rho/ROCK pathway or for their novelty for hitting new targets that haven't been previously explored in the literature. Furthermore, CCG-1423 (Rho inhibitor), z-DEVD-fmk (Caspase-3 inhibitor) and mesalamine (PPAR-γ agonist) were selected for their novelty for application in PNI. Moreover, dexamethasone hasn't been shown to target the Rho/ROCK pathway but was selected due to its anti-inflammatory properties similar to many therapies tested for PNI. Y-27623 was selected as it has a greater potency for ROCK than fasudil.

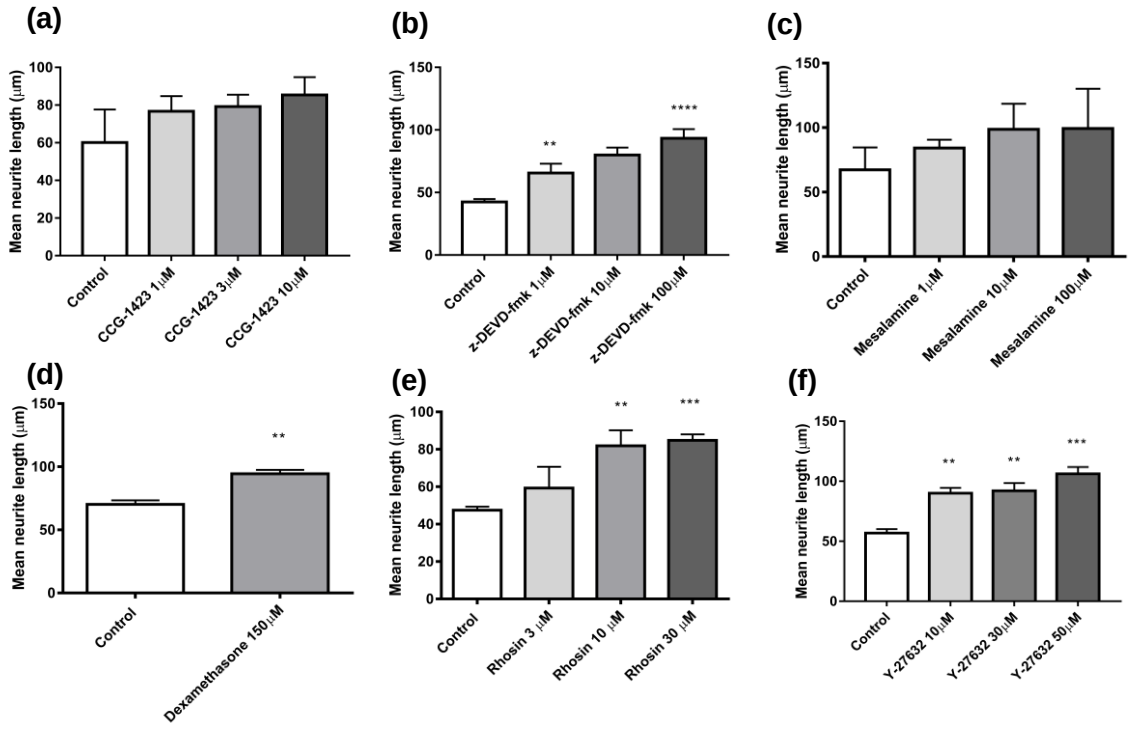

Figure 3.12: CCG-1423 Rho inhibitor), z-DEVD-fmk (Caspase-3 inhibitor), mesalamine (PPAR-γ agonist), dexamethasone, Rhosin (Rho inhibitor) and Y-27632 (ROCK inhibitor) increased neurite growth in the 3D EngNT co-culture consisting of SCL4.1/F7 and PC12 cell lines. *Significant increases in neurite length were seen in the presence of 1 μM and 100 μM z-DEVD-fmk and 150 μM dexamethasone in comparison to the no-drug control, after 72 h exposure. No significant increase in neurite growth was seen with the CCG-1423 or mesalamine. Co-cultures were immunostained to detect β-III tubulin (green). N=6, mean ± SEM for each condition. One-way ANOVA with Dunnett's post hoc test, **p < 0.01, ***p < 0.001 and ****p < 0.0001.*

3D EngNT co-culture models containing SCL4.1/F7 and PC12 cell lines, were used to investigate the capacity of Rhosin, CCG-1423, z-DEVD-fmk, Y-27632, mesalamine and dexamethasone in modulating neurite outgrowth (figure 3.12 and 3.13). Significant growth was seen with 1 µM and 100 µM z-DEVD-fmk and 150 µM dexamethasone. Rhosin and Y-27623 demonstrated the greatest effects on neurite growth in comparison to the other compounds screened (Figure 3.12). A further dose response was conducted for Rhosin with doses ranging from 1 to 100 µM for 72 h (Figure 3.13). A significant increase in neurite growth was seen at doses 10 µM, 30 µM and 100 µM, with the highest dose increasing the neurite growth by 99.2% in comparison with the no drug control.

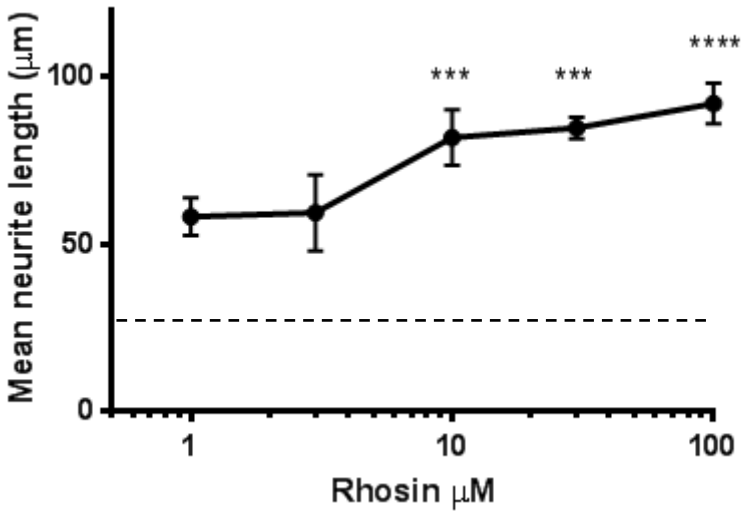

Figure 3.13: Rhosin increased neurite growth in the 3D EngNT co-culture in a dose dependent manner. *Significant increases in neurite length were seen with 10 µM, 30 µM and 100 µM doses of Rhosin, however, all doses increased neurite growth when compared with the no drug control (shown by dotted line) even though they were not statistically significant after 72 h exposure. Co-cultures were immunostained to detect β-III tubulin (green). N=6, mean ± SEM for each condition. One-way ANOVA with Dunnet's post hoc test, ***p < 0.001, ****p < 0.0001.*

3.2.5 Synergistic properties of drug treatments

Drug synergism was tested by combining dexamethasone and ibuprofen, rhosin and z-DEVD-fmk, and ibuprofen and fasudil (Figure 3.14 and 3.15). Only the latter drug combination elicited an increase in neurite growth in comparison to either drug given alone or with no drug treatment. The neurite growth increased by 71.1% in comparison to ibuprofen (55.2%) or fasudil (27.2%) treatments alone (Figure 3.15).

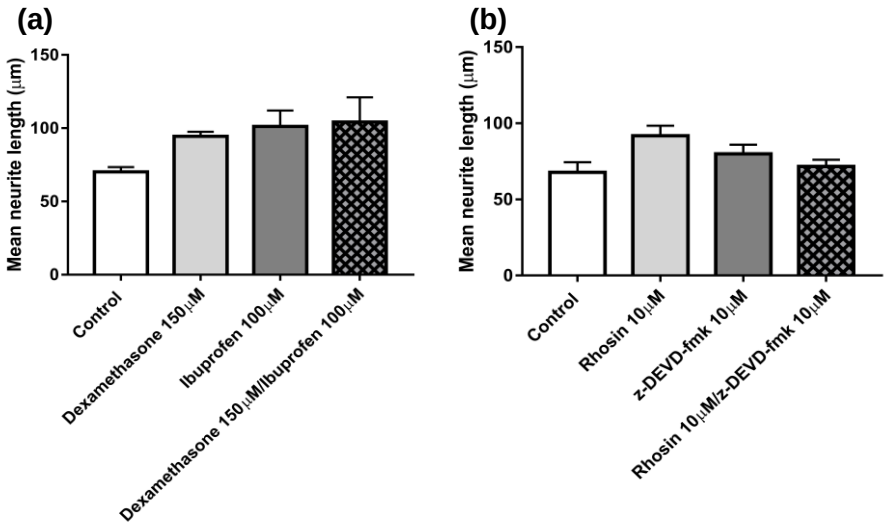

Figure 3.14: Drug synergism. *Dual treatments combining ibuprofen and dexamethasone or rhosin and z-DEVD-fmk gave no synergistic effect on neurite growth in the 3D EngNT co-culture. Co-cultures were immunostained to detect β-III tubulin (green). N=6, mean ± SEM for each condition One-way ANOVA with Tukey's post hoc test, no significance.*

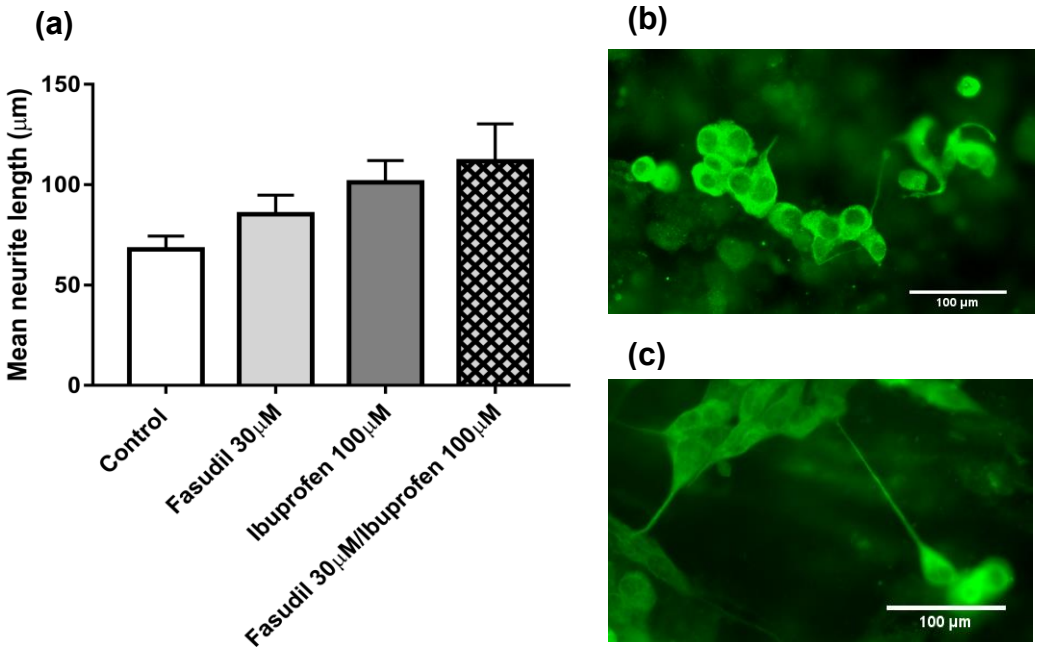

Figure 3.15: Ibuprofen and fasudil elicited a synergistic effect on neurite growth in the 3D EngNT co-culture. *However, no statistically significant increase in growth was seen with the dual treatment with 100 μM ibuprofen and 30 μM fasudil (a). Fluorescence micrographs of PC12 neuronal cells seeded on the gels with no drug treatment (b) and with dual treatment of 100 μM ibuprofen and 30 μM fasudil (c). Cultures were immunostained to detect β-III tubulin (green). Scale bar = 100μm. N=6 of co-culture gels, mean ± SEM for each condition. One-way ANOVA with Tukey's post hoc test, no significance.*

3.3 Discussion

There is a growing interest in the development of *in vitro* models that can accurately simulate the natural regeneration process of neurons following a PNI. Monolayer *in vitro* systems have been developed by co-culturing neurons with Schwann cells to study the influence of cell-to-cell interactions *(Clarke et al., 2011)*, however, more complex 3D co-culture systems have been developed to mimic the natural nerve environment more closely such as; explant cultures *(Lesuisse and Martin, 2002, Miller et al., 2001, Vikman et al., 2001, Yip et al., 1998),* self-assembled aggregate cultures *(Becq et al., 1999, Edoff and Jerregard, 2002, Jerregard, 2001, Knoops et al., 1991, Lee et al., 2002, Lillesaar et al., 2001, Ruscheweyh and Sandkuhler, 2001)* and scaffold based cell cultures *(Backstrom et al., 2000, Balgude et al., 2001, Borkenhagen et al., 1998, Dubey et al., 1999, Georgiou et al., 2013, Yu and Bellamkonda, 2001)*.

Despite this no models have yet been developed to screen the effect of drug therapies on axon regeneration. Here the effectiveness of different culture systems, in terms of suitability for use in PNI drug development, was studied by exploring the effect of small molecules on the length of neurites in the culture systems. Overall, small molecules known from previous *in vivo* studies to improve regeneration, increased neurite length in all the models tested regardless of the type of neurons and the complexity of the culture environment.

This study demonstrates that the 3D co-culture model containing neurons and Schwann cells aligned within a collagen hydrogel is an effective tool to screen drugs for pro-regenerative effects in the peripheral nerve. The four compounds used to assess the model; ibuprofen, pioglitazone, GW1929 and fasudil, all enhanced neurite growth mimicking results seen in previous studies. Ibuprofen has formerly been shown to promote neurite growth enhancement in primary neuronal cell cultures in a dose dependent manner *(Dill et al., 2010, Fu et al., 2007, Wang et al., 2009).* This effect of ibuprofen was further demonstrated in animal models of both the central and peripheral nervous system, with axonal sprouting induced by ibuprofen treatment following a

contusion injury *(Wang et al., 2009),* the promotion of axonal growth following spinal cord lesions (*Fu et al., 2007)*, and improved axonal areas and myelin in peripheral nerve repair (*Madura et al., 2011*). In this study a dose of 100 µM ibuprofen elicited the greatest effect on neurite length, with a 55.2% increase compared with the no drug control (Figure 3.2). An increase of dose to 200 µM did not result in an increase in neurite growth. This could provide an insight into the therapeutic window of ibuprofen treatment and could inform dose ranges to be tested in future animal models.

Pioglitazone, a PPAR-γ agonist, had also previously demonstrated benefit following nervous system injury by providing neuroprotection succeeding focal cerebral ischemia in rats *(Zhao et al., 2006)*, and promoting remyelination following a sciatic nerve crush injury in mice *(Eto et al., 2008).* In the co-culture pioglitazone stimulated an increase in neurite growth, even at a much lower dose than the other small molecules. The mechanism by which pioglitazone promotes neurite growth is an area that still needs to be explored, however, it could be assumed that it targets PPAR-γ for PNI based upon its known mechanism of action as an anti-diabetic *(Park et al., 2007, Smith, 2001)*. Ligand binding and cellular transactivation assays could be conducted to confirm this.

The effect of another PPAR-γ agonist, GW1929, was also investigated. The neuron regenerative effects of GW1929 previously seen *(Dill et al., 2010)*, were also mimicked using this model. The PPAR-γ antagonist GW9662 was used in this study as a negative control where it abolished neurite growth completely. A study conducted by Lezana *et al.* (2016) demonstrated a similar effect with GW9662 reducing neurite growth by 40% in DRG cultures with a 10 µM dose. Increasing the dose 10-fold seems to eradicate any neurite growth which could suggest that the baseline neurite growth (as seen with no drug treatment) is dependent on PPAR-γ activation.

A small molecule, fasudil that directly targets ROCK in the Rho/ROCK pathway was also tested within the 3D co-culture model. Hiraga *et al.* (2006) had demonstrated an increase in axon myelination and a significant improvement in functional recovery following a sciatic nerve crush injury with fasudil treatment in mice. It was suggested that the enhanced myelination of axons resulted in better regeneration and maturation of the

injured axons *(Hiraga et al., 2006)*. This was supported by fasudil preventing growth cone collapse and promoting outgrowth in a peroneal nerve interpositional graft model in rats *(Madura et al., 2007)*. The results from this study mimicked the regenerative effects of fasudil seen in other studies. Fasudil treatment within Ntera-2 neuron cultures *(Lingor et al., 2007)* and monolayer PC12 cultures *(Gopalakrishnan et al., 2008)* also elicited a substantial increase in neurite growth. Overall the small molecules tested in this study yielded results that corresponded to those in other models.

The versatility of the model was further investigated using different neuronal cell types. Similar patterns of dose-response were achieved following ibuprofen treatment when using either the PC12 or NG108-15 cell lines or primary neurons in the 3D EngNT co-culture model. With all cell types the optimal dose tested was 100 µM ibuprofen which increased neurite growth by ~60%. In contrast, in the monolayer cultures no neurite growth was seen with the PC12 cell line, indicating that the 3D EngNT co-culture environment was required in order for that cell line to extend neurites under the media conditions used in these studies. In previous studies PC12 cells have extended neurites without the need of a co-culture system, but through the enrichment of media with growth factors *(Minase et al., 2010, Gopalakrishnan et al., 2008)*.

The results observed from the monolayer NG108-15 and DRG cultures still demonstrated extensive neurite elongation following drug treatment. Interestingly, the extent of growth in these cultures was different to that seen in the 3D system. With ibuprofen treatment the optimal dose remained the same at 100 µM ibuprofen, however, the growth increase in response to the drug exceeded 100%, considerably higher than that seen in the 3D system. Also the 200 µM ibuprofen dose in the NG108-15 monolayer culture elicited an increase in neurite length in comparison to the control which was not reproduced in the 3D-engineered co-culture.

Differences were also seen between the monolayer and co-culture model with the other small molecules. The optimal dose of fasudil was 30 µM in the monolayer culture but no difference was seen between the 10 µM and 30 µM dose in the 3D co-culture system. Furthermore the 50 µM dose of fasudil elicited a substantial difference in neurite growth

in comparison to the no treatment control in monolayer cultures which was not reproduced in the 3D co-culture. The optimal dose also changed with GW1929 treatment, with 20 µM in the monolayer and 10 µM in the co-culture. Pioglitazone presented a clear dose response in the monolayer culture, however, this was not present in the 3D co-culture with a similar neurite growth seen in both the 1 µM and 5 µM doses. This difference in neurite growth between the monolayer and co-cultures has been established previously. A study compared the neurite growth of NG108-15 cells in 2-dimensional (2D) monolayer and a co-culture with Schwann cells in a spheroidal 3D collagen matrix. Despite neurites growing in both environments, the length and diameter of the neurites increased in the 3D co-culture as time increased *(Kraus et al., 2015)*.

Furthermore, the study of neurite outgrowth of DRG neurons at the interface of 2D and 3D growth environments demonstrated how structural and chemical cues impacted the growth of neurites. More neurite outgrowth was seen near the surface of the 3D collagen gel matrix and their extensions were significantly longer *(Kofron et al., 2009)*. Another model consisting of cross-linked porcine collagen also promoted axonal growth of DRG cells and the microstructural properties of the scaffold enabled Schwann cells from the culture to migrate along the scaffold resembling bands of Büngner *(Bozkurt et al., 2007)*. These findings suggest that 3D cell cultures provide an environment that closer mimics the *in vivo* environment in terms of spatial and mechanical cues which are not found in a 2D environment.

To fulfil the aim of the study in developing a model to be used as a screening tool for therapies for PNI, a metric was devised to compare the different *in vitro* models and to determine which one was most replicable. The dose administered in all models that represented a significant increase was the 100 µM ibuprofen dose, therefore only the data sets for this dose were analysed from each culture model used, by normalising them to their controls. This analysis showed that the monolayer models had marked variability in neurite length. Although the mixed population-DRG and NG108-15 monolayer cultures had comparable fold increases they had a large standard deviation (e.g. ± 60% in the

NG108-15 culture). Conversely, the 3D models were more consistent, with a standard deviation of ±40% independent of the cell type used (Figure 3.16).

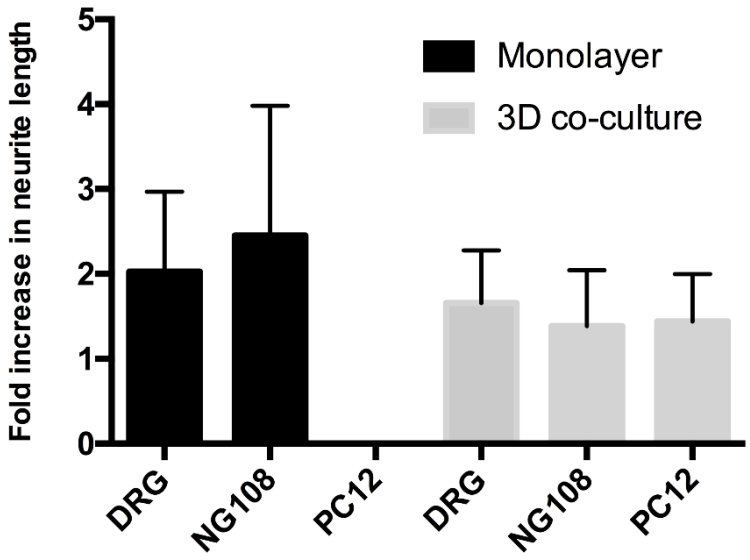

Figure 3.16: Fold increase in neurite length across models. *The data sets for the 100 µM dose of ibuprofen in the various different in vitro models were normalised to their own controls and presented as fold changes to the no drug control. Neurite growth increase was seen in all of the in vitro models except the monolayer PC12 cultures where no growth was seen. N=6 (N=3 for NG108-15 3D culture). Mean ± SD.*

Cell choice is an important consideration for *in vitro* experiments and there is invariably a trade-off between the ready availability, standardisation and reproducibility of immortalised cell lines (e.g. NG108-15, PC12, SCL4.1/F7) and the use of primary cells which behave more naturally but have additional limitations in terms of source and variability. Species differences may also be a consideration depending on the purpose of the experiment (as a precursor to animal studies then animal cells may be more appropriate, but in turn they may be less appropriate for modelling human physiology). The advantage of using cell lines is that the cell cultures are more reproducible and standardised as the variability present between individual animals and individual primary cultures is avoided. Furthermore, these studies were designed to follow the guidelines of the 3Rs – reduction, replacement and refinement; which encourages the reduction of animal usage in research *(Russel and Burch, 1959)*. Comparable effects were seen between cell lines and primary neurons following ibuprofen and fasudil treatment in this

study, indicating that the cell lines provided a valid prediction of the effects of drugs without the need for primary cells (requiring culling of an animal) in this instance.

In addition, the synergistic activity of neurons and Schwann cells plays a key role in nerve regeneration, therefore it is desirable to recreate this key cell-to-cell interaction in a model when screening the effects of drug therapies. Using a tool that is more biologically relevant than a monolayer culture of isolated cells may provide pertinent data on drug safety and efficacy to inform subsequent animal and clinical studies. The 3D EngNT co-culture model system allows the exploration of key regenerative events such as neurite formation, cell-to-cell interactions and optimal dosing regimens and could also be used to further the understanding of mechanisms of action. Another advantage is the cell alignment which further mimics the natural environment recreating the bands of Bünger following injury and also helps in the practicality of measuring neurite length. However, it may be of benefit to use primary cells when trying to understand more complex cellular and molecular biology.

On the contrary, 3D co-culture systems increase complexity and can introduce time restraints by restricting the number of samples produced *(Ko and Frampton, 2016)*, however, the developed protocol from this study (described in section 2.2, Figure 2.2) provides a more rapid approach. Each fabricated EngNT co-culture gel can be cut into 4 equal segments and subjected to a different dose, allowing multiple doses to be tested from one fabricated EngNT co-culture system. Furthermore, this method also provides a control within each EngNT gel manufactured. Further development would need to be conducted to ensure the model is reproducible in other laboratories, with intra and inter observer reliability and intra class correlation which needs to be scalable for large manufacture.

The results reported herein established an effective screening tool for drugs to treat PNI, therefore, other identified compounds were screened using this model. Currently no compounds directly targeting Rho have been studied in PNI, but a specific Rho inhibitor, Rhosin, has been shown to enhance neurite growth in synergy with NGF in a CNS model *(Shang et al., 2012)*. The structure of Rhosin consists of two-aromatic rings tethered by

a linker which binds to Rho A with a Kd of 354 nM inhibiting the GEF catalysed Rho A activation *(Shang et al., 2012)*.This study found that Rhosin could also be a beneficial treatment for PNI as it also enhanced neurite growth in the 3D co-culture model. The neurite growth increased in a dose-dependent manner with the highest dose of 100 µM eliciting an increase of 99.2%, which had the greatest effect of all the small molecules screened.

Another Rho signalling inhibitor was screened, CCG-1423, which has not been tested in any nervous system models previously. CCG-1423 treatment also resulted in an increase in neurite length, but this was not significant and was low in comparison to Rhosin.

Small molecules that target other parts of the Rho/ROCK pathway were also screened such as z-DEVD-fmk which is a caspase 3 inhibitor. ROCK I is a direct cleavage substrate following the activation of caspase 3 *(Chang et al., 2006)*. z-DEVD-fmk is a specific inhibitor of caspase 3 with a high affinity (K_i < 1 nM), which has demonstrated neuroprotective properties in a controlled cortical impact injury in mice *(Knoblach et al., 2004)*. Its local application in spinal cord injury reduced secondary tissue damage and maintained motor function *(Barut et al., 2005)*. This study has demonstrated that z-DEVD-fmk can also have beneficial effects on neurite regeneration *in vitro*. Neurite growth increased in a dose-dependent manner with the highest dose of 100 µM eliciting a significant result.

Drugs that work through mechanisms other than the Rho/ROCK pathway were also investigated such as mesalamine and dexamethasone which have anti-inflammatory properties. Like some of the other drugs tested in this study they are already approved for clinical use in other indications, therefore, as their safety profiles are already established they could be repurposed and rapidly translated to clinical treatment of PNI. Mesalamine is commonly used to treat inflammatory bowel diseases including ulcerative colitis and mild to moderate Crohn's disease, and dexamethasone is a corticosteroid which has many indications such as rheumatoid arthritis, severe allergies and respiratory problems. Mesalamine hasn't been tested for nerve regenerative properties whereas

dexamethasone has demonstrated positive effects in peripheral nerve regeneration. Dexamethasone increased functional recovery, increased gastrocnemius muscle mass, reduced the severity of Wallerian degeneration, and enhanced regenerated myelinated nerves in animal models of PNI *(Mohammadi et al., 2013a, Feng and Yuan, 2015)*. Both drugs demonstrated improvements in neurite growth in the 3D co-culture model in comparison with the no drug control and dexamethasone at a dose of 150 µM elicited a significant increase in growth.

Duan *et al.* (2012) reported a synergistic effect on neurite outgrowth when inhibiting both ROCK and COX-2 together in PC12 and Neuro-2a cell cultures, suggesting that dual treatment may have promise in the treatment of PNI. An extended drug treatment (3 days *in vitro*) lead to tolerance of ROCK inhibition and attenuation of neurite outgrowth. This tolerance appeared to correlate with upregulation of the COX-2 pathway *(Duan et al., 2012)*. A preclinical study combining the treatment of the ROCK inhibitor, fasudil, and COX-2 inhibitor, celecoxib, demonstrated a synergistic effect by decreasing COX-2 and ROCK-II activation in a spinal cord injury site following a hemi-section in rats *(Hou et al., 2015)*. Locomotor functional recovery was enhanced with the combined therapy but not when the two drugs were given alone *(Hou et al., 2015)*.

Another study investigated the dual treatment of the anti-inflammatory drug methylprednisolone and the PPAR-γ agonist rosiglitazone, which also demonstrated a positive synergistic effect. The combined treatment of methylprednisolone and rosiglitazone following a laminectomy and compressive spinal cord injury in animals, had a pronounced effect on attenuation of inflammation and apoptosis. Increased functional recovery was observed when the two drugs were administered together in comparison to using either drug treatment alone *(Li et al., 2016).*

Drug synergy had generated positive results in the treatment of spinal cord injury and so was further investigated in this study for PNI. However, no benefit was seen with the combination of two anti-inflammatory drugs with different mechanisms of action, ibuprofen (NSAID/PPAR-γ agonist) and dexamethasone (corticosteroid) which only resulted in a small non-significant increase in neurite growth. On the other hand, the

combination of Rhosin (Rho inhibitor) and z-DEVD-fmk (Caspase 3 inhibitor) resulted in a reduction in neurite growth with the dual treatment in comparison to the drugs given alone. In both cases this may be due to saturation of the pathway as both targets have the same downstream effector.

Conversely, the dual treatment of fasudil (ROCK inhibitor) and ibuprofen (NSAID/PPAR-γ agonist) resulted in a substantial increase of neurite length (71.1%) compared to either drug given alone. This mimicked the result seen previously with fasudil and celecoxib *(Hou et al., 2015)* suggesting that ibuprofen could be working through two mechanisms, as a PPAR-γ agonist and through its primary mechanism as a COX inhibitor. Drug synergy provides an exciting new area for drug development, as the combination therapy could treat multiple aspects of PNI such as neural viability, nerve regeneration and neuropathic pain.

In conclusion, this study has generated a model that represents some of the key features of PNI, providing for the first time a 3D co-culture model of PNI developed specifically for drug development. The model enables medium throughput drug screening with results that are consistent with the outcomes of previous studies. The findings from this chapter will be used to inform further studies in this body of work. The 3D co-culture model will be utilised in the identification and development of drug therapies for PNI in chapter 5.

Chapter 4: *In vivo* models to screen drugs for peripheral nerve regeneration.

4.1 Introduction

Regardless of advancements made in the development of reliable *in vitro* models to screen therapies for peripheral nerve injuries, animal models still play a key part in pre-clinical studies. They remain a mandatory requirement of regulatory bodies meaning they need to be conducted before new therapies can make it onto the market *(Geuna et al., 2016)*. To ensure the successful translation of drug compounds from the bench to the clinic; animal models need to enable a valuable prediction of human pathophysiology *(Greek, 2012)*. The selection of a validated and predictive model is, therefore, vital in ensuring that this can be addressed effectively. However, this stringent criteria has consequently reduced the success rates of drug therapies during the pre-clinical stages *(Denayer et al., 2014)*.

For application in PNI the *in vitro* models offer highly controllable systems of study for neurite outgrowth, however, the animal models allow the additional evaluation of functional recovery. They allow a holistic view of peripheral nerve recovery, as we are able to see whole body interactions *(Donaldson and Hoke, 2014)*. Yet, it can be expected that the responses of animals and humans can be compared when studying the level of organisation in simpler body systems, however, it is more difficult to obtain reliable results when more complex systems are studied as a whole *(Greek, 2012)*.

On the contrary, animal studies can permit the study of cellular and molecular changes, which is highly important in the field of PNI, as successful recovery relies on an orchestrated permissible cell environment *(Allodi et al., 2012)*. This includes the influence of the Schwann cells and the impact of a local immune and inflammatory response *(Gingras et al., 2003)*. Considering all of these factors, it is therefore vital to choose a model that answers a specific question and uses appropriate methods to derive meaningful conclusions *(Navarro, 2016, Denayer et al., 2014)*.

4.1.1 Stages of PNI

PNI can be separated into three main phases; the regeneration of axons, reinnervation of targets and recovery of function, with each phase depending upon the preceding stage for a successful outcome. These different phases of PNI can help determine the most adequate methods to use *(Navarro, 2016)*. The regeneration of axons involves the emergence of sprouts and their growth across the injury site. The axons that successfully regenerate will reinnervate the target organ and establish functional connections. Reinnervation is not always achieved, especially if a nerve transection has occurred, because regenerating axons have a high probability of regrowth misdirection *(Madison et al., 1996)*. The axons that reach the appropriate target will mature and increase in size and myelin thickness, which will in turn restore conduction properties *(Navarro, 2016)*. The final phase is then the restoration of function such as motor control and sensory discrimination.

Achieving functional recovery is the most clinically relevant outcome of successful peripheral nerve regeneration. Functional analysis provides evidence that not only has the nerve regenerated, but has also formed connections with the end target organ *(Navarro, 2016)*. However, previous literature has shown that function recovery does not always correlate with histological and electrophysiological data *(Munro et al., 1998, Nichols et al., 2005)*. This is due to regenerating axons producing more than one daughter branch, resulting in an overestimation of the number of functional axons in histological studies *(Navarro, 2016)*.

In conclusion, objective analytical methods should be used at each phase of nerve injury recovery for the quantitative assessment of regeneration and restoration of function. Previous literature demonstrates the wide variety of tests available that are commonly used to evaluate PNI recovery *(Nichols et al., 2005, Vleggeert-Lankamp, 2007)*. Some of these tests are discussed below.

4.1.2 Regeneration and functional evaluation

Each developed assay for PNI evaluation has its strengths and weaknesses, but they need to be selected based upon the type of data required to test a specific hypothesis. The technical difficulty, expense and time required to conduct the assessments also needs to be considered *(Nichols et al., 2005)*.

4.1.2.1 Axonal regeneration

Common tests to determine axonal regeneration are pinch and nerve conduction tests, alongside immunohistochemical and histological methods on harvested tissue, and retrograde and anterograde tracing *(Navarro, 2016)*. Histology is the most frequently used assessment for axonal counts and distinguishing nerve fibre populations *(Kemp et al., 2017, Vleggeert-Lankamp, 2007)*. Other parameters can be quantified including the number of myelinated or unmyelinated axons, myelinated axon diameter and area, myelin thickness, g-ratio, n-ratio (used to measure the maturity of regenerating nerves) and blood vessel profiles.

4.1.2.2 Reinnervation of target organ

More vigorous testing can be conducted for nerve reinnervation. They are usually non-invasive and can be performed at multiple intervals throughout the study, reducing the number of animals and the inter-individual variability. These methods quantify the amount of reinnervation, and thus the recovery of activity in the target organ *(Navarro, 2016)*.

An example is motor nerve conduction tests which involve the stimulation of the nerve with electrical pulses of increasing intensity, delivered by electrodes placed proximal to the injury and recording the compound muscle action potential (CMAP) from the corresponding target muscle. CMAP is a useful indicator of nerve regeneration as the amplitude is determined by the number of muscle fibres innervated. The latency to the CMAP is also informative, as it measures the conduction time taken to obtain a response *(Navarro, 2016).*

The weight of muscles distal to the injured nerve is another useful outcome measure as it is proportional to the degree of innervation *(Evans et al., 1995)*. The test is easy to perform through the harvest of muscle at the end-point of the study. The muscle weight from the nerve-injured side is compared with the contralateral uninjured side.

4.1.2.3 Functional recovery

The degree of functional recovery depends on the type of injury and repair provided, but also on the complexity of outcome measures used. An example of a simple but reliable measure is the sciatic static index (SSI) which involves the analysis of static footprints by measuring the toe spread. This technique allows the assessment of the degree of functional loss *(Baptista et al., 2007)*. Other tests specifically for motor function recovery include grasping tests, rotarod tests, sciatic functional index (SFI) and gait analysis *(Navarro, 2016)*.

The return of sensory function should also be considered in nerve recovery. Such tests include von Frey hair test, nociceptive electric stimulation and incremental electrical stimulation. However, it is difficult to assess sensory improvements independent of motor because most tests require a motor response to a sensory stimulus *(Nichols et al., 2005)*.

4.1.3 Experimental lesion paradigms

Two main experimental lesion paradigms have been adopted in the field of PNI; axonotmesis which results in the damage of the nerve endoneurium but the epineurium remains intact and neurotmesis which is a complete transection of the whole nerve (Figure 1.4). Each model evokes a different type of injury corresponding to clinical conditions of PNI observed in patients *(Donaldson and Hoke, 2014, Tos et al., 2009)*. A significant shortcoming of rodent models is that their regenerative process occurs more rapidly and completely than in humans *(Donaldson and Hoke, 2014)*. To address this, prolonged deinnervation is replicated in the animals using a chronic deinnervated model. Despite animal models not completely mirroring the condition in humans, the models

have still advanced the field of PNI providing systems to study novel regenerative therapies *(Donaldson and Hoke, 2014)*.

4.1.3.1 Axonotmesis

Axonotmesis is a commonly used injury model of PNI because damage to the axon is sufficient enough to trigger Wallerian degeneration, but the supporting structures remain intact, and there will be good recovery following injury as a result *(Mazzer et al., 2008)*. This injury type also provides a low-cost model and allows comparable regeneration in a variety of animals, ranging from rodents to nonhuman primates with low inter-animal variability *(Donaldson and Hoke, 2014, Ronchi et al., 2009)*.

The disadvantage of this model is the lack of a standardised crush protocol in terms of tools used, and the number and duration of crushes *(Donaldson and Hoke, 2014)*. However, a study compared six common crush methods and determined that they all produced similar axonal damage and regeneration *(Bridge et al., 1994)*. Furthermore, the consistency of the location of the crush is an issue, but, protocols establishing precise location through the use of anatomical markers have been used *(De Koning et al., 1986)*.

4.1.3.2 Neurotmesis

Neurotmesis provides an *in vivo* model of the most severe degree of nerve damage, which would mandate surgical repair in humans *(Donaldson and Hoke, 2014)*. The model can be used to study neuronal degeneration and regeneration as the nerve is transected and then the two stumps are re-joined with epineurial sutures. Again it is an inexpensive model that provides a platform to study regeneration in a similar manner as human nerve injuries *(Donaldson and Hoke, 2014)*. The regeneration is a lot slower and less likely to lead to complete recovery in comparison to the crush model, but this aids the identification of small differences between the groups *(Tos et al., 2009)*. Therefore, this is the preferential model investigating the potential of future therapies as significant differences between experimental groups will be easier to detect *(Tos et al., 2009)*.

A disadvantage is that when a rat has undergone a nerve transection and repair it is more likely to endure autotomy, especially in the commonly studied rat sciatic nerve. This results in the loss of functional recovery measures that can be performed and in severe cases the animal may need to be culled. The rate of incidence of autotomy can vary between rat strains, being more like to occur in Brown Norway and Sprague-Dawley rats, but not Lewis rats *(Donaldson and Hoke, 2014)*.

4.1.4 Selection of nerve model

Rodents are commonly used in PNI research as they are easily housed and handled, inexpensive and large numbers of genetically identical animals can be obtained. The larger size of rats allows the study of bigger gaps than in mice.

Many different nerves in the rat are commonly used for PN studies, however, the most commonly used is the sciatic nerve due to its large size *(Varejao et al., 2004)*. Its size ensures easy surgical access and helps facilitate microsurgical injury and repair. Also the size of sciatic nerve in a rat is equivalent to the human digital nerve making it a useful model in testing human-scale repair approaches. In addition, the rat sciatic nerve is a useful model to assess motor function recovery as there are several automated behavioural tests that are applicable *(Tos et al., 2009)*.

Using the rat sciatic nerve model means the data are comparable to most of the previous literature in the PNI field, however, more importantly it is more clinically translatable as this model focuses on limb surgery which is one of the most common PNI in humans requiring surgery *(Tos et al., 2009)*.

4.1.5 The "Three Rs"

When developing *in vivo* models it is important to consider the "Three Rs" concept which is based on three principles; 1.) Replacement, which means the use of non-animal options should be considered if appropriate such as; cell cultures, human volunteers or computational models; 2.) Reduction, which means the use of methods that enable the obtainment of information from a fewer number of animals or more information from the

same number of animals and 3.) Refinement, which means the use of methods that enhance animal welfare and act to reduce pain, distress or suffering of the animals.

These concepts have been adhered to within this body of work by developing a robust *in vitro* co-culture system as an initial assay to screen a large database of drugs. The subsequent use of *in vivo* studies was only included when necessary to further pre-clinical studies that are required for drug therapies. Further to this, the most suitable *in vivo* models were used to ensure the number of animals required was reduced.

4.1.6 Aims of chapter 4

The aim of this chapter was to determine an *in vivo* model to screen the regenerative effects of drug agents in pre-clinical studies. Two models were tested; a transection and a crush to determine the different regenerative and functional outcome measures that could be evaluated from each model. An important objective was to identify a model that could provide an injury detrimental to function but with a relatively short recovery period, to enable both clinically relevant but also rapid screening of drug therapies. The ideal PNI models were optimised and utilised to screen identified drugs. As ibuprofen demonstrated positive effects *in vivo* in previous literature, it was used in pilot studies to determine the effectiveness of the models in measuring regeneration and functional recovery. Also, as ibuprofen elicited the greatest effect on neurite growth in chapter 3, another aim included investigating whether there is a correlation between the effects seen in the co-culture *in vitro* model and the effect seen *in vivo*. This led to the objective of determining whether the *in vitro* model could be used as a predictive tool of *the in vivo* outcomes.

4.2 Results:

4.2.1 Automatic axon count protocol

Following nerve injury and repair, rat sciatic nerves were dissected and transverse sections were assessed to determine the number of axons present in specific regions of the proximal and distal stumps. To ensure reproducibility and replicability of axon number quantification; a robust protocol was needed. An automated protocol was developed using high contrast tile-scans taken on a LSM confocal microscope and analysed using Volocity software. The analytical software protocol consisted of multiple stages; firstly the region of interest was manually selected by drawing a line at the interface between the perineurium and endoneurium, which allowed the identification of individual axons by automated selection of all objects with a fluorescence intensity above a minimum threshold (Figure 4.1 (a), (b)). Extra analysis tasks were then added to exclude any objects that were not axons by size or any objects that were touching. In order to ensure that the automated protocol consistently provided reliable data, 3 areas on each section were selected at random and the number of axons within the area were counted manually and compared with the automated count. If the two counts matched the automatic count was accepted (Figure 4.1 (c) and (d)). If there was a difference of more than 10% then the parameters of the automated analysis were adjusted accordingly. This ensured that reliable data were obtained from the process and that any variability between samples that may have skewed the automated data were accounted for.

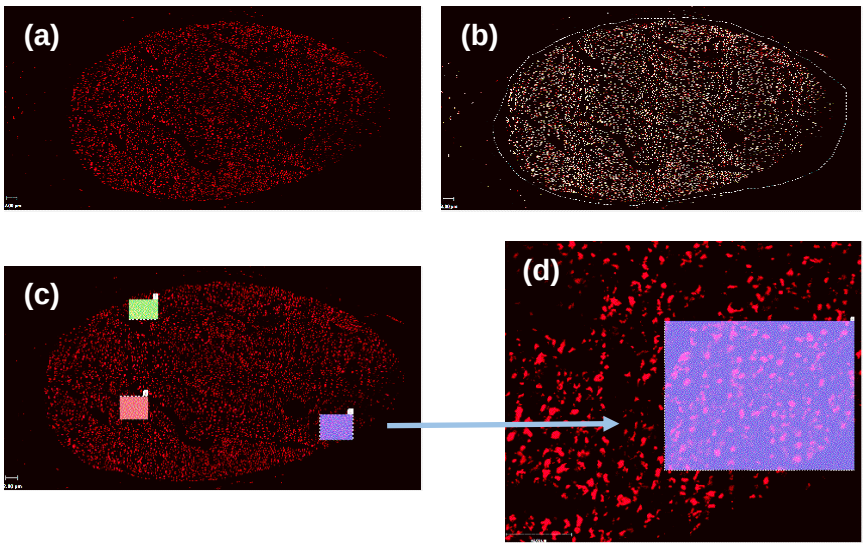

Figure 4.1: Axon count protocol optimisation. *Tile scans taken on a LSM confocal microscope and analysed using an automated quantification protocol on the Volocity software which identified individual neurofilament-positive axons from the entire section. The endoneurium was selected as the region of interest, then automated identification of axons was performed using a set of software protocols (a), (b) and randomised areas selected for manual counts to ensure accuracy of the count (c), (d).*

4.2.2 Optimisation of electrophysiology protocol

The muscle response to stimulation (1.2 mA) of the proximal nerve was investigated using electrophysiology. Compound muscle action potentials (CMAP) were recorded from the gastrocnemius muscle in the rat to develop a consistent protocol. Different positions of both the stimulating and recording electrodes were analysed. The position of the recording and stimulating electrodes impacted the CMAP, latency and area under the curve (AUC) of the trace. The orientation of the stimulating electrode had an effect on the CMAP and latency but not the AUC when positioned on top of the nerve and beneath (Figure 4.3). On the contrary, the position of recording electrode had no effect on the latency. Also if the electrode was placed higher or in the middle of the muscle there was no difference in the CMAP, however, the CMAP reduced when the electrode was moved further away from the stimulated nerve (Figure 4.2). The AUC reduced if the electrode was placed in the middle or the lower part the muscle.

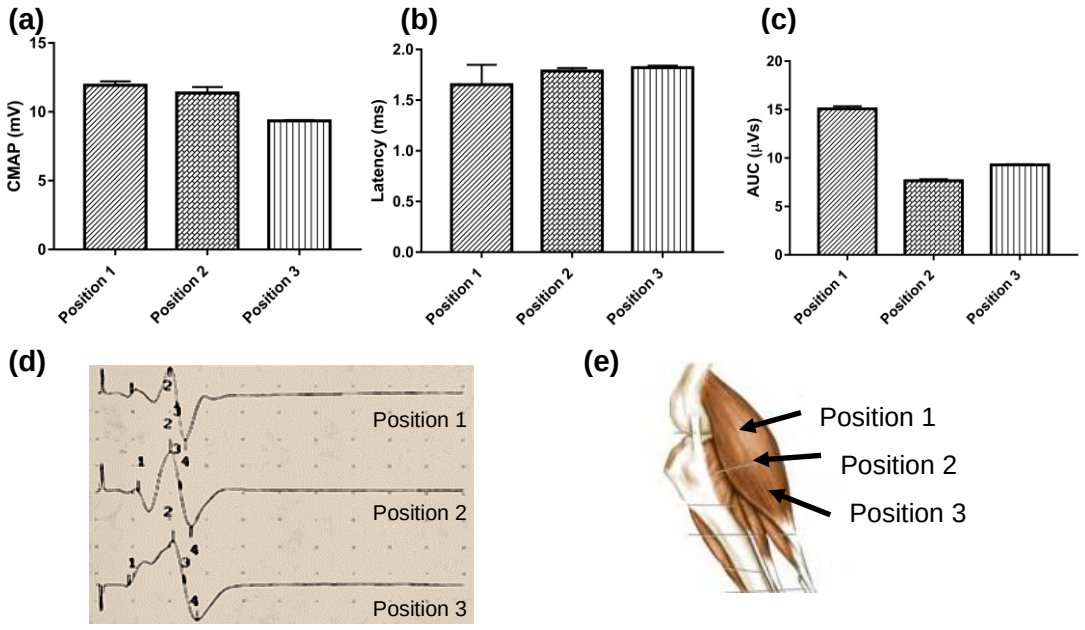

Figure 4.2: Position of the recording electrode in the gastrocnemius muscle. *Changing the position of the recording electrode had an effect on the CMAP but not the latency, determined from the electrophysiology trace recording (d).The electrode was placed at the top, middle and bottom of the muscle (e). The CMAP decreased as the electrode was moved further away from the nerve (a), this had no effect on the latency (b) but a clear effect on the AUC (c). N=3, mean ± SEM for each condition.*

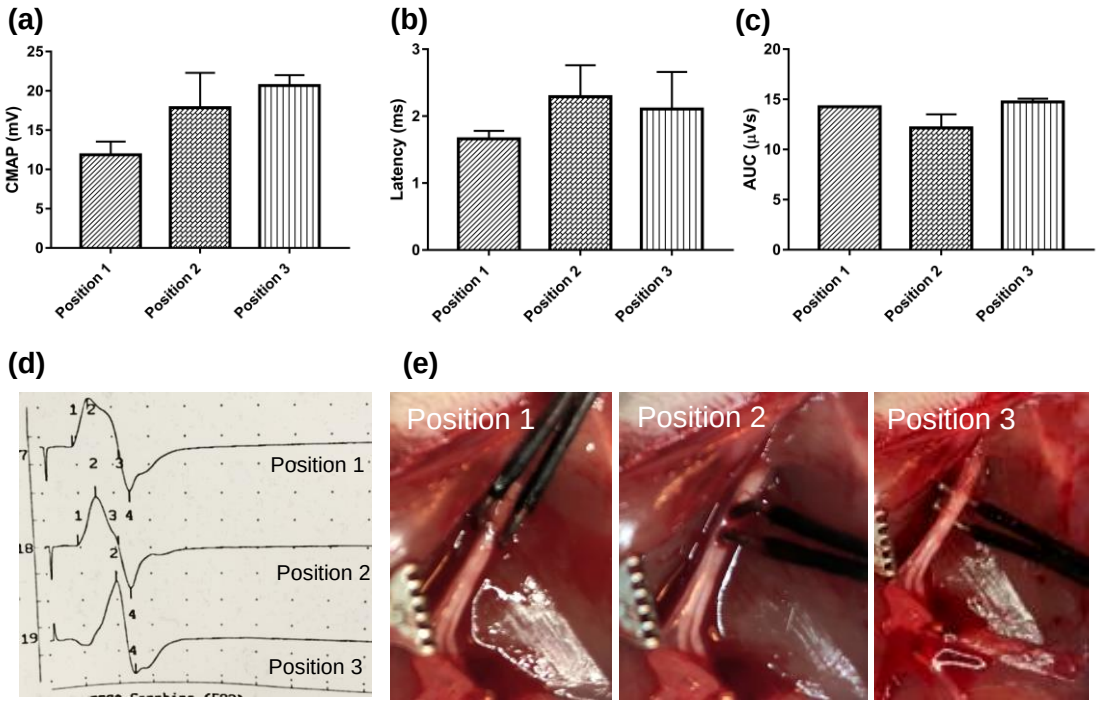

Figure 4.3: Position of the stimulating electrode on the surface of the sciatic nerve. *Changing the position of the stimulating electrode had an effect on the CMAP and the latency, determined from the electrophysiology trace recording (d).The electrode was placed in different positions on the nerve (e). The CMAP increased when the electrode was repositioned and when the nerve was stimulated from beneath (a) the same was seen with the latency (b) but a little effect on the AUC (c). N=3, mean ± SEM for each condition.*

From these findings position 3 of the stimulating electrode (Figure 4.3 (e)) and position 2 of the recording electrode (Figure 4.2 (e)) were used subsequently. The rationale for these positions was the minimal SEM seen between the recordings at these positions. Also a bigger CMAP was reached when conducting electrophysiology using position 3 of the stimulating electrode which provides a much clearer outcome measure.

Following the optimisation of these outcome measures the suitability of an animal model to screen drugs for PNI was investigated. The regenerative and functional outcomes were analysed following two common nerve injury models; a transection injury with primary repair and a crush injury. Other functional outcomes used in this study including von Frey, SSI and gastrocnemius muscle mass, which were conducted following standard published methods *(Bervar, 2000, Arguis et al., 2008)*.

4.2.3 Comparison between a transection and crush injury model

4.2.3.1 Quantification of neuronal growth

Rat sciatic nerves were dissected at day 1, 2, 7 and 21 days post-injury in a transection model and at 28 days in the crush injury. Transverse sections with 10 µm thickness were taken to determine axon number as a quantification method to assess neuronal growth. The neurofilament-positive axons present in the proximal and distal stumps were quantified using the protocol outlined in section 4.2.1.

Following a transection injury the analysis demonstrated an initial loss in axon number 24 h post-surgery, however, by day 2 there was an increase in the number of neurofilament-positive axons in the distal stump which continued to increase over time (Figure 4.4 (a)). Moreover, it was found that the number of axons in the distal stump exceeded the quantity of the axons in the proximal stump in the same animal at 21 days post-surgery (~110%) (Figure 4.4 (b)).

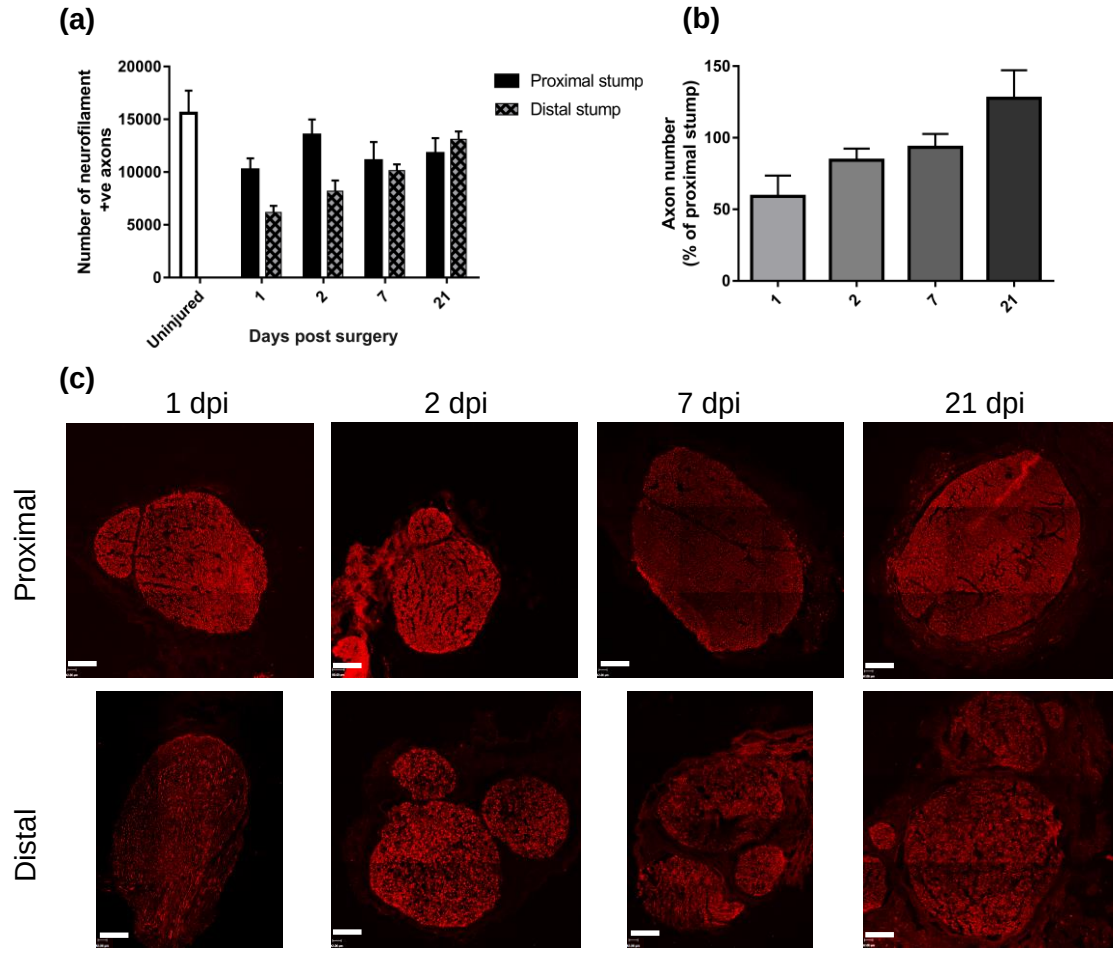

Figure 4.4: Axon number in the distal stump increased over time in a transection injury model in rat sciatic nerve. *Axons were quantified by counting the number of neurofilament-positive cells in the proximal stump and distal stump. The number of axons increased from 1 day post-injury (dpi) to 21 dpi in the distal stump (a). By 21 dpi the number of axons in the distal stump had exceeded the proximal stump (b). Micrographs are 10 µm transverse sections showing neurofilament positive neurites (c). Scale bar = 100 µm. N = 3, mean ± SEM for each condition.*

The same effect was seen in the analysis following a crush injury with a loss in axon number following surgery (Figure 4.5 (a)). In addition, as sections were taken more distal to the injury site the number of axons increased (Figure 4.5 (b)).

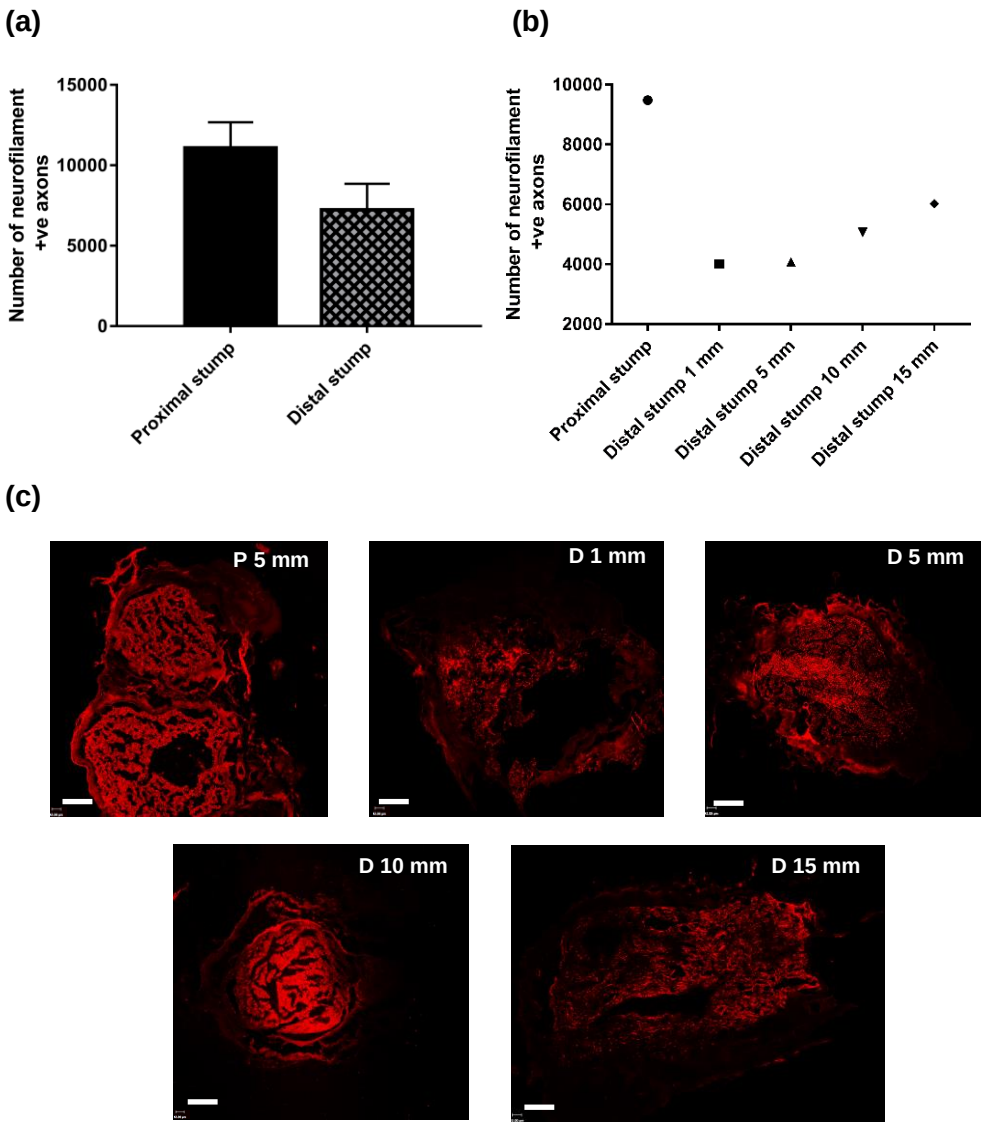

Figure 4.5: Axon number following a crush injury model in rat sciatic nerve. *Axons were quantified by counting the number of neurofilament-positive cells in the proximal stump and distal stump. The number of axons decreased following injury (a). The number of axons increased the more distal to the injury the sections were taken (b). P = proximal, D = distal. Micrographs are 10 µm transverse sections showing neurofilament positive neurites (c). Scale bar = 100 µm. N = 3 (a), N=1 (b), mean ± SEM for each condition.*

From the automated count on Volocity the cross-sectional area of each individual axon was also quantified from the immunohistochemical staining with neurofilament which was used to obtain axon diameter. Following the transection injury the mean axon diameter did not change from 1 dpi to 21 dpi in the proximal or distal stumps (~4 µm for all groups) (Figure 4.6).

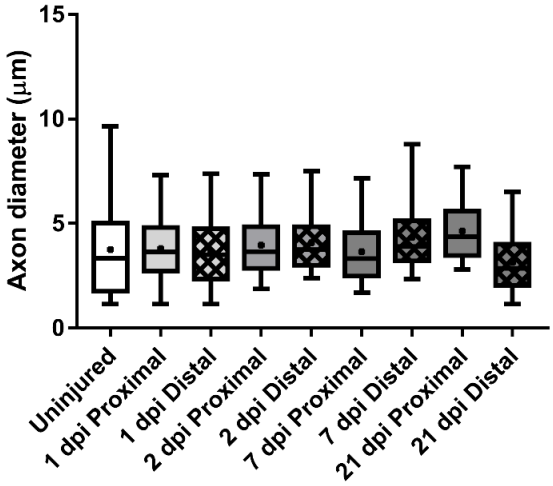

Figure 4.6: Axon diameter in the proximal and distal stump in a transection injury model in rat sciatic nerve. *Axon diameter of the neurofilament- positive cells was quantified in the proximal stump and distal stump at various days post injury (dpi). No changes in the axon diameter were observed between the groups. N=3, box plots showing distribution of axon diameter with boxes extending from the 2nd to 98th percentiles , + indicates mean, data are 6000-12000 axons from 3 rats.*

4.2.3.2 Functional outcomes

Motor recovery was investigated using techniques that study muscle reinnervation such as; electrophysiology, muscle mass and SSI, and sensory improvements were explored using von Frey. Analysis was conducted at the 21 day end point in the transection injury and the 28 day end point in the crush injury. In both models there was a reduction in function following injury. This function returned to baseline within 28 days in the crush injury model, but no recovery was seen at 21 days in the transection model.

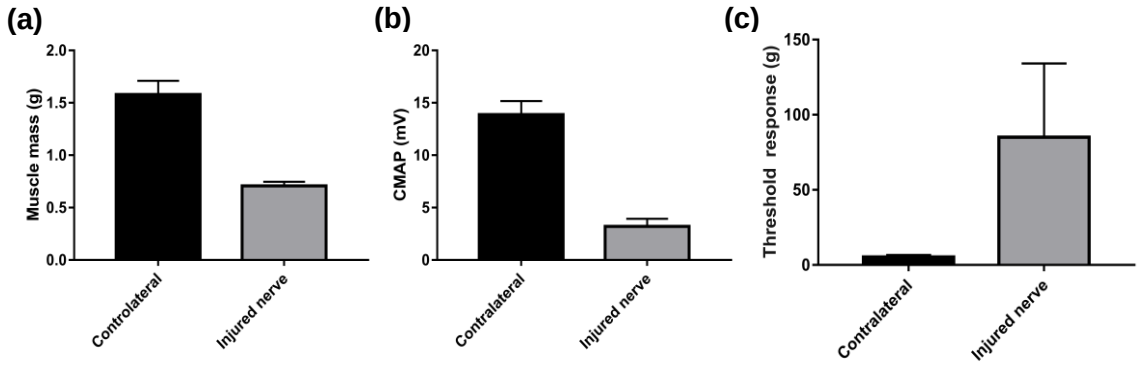

Figure 4.7: Functional outcomes 21 days following a transection injury with primary repair in a rat sciatic nerve. *The function on the nerve-injury side was reduced in comparison with the uninjured side, demonstrated in all outcome measures. The muscle mass and CMAP was reduced (a), (b). The von Frey threshold response increased in the nerve-injury side (c). N=3, mean ± SEM for each condition.*

Motor function had declined by 21 days post-surgery in the transection model demonstrated by a reduction of CMAP by ~80%. There was also a reduction in the gastrocnemius muscle weight by ~60%, both measurements were in comparison to the uninjured, contralateral hind paw (Figure 4.7 (a), (b)). Furthermore, sensation was also lost by 21 days following injury, as a much higher threshold (g) stimulus was needed to elicit a paw retraction response from all animals (Figure 4.7 (c)).

Following the crush injury the muscle mass had reduced in the nerve-injured hind leg in comparison to the contralateral uninjured side in all animals (Figure 4.8 (b)). The SSI and sensory threshold response were both reduced in the nerve-injured side in comparison with the contralateral side following injury but returned to baseline after 28 days, demonstrating full recovery of function (Figure 4.8 (a), (c)). The CMAP had reduced with a corresponding increase in latency following injury. A higher stimulus intensity was needed to achieve a supramaximal response in the injured nerve in comparison to the contralateral (Figure 4.9).

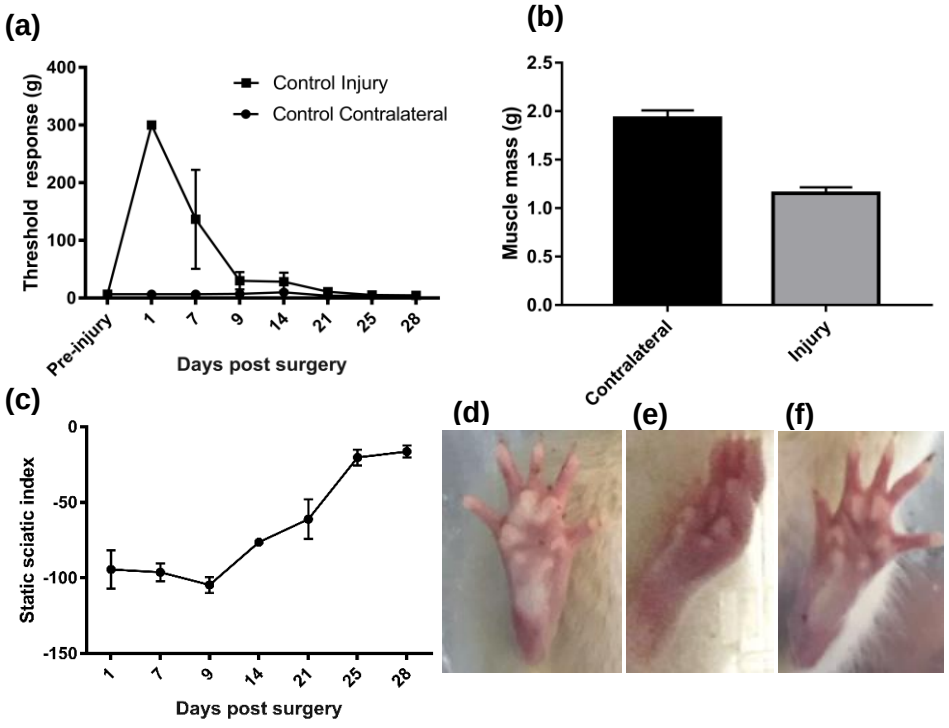

Figure 4.8: Functional recovery following a crush injury in a rat sciatic nerve. *Von Frey (a) and SSI (c) analysis demonstrated that sensory function was restored by 28 days post-injury. Hind paw images used to conduct SSI quantitation in contralateral paw (d), at 1dpi (e) and 28 dpi (f). The mass of the gastrocnemius muscle on the injured side was not restored back to that seen in the contralateral side (b). N=3, mean ± SEM.*

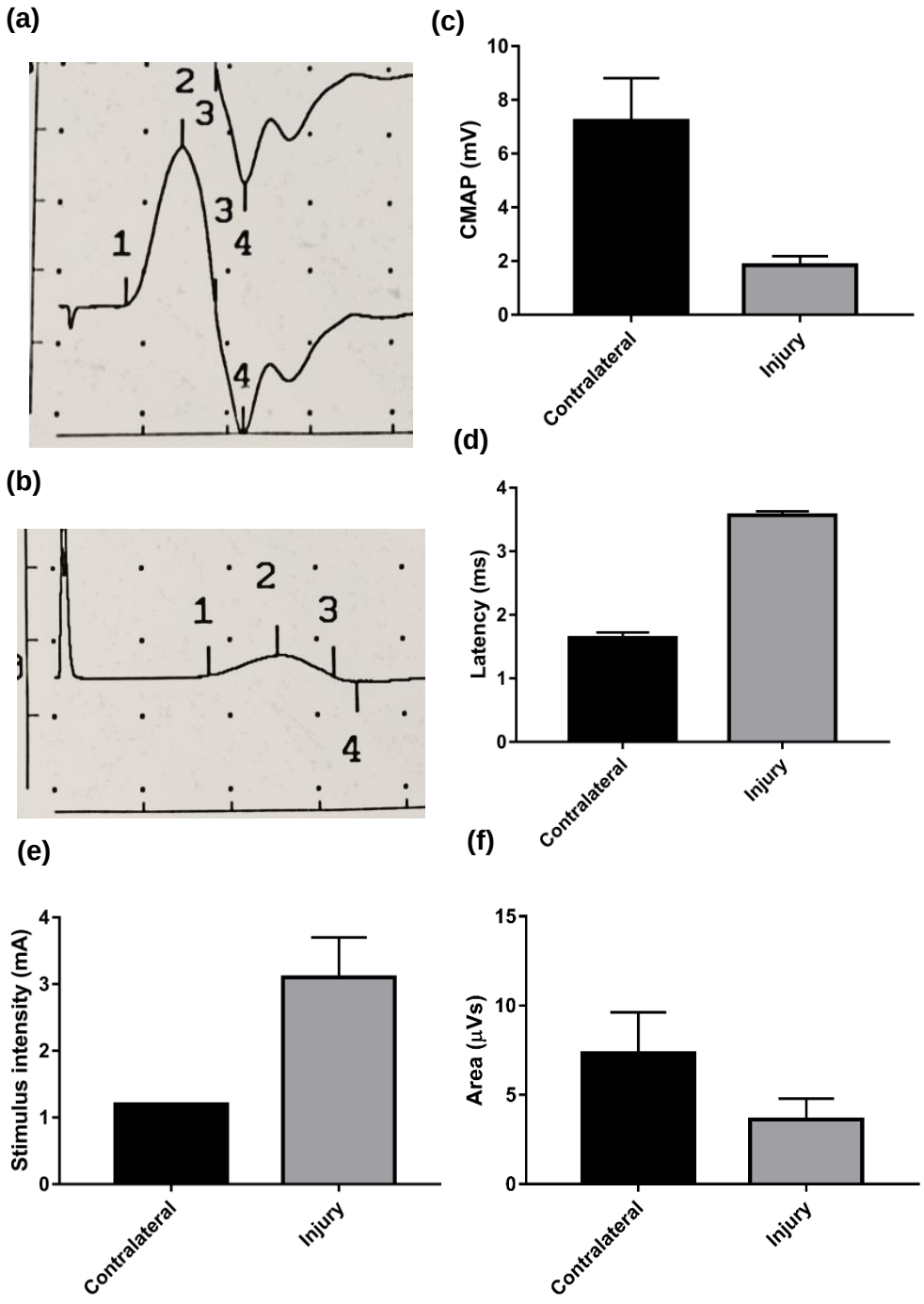

Figure 4.9: Electrophysiological evaluation of sciatic nerve 28 days after a crush injury. *The sciatic nerve was stimulated proximal to the repair site and the CMAP was recorded from the gastrocnemius muscle. The electrophysiological traces for the contralateral (a) and injured nerve (b). The CMAP amplitude reduced in the injury side in comparison with the contralateral non-injured side (**c**). Furthermore the latency had increased in the injured side (d), the stimulus intensity needed to produce a response increased in the injured side (e), therefore, overall there was a corresponding reduction in the area under the curve in the trace (f). N=3, means ± SEM.*

4.2.3.3 Vascularisation following a transection injury

Vascularisation was examined via immunohistochemical staining of transverse sections for RECA-1. Analysis revealed the presence of blood vessels throughout the injured nerves in both the proximal and distal sections, however, there was a higher number of blood vessels in the proximal stump. Trends were also seen in the number of blood vessels present at the various time points following the injury, however, no clear trends could be established. Vasculature in the uninjured, contralateral nerves was also examined, revealing approximately 26 blood vessels per nerve with a mean diameter of 9.5 µm (Figure 4.10).

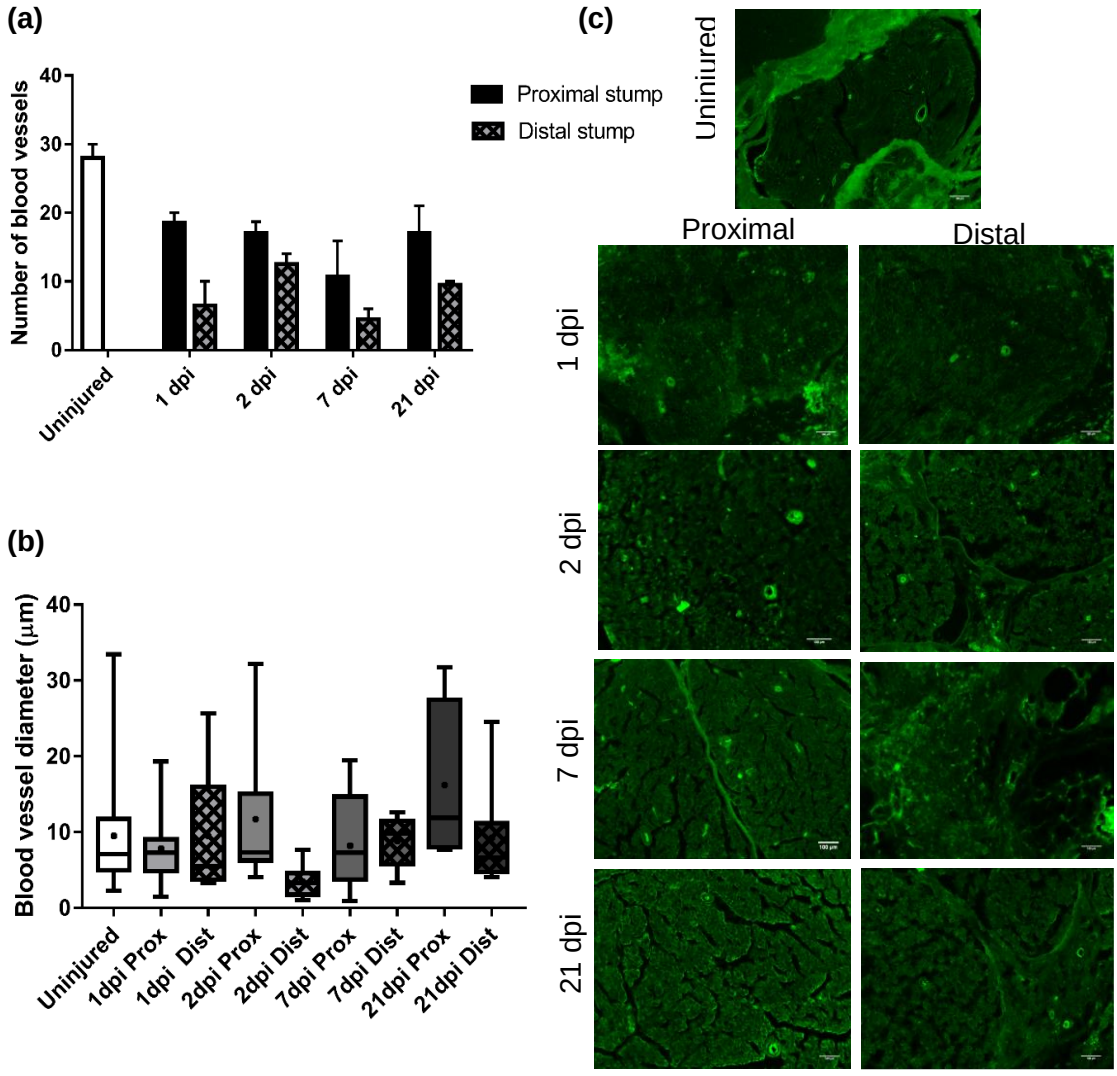

Figure 4.10: Vasculature changes at various time points following a transection injury. *Quantitative analysis of number (a) and diameter (b) of blood vessels by RECA-1 (green) immunostained 10 µm transverse sections from the proximal and distal stump. N=3, mean ± SEM for each condition. Box plots show the distribution of blood vessel diameter with boxes extending from the max to min, + indicates mean.*

From the pilot studies it was found that the crush injury model provided a more rapid approach to screen potential drug therapies, as the functional recovery returned to baseline within 28 days. This didn't occur within the transection model and would require a longer period of time, however, it is still a beneficial model for screening drugs in PNI as it enables the evaluation of drug therapies in a more severe injury model. The exploration of these two models helped identify suitable outcome measures to evaluate the regenerative capacity of drug therapies. In both models the histological analysis demonstrated a clear loss of axons and so both time periods, 21 and 28 days, in the transection and crush model respectively would provide a platform in which a change in the axon number could be identified. Histology methods were also used to investigate vascularisation and cell phenotype changes following a PNI, however, the immunohistochemistry images of biomarkers s100 and c-Jun for Schwann cells did provide clear results and would need quantifying (shown in appendix 2). In addition, initial pilot studies using qPCR to evaluate Schwan cell phenotype gave promising results, however, there were insufficient data to study in this body of work (data in appendix 2). Furthermore, the functional recovery could be studied with the techniques utilised in the pilot studies, however, it was found that it is more beneficial to conduct the outcome measures at various time points throughout the study and not just at the end-point. This is particularly useful in the crush injury model because the function returned to baseline in all animals, so improvements in function with drug treatments may be missed if only the end point was considered. Electrophysiology, von Frey, SSI and muscle mass will be used in future *in vivo* studies in this body of work.

4.2.4 Transection and crush injury treated with ibuprofen delivered through osmotic pumps

4.2.4.1 Quantification of neuronal growth

Rat sciatic nerves were dissected at 21 days in the transection model and 28 days in the crush injury model. 10 μm transverse sections were taken from the proximal and

distal segments of the nerve 5 mm away from the injury site to determine axon number as a quantification method to assess neuronal growth. The neurofilament-positive axons present were quantified using the protocol outlined in section 4.2.1. There was a higher number of axons in the distal stump with ibuprofen treatment (7µg and 70µg) in comparison with the no drug control group in the transection model (Figure 4.11) but this trend was not as prominent in the crush model (Figure 4.12). However, a dose of 7 µg/day ibuprofen increased the number of axons in the distal section of nerve as a percentage of the proximal in comparison with the no drug control group in the crush model but no statistical significance was seen (Figure 4.12 (b)).

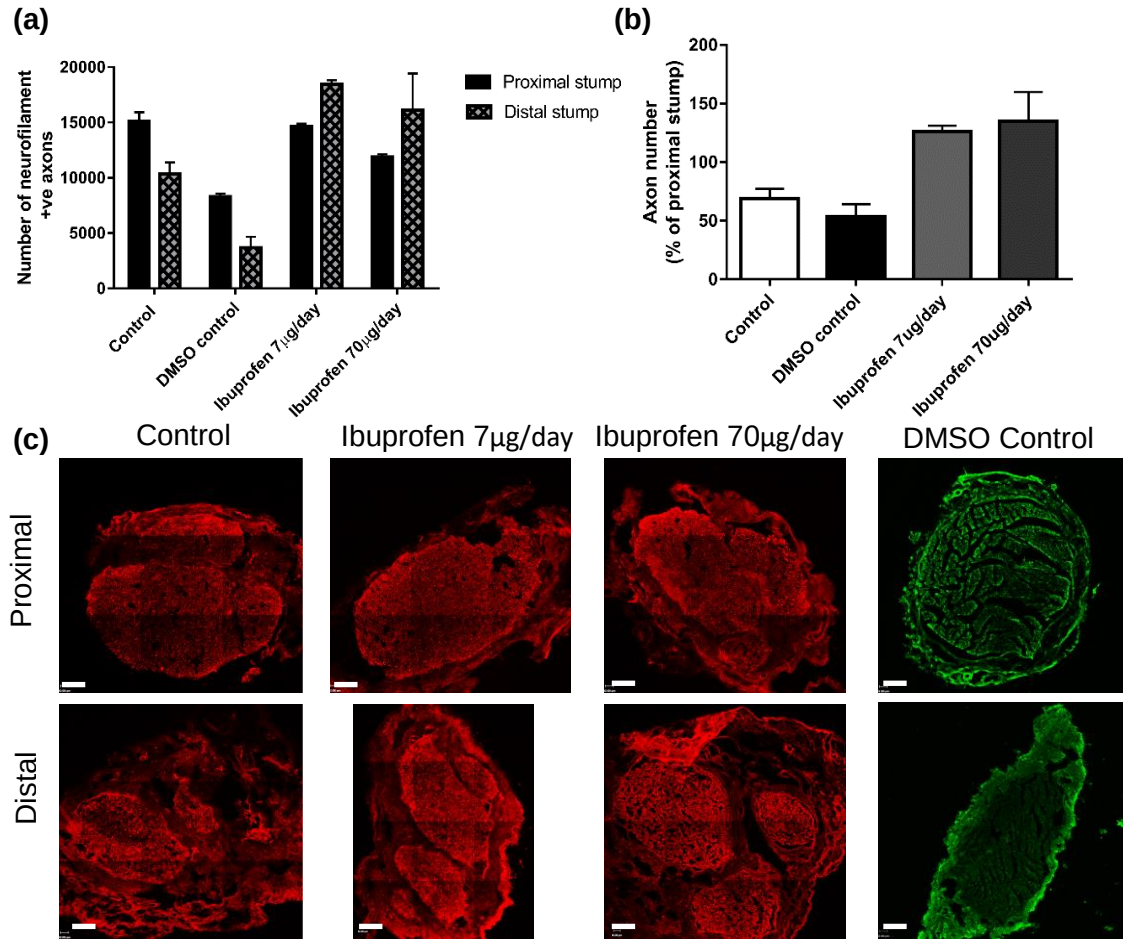

Figure 4.11: Quantification of axons in the proximal and distal stump following drug treatment in the transection model. *The number of axons in the distal stumps increases with ibuprofen treatment in comparison with the no drug control (a). The axon counts were also expressed as a percentage of the proximal stump in each animal (b). Micrographs are transverse sections showing neurofilament positive neurites at 5 mm proximal and distal to the injury site (c). Scale bar = 100 µm. N=3, means ± SEM.*

A similar effect was observed in the transection model with the number of axons in the distal stump exceeded the quantity of the axons in the proximal stump with both doses of ibuprofen (121% at 7 µg/day and 150% at 70 µg/day) (Figure 4.11 (b)).

Due to the poor solubility of ibuprofen, DMSO was used to dissolve the drug into the saline vehicle to load the osmotic pumps. Therefore, to determine its effects, 10% (v/v) DMSO was given to a separate group for 3 weeks at a release rate of 0.11 µl/hr. Analysis demonstrated that DMSO resulted in a loss of axons in the distal and proximal stumps. The number of axons were lower (~15%) than the no drug control group. Due to the negative effects of DMSO its use was avoided in the crush model study and the ibuprofen sodium salt was used as it is more soluble.

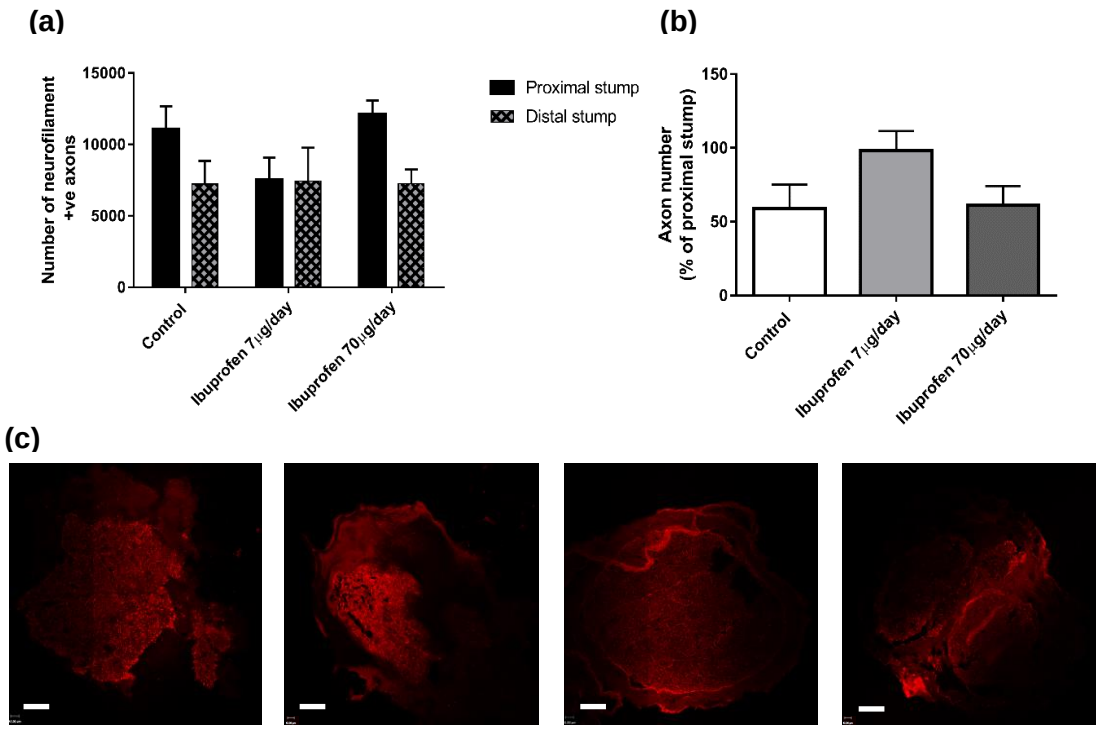

Figure 4.12: Axon number in a crush injury in a rat sciatic nerve. *Axons were quantified by counting the number of neurofilament-positive cells in transverse sections through the proximal and distal nerve segments 5 mm away from the crush site. There was no difference in the number of axons in the distal nerve between the groups (a). However, a dose of 7 µg/day ibuprofen increased the number of axons in the distal nerve segment as a percentage of the proximal in comparison with the no drug control (b). Micrographs are 10 µm transverse sections showing neurofilament positive neurites (c). Scale bar = 100 µm. N=3 (no drug control) N=2 (ibuprofen treatment groups), mean ± SEM for each condition.*

Furthermore, the mean axon diameter didn't change between the different groups in the proximal or distal stumps (~4 µm). In the transection injury the largest axon diameter in the distal stump increased slightly by ~3 µm with 7 µg/day and 70 µg/day ibuprofen treatment (Figure 4.17(a)). In the crush model the mean axon diameter didn't change between the different groups in the proximal stump, however, the mean axon diameter was larger in the distal stump with 7 µg/day ibuprofen treatment.

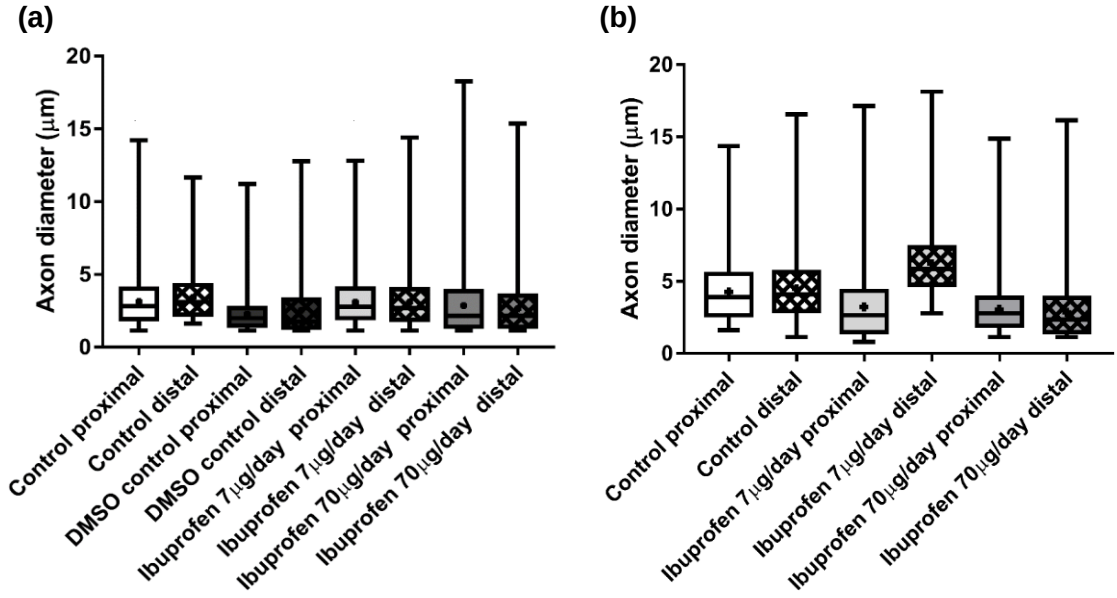

Figure 4.13: Axon diameter in the proximal and distal stump in a transection and crush injury model in rat sciatic nerve. *Axon diameter of the neurofilament-positive cells in the proximal stump and distal stump were measured. Minimal differences in the axon dimeter were seen between the groups in the transection model (a) and the crush model (b). N = 3 (no drug control), N=2 (ibuprofen treatment groups) (b), box plots show min and max, + indicates mean, data are 6000-12000 axons from 2-3 rats.*

4.2.4.2 Functional recovery

Motor and sensory recovery was studied at the 21 day end point in the transection model using muscle weight, static sciatic index, electrophysiology, and von Frey analysis. Sensation had recovered better with 7 µg/day treatment but not with 70 µg/day in comparison with the no drug control as demonstrated by a reduction in the threshold (g) needed to achieve a paw withdrawal response. The sensory recovery of the DMSO group was less than that seen with no drug treatment (Figure 4.14 (a)). The gastrocnemius muscle was harvested and weighed immediately. There was no

difference in muscle mass between any of the groups (Figure 4.14 (b)). Furthermore, no difference was seen between the groups with the SSI as they all still presented with a SSI of -100 (Figure 4.15).

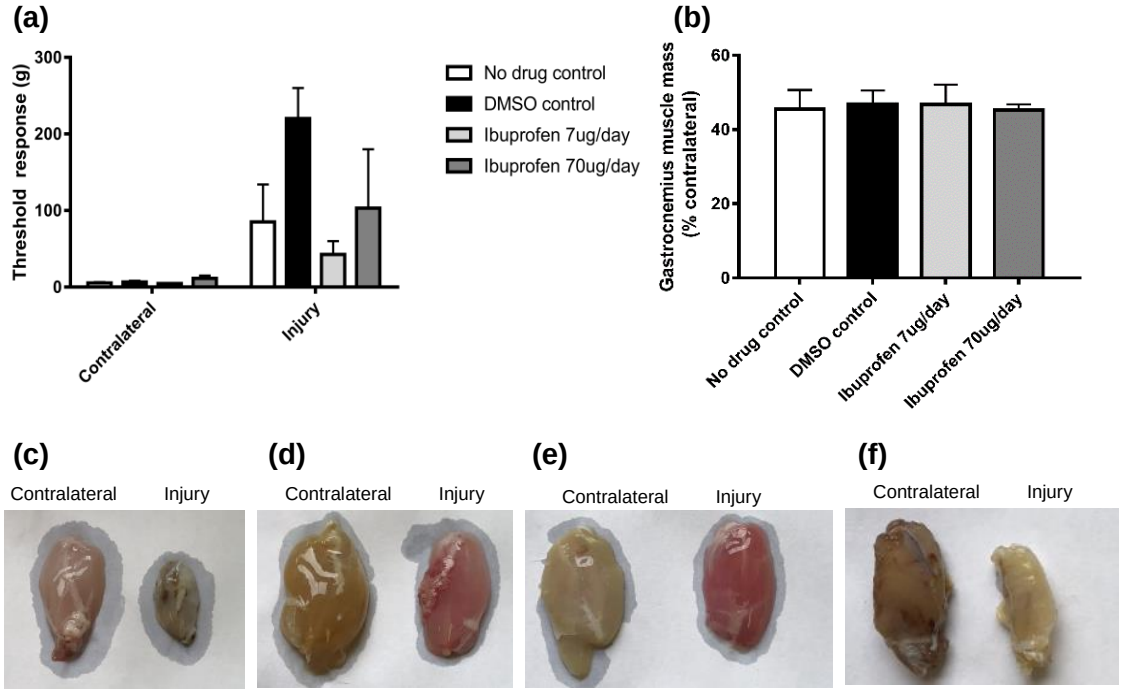

Figure 4.14: Functional recovery following a transection injury in a rat sciatic nerve. *A reduction in the threshold sensory recovery was seen with ibuprofen treatment at a dose of 7µg/day but not with 70µg/day using von Frey as an outcome measure (a). No difference was seen between the groups with muscle mass (b). Images of the harvested gastrocnemius muscle from the right (uninjured) and left (injured) hind legs from the no drug control (c), 7µg/day ibuprofen (d) 70µg/day ibuprofen (e) and DMSO control (f) groups. N=3, mean ± SEM.*

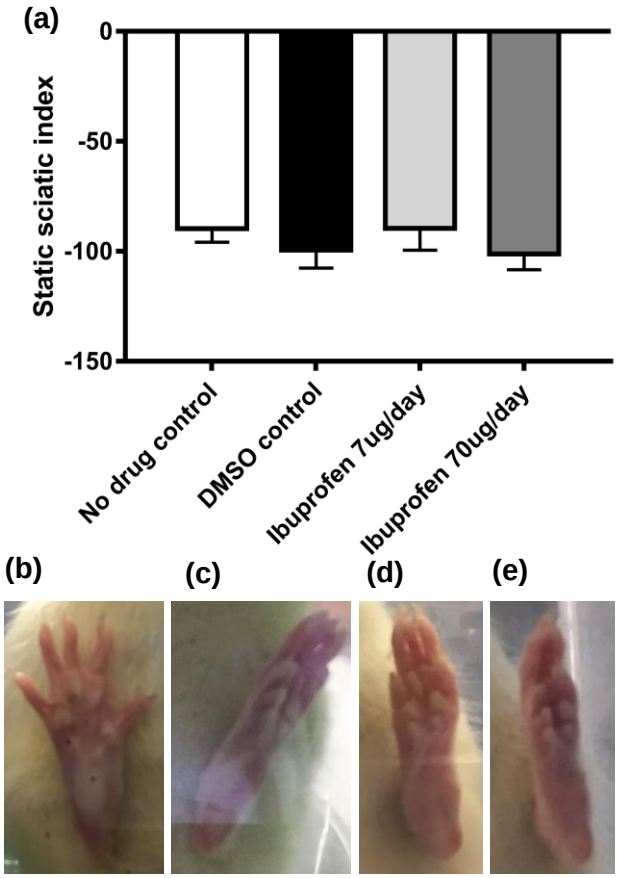

Figure 4.15: SSI following a transection injury in a rat sciatic nerve. *A small difference in the SSI was seen between the groups (a). Hind paw images used to conduct SSI quantitation; no drug treatment (b), DMSO (c), ibuprofen 7 µg/day (d) and ibuprofen 70 µg/day (e). N=3, means ± SEM.*

CMAP was recorded from the contralateral side and injured side in all animals. A dose of 7 µg/day and 70 µg/day ibuprofen elicited a CMAP slightly higher to that seen with the no drug control group. Moreover, the groups treated with either dose of ibuprofen needed a lower stimulus intensity to get a response. There were no differences seen in the latency between these three groups. On the contrary, the DMSO group presented a higher CMAP but also a higher latency and stimulus intensity than all groups (Figure 4.16)

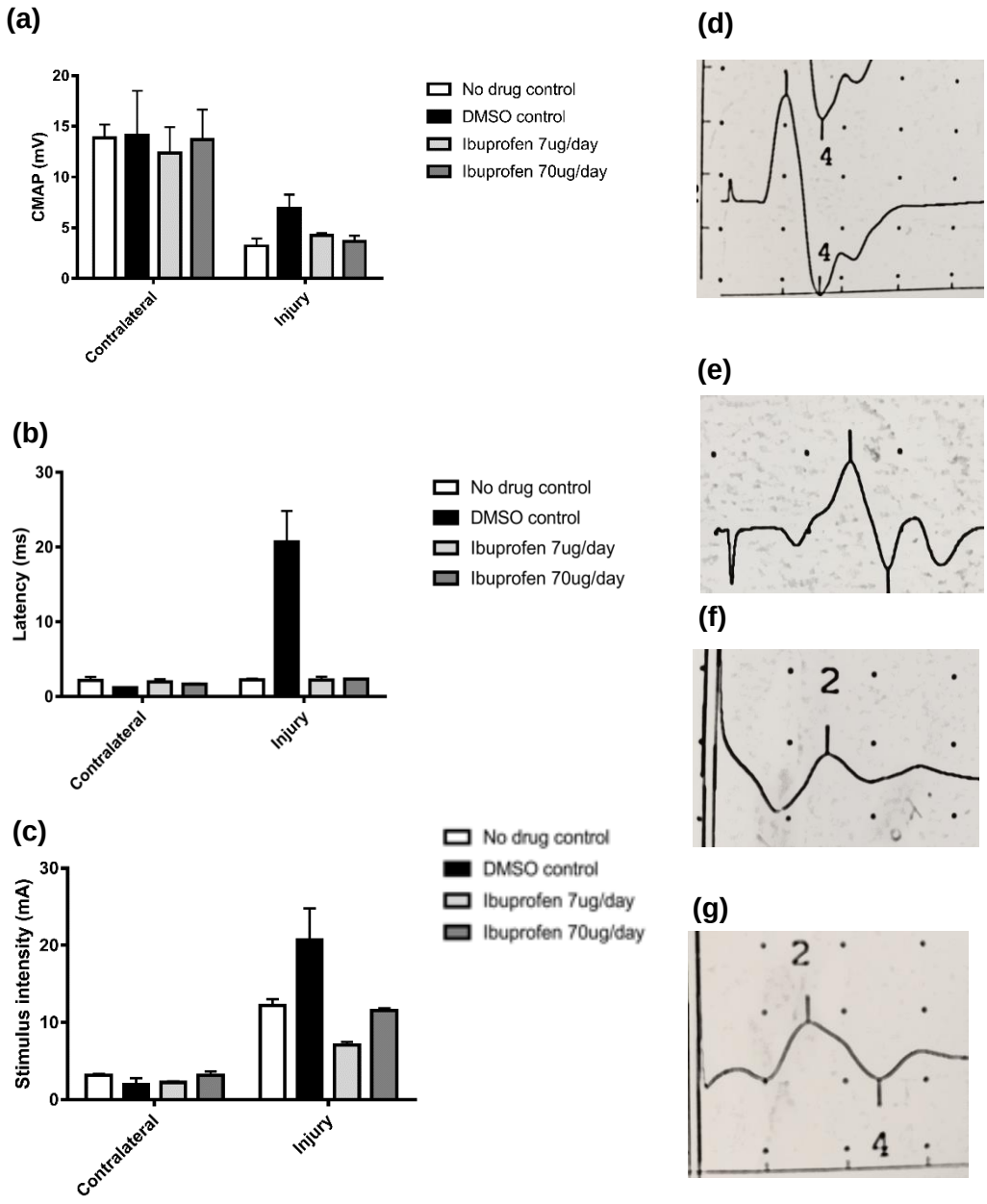

Figure 4.16: Electrophysiological evaluation of sciatic nerve 21 days after a transection injury in the sciatic nerve. *The sciatic nerve was stimulated proximal to the repair site and the CMAP was recorded from the gastrocnemius muscle. The CMAP amplitude increased in the ibuprofen 7 µg/day, ibuprofen 70 µg/day and DMSO control group (a). No difference were seen between the latencies with ibuprofen treatment in comparison to the no drug controls (b).The stimulus intensity reduced with both ibuprofen doses (c).The electrophysiological traces for the no drug treatment (d) DMSO control group (e), ibuprofen 7 µg/day (f) and ibuprofen 70 µg/day (g). N=3, means ± SEM.*

Functional recovery was studied at the 28 day end point in the crush injury model using electrophysiology and muscle weight, whereas the SSI and von Frey analysis was conducted throughout the experiment every 2-3 days. Sensation was recovered in all animals by 28 days post-injury, however, the animals that received 7 µg/day treatment

of ibuprofen recovered quicker in comparison with no drug treatment (Figure 4.17). Furthermore, the response threshold was lower with 70 µg/day treatment of ibuprofen in comparison with the control from day 4 until day 16 dpi, but was the same as the no drug control from 21 days post-injury. The gastrocnemius muscle was harvested and weighed immediately. Both 7 µg/day ibuprofen and 70 µg/day ibuprofen elicited an increase in the muscle mass as a percentage of the contralateral in comparison with the no drug control (Figure 4.18). Furthermore, recovery was seen with ibuprofen treatment at a dose of 7µg/day but not with 70µg/day using SSI as an outcome measure (Figure 4.19).

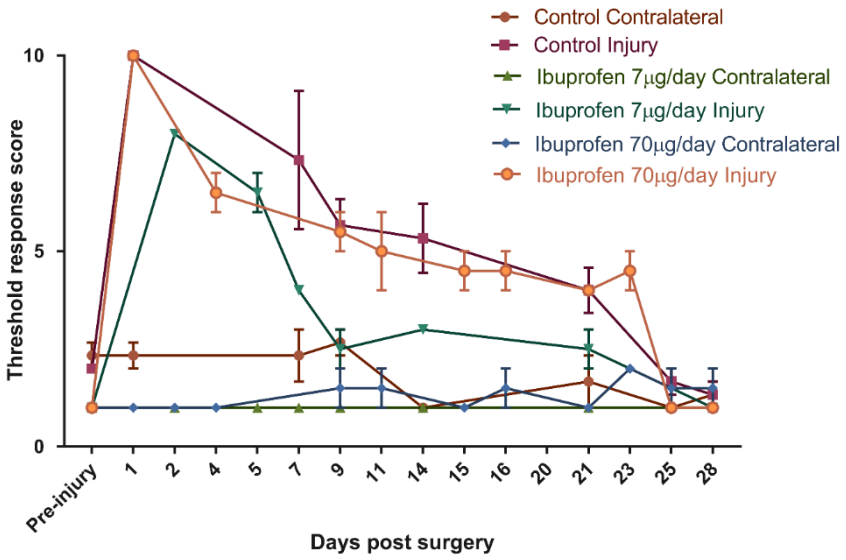

Figure 4.17: ***Sensory recovery following a crush injury in a rat sciatic nerve.*** *Sensory recovery improved with ibuprofen treatment at a dose of 7µg/day by 28 days following injury, but not with 70µg/day ibuprofen in comparison to the no dug treatment control, using von Frey as an outcome measure. N=3, (no drug control) N=2 (ibuprofen treatment groups), mean ± SEM.*

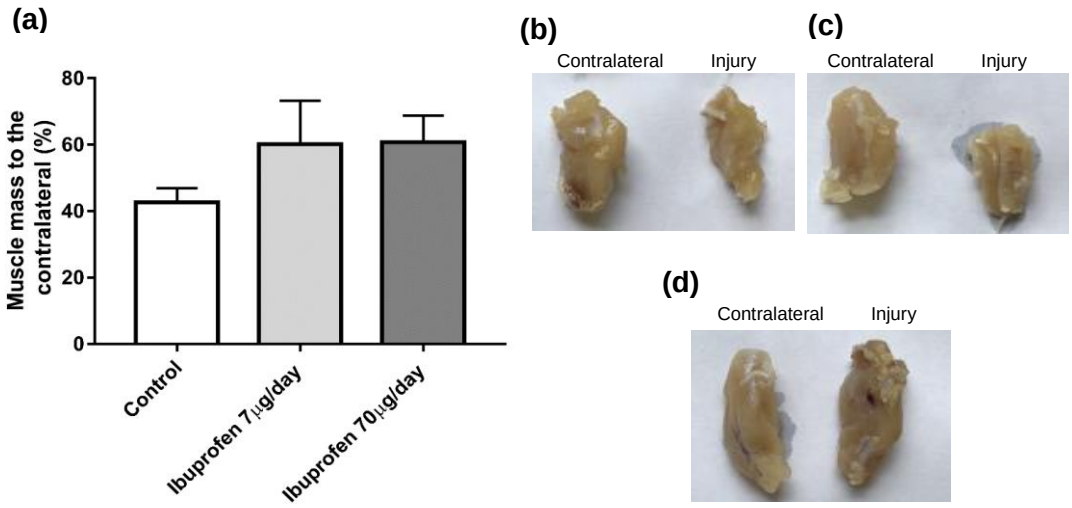

***Figure 4.18:* Gastrocnemius muscle mass following a crush injury in a rat sciatic nerve.** *An increase in muscle mass was seen with an ibuprofen treatment at a dose of 7μg/day and 70μg/day in comparison with the no drug treatment (a). Images of the harvested gastrocnemius muscle from the right (uninjured) and left (injured) hind legs from the no drug control (b), 7μg/day ibuprofen (c) and 70μg/day ibuprofen (d) groups. N=3 (no drug control) N=2 (ibuprofen treatment groups), mean ± SEM.*

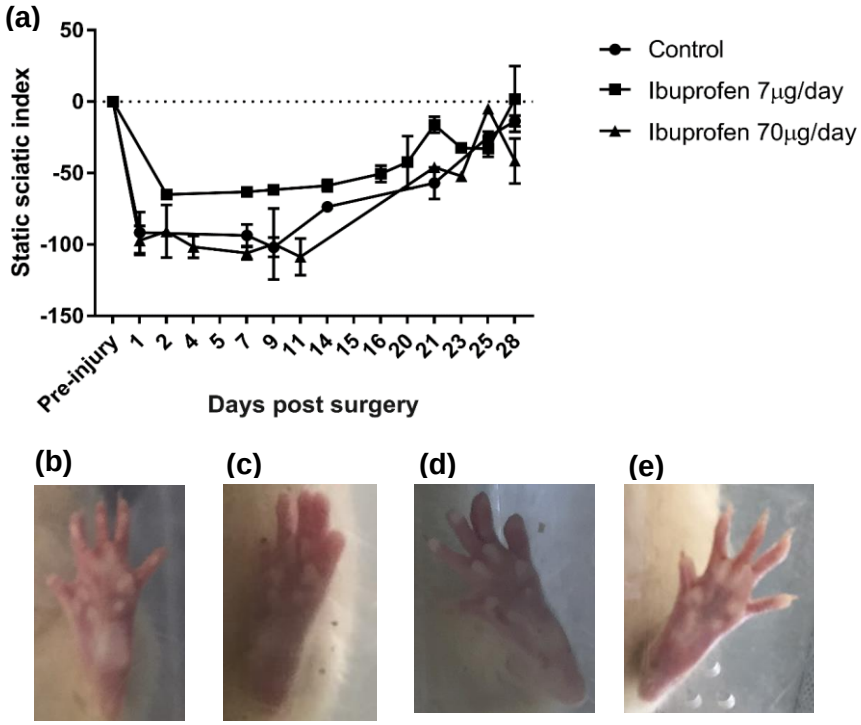

***Figure 4.19:* SSI following a crush injury in a rat sciatic nerve.** *A dose of 7μg/day but not with 70μg/day elicited a much quicker recovery of function through SSI analysis in comparison to the no drug treatment (a). Hind paw images used to conduct SSI quantitation; healthy nerve (b), no drug treatment (c), ibuprofen 7 μg/day (d) and ibuprofen 70 μg/day (e). N=3 (no drug control) N=2 (ibuprofen treatment groups), means ± SEM.*

CMAP was recorded from the contralateral side and injured side in all animals. Both doses of ibuprofen elicited a CMAP similar to that seen with the no drug treatment (Figure 4.20 (a)). However, the latency was reduced in both groups with ibuprofen treatment in comparison with the no drug control group (Figure 4.20 (b)).

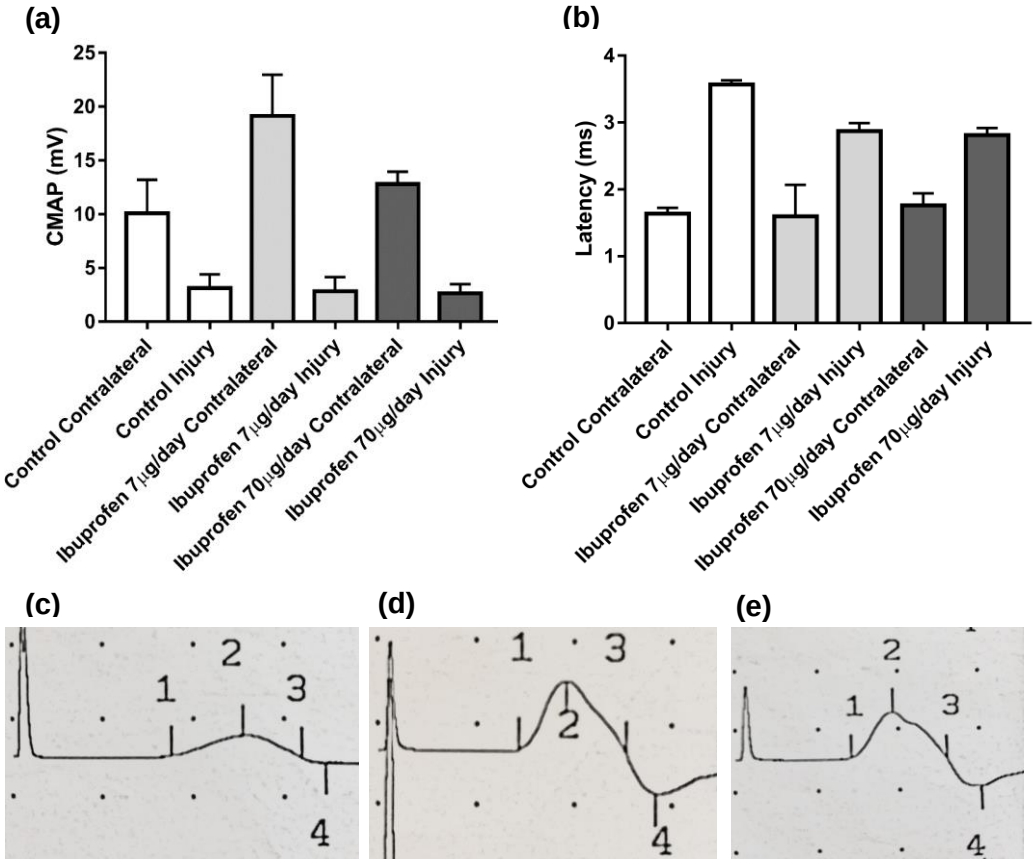

Figure 4.20: Electrophysiological evaluation of sciatic nerve 28 days after a crush injury in the sciatic nerve. *The sciatic nerve was stimulated proximal to the injury site and the CMAP was recorded from the gastrocnemius muscle. No difference was seen with the CMAP between the groups (a). The latency reduced in both groups with ibuprofen treatment in comparison to the no drug control (b). The electrophysiological traces for the no drug treatment (c) ibuprofen 7 μg/day (d) and ibuprofen 70 μg/day (e). N=3 (no drug control) N=2 (ibuprofen treatment groups), means ± SEM.*

4.2.4.3 Vasculature

The vascularisation was examined via immunohistochemical staining of transverse sections for RECA-1 at 21 days following a transection injury and 28 days in the crush injury. Analysis revealed the presence of blood vessels throughout the injured nerves in both the proximal and distal sections, however, there was a higher numbers of blood vessels in the proximal stump in both injury models.

In the transection injury model, the number of blood vessels in the distal stump increased following treatment with a dose of 7 µg/day ibuprofen and 70 µg/day ibuprofen in comparison with the no drug control (Figure 4.21 (a)). No difference was seen in the mean blood vessel diameter between the groups, however, larger blood vessel diameters were found in the no drug control (Figure 4.21 (b)).

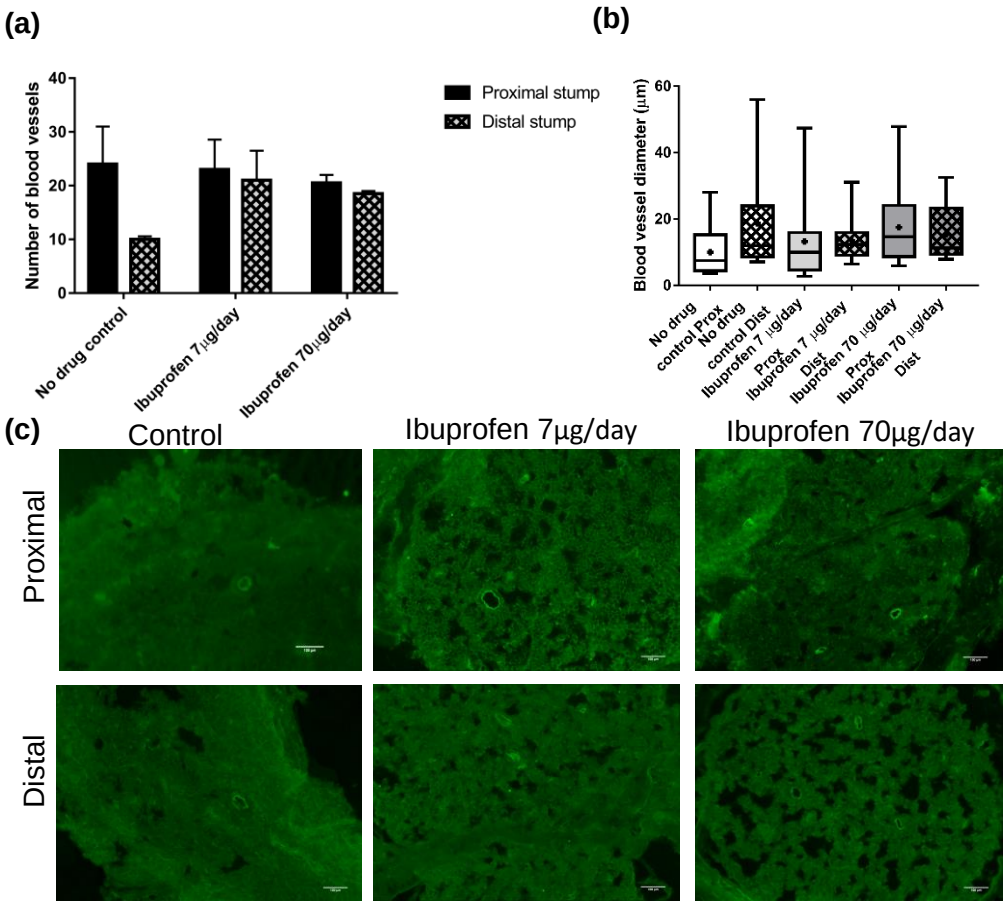

Figure 4.21: Vasculature changes following a transection injury. *Quantitative analysis of number (a) and diameter (b) of blood vessels by RECA-1 (green) immunostained 10 µm transverse sections from the proximal and distal stump (c). N=3, mean ± SEM for each condition. Box plots show the distribution of blood vessel diameter with boxes extending from the max to min, + indicates mean.*

The same was not seen in the crush injury model, as there was no difference in the blood vessel number, however, a small increase in the mean blood vessel diameter was observed with 70 µg/day ibuprofen treatment in comparison with the no drug control (Figure 4.22 (a), (b)).

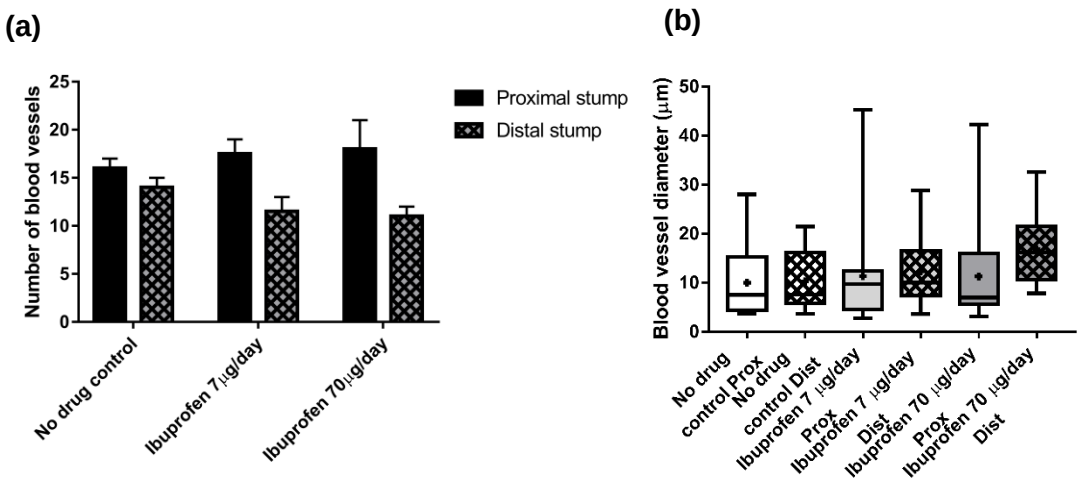

***Figure 4.22:* Vasculature changes following a crush injury.** *Quantitative analysis of number (a) and diameter (b) of blood vessels by RECA-1 immunostained 10 µm transverse sections from the proximal and distal stump. N=3, mean ± SEM for each condition. Box plots show the distribution of blood vessel diameter with boxes extending from the max to min, + indicates mean.*

4.3 Discussion

The 3Rs policy can be met to a substantial degree in PNI research through the use of *in vitro* models, however, *in vivo* testing is unavoidable for translating therapies to the clinic. *In vitro* models have the capacity to determine the basic effects of a treatment on Schwann cell migration and neurite outgrowth and so can aid the selection of the most promising therapies to be taken forward into pre-clinical *in vivo* studies *(Greek, 2012)*. This way the *in vivo* studies can be better targeted to answer more fundamental questions about safety and efficacy using a smaller number of animals. This pilot study explored the use of standard *in vivo* injury models and the regenerative and functional outcome measures as tools to screen drugs for PNI.

4.3.1 Optimisation of functional outcomes

Histological and morphological analysis is the most common method for the study of peripheral nerve regeneration *(Geuna et al., 2009)*. Although functional recovery is the main assessment tool of the nervous system in the clinic, exploring the nerve morphology in experimental studies provides more information about the regeneration processes, which can be related to the nerve function.

Histology is considered a descriptive method, however, more recently it is being used for quantitative analysis *(Raimondo et al., 2009)*. Morphometric analysis can be used to quantify the number of cells present, measure the diameter of cells or structures and the area which is occupied by the tissue or injury. The accuracy of these measurements is increased by determining the intensity or area fraction of positive staining in the immunofluorescent techniques *(Carriel et al., 2014)*.

One of the most commonly used antibodies to quantify axon regeneration is neurofilament and its intensity is significantly higher in healthy nerves as compared to the newly-formed axons. However, when there is high levels of regeneration the intensity values are similar to healthy nerves *(Carriel et al., 2014)*. Neurofilament protein is found in the cytoplasm of neurons and is associated with axonal growth *(Wang et al., 2012)*. There are three major subunits of neurofilament that differ in molecular weight;

neurofilament light chain (NF-L) (68 kDa), neurofilament medium chain (NF-M) (150 kDa), and neurofilament heavy chain (NF-H) (190-210 kDa) *(Johns, 2014)*. The morphology, function and transport of neurofilament in neurons is regulated by its phosphorylation *(Wang et al., 2012)*. Neurofilament phosphorylation occurs mostly around the NF-H C-terminal region, and these multiple phosphorylated sites are ideal targets in antibody-based assays *(Ghonemi et al., 2013)*. The neurofilament antibody used in this study was selected because it reacts with both NF-M and NF-H and neurofilaments with high and low degrees of phosphorylation, therefore, staining the entire axon population.

Neurofilament immunofluorescence staining was used in this study to quantify axon number through an automated axon count protocol developed using Volocity software. Manual analysis of peripheral nerve sections can be time consuming and lead to human error, therefore, more automated and semi-automated tools have been developed *(Romero et al., 2000, Vita et al., 1992)*. Despite the great efficiency with automated methods, errors can still occur due to the failure of the software to recognise and separate small axons or differentiate non-axonal artefacts *(Mezin et al., 1994, Savy et al., 1988)*. For this reason semi-automated axon analysis has been implemented to achieve improved efficiency but with high accuracy *(Isaacs et al., 2014).* In order to circumvent these limitations in this study, manual checks were used when the axon recognition was not fully distinctive in the automatic counts. If a difference of more than 10% was observed between the automatic and manual count, then the parameters were refined until an accurate count was obtained. This is the first reported protocol that uses the combination of a tile scan of an entire nerve section and Volocity software to quantify axon number. Further validation is required before wider use to ensure that it is as robust as other automated quantification tools already available.

Furthermore, most protocols quantifying histological or morphological analysis of axons use transverse sections rather than longitudinal sections as the cross-sectional area of the nerve is needed. Longitudinal sections can be useful when analysing axon growth and reinnervation as you can trace the full length of individual axons. However,

transverse sections have advantages by enabling a simpler and less time extensive quantification of axon number and myelination, which can't be conducted in longitudinal sections without specialised equipment.

Many studies use random or targeted sampling strategies to select fields for axon counting *(Marina et al., 2010, Reynaud et al., 2012, Teixeira et al., 2014)*. When sampling tissues or sections it is important to ensure that there is an equal opportunity for any of the objects to be included in the sample *(Geuna et al., 2000)*. Sampling methods for axon number assume axon density is homogenous across the nerve but it has been shown that this is not the case *(Chauhan et al., 2006).* A study conducted in the optic nerve of mice demonstrated a large regional variation in the axon density on nerve sections, as well as, variations between individual animals *(Zarei et al., 2016)*.

Therefore, this study implemented the use of entire transverse sections to obtain axon counts. Despite the inclusion of all axons present within the tissue there are still limitations to using this method. A transverse section is a single snapshot of the number of axons at a determined distance from the injury site and doesn't consider the extent these axons have regenerated in terms of length. Nerve fibre quantification is dependent on the distance from the nerve injury. Therefore, two methods of analysis can be implemented; the first is to obtain data from multiple sections along the nerve and take a mean or a second is to use a single section but ensuring the section is taken at the same location along the nerve between experimental groups. If adequate sampling techniques are employed then bias can be reduced *(Geuna et al., 2000, Larsen, 1998)*.

Histology techniques make it challenging to analyse the entire nerve and they do not provide any indication of the extent of functional recovery, therefore, other techniques such as nerve conduction/electromyography studies need to be used to evaluate peripheral nerve continuity and function *(Diao et al., 2004)*.

Nerve conduction velocity is one of the most thoroughly studied aspects of nerves and can be used as a tool to monitor regeneration *(De Koning et al., 1986)*. Also in animal studies, injured nerves can be compared to the contralateral uninjured nerve. Recording electrodes can be placed into the target muscle to record compound muscle action

potentials to study motor recovery *(De Koning et al., 1986)*. In this pilot study, the positioning of the electrodes impacted the CMAP and therefore this was optimised and standardised for this body of work. Furthermore, electrophysiology results presented here demonstrated inconsistencies, so the protocol was refined to ensure consistent supramaximal stimulation, which has a characteristic wave form, in order for electrophysiology to be applied reliably in subsequent parts of the study (Chapter 5 and 6).

In the rat sciatic nerve model there are many tests that study the functional recovery, gait and posture *(Nichols et al., 2005)*. One of the most commonly used tests is the sciatic functional index (SFI) as it provides a non-invasive and quantitative method to evaluate functional recovery of walking ability *(Martins et al., 2006).* SFI was introduced as a method to assess reinnervation after an experimental sciatic nerve lesions, however, is not always a practical choice of evaluation due to the need of sophisticated equipment needed and the more complex analysis involved. The static sciatic index (SSI) is a simple and practical alternative that can be performed. A study comparing the two techniques; SFI and SSI in a transection and crush model in the mouse sciatic nerve determined that SSI can be used as an alternative for SFI demonstrated by high correlation coefficient (r=0.892) *(Baptista et al., 2007)*. Furthermore, they compared an ink and a photo method to obtain the 1–5 toe spread (TS) and 2–4 toe spread (ITS) measurements and determined that the photo method showed better reproducibility *(Baptista et al., 2007)*.

4.3.2 Selection of in vivo injury models

There are several injury models used for PNI but most commonly a crush or transection with primary repair of a nerve in rodents are used to test potential treatments *(Angius et al., 2012)*. The complexity of such models echoes that of the human clinical situation and provides useful systems-level information. An animal model should be chosen through the consideration of several factors and careful definition of the research question.

Rodents are commonly used and the rat is usually the animal of choice due to its larger size. Mice are also often used due the availability of many transgenic strains *(Tos et al., 2009)*. There is still debate between using hindlimb and forelimb models but there is no strong evidence to use one over the other *(Bontioti et al., 2003, Nichols et al., 2005)*. The model should be based on the specific requirements for the study and the researcher's expertise ensuring that the limitations are considered *(Tos et al., 2009)*. The sciatic nerve was chosen for this study as it is the largest nerve in the rat providing plenty of tissue to conduct multiple histological and morphological analysis and because it is the most clinically relevant due to its similar size to the nerves in human digits.

The selection of a particular injury type should also be decided upon the study aims. Neurotmesis is preferred for pre-clinical tests for the evaluation of new therapeutic agents as it is easier to identify significant differences in morphological, functional and electrophysiological measures. Axonotmesis is used when reproducible regeneration is required such as in the development of new therapeutic agents *(Tos et al., 2009)*. There is a need for more reproducible models to enable rapid screening of compounds in earlier drug development stages, but also for a model to be used as a pre-clinical study to aid the future translation of drug therapies. Due to the differences in severity between the two models they were both tested for their appropriateness for drug screening.

In this study the axonotmesis model was more reproducible as the function of all the animals returned to the baseline 28 days following a crush injury to the sciatic nerve. This mirrored what have been seen in previous studies *(Pavic et al., 2011, Ramli et al., 2017).* However, one study suggested full regenerative recovery would be unlikely to occur after 28 days as the sciatic recovery rate was found to be 2.20 ± 0.3 mm/d *(Hadlock et al., 2005)* meaning the axons wouldn't have fully regenerated over the distance between injury site and foot. Overall, the quicker recovery time rendered the crush model more effective in the rapid initial screening during the development of new drug compounds.

However, a limitation of the crush model is the standardisation of the crush injury in terms of force and pressure administered *(Tos et al., 2009)*. The method to crush nerve in this

study was conducted manually and the methodology by completely closing the tweezers for the same time in each animal meant the pressure remained consistent. This provided a standardised method which was reproducible and reliable in this study *(Benito et al., 2017)*. Other studies have devised a clamp that provides a reproducible force, pressure and duration of compression *(Beer et al., 2001)*, that has been used in rat sciatic nerve models *(Amado et al., 2008, Luis et al., 2008, Varejao et al., 2004)*.

Axonal regeneration and functional recovery is much slower in a transection injury with recovery taking approximately 4 times as long, as there is complete discontinuation of the nerve structure. For example functional recovery in a rat median nerve begins after 12 days and reaches the plateau at 28 days following axonotmesis, whereas, it begins after 30 days and reaches the plateau at 120 days in neurotmesis *(Tos et al., 2009)*. However, this extended recovery time could allow for the progression of regeneration to be quantified more easily in greater detail.

There are advantages in using the axonotmesis model over neurotmesis including the method being less technically challenging and therefore the researcher doesn't require complex microsurgical training. Furthermore, there is less likely to be inter-animal variability in the post-operative outcomes *(Varejao et al., 2004)*, and autotomy is less likely to occur.

With any injury model there are still limitations in correlating the experimental model with the clinical outcome. In many animal studies young and healthy animals are used which doesn't relate to older human subjects with additional long-term conditions *(Tos et al., 2009)*. Older animals presenting with other chronic illnesses such as diabetes or infections should be considered to test the effectiveness of therapies in PNI *(Jolivalt et al., 2008, Zochodne et al., 2007)*. Furthermore, within the clinic human subjects usually have a delay in surgical repair which highly impacts the regenerative capacity. This is not replicated in most animal models as the repair tends to be conducted immediately after injury and therefore leads to discrepancies when comparing regeneration between humans and rodents *(Richardson, 1997)*. In addition, the sex and strain of the rodent subjects need to be considered as it has been found that nerve regeneration is more

pronounced in females due to the neuroprotective effects of sex hormones *(Kovacic et al., 2003, Kovacic et al., 2004, Richardson, 1997, Roglio et al., 2008)*. The use of different strains does not seem to impact regenerative capacity but more the likelihood of autotomy with Lewis rats presenting with the lowest incidence of autotomy *(Tos et al., 2009)*.

4.3.3 Comparison of in vivo models and the effect of ibuprofen in these models

Regeneration and functional recovery was measured 21-28 days post-injury after ibuprofen was delivered locally through osmotic pumps in a crush and transection injury. Histological analysis demonstrated an increase in axon number in the distal stump in the treatment group at 21 days in the transection model and at 28 days in the crush model in comparison to the corresponding no drug control groups.

In the transection model it was found that the number of axons increased in the distal stump over time following injury. Interestingly at 21 days post-injury the number of axons in the distal stump exceeded those in the proximal stump in the same animal, suggesting neurite branching. Following local treatment of ibuprofen at a dose of 7 µg/ day and 70 µg/day the number of axons in the distal stump increased in comparison to the no drug control group. A dose dependent response was seen in the percentage of axons in the distal stump as a proportion of those in the proximal stump with 140% and 155% increases seen with 7 µg/ day and 70 µg/day doses of ibuprofen respectively. Furthermore, larger axon diameters were seen with 70 µg/day ibuprofen in comparison to the lower dose and no drug control. As ibuprofen is a poorly soluble drug it was dissolved in a 10% DMSO solution in saline to be delivered *via* the osmotic pumps. The effect of DMSO was tested in a separate group of animals to determine whether it had an effect on nerve regeneration. Treatment with 10% DMSO solution led to a reduction in the number of axons in the distal stump. The number in the proximal stump was lower than that seen in the other experimental groups but it is hard to distinguish whether this was due to animal inter-variability or an effect of DMSO. The percentage of axons in the distal stump as a percentage of the proximal

is similar to the no drug control group indicating it may be due to the former or neurotoxicity. Overall this could have limited the effect of ibuprofen *in vivo* and would need to be explored further. Later studies were all conducted using the ibuprofen sodium salt as it is more soluble and avoided the use of DMSO.

The same ibuprofen treatment resulted in a different effect in the crush model as only the 7 µg/ day dose increased the axon number and axon diameter in the distal stump in comparison to the no drug control. Furthermore, the number of axons didn't exceed the number in the proximal stump suggesting there was less branching in the crush model than the transection. Interestingly as sections were taken at increasing distances distal from the injury site the number of axons increased. This could indicate that there was still a degree of branching in the distal stump following a crush injury but it occurred more distally that in the transection model. This could be investigated further by analysing axon numbers in transverse sections as multiple positions along the distal stump in the nerve.

The number and density of axons are good indicators of nerve regeneration, however, they need to be interpreted carefully because a high number of axons can not only indicate regeneration, but also aberrant sprouting *(Raimondo et al., 2009)*. Also a high fibre density doesn't always reflect good regeneration but could be due to a large number of small axons *(Raimondo et al., 2009)*.

This is the first study to show ibuprofen treatment having a beneficial effect on axon number and also the first to report the effect of the local delivery of ibuprofen in peripheral neve injury.

In both the transection and crush models function was lost following injury, however, it was evident that some functional recovery had occurred in the crush model by 28 days. In the transection model the outcomes measured by von Frey, static sciatic index and muscle mass remained low at 21 days post-injury. Treatment with 7 µg/ day and 70 µg/day improved sensation as the threshold response (g) needed to obtain a response was lower than for the no drug control. However, there was no difference seen with the SSI and muscle mass between the experiment groups.

The results seen with the electrophysiological data correlated with the histology to a certain extent, as the CMAP was greater with a dose of 70 µg/day ibuprofen, meaning the nerve may contain more axons. However, there was no difference in the latency between experimental groups meaning that both groups have a similar number neurons with a fast conduction velocity. A previous study had seen the return of nerve conduction velocity following 3 weeks systemic treatment with ibuprofen in PNI *(Madura et al., 2011)*. However, the injury model was an interpositional graft in the tibial nerve and electrophysiological tests were conducted after 3 months and therefore the 3 weeks drug treatment used in this study may not have been long enough to see a change in function.

In the crush model sensation returned to baseline in all animals by 28 days, however, treatments of both 7 µg/ day and 70 µg/day improved sensory recovery seen by a lower threshold (g) stimulus needed to obtain a response from the animals. The group with a dose of 7 µg/ day ibuprofen presented with the best sensory recovery.

To assess target organ reinnervation the gastrocnemius muscle mass was recorded. Denervation of a target muscle is a consequence of PNI and causes muscle atrophy. Reinnervation will restore muscle function and therefore stop atrophy *(Feng and Yuan, 2015)*. The results show that the muscle mass in the injured hind leg has reduced considerably in comparison to muscle in the uninjured hind leg. The muscle mass was higher in the ibuprofen treatment groups at 60% of the contralateral in comparison to the 40% in the control. These results were consistent with the SSI as the ibuprofen treated groups returned to baseline quicker, especially the 7 µg/ day dose which presented with better recovery throughout the 28 days.

This correlated with results seen using electrophysiology, as the latency was longer in the control group, meaning the nerve may contain a higher population of axons with a lower conduction velocity. However, no difference was seen in the CMAP between the groups.

In addition to investigating axon regeneration and functional recovery, vascularisation and the presence and phenotypes of Schwann cells were also explored. These cellular

changes are important to study as their combined interactions have been shown to facilitate initial Schwann cell guidance and regeneration *(Cattin et al., 2015)*. It is well established that there is activation of Schwann cells in the distal stump following nerve injury and it is of interest to determine the action of drugs within these cells. To understand the benefits this could have clinically, we first need to understand how drug agents could manipulate Schwann cell activity. The pilot qPCR data demonstrated that the gene expression in Schwann cell changed considerably following a transection injury with the upregulation of biomarkers indicating the Schwann cells are switching to a myelinating phenotype, over the 21 day period. The findings from this study are not conclusive due to the lack of n numbers and further analysis is needed to produce a readout that is consistent with previous data. This will provide a baseline which will allow the investigation of the effectiveness and mechanism of action of potential drug therapies that will be taken forward *in vivo* tests.

Vascularisation has shown to play in role in the success of peripheral nerve regeneration *(Cattin et al., 2015)*, however, the effect of drug treatments on nerve vascularisation hasn't yet been explored. The number of blood vessels increased with 7 µg/day and 70 µg/day ibuprofen treatment following a transection injury, however blood vessels with larger diameters were in the control group. The opposite was seen in the crush injury with no difference in blood vessel number but the blood vessel diameter was slightly larger in the group with 70 µg/day ibuprofen treatment. The higher number of smaller blood vessels in the ibuprofen treatments group in the transection model could be due to newer blood vessels being formed through angiogenesis in the presence of the drug. This is just speculation and further in depth analysis of the revascularisation on the nerve following dug treatments would be needed to determine the mechanism.

4.3.4 Correlation between in vitro and in vivo effects

It would be greatly beneficial to have an *in vitro* model that predicted the outcome of the *in vivo* model. To evaluate this a metric was devised to compare the different *in vitro* models used in chapter 3 determine which one best predicted the effect seen *in vivo*. The *in vivo* model demonstrated a two-fold increase in neurite number following 7 µg/day of ibuprofen administered locally for 21 days. The dose administered *in vivo* was approximately equivalent to the 100 µM dose the cells were subjected to *in vitro*. Therefore, the data sets for this dose were analysed from each culture model, by normalising them to their controls. This analysis showed that the monolayer models had marked variability in neurite length. Although the DRG and NG108-15 monolayer cultures had comparable fold increases they had a large standard deviation (e.g. ±60% in the NG108-15 culture) (Figure 4.32). Conversely, the 3D models were more consistent, with a standard deviation of ±40% independent of the cell type used. Furthermore, the 3D EngNT co-culture with DRG neurons demonstrated a fold increase in neurite length that is most comparable to the *in vivo* model.

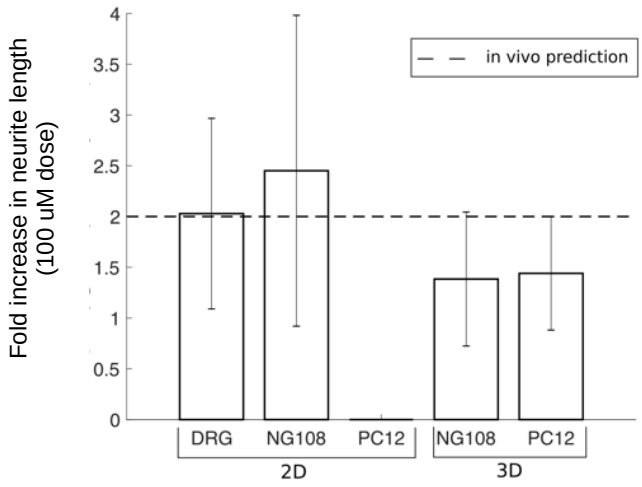

Figure 4.23: Comparison of effects of ibuprofen on axon growth in vitro and in vivo.

There are limitations in comparing the two models used in this study, as the *in vitro* model analyses axon length and the *in vivo* measures axon number and so they cannot be

directly correlated. Therefore, it would be better to use the same analytical method in both models to devise a metric allowing them to be compared directly.

In conclusion, this chapter determined that a crush *in vivo* model was a more rapid model for initial screening of the regenerative effects of drug agents in pre-clinical studies. The model has the advantage of isolating the rate of neurite extension from the pathfinding across the interface required in transection. The transection model could also be used for drug screening but would require a longer repair duration to enable in depth analysis of the effect of drugs on regeneration. Both the transection and crush injury were useful to determine different regenerative and functional outcome measures that could be evaluated from each model.

Chapter 5: Development of a controlled release drug delivery platform.

5.1 Introduction

Some small molecules that improve nerve regeneration rate in experimental models have been identified, however, the potentially damaging side effects associated with their sustained systemic administration has restricted clinical translation *(Yang and Pierstorff, 2012)*. In the past decades, local drug delivery systems have become more attractive because of these drawbacks of conventional drug treatments *(Yang and Pierstorff, 2012)*. These side effects can be reduced through decreasing drug concentrations, however, this may reduce the therapeutic efficiency of the drug and is not a sustainable solution *(Yang and Pierstorff, 2012)*. Therefore the development of local drug delivery platforms could be advantageous not just due to reduction of side effects but also for drugs with physical chemical problems such as non-optimal solubility.

5.1.1 Local drug delivery for PNI

Despite the growing interest in the development of drug therapies for PNI, research using local drug delivery platforms is lacking. No study has been published in which a suitable treatment duration for any agent has been identified, however, as regeneration of nerves in humans takes a remarkable time (months-years), treatment durations may need to extend to this amount of time, depending on the role of the drug. Long term oral treatment can lead to long term side effects with minimal efficiency but also problems with patient compliance. Therefore, a device that can deliver drugs locally to the injured nerve over a sustained period could be beneficial.

Many advancements have been made in targeted therapeutics for PNI to deliver cells types, proteins, platelet-rich plasma and gene therapy to promote nerve regeneration *(Federici et al., 2007, Kuffler, 2014, Bhangra et al., 2016, Busuttil et al., 2017).* These therapies are delivered through the use of conduits that are surgically inserted into the injury site. These interventions have proven beneficial in promoting nerve regeneration via the induction of axon outgrowth and neurological recovery *(Kuffler, 2014).* As other

therapeutics have been successfully delivered locally through conduits this provides a platform that could be feasible for drug therapies.

Tissue engineering approaches have developed synthetic and natural biomaterials as alternative strategies for the surgical treatment of PNI to autologous nerve grafting *(Subramanian et al., 2009)*. These materials could not only provide a new approach of delivering small molecules but also the possibility of dual therapies of drug treatments alongside cell or gene therapies within the same device.

The existing materials are biocompatible and include synthetic polymers, or materials that occur naturally in the body such as collagen and fibrin. These materials have the potential to provide a controlled-release delivery device that would naturally biodegrade in the body over time. As a result this makes the therapy less invasive for the patient, by eradicating the need for additional surgery to remove the device after treatment. Bio-degradable polymers possess weak bonds such as ester, amide, and anhydride bonds that break down by hydrolysis or enzyme degradation *(Fu and Kao, 2010)*.

On the other hand, non-degradable polymers are still extensively used for drug delivery for other clinical applications due to their robust structure, durability, mechanical strength and relatively slow release. They have two types of release 1.) Reservoir-type where the material has a coating which controls the release rate with its thickness and permeability and 2.) Matrix-type where the drug is released through a diffusion and concentration gradient *(Fu and Kao, 2010)*.

Extensive work has been conducted to develop both degradable and non-degradable biomaterials to deliver drugs to other tissues for various clinical conditions. Most of these controlled-release systems have demonstrated biocompatibility and effectiveness which can be tested for application in a neural environment. They need to possess certain properties to be used clinically such as; chemically inert, free of leachable impurities, have a suitable physical structure and be readily processable *(Brannon-Peppas, 1997)*. They also need to provide constant drug levels without producing drug concentration peaks. The ideal delivery system needs to have a zero order release meaning the

release rate does not change with time. Examples of current drug delivery systems include; tubes, fibres, laminates, and microspheres.

5.1.2 Ethylene vinyl acetate (EVA)

EVA is a non-degradable polymer approved for use in a vast range of clinical applications including transdermal drug delivery, contraceptive insertions, subcutaneous implants and mucosal contact forms *(Zhang, 2015)*. The polymer is flexible, inexpensive, and biocompatible as it does not cause an inflammatory response in tissues and so is commonly used in diffusion-controlled systems for release over a substantial period of time *(Fu and Kao, 2010)*. Its success has encouraged research into the use of EVA-based controlled-release systems for other clinical areas, however, to date it hasn't been used in PNI.

EVA is used clinically to deliver drugs such as; hormonal contraception in intravaginal rings (NuvaRing®) and implant devices (Nexplanon® and Implanon®); pilocarpine for glaucoma (Ocusert®) and buprenorphine for opioid addiction (Probuphine®) *(Schneider et al., 2017)*. Furthermore there are many more studies exploring the use of an EVA matrix system for other clinical applications. One such study explored the possibility of delivering atenolol (a beta-adrenergic receptor blocker) through a transdermal controlled release EVA matrix. They found the matrix successfully released the drug following a diffusion-controlled model and the dose released can be controlled by changing the drug load and temperature *(Kim and Shin, 2004)*.

Another study explored the use of EVA to deliver phenytoin (an anti-epileptic) to reduce seizures in a rat epileptic model *(Tamargo et al., 2002).* The EVA polymeric formulation demonstrated the ability to deliver phenytoin in a controlled-manner for a calculated period of 3.5 years using a 50% drug loaded cylinder (5 mm diameter and 4 mm height) *(Tamargo et al., 2002).*

As EVA has been well-studied, a wide range of pharmaceutical manufacturing processes can be used to tailor its properties and compatibility to a broad variety of small molecules. These include soluble and insoluble drug molecules, peptides, nucleic acids and proteins

(Schneider et al., 2017). Evidence shows that EVA is inert toward drug molecules and highly compatible with the human body making it an ideal polymer for use as an implantable long-term drug delivery system.

5.1.3 Polycaprolactone (PCL)

PCL is a FDA approved aliphatic polyester which is biocompatible and biodegradable. An example of its clinical use is the implant for hormonal contraception delivery (Capronor®). It has a slow degradation rate of 2-3 years which occurs by hydrolysis of its ester bonds *(Chang et al., 2018)*.

PCL has been extensively investigated for PNI as a nerve conduit to act as a guide for axon regeneration. PCL nanofibre conduits improved motor and sensory function following nerve defect in a rat tibial nerve in comparison to hollow conduits *(Neal et al., 2012)*. Another study demonstrated that electrospun PCL/lignin nanofibers promoted Schwann cell proliferation and DRG neuron outgrowth when culturing the cells on the surface of the material *(Wang et al., 2018)*. Moreover, ultrathin PCL films aided the regenerating nerve tissue and Schwann cells to bridge a 10 mm gap in the sciatic nerve of a rat *(Sun et al., 2010)*. Currently, a Phase I clinical trial is recruiting participants to evaluate the use of PCL nerve conduits as a therapy in sensory digital nerve surgery (gap size 5-20 mm) *(ClinicalTrials.gov, 2016)*.

Drug loading into PCL has also been investigated, however, there is no known literature that has tested the effect of these conduits using *in vitro* or *in vivo* models of PNI. The published study explored the ideal properties and structure of PCL/ibuprofen conduits to be used as drug delivery systems. It was found that manufacturing the conduits using vertical extrusion provided appropriate mechanical properties, dimensions and a suitable drug release profile *(Salmoria et al., 2016).* Moreover, polycaprolactone-b-polyethylenoxyde (PCL-b-PEO) micelles loaded with FK506 (Tacrolimus) were studied in a rat sciatic nerve crush injury. The injected micelles increased the animals' endurance time on the rota-rod apparatus *(Allen et al., 2000)*.

5.1.4 Poly (Lactic-co-Glycolic) acid (PLGA)

PLGA is a biocompatible and biodegradable co-polymer which is FDA approved for clinical use in humans. The co-polymer is made up of two components; poly(lactic) acid (PLA) and poly(glycolic) acid (PGA) and the degradation rate of the material can be tailored based on the molecular weight and the copolymer ratio. PLGA degrades by hydrolysis of its ester bonds in the presence of water, through bulk or heterogeneous erosion. Furthermore, the surface properties of the material can be modified to provide better interactions with small molecules *(Gentile et al., 2014)*.

PLGA has been used previously in the development of sustained release systems for PNI to deliver growth factors, hormones and drugs. NGF-loaded PLGA microspheres were tested for PNI in a 2 mm gap injury in the rat sciatic nerve. It was found that the release of NGF microspheres enhanced the regeneration by increasing fibre number and myelin sheath thickness, as well as improving functional recovery seen with SFI *(Wang et al., 2014)*.

Furthermore, an additional study explored the release of NGF from multi-ply alginate/chitosan conduits coated with layers of PLGA. The *in vitro* results demonstrated an appropriate release profile and so the multi-ply NGF-loaded conduit shows promise as a suitable formulation to deliver NGF for the treatment of peripheral nerve regeneration *(Pfister et al., 2008)*.

Another study investigated the beneficial effect of delivering basic fibroblast growth factor (bFGF) from PLGA microspheres in a 10 mm defect in a rat sciatic nerve on peripheral nerve regeneration. They demonstrated enhanced functional recovery through electrophysiology and SFI alongside increased axon dimeter and myelin sheath thickness *(Si et al., 2017)*. Moreover, neurotrophic factor (NTF)-loaded PLGA microspheres for local delivery in repaired transection injury in a rat sciatic nerve demonstrated a slow release of neurotrophic factors which led to improved regeneration of motor and sensory axons *(Santos et al., 2016)*.

Furthermore, the hormone erythropoietin (EPO) encapsulated into PLGA microspheres provided a sustained release profile of two weeks and demonstrated an improvement in the SFI and motor conduction nerve velocity (MCNV) following treatment with the microspheres in a 2 mm nerve defect in a rat sciatic nerve *(Zhang et al., 2015)*.

In addition, drug-loaded PLGA microspheres were tested in a 10 mm nerve defect in a rat sciatic nerve. The rapamycin-loaded PLGA microspheres demonstrated no significant difference in functional recovery between the different groups but reduced the secondary nerve injury *(Ding et al., 2015)*.

5.1.5 Mesoporous silica nanoparticles (MSN)

In the field of nanotechnology, nanoparticles (<100 nm) have been developed as efficient drug carriers as they possess physicochemical and biological properties that allow them to be taken up more readily by cells. These are extremely useful in the delivery of bioactive compounds but could also be used for a sustained drug delivery *system (Wilczewska et al., 2012)*.

MSN nanoparticles are ordered hexagonal arrays of cylindrical mesopores. These nanoparticles are widely used in the biomedical field due to low toxicity, permeability, inertness and high biocompatibility. The outer surface usually contains free silanol groups, which enables the chemical modification of the particle surface to improve drug release such as; charged small molecules, proteins, and antibodies *(Giret et al., 2015)*.

Drugs have been successfully loaded into MSNs for the development of drug delivery systems. Ibuprofen was used to test the release properties of MSNs and the results demonstrated a high loading content of the poorly soluble drug and a release rate of 96.3% *(Zhang et al., 2011)*.

Moreover, the properties of MSNs were explored in order to load another poorly-water soluble drug, telmisartan. The study found that the reduction of the pore size (volume and diameter) and the chemical modification of the nanoparticles involving the presence of ionic interactions between the MSNs and drug, improved drug uptake and release *(Zhang et al., 2010)*.

5.1.6 Electrospinning

Electrospinning is a broadly used method to manufacture fibres with different sizes, shapes and functional properties, from natural or synthetic polymers. It can be applied to many fields including tissue engineering, pharmaceuticals and biotechnology as the fibres have high surface-to-volume ratio and tunable porosity *(Bhardwaj and Kundu, 2010)*.

Electrospinning has been studied for use in developing therapies for peripheral nerve regeneration, most commonly the fabrication of aligned nanofibres or conduits for nerve guidance but also to deliver small molecules. Most recently, a study developed methylcobalamin-loaded electrospun PCL nanofibres as a local delivery system. The fibres were wrapped around a crush injury in a rat sciatic nerve and as a result improved nerve conduction velocity recovery and enhanced myelination *(Suzuki et al., 2017)*.

Another study developed a blend of polycaprolactone and bovine serum albumin (BSA) to prepare nerve growth factor (NGF)-loaded electrospun nanofibers. The material was tested on PC12 neuronal cultures and demonstrated a sustained release of NGF, which induced neurite outgrowth in the PC12 cells *(Valmikinathan et al., 2009)*.

Electrospun PLGA has been explored for peripheral nerve regeneration, but only for use in the manufacture of aligned nanofibre, electrospun conduits *(Lee et al., 2009, Li et al., 2012, Wang et al., 2011)* or cell-seeded conduits *(Schuh et al., 2015)*. These formulations demonstrated positive effects in PNI; supporting and enhancing nerve cell growth using *in vitro* and *in vivo* models. PLGA/gelatin electrospun nanofibres have demonstrated ideal properties to act as a drug delivery system to deliver fenbrufen as a treatment for rheumatoid arthritis or osteoarthritis *(Meng et al., 2011)*, however, to date this approach has not been used to deliver drugs locally for peripheral nerve regeneration.

In conclusion, there are many advantages of using a biomaterial preparation to deliver drugs locally for treatment in PNI; they are currently widely used for other clinical applications and most are biodegradable. Films and nanofibrous sheet formulations

provide ideal handling properties for wrapping around an injured nerve. In addition, they can be loaded with a range of small molecules and the dose, rate and duration of drug release can be precisely controlled through controlling the material formulation. Finally local delivery can help alleviate the side effects associated with systemic administration. Moreover, their use doesn't require the need for additional surgery in patients with a PNI as most will have their nerves exposed during surgical repair, so wrapping a drug-loaded material around the repaired nerve at that stage is no more invasive than the repair surgery itself. Furthermore, the use of a degradable material means that there is no need for a second procedure to remove the device.

5.1.7 Aim of chapter 5

The aim of this chapter was to manufacture and test drug-loaded biomaterials for use as drug delivery systems for the treatment of PNI. Standard techniques were used to characterise the drug-loaded biomaterials. Once a suitable release profile was obtained the materials were tested in the two nerve injury models optimised and applied in chapter 4; namely a crush and a transection with primary repair. This allowed the comparison of delivery from the drug-loaded biomaterials with the delivery from the osmotic pumps from the results shown in chapter 4, which are an established experimental tool to deliver drug locally to tissues. Ibuprofen was used as an exemplar drug as it has proved beneficial for nerve regeneration *in vitro* and *in vivo* in this body of work as well as in previous literature.

5.2 Results

5.2.1 Characterisation of biomaterials

5.2.1.1 Ethylene vinyl acetate (EVA)

Scanning electron microscope (SEM)

The composition and morphology of EVA membranes loaded with and without ibuprofen were analysed using SEM following cryogenic fracture in liquid nitrogen (7 mm x 12 mm x 0.5 mm) (Figure 5.1). The membranes displayed similar patterns of porosity which appeared homogeneous, however, the pore size changed following drug loading with pores ~5 µm in the control and ~ 25 µm in the ibuprofen loaded material (Figure 5.1 (d)). Drug loading was successful as demonstrated by the small crystals of drug deposited within the pores over the surface of the membrane (Figure 5.1 (c), (d)).

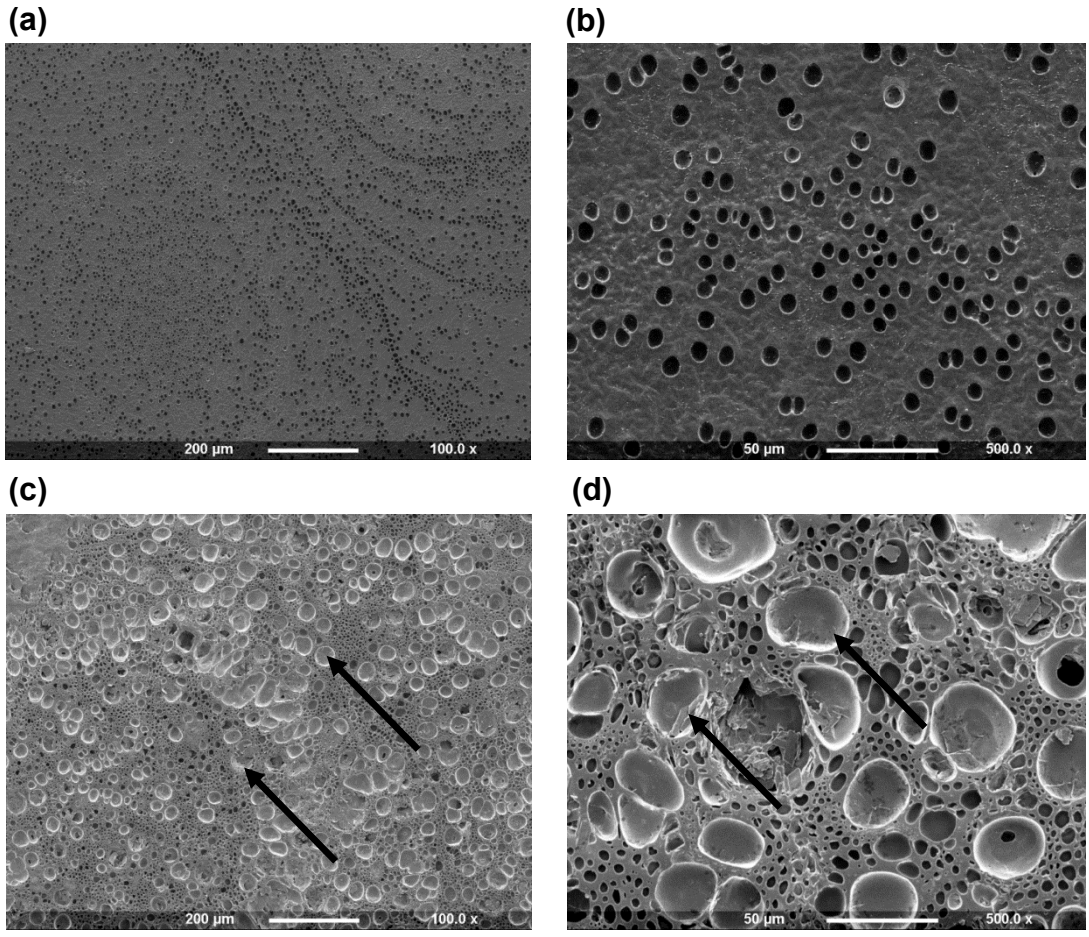

Figure 5.1: SEM images of blank and ibuprofen-loaded EVA membranes. *The images were taken following cryogenic fracture of blank EVA membranes (a), (b) and ibuprofen loaded EVA membranes (c), (d). Drug deposited in pores indicated with black arrows.*

For PNI application it would be more advantageous to have a tube or wrap to place around the injured nerve rather than a flat membrane, as this would ensure the device remained at the injury site once it has been implanted and that the drug is delivered directly to the injured tissue. Therefore, this study explored the possibility of manufacturing of EVA tubes for drug delivery for PNI.

The composition of EVA tubes with and without ibuprofen were analysed using SEM following cryogenic fracture in liquid nitrogen (7 mm x 12 mm x 0.5 mm) (Figure 5.2). Drug loading can be seen by the small crystals of drug deposited throughout the material (Figure 5.2 (c), (d)). It is evident that the manufacturing process using chloroform to form EVA tubes (described in section 2.11.2) helps to fuse the two surfaces, however, there are inconsistencies in the inner diameter. This could have an impact on the ability to implant the tube correctly without it being too tight-fitting around the nerve causing tension. All diameters were measured for consistency before implanting *in vivo*.

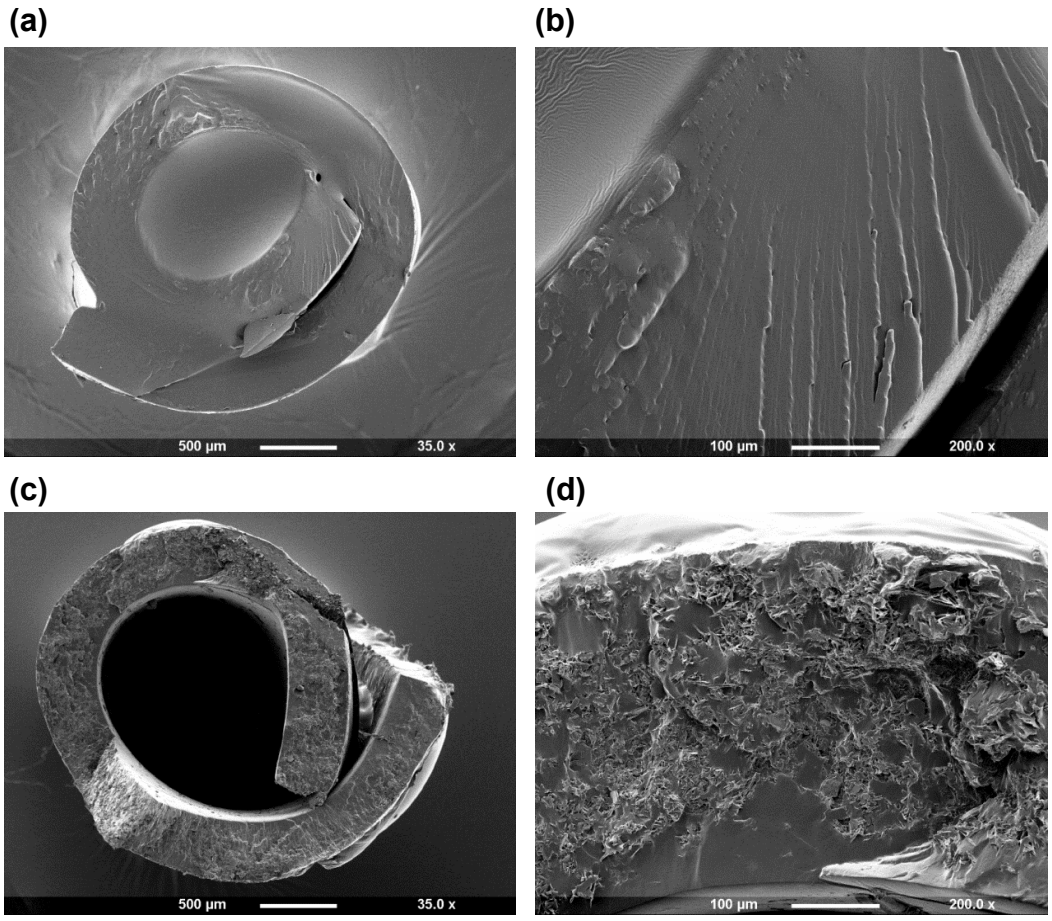

Figure 5.2: SEM images of blank and ibuprofen-loaded EVA tubes. *The images were taken following cryogenic fracture. (a), (b) blank EVA membranes and (c), (d) ibuprofen loaded EVA membranes.*

Fourier transform infrared spectroscopy (FT-IR)

The absorbance FTIR spectra of pure ibuprofen and ibuprofen-loaded EVA membranes were measured over the spectral region 500 to 4000 cm^{-1}.

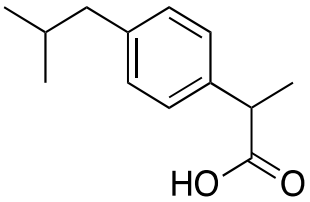

Figure 5.3: Chemical structure of ibuprofen.

As expected the spectrum of pure ibuprofen shows multiple vibrations corresponding to its structure; the band at ~ 3000 cm^{-1} could relate to the OH group, the band ~1700 cm^{-1} represents the stretching of the C=O group and the wide bands between 800 -1500 cm^{-1} likely corresponds to the phenyl group *(Xu et al., 2017)*. In the case of ibuprofen loaded-EVA there is a slight shift in the bands, which could be indicative of interaction between the drug and material suggesting successful drug incorporation. The major ibuprofen peaks are present, however, the shift in peaks indicates both the polymer and drug are present in the formulation and that there could be an interaction between the two (Figure 5.4).

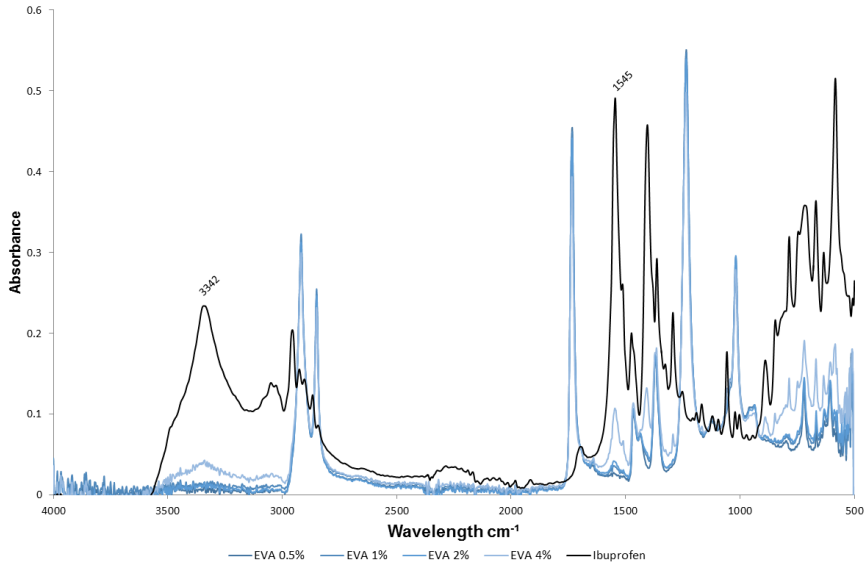

Figure 5.4: FTIR spectrum for pure ibuprofen and EVA with different loading concentrations of ibuprofen. *Each spectrum was acquired from four consecutive scans of a single sample.*

Drug release

In vitro drug release from ibuprofen-loaded EVA membranes and tubes was measured every hour for 4 h and then every 24 h for 10 days. Each time the solution was completely removed and replaced with fresh water. The drug concentration in the solution was measured using UV-Vis spectroscopy and a calibration curve (Figure 2.11). The release from ibuprofen-loaded EVA was rapid in the first 4 h and then plateaued at 24 h. Increasing the drug loading had no effect on the release profile, however, over 30% of the drug was released in the first 4 h with a 4% drug load while only 12% was released with the 0.5% drug load. Furthermore, the 2% drug load achieved the highest release over 10 days at 92%, whereas, for 0.5%, 1% and 4 % drug loads 84%, 65% and 67% drug release respectively were observed. Therefore, the 2% drug load concentration was taken forward for further investigation. Furthermore, it was found that a tube geometry slowed the release profile in the first few days with the release plateauing at 5 days (Figure 5.5).

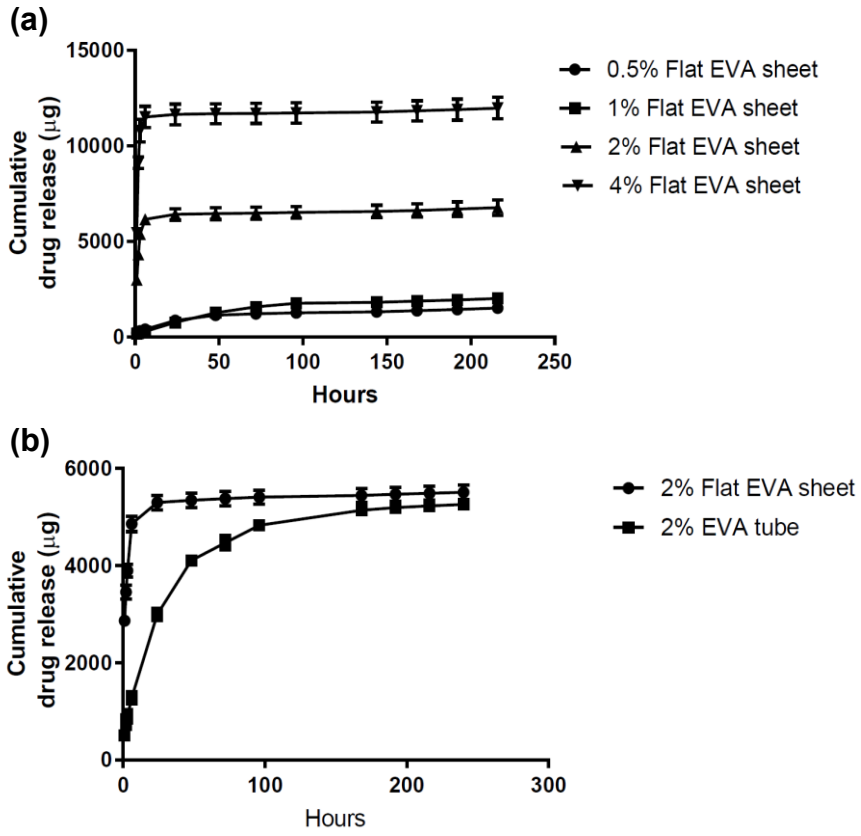

Figure 5.5: Drug release from ibuprofen-loaded EVA. *Comparison of increasing concentration drug loads (a) and comparison of release from an EVA membrane and tube (b). N=3, mean ± SEM.*

The geometry of the EVA tubes presents differently to the EVA membranes and a change in the release was seen (Figure 5.5). Drug release was blocked from one surface (either internal or external) by coating with blank EVA allowing drug release from the opposite surface to be measured. The external surface had a cumulative drug release of 6165 µg in 14 days in comparison to 4970 µg from the internal surface. The overall release was similar from both surfaces with 91% from the external surface and 87% from the internal surface, as the initial drug loading was 6770 µg and 5810 µg respectively

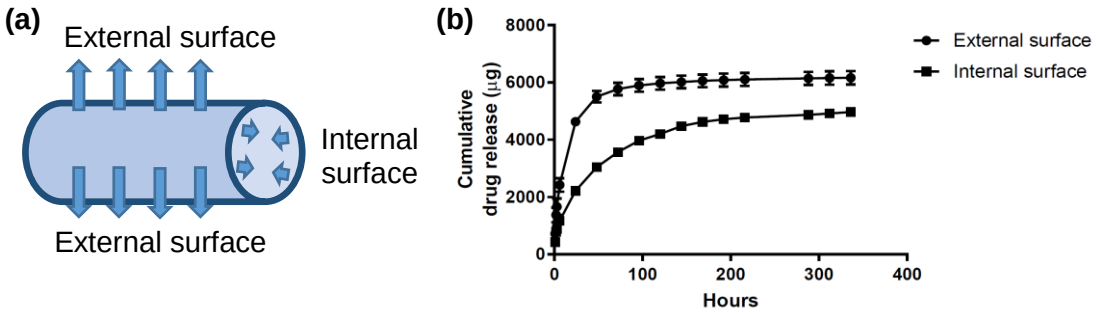

Figure 5.6: Drug release from the internal and external surfaces of ibuprofen-loaded EVA. *Representation of an EVA tube (a) and comparison of release from the internal and external surface of the EVA tube (b). N=3, mean ± SEM.*

5.2.1.2 Polycaprolactone (PCL)

Scanning electron microscope (SEM)

The composition and morphology of the PCL membranes (7 mm x 12 mm x 0.5 mm) either blank or loaded with 2% ibuprofen were analysed using SEM (Figure 5.7). No pores could be seen on the membrane and small crystals of drug were deposited over the surface of the membrane (Figure 5.7 (b)). Drug loading was not homogenous and was randomly deposited.

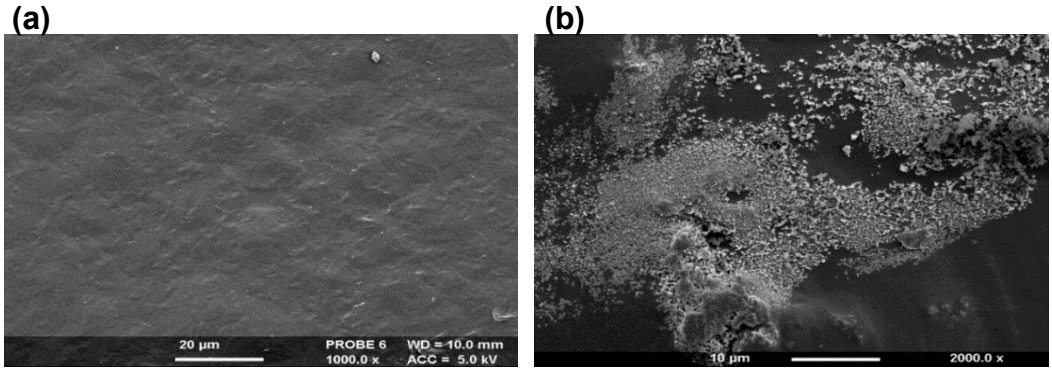

Figure 5.7: SEM images of blank and ibuprofen-loaded PCL membranes. *Blank PCL membranes (a) and ibuprofen loaded PCL membranes (b).*

Drug release

In vitro drug release from ibuprofen-loaded PCL membranes was measured every hour for 4 h and then every 24 h for 10 days. Each time the solution was completely removed and replaced with fresh water. The drug concentration in the solution was measured using UV-Vis spectroscopy and a calibration curve (Figure 2.11). The release from ibuprofen-loaded PCL was rapid in the first 4 h and then plateaued and remained constant after 24 h. The release reached ~80% of the starting drug load after 10 days (Figure 5.8).

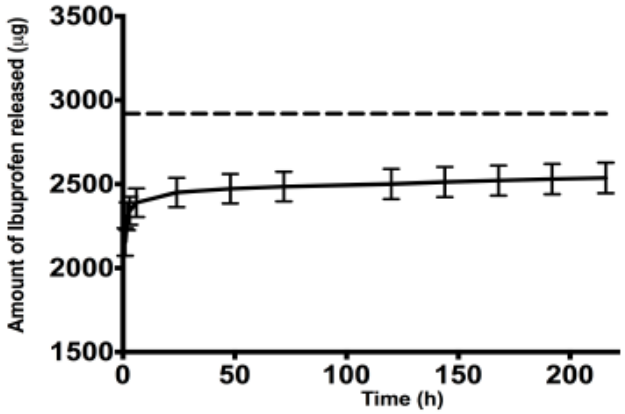

Figure 5.8: Drug release from ibuprofen-loaded PCL. *The initial drug load is shown by the dotted line. N=3, mean ± SEM.*

5.2.1.3 Poly (Lactic-co-Glycolic) acid (PLGA)

Scanning electron microscope (SEM)

The composition and morphology of the electrospun PLGA nanofibres with and without ibuprofen were analysed using SEM (Figure 5.9). The nanofibres with a 1:7 ratio of drug to polymer were smooth and randomly aligned. The 1:7 formulation resulted in the fabrication of 100 nanofibres with an average diameter of 0.92 µm.

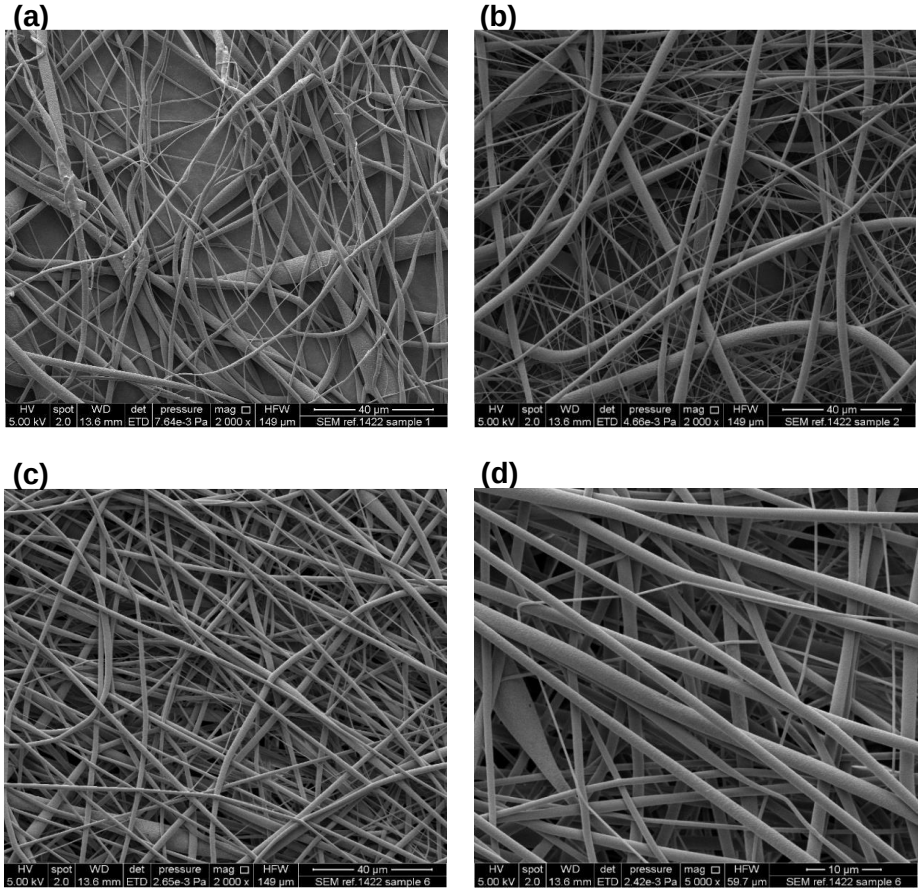

Figure 5.9: SEM images of blank and ibuprofen-loaded electrospun PLGA nanofibres. *Blank PLGA nanofibres (a), (b) and ibuprofen-loaded PLGA nanofibres (c), (d).*

Drug release

In vitro drug release from ibuprofen-loaded PLGA nanofibres was measured every hour for 4 h and then every 24 h for 7 days. Each time the solution was completely removed and replaced with fresh water. The drug concentration in the solution was measured using UV-Vis spectroscopy and a calibration curve as before (Figure 2.11). The ibuprofen-loaded PLGA nanofibres demonstrated first order kinetics with a steady release, however, 100 % of the drug was released within 7 days (Figure 5.10).

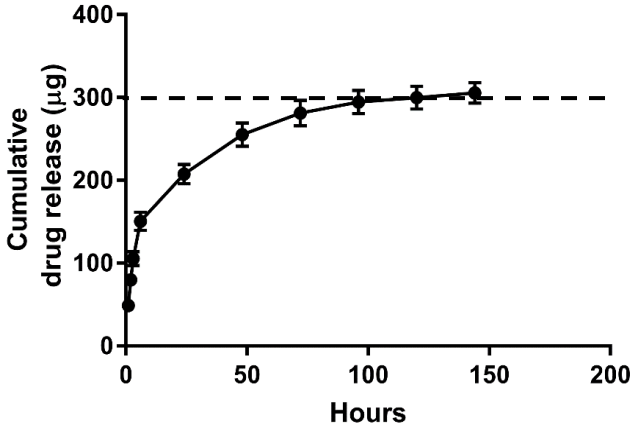

Figure 5.10: Drug release from ibuprofen-loaded electrospun PLGA nanofibres. *The initial drug load is shown by the dotted line. N=3, mean ± SEM.*

5.2.1.4 Mesoporous silica particles (MSN)

Scanning electron microscope (SEM) and transmission electron microscope (TEM)

The composition and morphology of the MSN were analysed using SEM and TEM (Figure 5.11). The MSNs presented a spherical shape with an average diameter of 100 nm. The SEM analysis showed that the nanoparticles formed clusters (Figure 5.11 (a)), however, the TEM images illustrate the ordered arrangement of the nanometer channels and the uniformity of pores (Figure 5.11 (b)).

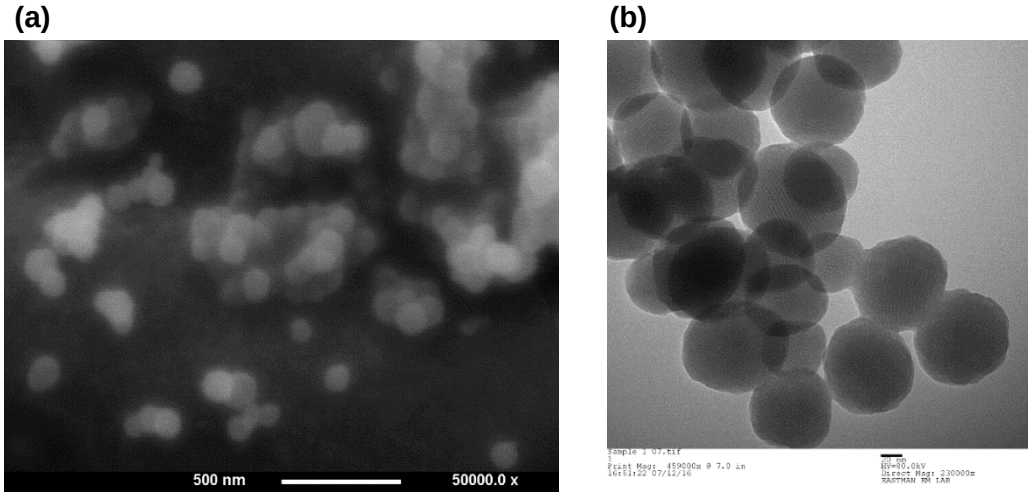

Figure 5.11: SEM (a) and TEM (b) images of blank mesoporous silica nanoparticles.

5.2.1.5 MSN loaded PCL

Scanning electron microscope (SEM)

The composition and morphology of the PCL membranes (7 mm x 12 mm x 0.5 mm) embedded with ibuprofen-loaded MSN were analysed using SEM (Figure 5.12). No pores could be seen on the membrane which was similar to the ibuprofen-loaded PCL (section 5.2.1.2). However, the loading was more homogenous with MSN loading *c.f.* pure drug (Figure 5.12 (b), (c)) and less drug was deposited on the surface of the PCL.

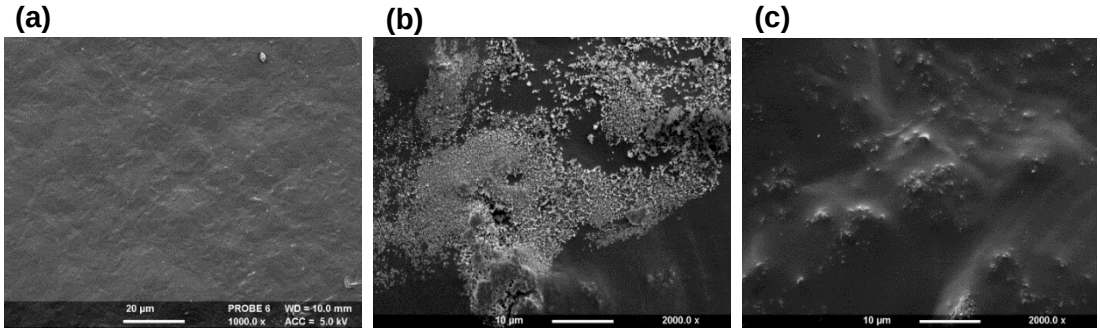

Figure 5.12: SEM images of blank, ibuprofen-loaded PCL membranes and MSN-loaded PCL membranes. *Blank PCL membranes (a), ibuprofen-loaded PCL membranes (b) and ibuprofen-loaded MSN embedded PCL (c).*

MSN drug loading

In initial studies 10 mg of MSN were added to 10 mL of 10 mg/mL ibuprofen solution which resulted in 7% drug loading after 1 h and 33% drug loading after 24 h (data not shown). Further studies were conducted to explore drug loading in other MSN and drug formulations. Different MSN and drug ratios were incubated for 24 h. A ratio of 1:50, consisting of 10 mg MSN and 10 mL of 50 mg/mL ibuprofen solution, gave the best drug loading at 72% (Figure 5.13).

1:1	10 mL 5 mg/mL ibuprofen with 50 mg MSN
1:2	10 mL 5 mg/mL ibuprofen with 25 mg MSN
1:5	10 mL 25 mg/mL ibuprofen with 50 mg MSN
1:10	10 mL 50 mg/mL ibuprofen with 50 mg MSN
1:50	10 mL 50 mg/mL ibuprofen with 10 mg MSN

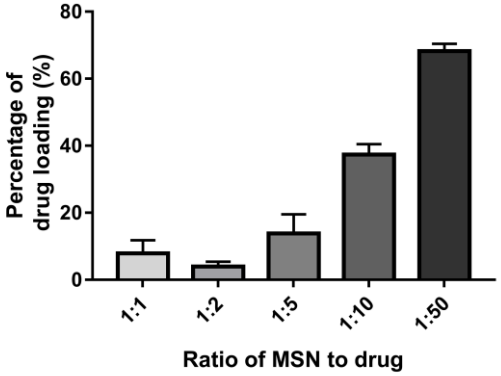

Figure 5.13: Drug loading (w/w) into different MSN formulations*. N=3, mean ± SEM.*

Drug release

In vitro drug release from MSN-loaded PCL membranes was measured every hour for 4 h and then every 24 h for 14 days. Each time the solution was completely removed and replaced with fresh water. The drug concentration in the solution was obtained using UV-Vis spectroscopy and a calibration curve as before (Figure 2.11). The release of ibuprofen was slower when loaded into MSN and then embedded into PCL in comparison to when loaded into PCL alone (Figure 5.14). After 14 days ~80% of drug was released in the ibuprofen loaded PCL (Figure 5.14 (a)), whereas, only ~20% of ibuprofen was released from the MSN-loaded PCL (Figure 5.14 (b)). Embedding the drug into MSN and PCL produced a dual release mechanism which improved the controlled release of ibuprofen.

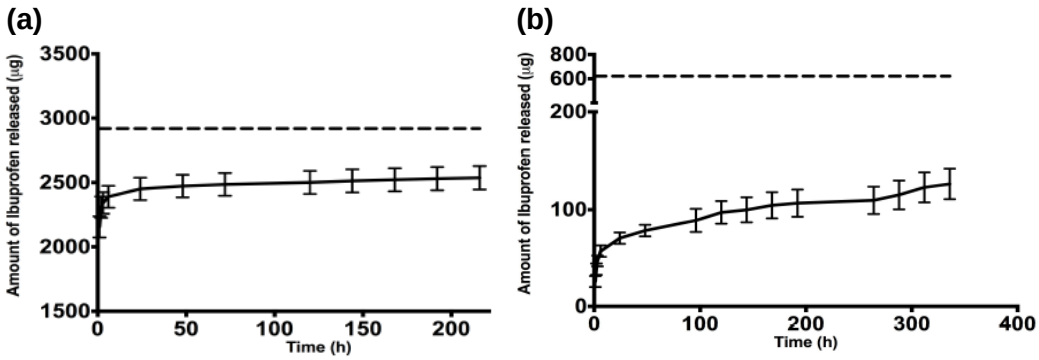

Figure 5.14: Drug release from ibuprofen-loaded PCL (a) and ibuprofen-loaded MSN embedded in PCL (b). *The initial drug load is shown by the dotted line. N=3, mean ± SEM.*

EVA tubes, PLGA nanofibres and ibuprofen-loaded MSN embedded PCL membranes all demonstrated suitable properties to be developed and used as drug delivery platforms for PNI. EVA tubes and PLGA nanofibres possess an additional advantage of having simplistic manufacturing protocols and so were therefore taken forward and tested *in vivo*.

5.2.2 Effect of ibuprofen-loaded EVA on nerve regeneration.

5.2.2.1 Quantification of neuronal growth.

EVA tubes with and without ibuprofen were surgically implanted into a rat sciatic nerve transection model as a wrap around a primary repair. The material had appropriate handling properties in terms of stiffness, strength, stability, size and shape and was surgically implanted around the injury with ease (Figure 5.15 (a)). Following 21 days the tubes were still in place but had contracted around the nerve. There were no visual abnormalities around the injury site during the harvest (Figure 5.15 (b)).

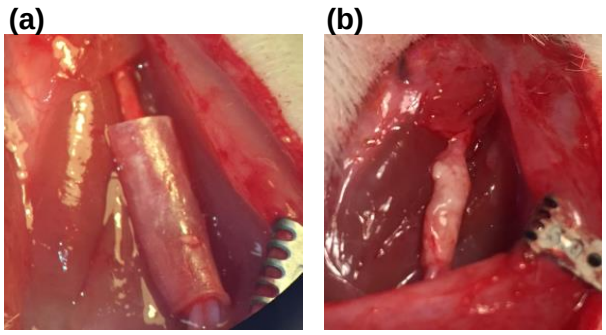

Figure 5.15: Implanted EVA tubes. *Surgically implanted EVA tubes (a) and harvesting tubes at 21 days post injury (b).*

The regenerative effect of ibuprofen treatment released from EVA was analysed histologically. Transverse sciatic nerve sections were stained with neurofilament to quantify axon numbers (Figure 5.16 (c)). The results demonstrated that a dose of ~17 µg/day ibuprofen increased the number of axons in the distal stump in comparison to no drug treatment (Figure 5.16 (a)). Furthermore the number of axons as a percentage to the proximal stump was higher in the ibuprofen treatment group in comparison to the control group with 160% and 105% respectively (Figure 5.16 (b)).

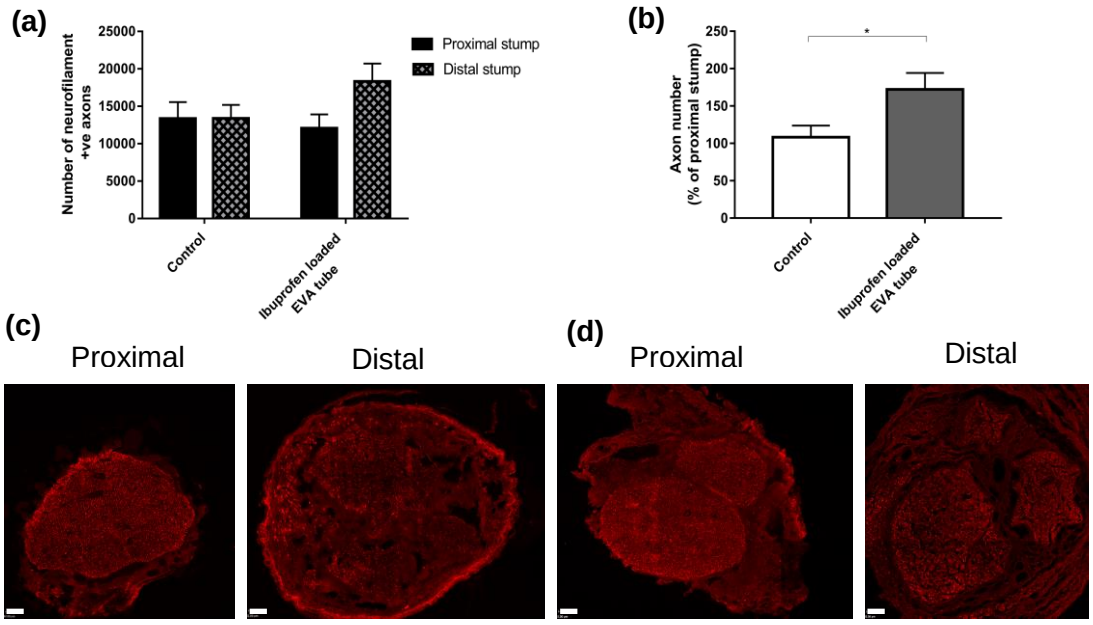

Figure 5.16: Axon number in a transection injury model with an implanted ibuprofen-loaded EVA tube. *Axons were quantified by counting the number of neurofilament-positive cells in the proximal stump and distal stump. The number of axons in the distal stump increased in the group with an implanted ibuprofen-loaded EVA tube in comparison to the blank EVA tube (a). Also the number of axons in the distal nerve stump exceeded those in the proximal stump (b). Micrographs are 10 µm transverse sections showing neurofilament positive neurites at 5 mm proximal and distal to the injury site in the control group (c) and ibuprofen treatment group (d). Scale bar = 100 µm. N=6, mean ± SEM for each condition. Two-way ANOVA (a), and two-tailed t-Test (b), *p < 0.05.*

5.2.2.2 Myelinated axon quantification.

Semi-thin sections (0.5 µm) were taken at specific regions in the proximal stump (5 mm from injury site) and distal stump (5 and 10 mm from injury site) following 21 days and stained with toluidine blue to evaluate the extent of regeneration and cellular features of the nerve tissue (Figure 5.18). Axon myelination had reduced in the distal stump following injury in comparison to the proximal stump (Figure 5.18), however, there is evidence that axon myelination is still present 5 and 10 mm distal to the injury

site (Figure 5.17). The results showed that there were more myelinated axons in the treatment group in comparison to the control group at 5 mm in the distal stump but no difference at 10 mm, however, this was not statistically significant (Figure 5.17 (a)). The G-ratio was also higher in the ibuprofen group (Figure 5.17 (d)), whereas, the myelin thickness was greater in the control group (Figure 5.17 (c)), however, neither result was statistically significant. No difference was seen in the mean myelinated axon diameter (Figure 5.17 (b)).

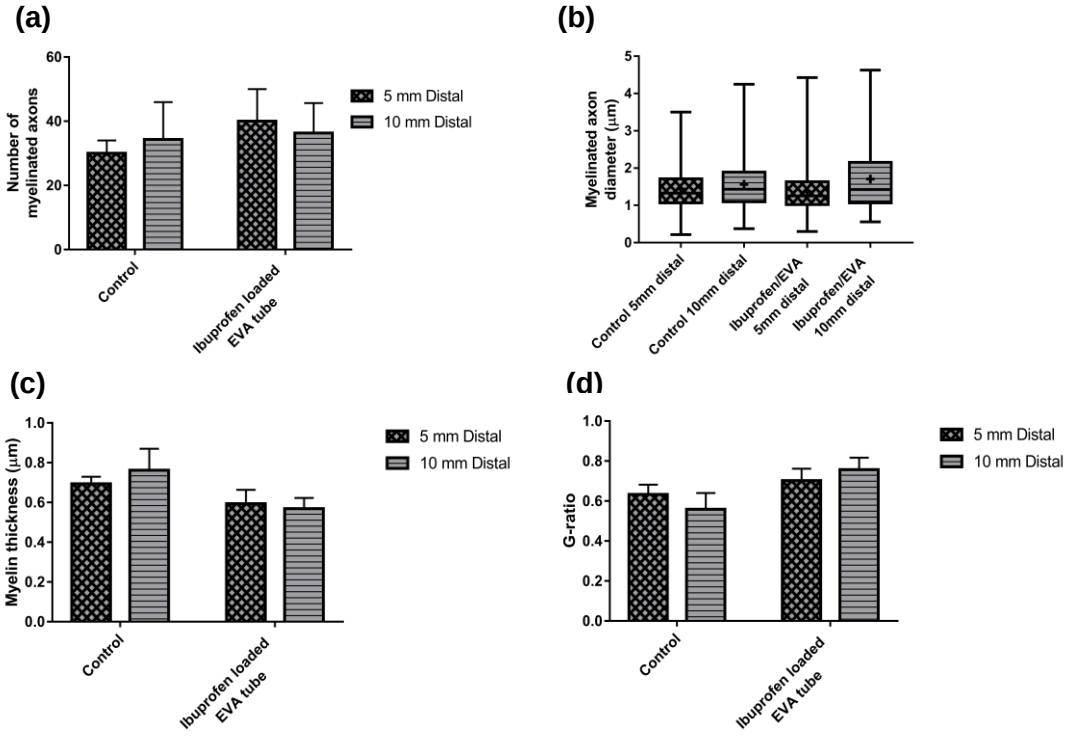

Figure 5.17: Myelination quantification following a transection injury treated with ibuprofen-loaded EVA. *SEM images were used to quantify the number of myelinated axons, myelin thickness, G-ratio and myelinated axon diameter per three 8600 µm² fields. There was a higher number of myelinated axons in the distal stump of the control group in comparison to the treated group (a), however there was no difference seen in other quantification measures (b), (c) and (d). Box plots show the distribution of myelinated axon diameters with whiskers showing max to min which a horizontal line indicating the median and + indicating the mean. N=3, mean ± SEM, Two-way ANOVA (a), (c), (d), One-way ANOVA with Tukey's post hoc test (b), no significance.*

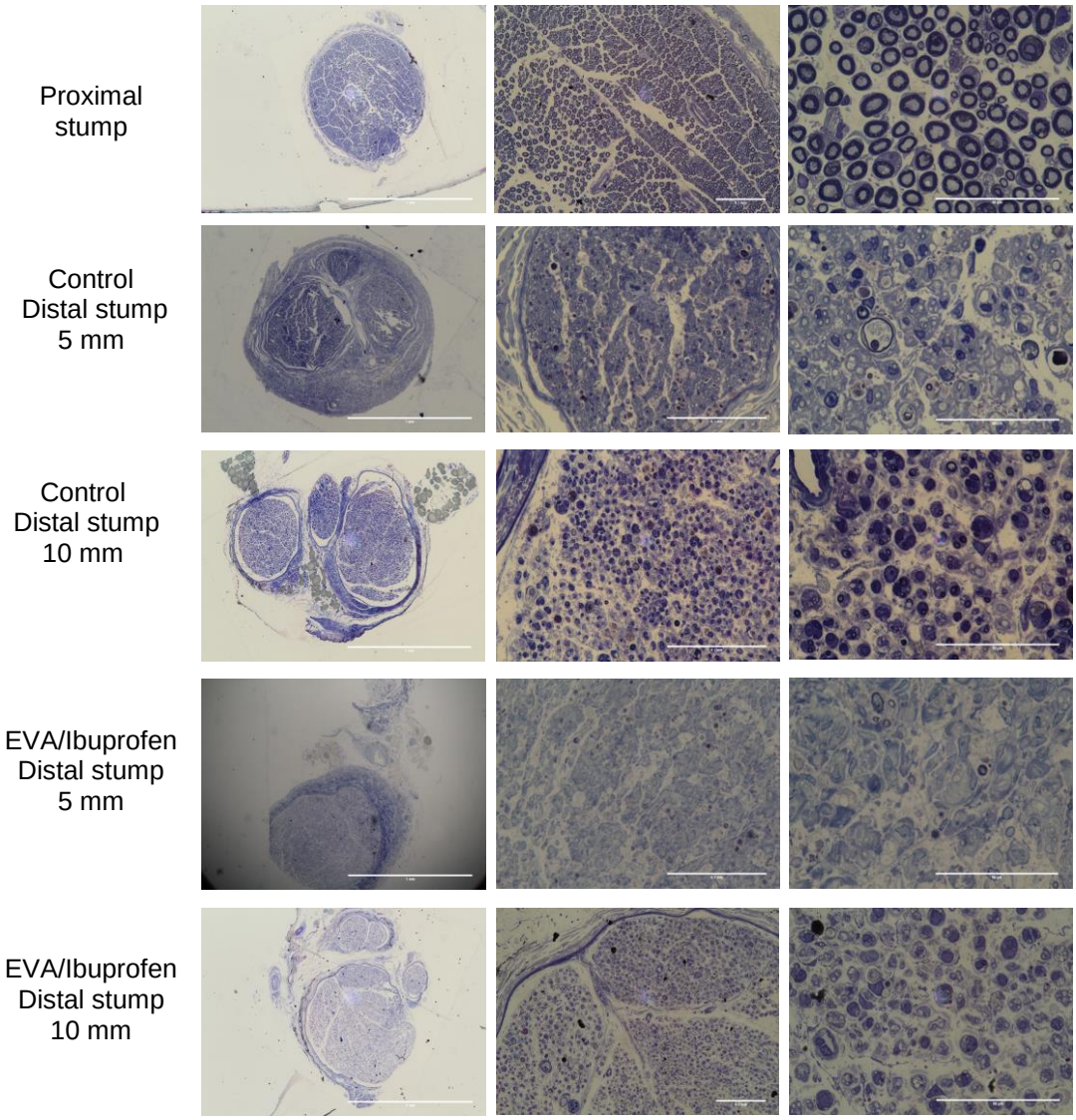

Figure 5.18: Distribution of neural tissue growth at multiple regions in the sciatic nerve at 21 days following a transection injury. *Representative semi-thin sections stained with toluidine blue show the differences in density and distribution of neural tissue growth between the proximal and distal stump at x 5, x 20 or x 40 and x100 magnification.*

5.2.2.3 Functional recovery.

Motor and sensory recovery was studied at the 21 day end point using muscle weight, static sciatic index, electrophysiology, and von Frey analysis. The animals in the treated group demonstrated a better response to sensory stimulation than the control group. The threshold response to the von Frey filaments was lower with the treatment of ibuprofen-loaded EVA (Figure 5.19 (a)). Moreover, the gastrocnemius muscle was harvested and weighed immediately. There was a small increase seen in the muscle mass in the treated group in comparison to the control group, however, the difference was not statistically significant (Figure 5.19 (b)). Furthermore, no difference in SSI was seen between the two groups. No improvement in the toe spread was seen between all the groups as they all still presented with a SSI of 100 (Figure 5.20).

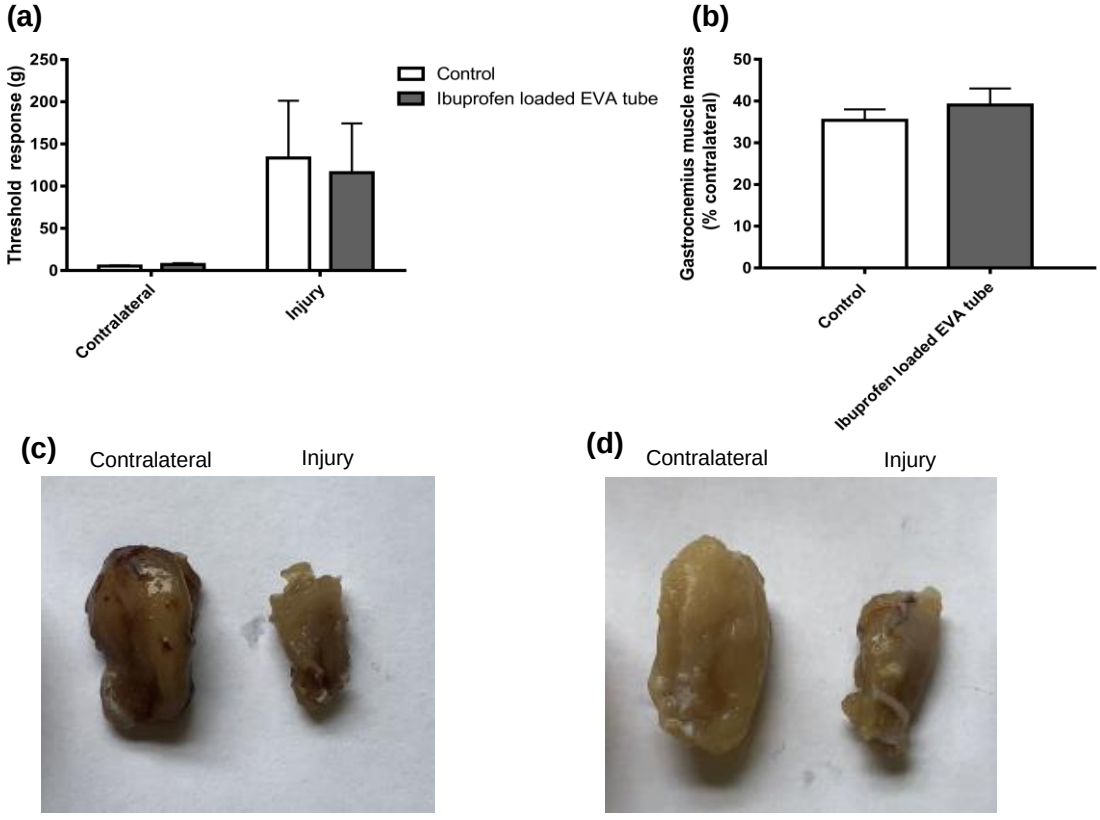

Figure 5.19: Von Frey and muscle mass following a transection injury treated with ibuprofen-loaded EVA. *A lower threshold response was seen in the ibuprofen treatment group in comparison to the control group (a). No difference was seen between the groups with muscle mass (b). The harvested muscle from the control (c) and ibuprofen treatment group (d). N=6, mean ± SEM, Two-way ANOVA (a), two-tailed T-test (b), no significance.*

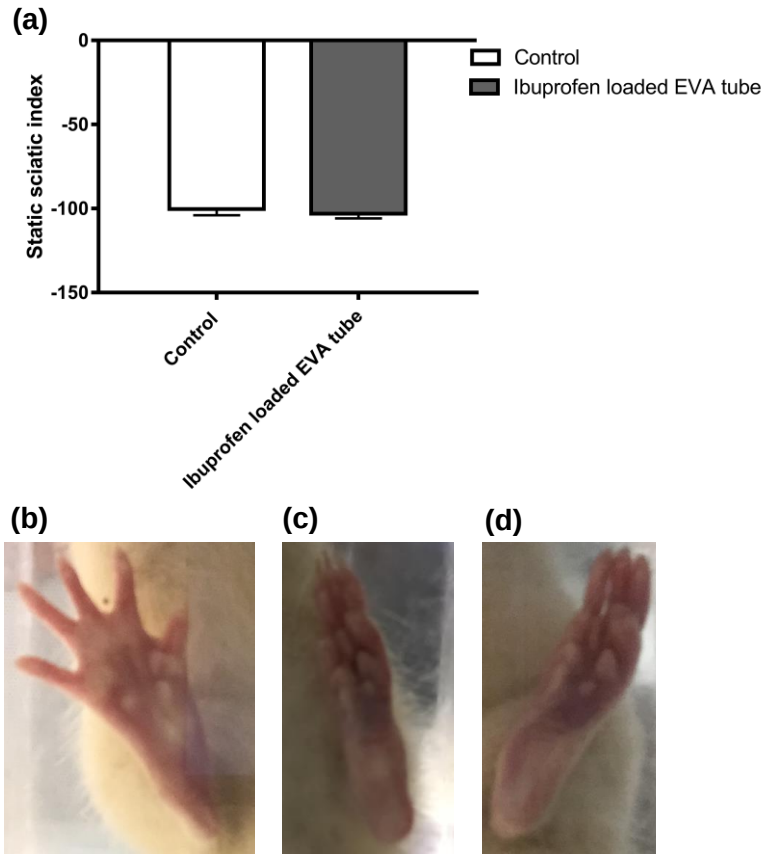

Figure 5.20: SSI following a transection injury treated with ibuprofen-loaded EVA. *No difference in the SSI was seen between the two groups (a). Hind paw images used to conduct SSI quantitation; contralateral side (b), injury side in the control group (c), and the ibuprofen treated group (d). N=6, means ± SEM, Two-tailed T-test, no significance.*

CMAPs were recorded from the contralateral side and injured side in all animals. The CMAP has reduced significantly in the injured side in comparison to the contralateral side but no difference was seen between the two groups (Figure 5.21 (a)). The latency had slightly increased in the treated group (Figure 5.21 (b)), however, the stimulus intensity to achieve a response was lower in the ibuprofen treatment group in comparison to the control group (Figure 5.21 (c)).

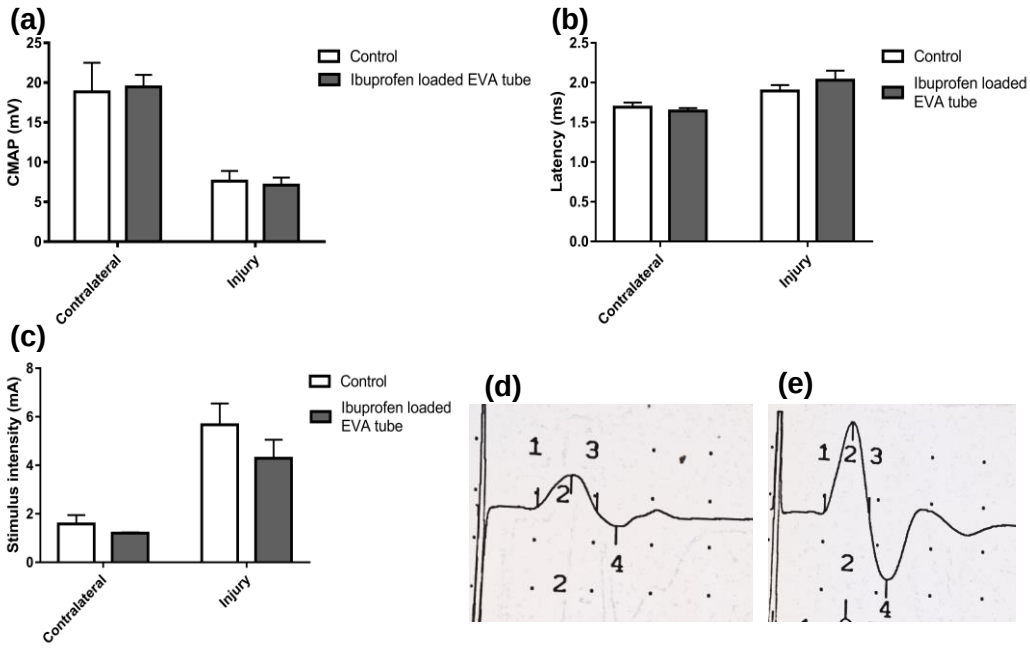

Figure 5.21: Electrophysiological evaluation of a transection injury treated with ibuprofen-loaded EVA. *The sciatic nerve was stimulated proximal to the injury site and the CMAP was recorded from the gastrocnemius muscle. Representative electrophysiological traces are included for the control group (d) and ibuprofen treatment group (e). No difference was seen with the CMAP between the groups (a). The latency was lower in the control group but not statistically significant (b), however, the stimulus intensity was lower in the ibuprofen treatment group (c). N=6, means ± SEM, Two-way ANOVA, no significance.*

5.2.2.4 Macrophages

Macrophages were identified and quantified in the distal stump at 21 days post-injury. The total number of macrophages were quantified immunohistochemically by staining for CD68. This sub-population of $CD68^{+}$ macrophages were then also analysed for immunoreactivity for arginase-1 which was used to establish the proportion of the M2 macrophage phenotype. The results indicate that there was a small decrease in the number of M2 macrophages in the ibuprofen treatment group but it wasn't statistically significant (Figure 5.22).

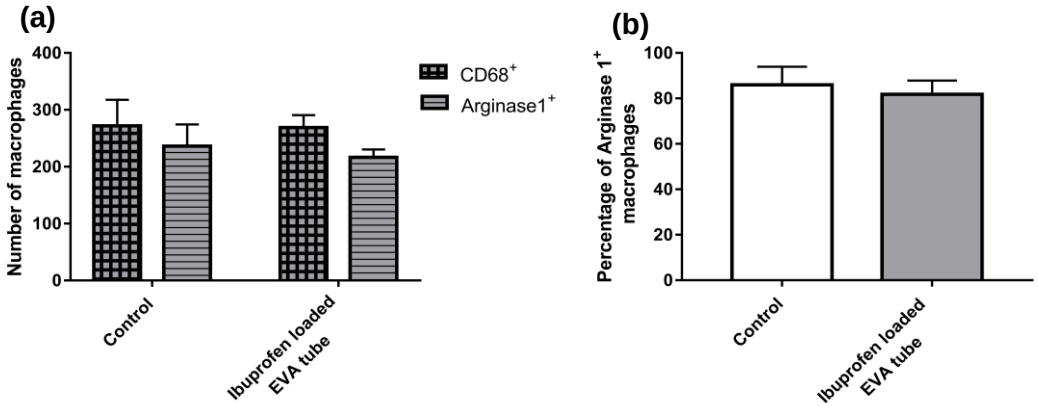

Figure 5.22: Macrophage presence and phenotype following a transection injury treated with ibuprofen-loaded EVA. The total number of macrophages *were quantified by counting the number of CD68 positive cells 5 µm into the distal stump. From these the M2 macrophage population could also be quantified (a). The population of M2 macrophages was quantified as a percentage of the total number of macrophages (b). N=6, mean ± SEM for each condition. Two-way ANOVA (a,) two-talied T-test (b) no significance.*

5.2.2.5 Vasculature

Analysis revealed larger blood vessel diameter in the distal stump of the ibuprofen treated group in comparison with the control group. Vasculature in the injured nerves in the ibuprofen-treated group revealed ~ 25 blood vessels per nerve with a mean diameter of ~18 µm, whereas, the control group presented ~ 15 blood vessels per nerve with a diameter of ~12 µm (Figure 5.23)

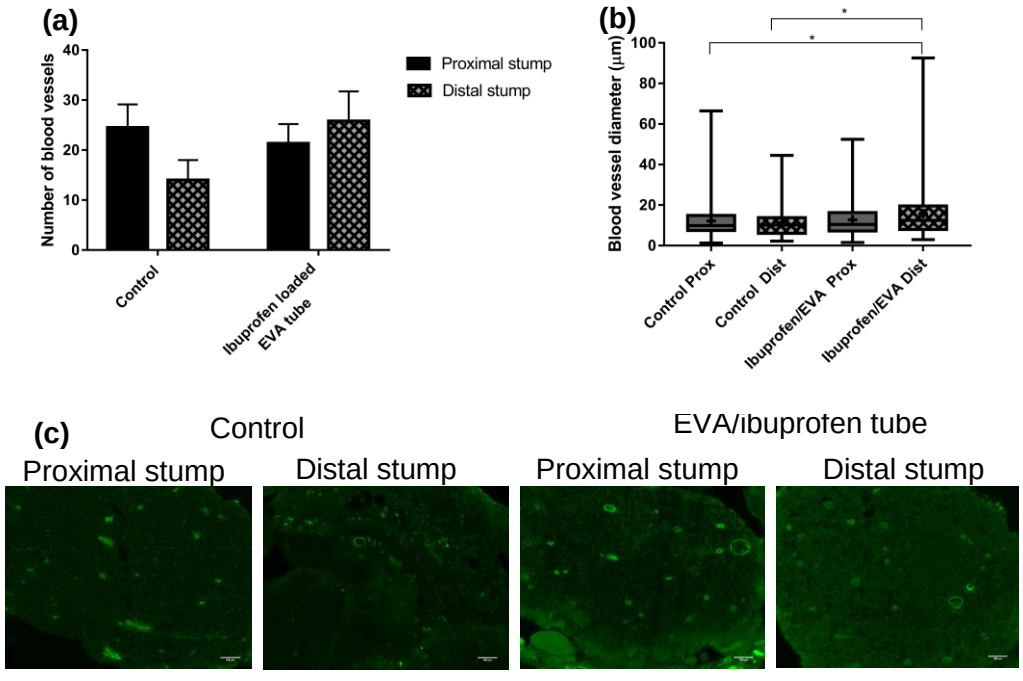

Figure 5.23: Vasculature changes following a transection injury treated with ibuprofen-loaded EVA. *Quantitative analysis of the number (a) and diameter (b) of blood vessels by RECA-1 (green). Immunostained 10 µm transverse sections from the proximal and distal stumps (c). Scale bar = 100 µm. N=6, mean ± SEM for each condition, Two-way ANOVA (a) One-way ANOVA with Tukey's post hoc test (b), *p < 0.05. Box plots show the distribution of blood vessel diameter with boxes extending from the max to min, + indicates mean.*

5.2.2.6 Residual drug release

The EVA tubes implanted in the *in vivo* experiments were harvested to measure the residual amount of drug. This was conducted by re-dissolving the EVA tubes in chloroform and measuring the amount of drug remaining using UV-Vis spectrophotometry. It was found that the EVA tubes provided a consistent system delivering the same dose to each animal, as ~96% of the drug was released from all 6 tubes in the 3 week period (Figure 5.24).

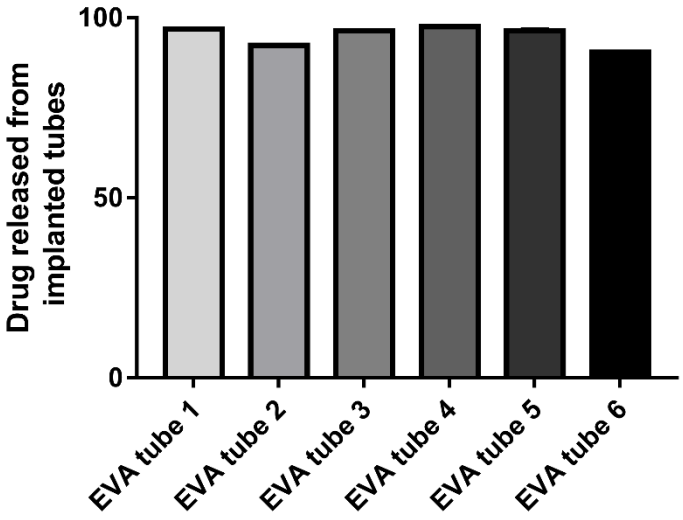

Figure 5.24: Drug released from EVA tubes implanted in vivo. *The residual drug was measured by re-dissolving the EVA tubes in chloroform. All 6 tubes released ~96% of the initial drug load within 3 weeks.*

5.2.3 Effect of ibuprofen-loaded PLGA on nerve regeneration.

5.2.3.1 Quantification of neuronal growth

PLGA nanofibre sheets loaded with and without ibuprofen were surgically implanted into a rat sciatic nerve as a cuff around a crush injury for 7 or 28 days.

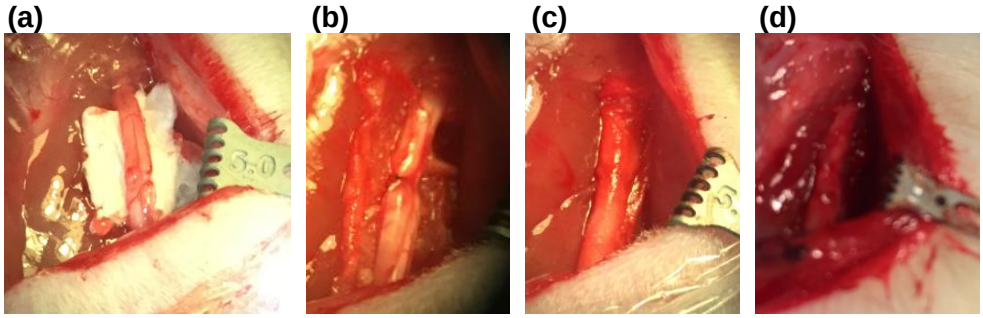

Figure 5.25: Implanted PLGA nanofibre wraps. *Surgically implanted PLGA (a), (b), (c) and harvesting of nanofibres at 28 days post-injury (d).*

The PLGA nanofibres had appropriate handling properties in terms of stiffness, strength, stability, size and shape and was surgically implanted around the injury with ease (Figure 5.25 (c)). The material was still in place wrapped around the nerve at 7 and 28 days. There were no visual abnormalities seen around the injury site during the harvest (Figure 5.25 (d)). The regenerative capacity of ibuprofen treatment released from this biomaterial was analysed histologically at both 7 and 28 days post-injury. Transverse sciatic nerve sections were stained with neurofilament to quantify axon numbers. The results demonstrated that ibuprofen increased the number of axons in the distal stump in comparison to the control at 28 days post-injury but not at 7 days, however, the differences were not statistically significant (Figure 5.26).

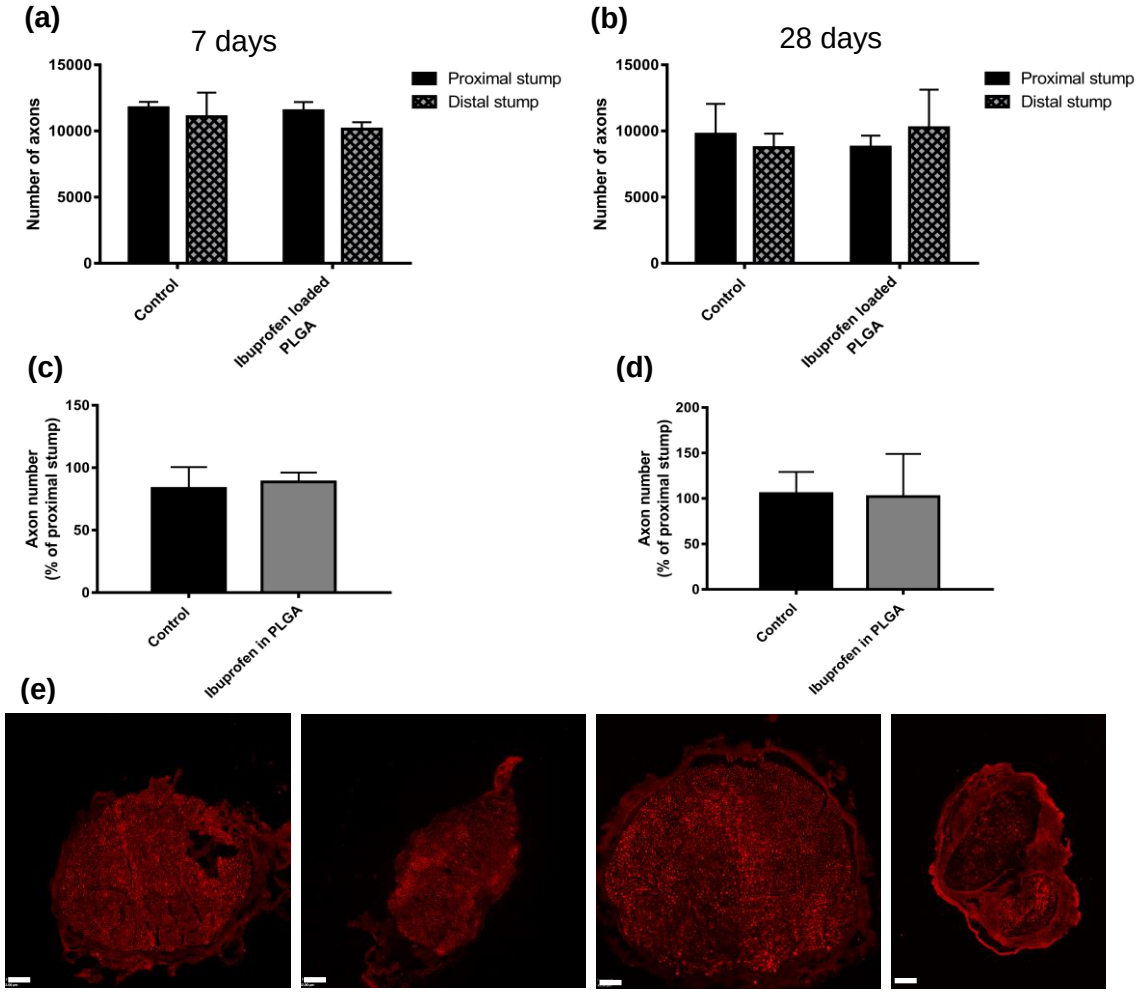

Figure 5.26: Axon number in a crush injury model with implanted ibuprofen-loaded PLGA nanofibres. *Axons were quantified by counting the number of neurofilament-positive cells in the proximal stump and distal stumps. The number of axons in the distal stump increased in the group with implanted ibuprofen-loaded PLGA nanofibers in comparison to the control at 28 days (b), (d), but not at 7 days (a), (c). Micrographs are 10 µm transverse sections showing neurofilament positive neurites (e). Scale bar = 100 µm. N=3 (7days), N=4 (28 days), mean ± SEM for each condition. Two-way ANOVA (a), (b), and two-tailed T-Test (c), (d), no significance.*

5.2.3.2 Functional recovery

Functional improvements were also studied in addition to histologically analysis. Motor recovery was investigated using techniques that study muscle reinnervation such as; electrophysiology, muscle mass and SSI, and sensory improvements were explored using von Frey. Muscle mass and electrophysiology were conducted at the 7 and 28 day end point and SSI and von Frey were measured every 2-3 days throughout the experiment. No difference was seen in the threshold response to the von Frey filaments between the two groups after 7 days (Figure 5.27 (a)). However, the threshold response returned to baseline quicker with ibuprofen-loaded PLGA nanofibres after 28 days with statistical significance at 20 and 22 days post-injury in comparison with the control group (Figure 5.27 (b)).

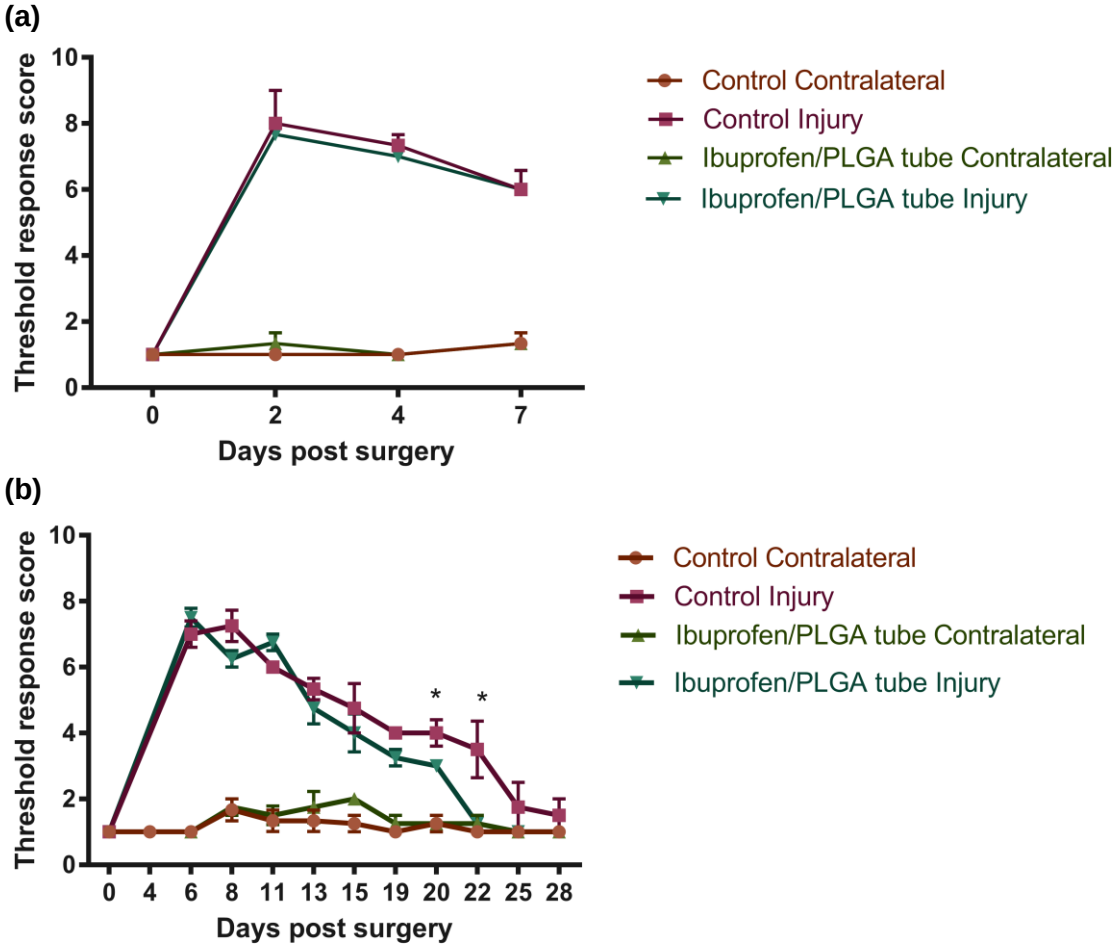

Figure 5.27: Von Frey following a crush injury treated with ibuprofen-loaded PLGA nanofibres. *The threshold response returned to baseline quicker in the ibuprofen treatment group in comparison to the control group after 28 days (a) N=3 (7 days), N=4 (28 days), mean ± SEM, Multiple T-tests between the injured groups at each time point *p<0.05.*

Furthermore, the SSI was continuously lower in the ibuprofen treatment group from day 4 with statistical significance seen at days 6 and 8. The SSI also returned to baseline quicker in the ibuprofen treatment group than the control. This occurred by 22 days post-injury with ibuprofen-loaded PLGA nanofibers, but by day 28 in the control group (Figure 5.28).

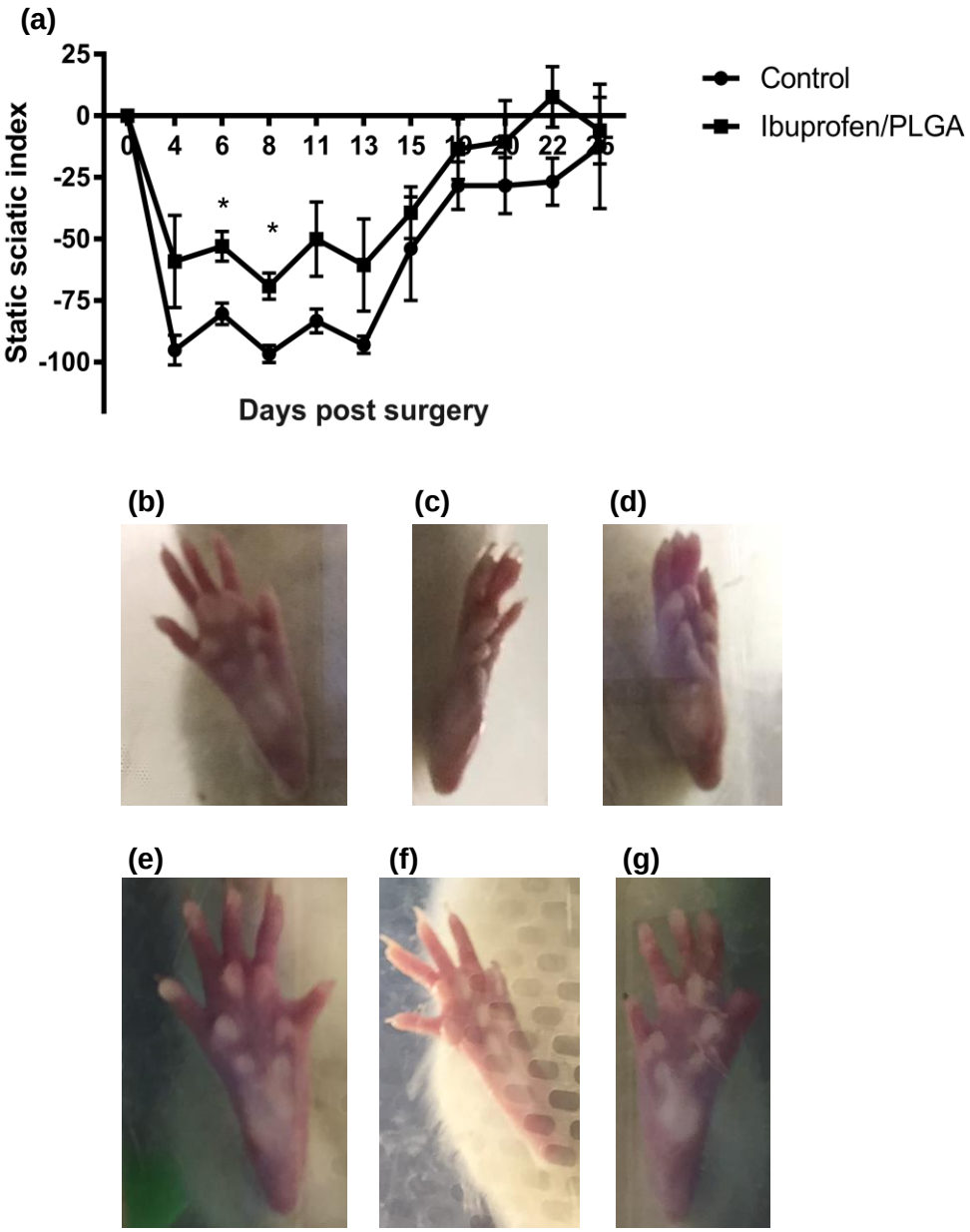

***Figure 5.28:* SSI following a crush injury treated with ibuprofen-loaded PLGA nanofibres.** *A **s**ignificant difference in the SSI was seen between the two groups (a). Hind paw images used to conduct SSI quantitation; contralateral side (b), control group (b) and treatment group (d) at 8 days and contralateral side (e), control group (f) and treatment group (g) at 28 days. N=4, means ± SEM, multiple T-tests, *p<0.05.*

The gastrocnemius muscle was harvested and weighed immediately. The muscle mass had reduced in the nerve-injured hind leg in comparison to the contralateral side in all animals. Moreover, the muscle mass had reduced further from 7 days to 28 days but no difference was seen between treatment and control group (Figure 5.29).

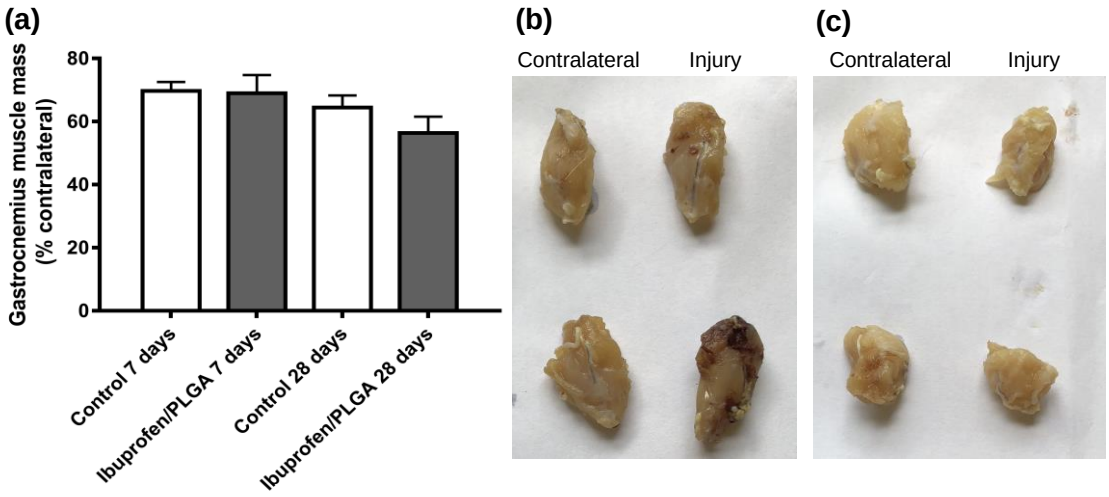

Figure 5.29: Gastrocnemius muscle mass following a crush injury treated with ibuprofen-loaded PLGA nanofibres. *No difference was seen between the groups with muscle mass (a). Harvested muscle from the control (top) and ibuprofen treated group (bottom) at 7 days (b) and 28 days (c). N=3 (7 days), N=4 (28 days), mean ± SEM, One-way ANOVA with Tukey's post-hoc test, no significance.*

CMAPs were recorded from the gastrocnemius muscle in the contralateral and injured side in all animals. The CMAP had reduced in the injured side in comparison with the contralateral side at 7 days (Figure 5.30 (a)). On the other hand, by 28 days the CMAP had increased in the ibuprofen treated group and was even higher than that seen in the corresponding contralateral muscle. (Figure 5.30 (b)). The latency was higher in the injured nerve of the control group than the ibuprofen treatment group (Figure 5.30 (c), (d)), however, the stimulus intensity to achieve a response was lower in the ibuprofen treatment group in comparison with the control group (Figure 5.30 (e), (f)).

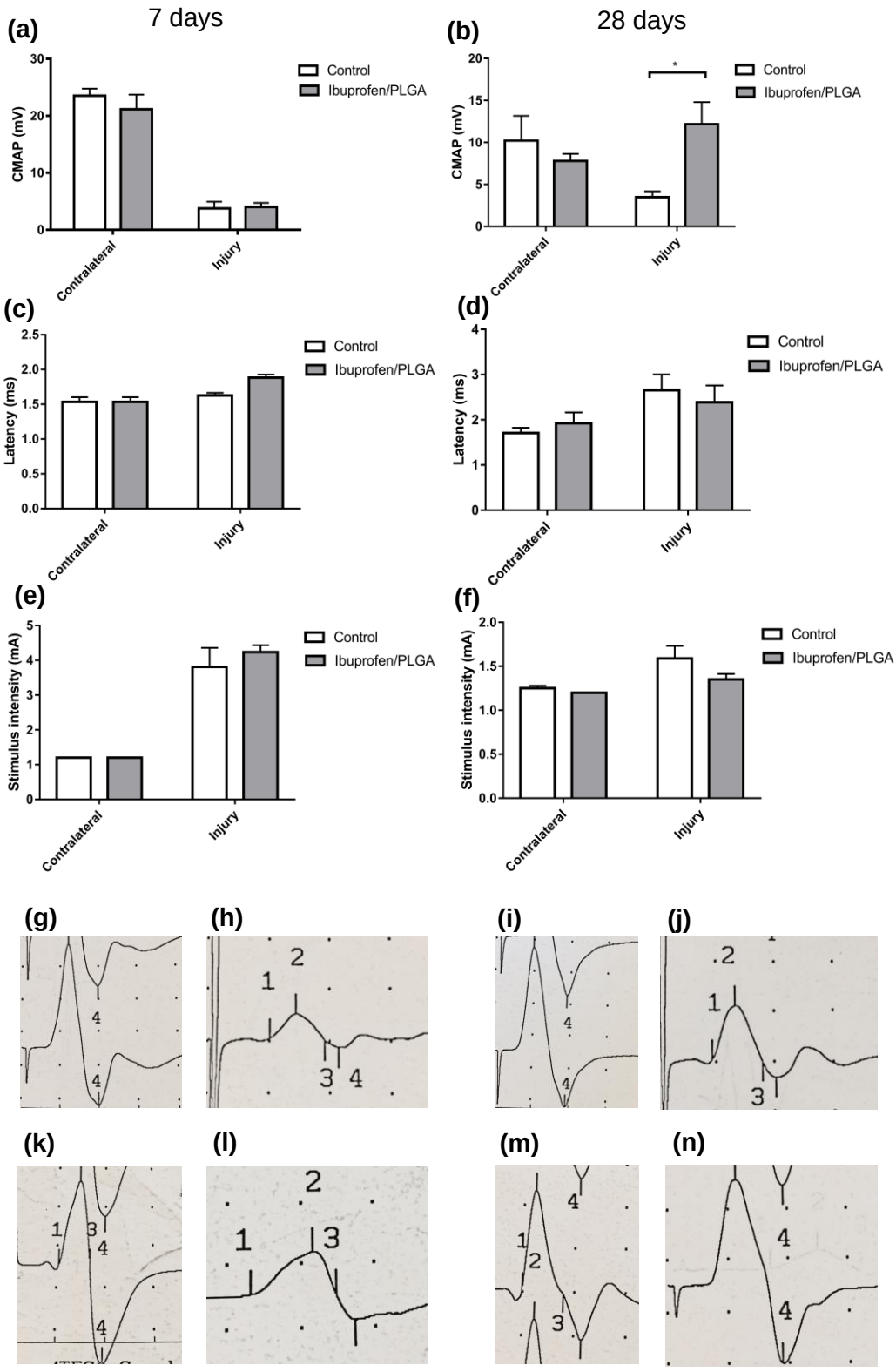

Figure 5.30: Electrophysiological evaluation of a crush injury treated with ibuprofen-loaded PLGA nanofibres at 7 and 28 days. *The CMAP was significantly higher in the treatment group at 28 days (a) but not at 7 days (b). No difference was seen in the latency at 7 (c) or 28 days (d). The stimulus intensity was lower in the ibuprofen treatment group at 28 days (f) but there was no difference at 7 days (e). The electrophysiological traces for the control group: contralateral (g) and injury side (h) at 7 day and contralateral (k) and injury side (l) at 28 days and the treatment group: contralateral (i) and injury side (j) at 7 day and contralateral (m) and injury side (n) at 28 days. N=3 (7 days), N=4 (28 days), means ± SEM, Two-way ANOVA, *p<0.05.*

5.2.3.3 Vasculature

Vascularisation was examined via immunohistochemical staining of transverse sections for RECA-1. Analysis revealed the presence of blood vessels throughout the injured nerves in both the proximal and distal sections, however, there was a higher number of blood vessels in the proximal stump in comparison with the distal stump. There was no difference in blood vessel diameter between the treated and control group at 7 or 28 days, however, there was an increase in blood vessel number observed with ibuprofen treatment at 28 days post-injury (Figure 5.31).

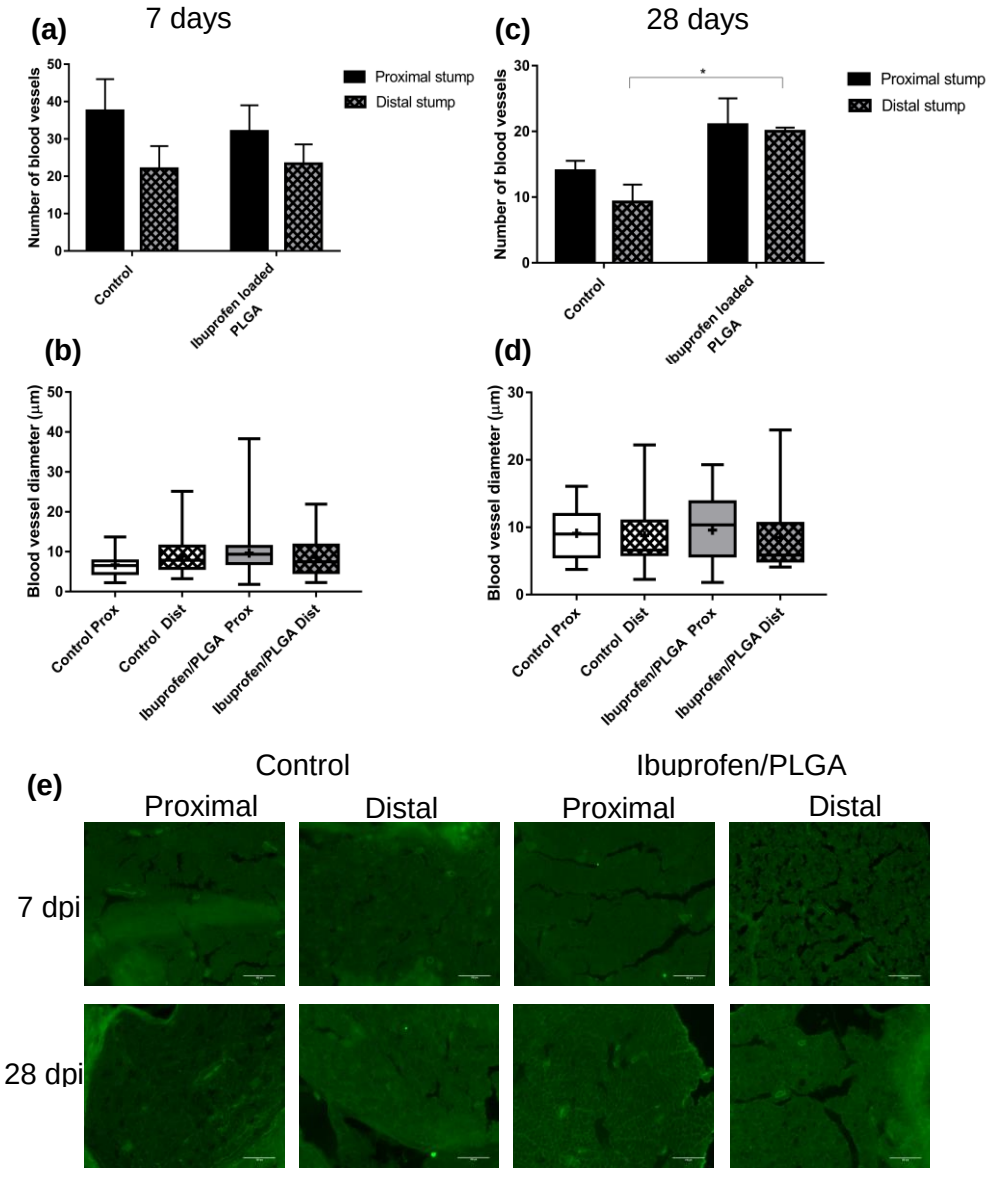

Figure 5.31: Vasculature changes following a crush injury treated with ibuprofen-loaded PLGA nanofibres. *Quantitative analysis of the number (a) and diameter (b) of blood vessels for 7 days and the number (a) and diameter (b) of blood vessels by RECA-1 (green). Immunostained 10 µm transverse sections from the proximal and distal stumps (c). Scale bar = 100 µm. N=3 (7 days), N=4 (28 days), mean ± SEM for each condition. Two-way ANOVA (a), (c), One-way ANOVA with Tukey's post-hoc test (b), (d). *p<0.05. Box plots show the distribution of blood vessel diameter with boxes extending from the max to min, + indicates mean.*

5.3 Discussion

5.3.1 Biomaterial drug release and characterisation.

Regenerative medicine is defined as “improving the self-healing capacity of the human body through the use of material scaffolds, cellular or biologically active components” *(Hopkins et al., 2015)*. This field is coupled with tissue engineering to combine their principles of engineering, materials, clinical science and biology *(Hopkins et al., 2015)*. This combinative approach bringing different disciplines together should be propelled into the PNI field when considering new therapies.

Not only are there currently no drug therapies for PNI, but there is also a lack of research into platforms to deliver such therapies. There are drugs moving into clinical trials, however, they are mostly immunosuppressants that have severe side effects associated with their systemic administration *(Tung, 2009)*. This doesn’t only identify a need for the discovery of novel compounds for PNI but also for alternative drug delivery methods. Drug treatments need to be able to promote nerve regeneration, reduce tissue atrophy, and improve functional recovery through the use of a minimally-invasive treatment. The systemic administration of drugs can lead to several drawbacks, including damage to healthy organs and insufficient amounts of drug reaching the target site. Many studies are beginning to develop better delivery systems to improve the efficiency of drug treatments, and this now needs to be driven into the PNI field.

This chapter was successful in instigating initial stages in the fabrication of drug loaded materials for local delivery in PNI.

5.3.1.1 EVA

Drug loading into EVA was efficient and provided sustained release over 3 weeks. This was the initial target treatment duration, as a previous study had seen positive effects on regeneration following three weeks systemic ibuprofen treatment *(Madura et al., 2011).* In that study it was considered that this treatment duration was suitable because it provided drug throughout the acute inflammatory phase and the majority of the myelin sheaths would have been removed during this time. Moreover, functional Rho is thought

to be needed for correct axon path-finding and a fine-tuned regeneration process *(Madura et al., 2011)*. Ibuprofen treatment led to improvements in the tibial functional index (TFI), as well as, increases in axon size and myelination following an interpostional graft in the tibial nerve in rats *(Madura et al., 2011)*.

Even though the release was sustained for three weeks with the EVA membranes there was an initial burst seen in the first 4 hours with 60% (4.2mg) and 20% (1.1 mg) of drug released from the membranes and tubes respectively. Within 24 hours this subsided and the release became more constant. This mirrored the results seen in a previous study that also observed a high burst of release of ibuprofen from EVA in the first few hours with 50% of the initial loaded drug released within the 24 hours. The release subsided after 48 hours with the remainder of the drug released in 10 days *(Thai et al., 1999)*.

The release rate seen in the present study was not ideal as a steady release of drug is needed to provide regular dosing over the treatment period. The system's properties need to be tailored so the material integrates with the damaged tissue and remains intact until the nerve fibres have restored connections and no longer require support from the materials *(Willerth and Sakiyama-Elbert, 2007)*, a time duration that hasn't yet been established in the field. It was evident that the geometry of the EVA affected the release rate with the tubes displaying a more desired release. Fabricating the EVA into tubes improved the release rate as they didn't exhibit the initial burst of release that was seen with the flat membranes and the drug was released in a more controlled manner. On the contrary, 96% of the initial drug load was released by 10 days, whereas, only 84% was released by the membranes.

Two methods were used in the fabrication of tubes (data not shown). The first approach involved dipping a glass rod in the EVA and ibuprofen solution 10-15 times with subsequent drying in between *(Chandy and Rao, 2002)*. The disadvantage of this method was the lack of reproducibility between the samples. Therefore, a second method was tested which involved wrapping the EVA membrane around a needle and fusing the edges together with solvent *(Day et al., 2004)*. A limitation of this method was the complete fusion on the two edges (Figure 5.2), however, this method enabled the

manufacture of similar sized EVA tubes with the same ibuprofen load. Therefore, these tubes were taken forward and used for *in vivo* testing.

EVA is a well-studied biomaterial used for a wide range of pharmaceutical products. It is biocompatible and inert toward drug molecules so can be used to deliver a broad variety of small molecules. These include soluble and insoluble drug molecules, peptides, nucleic acids and proteins *(Schneider et al., 2017)*. Therefore, its properties have been well established and the ideal system for PNI can be fabricated utilising previous knowledge.

A study had explored the possibility of delivering atenolol through a transdermal controlled release EVA matrix. Drug was successfully released from the diffusion-controlled system and the dose yielded was controlled by changing the drug load and temperature. There was linear relationship seen between the drug load and release rate *(Kim and Shin, 2004)*. Another study embedding triprolidine into EVA for transdermal application also displayed a clear relationship between the release and drug load and temperature. Increasing the ratio of vinyl acetate co-monomer or plasticiser also improved the release rate, as this acted to increase the permeability coefficient *(Shin and Lee, 2002)* .

Studies have also seen longer duration periods. Dexamethasone-loaded EVA was developed for peritumoral oedema and a 50% drug load resulted in a steady release over 30 days. *(Tamargo et al., 1991)*. Moreover, an EVA polymeric formulation loaded with phenytoin to treat epilepsy displayed the ability to deliver phenytoin in a controlled-manner for a period of 3.5 years using a 50% drug loaded cylinder *(Tamargo et al., 2002)*.

Despite EVA exhibiting a short release duration in this study it still demonstrated promising results to be used as a material to deliver drug locally for PNI as it is relatively easy to manufacture and has suitable handling properties. However, the material is non-biodegradable and would require recurrent surgery for removal making the therapy more invasive to patients. Therefore, for PNI application a biodegradable would be more efficient.

5.3.1.2 PCL and MSN

Ibuprofen-loaded PCL also demonstrated a high burst of drug in the first four hours releasing 22% of drug within this time, however, only a total of 26% of drug was released by day 10. This shows an initial burst followed by minimal release which is typical behaviour of a biodegradable material during the degradation process *(Yang and Pierstorff, 2012)*. This mirrored the results seen in a previous study where PCL loaded with 15% ibuprofen also had rapid release in the first 4 hours. The study investigated the use of vertical extrusion to manufacture PCL conduits and it proved to produce conduits with optimal mechanical properties and more efficient release profiles *(Salmoria et al., 2016)*. Another study explored combining PCL and collagen and it was found that increasing the drug to material ratio improved drug encapsulation. However, there was still a large burst of drug and not all the drug got released *(Prabu et al., 2006)*. Moreover, the combination of collagen and PCL to deliver insulin was explored and again a burst release was observed with most drug being released within 2 hours. It was suggested that the hydrophobicity of the matrix led to a poor interaction between the polymer and drug. The drug entrapment was maximum when a polymer to drug ratio 1:2 was used *(Kanungo et al., 2013)*.

Despite this PCL is still a commonly used biomaterial and has been used in studies for PNI. For example, polycaprolactone-b-polyethylenoxyde (PCL-b-PEO) micelles loaded with FK506 (Tacrolimus) were studied in a rat sciatic nerve crush injury. The injected micelles increased the animals' endurance time on a rotor-rod apparatus *(Allen et al., 2000)*.

Synthetic materials have many advantages for use as scaffolds as they can be tailored to offer a wide range of mechanical properties and degradation rates. These materials can also be used together to combine the optimal properties of each *(Willerth and Sakiyama-Elbert, 2007)*.

This concept was used in this study to explore the effect of combining MSN and PCL. A MSN and drug ratio of 1:50 was used to achieve 70% drug loading. This mimicked the successful loading of MSN with ibuprofen previously seen *(Zhang et al., 2011)*. The MSN

was then embedded into the PCL membranes. This combination of two release mechanisms improved the release profile as it caused the loss of the initial burst of drug and provided a more controlled release which continued for 14 days.

This provided a promising system to be used as a drug delivery platform for PNI. However, inconsistencies were found in the drug loading of the nanoparticles and so more development is needed before it could be tested further *in vivo*.

5.3.1.3 PLGA

Electrospinning PLGA with ibuprofen resulted in smooth, uniform and bead-free nanofibers with a diameter of ~900nm. The presence of ibuprofen in the nanofibres was confirmed using thermo-gravimetric analysis and differential scanning calorimetry (conducted by Dr Craig's lab, UCL School of Pharmacy (data not shown)), and its compatibility with the PLGA was evaluated using FTIR spectroscopy. From the results the material and drug were compatible and there appeared to be no strong bonds between the two.

The drug release from the PLGA was controlled exhibiting first order release, however, all the drug had been released within 1 week. This was better than results seen in a previous study where electrospun PLGA loaded with 10% ibuprofen exhibited a rapid release over the first 8 hours which slowed until the material degraded at 6 days *(Canton et al., 2010)*.

A recent study demonstrated how aligning the nanofibres within the conduits changed their properties by improving the materials flexibility, reducing the pore size, and slowing the degradation rate *(Subramanian et al., 2012)*. This technique could be applied as a means to improve the release rate of the nanofibres. In another study FK506 had been encapsulated into a PLGA diffusion system which maintained a steady drug level for 20 days *(Labroo et al., 2016)*. Furthermore, FK506 was microencapsulated into PLGA and then embedded into fibrin gels which provided a high release of the drug for 9 days but the release rapidly declined by 10-15 days *(Tajdaran et al., 2015)*.

As PLGA is biodegradable it would remove the requirement for additional surgery for removal making the therapy less invasive to patients. Therefore, PLGA is a good candidate for the development of a drug delivery platform for PNI.

5.3.2 In vivo local delivery of ibuprofen from biomaterials

As both EVA and PLGA demonstrated suitable drug release profiles, they were both tested in *in vivo* PNI animal models. They both presented suitable handling properties for surgical implanting. Both materials were placed around the nerve like a cuff and no additional suturing was required to hold the materials in place. In addition, no inflammation or abnormalities were seen during the tissue harvest.

This study has two main findings; 1.) Further evidence that ibuprofen is an effective drug for use in PNI supporting earlier findings in chapter 4, and 2.) The biomaterial based devices (EVA and PLGA) are suitable systems to deliver drugs locally to peripheral nerves. Once the materials had been manufactured and presented consistent release profiles *in vitro* they were implanted into two *in vivo* models of PNI; EVA tubes in a transection injury with primary repair and PLGA nanofibres in a crush injury. The materials were tested in different injury models because the EVA tube could not be wrapped around a crush injury.

5.3.2.1 EVA tubes in a transection injury with primary repair

Regeneration and functional recovery was measured 21 days post-injury. Histological analysis of cross sections through the proximal and distal stumps demonstrated an increase in axon number in the distal stump in the treatment group. This is an effect that hasn't before been reported with ibuprofen treatment in PNI. Interestingly, the number of axons in the distal stump exceeded those in the proximal stump in the same animal, the same as was seen following ibuprofen treatment in chapter 4. This is further evidence that there may be more than one daughter branch in the regenerating axons. Delivering ibuprofen through EVA resulted in a larger dose (~17µg/day) and, therefore, a larger effect on axon growth than that seen osmotic pumps (7µg/day). The

number of axons in the distal stump were 172% and 127% of the number of axons in the proximal stump, for the EVA tubes and osmotic pumps respectively. It could also be suggested that EVA provides additional growth support to the neurons as the number of axons in the distal stump in the EVA control group were higher than those seen in osmotic pump control group. The number of axons in the distal stump were 108% and 68% of the number of axons in the proximal stump for the EVA tubes and osmotic pumps respectively. The entubulation of the nerve with biomaterials could be beneficial, as it creates a closed environment which helps guide axonal growth towards the target *(Babu et al., 2008)*. There are additional drawbacks from the use of local injections or experimental delivery devices such as osmotic pumps as they result in the leakage of drug into surrounding tissues *(Kanje et al., 1988)*, therefore, a device that creates a chamber around the nerve would be beneficial.

Light microscopy analysis at the distal stump (5 mm and 10 mm from the injury site) showed that there was no statistical difference between the numbers of myelinated axons present between the groups. However, it may have been difficult to analyse myelination at 21 days as the axons may not have fully undergone the de-myelinating stage of Wallerian degeneration. A study showed that following a transection injury the mean fibre diameter began to increase between 50 and 150 days, so 21 days may be too early to detect a difference *(Ikeda and Oka, 2012)*. Furthermore, mean axon diameter and myelin thickness do not provide accurate measures of recovery because regenerating nerves have a high prevalence of thin, non-functional fibres with relatively thick sheaths *(Ikeda and Oka, 2012)*.

The results seen are consistent with the electrophysiological data to a certain extent, but the latency was shorter in the control group, meaning the nerve may contain fewer axons with a slower conduction velocity in comparison the treatment group. There was no difference seen in the myelin thickness and G-ratio between the two groups and no difference in the CMAP amplitude. This may mean that the control group has a large number of non-conducting degenerating neurite sprouts at this time post-injury.

A previous study had seen the return of nerve conduction velocity back to baseline following ibuprofen treatment in PNI *(Madura et al., 2011)*. However, the injury model was an interpositional graft in the tibial nerve and electrophysiological tests were conducted 3 months after injury making it difficult to compare with our study.

To further access target organ reinnervation the gastrocnemius muscle mass was recorded. Denervation of a target muscle is a consequence of PNI and causes muscle atrophy. Reinnervation will restore the muscles function and therefore stop atrophy *(Feng and Yuan, 2015)*. The results show that the muscle mass in the injured hind leg has reduced considerably in comparison to muscle in the uninjured hind leg. The muscle mass was slightly higher in the treatment group than the control but it was not significant. These results were consistent with the SSI as both groups still had an index of -100 showing no improvement at all.

Lastly, sensory recovery was conducted using von Frey filaments. The treatment group displayed a lower threshold response than the control group suggesting that these animals have regained some sensation in their hind paw.

In addition, to investigating axon regeneration and functional recovery, this study also explored the vascularisation, and the presence and phenotype of macrophages. These cellular changes are important to study as their combined interactions have been shown to facilitate initial Schwann cell guidance and regeneration *(Cattin et al., 2015)*. In both groups there was a large number of CD68 and Arginase-1 positive cells indicating there was a high number of macrophages present following injury, but, no differences were seen between the two groups. There were also CD68/Arginase-1 double positive cells present in both groups, which is consistent with previous studies that indicate the importance of M2 phenotype macrophages in nerve repair *(Mokarram et al., 2012, Scheib and Hoke, 2013)*. It has been shown that ibuprofen can influence the innate immune system by influencing the secretion of interleukin-6 (IL-6) from macrophages in a dose-dependent manner *(Hockertz et al., 1992)*. A mouse knockout model indicated that IL-6 does not impair nerve recovery following a sciatic nerve injury *(Inserra et al., 2000)*. However, the biological events following a peripheral nerve

injury are complex and the effect of ibuprofen on macrophages would need to be investigated in more detail.

Finally, vascularisation was higher in the treatment group in terms of the number of blood vessels and blood vessel diameter observed in the distal stump. Also the number of blood vessels in the distal stump exceeded those seen in the proximal stump. Vascularisation is known to play in role in the success of peripheral nerve regeneration *(Best and Mackinnon, 1994)*, however, the effect of drug treatments is yet to be explored.

5.3.2.2 PLGA nanofibres in a crush injury

Regeneration and functional recovery was measured 7 and 28 days post-injury. Histological analysis demonstrated an increase in axon number in the distal stump in the treatment group at 28 days. Interestingly, the number of axons in the distal stump exceeded those in the proximal stump in the same animal, the same as was seen following treatment with ibuprofen-loaded EVA tubes (section 5.3.5.1) and ibuprofen treatment in chapter 4. As for EVA, it could also be suggested that PLGA nanofibres provide additional growth support to the neurons, as the number of axons in the distal stump in the PLGA control group at 28 days were higher than those seen in the osmotic pump control group in the crush model. Evidence of this in other studies is the regeneration and functional recovery seen in a 10 mm gap model in a rat sciatic nerve model repaired with an electrospun blend of PLGA and PCL. The material aided the reconnection of the nerve stumps and the reinnervation of the target muscle *(Panseri et al., 2008)*. Furthermore, aligned PLGA nanofibers facilitated the formation of longitudinal columns of Schwann cells *(Subramanian et al., 2012)*, and PLGA-peptide treatments resulted in the extension of Schwann cells and the recovery of motor and sensory function in a 10 mm gap model in a rat sciatic nerve *(Nune et al., 2017)*.

The electrophysiological results indicate that ibuprofen treatment improves functional recovery as the CMAP amplitude was greater in the treatment group at 28 days post-injury. Moreover, the latency and stimulus intensity required to evoke a response were

both lower in the treatment group. This suggests that there is better target muscle reinnervation with ibuprofen treatment, which is similar to what was seen in a previous study with ibuprofen improving the nerve conduction velocity, despite a different model being used *(Madura et al., 2011)*.

The results from the gastrocnemius muscle mass showed no difference between the no drug control and treatment groups at 7 days and a small difference at 28 days. A previous study demonstrated that atrophy is likely to have occurred by 14 days post crush injury with a loss of 60% of muscle mass as a ratio of the injury to the contralateral muscle, which increased back to 70% by 28 days *(Wu et al., 2015)*. This may indicate that the drug treatment had no direct effect on the muscle atrophy, as no difference was seen between the two groups at 7 days when atrophy occurs was likely to occur. On the other hand, a difference was seen at 28 days which may indicate that the drug treatment plays a role in the regeneration of the muscle. The results here are not robust enough to allude a mechanism but further work using morphometric analysis of muscle sections could be used to explore this hypothesis. The results from the electrophysiology were not consistent with the gastrocnemius muscle mass results but were with the SSI. The SSI returned to baseline within 28 days in the control group but by day 22 in the treatment group. The SSI was significantly lower in the treatment group from day 4 post-injury. This mirrored the previous study that recorded an improvement in the TFI following ibuprofen treatment *(Madura et al., 2011)*. Lastly, sensory recovery was conducted using von Frey filaments. The treatment group displayed a significantly lower threshold response than the control group from day 13 post-injury. Furthermore, sensory function returned to baseline by day 22 in the treatment group but not until day 28 in the control group. All these measures indicate that function is returned 1 week earlier with ibuprofen treatment than with no treatment.

In addition, this study also explored the effect of drug treatment on vascularisation. It was found that ibuprofen released from PLGA had no effect on the number of blood vessels observed in the distal stump, but the blood vessel diameter was larger in the ibuprofen treatment group in comparison with the control group.

In conclusion, the aim of this chapter was achieved as there was successful manufacture and *in vivo* testing of drug-loaded biomaterials as drug delivery systems. Many FDA approved nerve conduits such as NeuroTube, NeuroFlex, NeuroMatrix and NeuroGen are made from collagen, PGA and PLGA, so using these materials to develop new drug delivery platforms is ideal. This study has expanded the research in drug delivery systems for PNI that have displayed optimal properties including sufficient drug release, handling for surgical implanting and efficacious effects on nerve regeneration.

Chapter 6: Investigating the correlation between PPAR-γ affinity and regenerative capacity

6.1 Introduction

6.1.1 Peroxisome proliferator-activated receptor gamma (PPAR-γ)

Peroxisome proliferator-activated receptors (PPARs) belong to the nuclear hormone receptor superfamily of ligand-activated transcription factors *(Hunter et al., 2001)*. PPARs regulate genes associated with lipid and metabolic homeostasis, energy balance, and cellular differentiation *(Cao et al., 2012, Quintanilla et al., 2014)*. There are three subtypes of PPARs; PPAR-α, PPAR-δ and PPAR-γ which share tissue expression and ligand activation profiles but still fulfil unique roles within the cell.

PPARs bind to specific sequences in the promoter regions of target genes *(Kersten et al., 2000).* PPAR-γ activation induces cellular metabolism leading to cell growth and differentiation. It is predominantly expressed in adipose and vascular tissue, and has a main role as a key adipogenic determination factor *(Cao et al., 2012, Quintanilla et al., 2014).* PPAR-γ is also found within the skeletal muscle; suggesting a role in muscle cell function and in particular myogenesis *(Hihi et al., 2002, Kruszynska et al., 1998)*. It is difficult to fully assess the effects of PPAR-γ as most of the agonists have a low affinity for the receptor which means high concentrations are needed to see a physiological effect *(Park et al., 2004)*. Despite this there is evidence from rodent studies that that PPAR-γ may have a role in neuronal development, improvement of neuronal health and pain signalling *(Wada et al., 2006)*.

6.1.2 PPAR-γ in peripheral nerves

The role of PPAR-γ in nerve tissue remains unclear, however, immunohistochemical analysis has demonstrated the localisation of PPAR-γ in Schwann cells of myelinated fibres and endothelial cells in rat peripheral nerves *(Yamagishi et al., 2008)*. This was reinforced by another study in which immunofluorescence staining demonstrated the expression of PPAR-γ within Schwann cells of healthy and regenerating nerves 1 week

following a crush injury *(Cao et al., 2012)*. The expression of PPAR-γ was found to increase during the inflammation process, which may promote the activation of Schwann cells as an immune cell *(Zhang et al., 2010)*. Moreover, the presence of PPAR-γ has been confirmed in axons within a rat sciatic nerve and PPAR-γ activation increased at 2, 4, and 6 h after a nerve ligation or crush injury *(Lezana et al., 2016)*. Another study found PPAR-γ was also expressed in human neuroblastoma cells and identified a correlation between expression and the maturational stage of the cell, thus indicating that PPAR-γ has a role in nerve cell biology *(Han et al., 2001)*, including the development and health of neurons *(Quintanilla et al., 2014)*. The natural PPAR-γ agonist PGJ2, a prostaglandin, was found to increase PPAR-γ expression resulting in two effects on PC12 cultures; the protection of PC12 cells from nitrosative-induced cell death and, the stimulation of neurite outgrowth *(Jung et al., 2003)*. Moreover, treatment with another PPAR-γ agonist, troglitazone in a primary rat hippocampal culture induced neurite outgrowth and axon length *(Quintanilla et al., 2013)*. This was echoed in another study in which treatment of rosiglitazone increased the activation of PPAR-γ in rat primary cortical neurons resulting in increased neurite outgrowth. The opposite was seen when treating the neurons with the PPAR-γ antagonist, GW9662 *(Lezana et al., 2016)*. Moreover, the effects of PPAR-γ ligands can also improve neuro-inflammation and be used to treat neuropathic pain *(Quintanilla et al., 2014)*.

Further studies have indicated that PPAR-γ activation has beneficial effects against oxidative stress, mitochondrial dysfunction, and apoptosis in several cell-based models for degenerative diseases such as Alzheimer's disease, Huntington's disease, amyotrophic lateral sclerosis, and spinal cord injury. PPAR-γ activation in mice models of the diseases listed above resulted in decreased cognitive decline *(Quintanilla et al., 2014)*. Finally, evidence suggests that PPAR-γ has an effect on neuronal differentiation through influencing transcription and the activation of secondary pathways impacting cell morphology and protein expression *(Cao et al., 2012)*. It is evident that there are many possible benefits for the development of PPAR-γ agonists for the treatment of peripheral nerve injury.

6.1.3 NSAID affinity for PPAR-γ

NSAIDs are commonly used within the clinic for their anti-inflammatory, anti-pyretic, and analgesic properties *(Lehmann et al., 1997)*. Their mechanism of action as inhibitors of prostaglandin synthesis is through the inhibition of cyclooxygenase (COX) 1 and 2 *(Kopp et al., 2012)*. As a result of their demonstrated inhibition, NSAIDs have previously been studied for neuropathic pain because of their activity on prostaglandins. Neuronal cell death triggers glial activation which in turn induces the release of prostaglandins and other inflammatory agents including cytokines, growth factors, purines and amines *(Scholtz and Woolf, 2002)*. Moreover, transcriptional changes induce the prostaglandin synthesizing enzyme COX-2 resulting in prostanoid production *(Durrenberger et al., 2004)*, which in turn sensitises peripheral nerve terminals causing peripheral nerve pain. This knowledge led to extensive research on COX-2 inhibitors for neuropathic pain *(Schafers et al., 2004, Yaksh et al., 2001).* PPAR-γ can instigate its own anti-inflammatory response through the negative regulation of macrophage activation and the inhibition of inflammatory cytokine production in monocytes *(Kapadia et al., 2008, Park et al., 2007, Zhou et al., 2003)*.

The focus in the PNI field has recently shifted to study NSAIDs for nerve regenerative as they have demonstrated positive effects in *in vitro* and *in vivo* studies *(Fu et al., 2007, Madura et al., 2011, Xing et al., 2011)*. It has been suggested that this pro-regenerative activity is a result of the inhibition of the Rho/ROCK pathway. PPAR-γ is essential for coupling NSAID drugs to Rho inhibition to acquire the induction of neuronal growth *(Dill et al., 2010)*.

Ligand activation of PPAR-γ in neuronal cells results in the upregulation of the protein tyrosine phosphatase, Src homology region 2–containing protein tyrosine phosphatase-2 (SHP-2). SHP-2 binds to the GEF, Vav, causing dephosphorylation and inactivation of Vav. This acts to retain this protein complex in the cytosolic fraction, and inactivates the Vav protein through dephosphorylation *(Wakino et al., 2004)*. Inactivation of Vav suppresses the conversion of inactive GDP-Rho to active GTP-Rho resulting in the downregulation of ROCK activity *(Wakino et al., 2004)* (Figure 1.10).

The development of potent, selective and cell permeable inhibitors of protein tyrosine phosphatases (PTPs) is challenging due to the conserved and highly polar nature of the active site coupled with the fact that anionic phosphate is the key recognition motif *(Barr, 2010)*. This mechanism is supported by an *in vivo* study in adult rats, which demonstrated suppression of Rho/ROCK activity was consistent with upregulated SHP-2 expression and inactivation of Vav following 4 weeks treatment with the PPAR-γ agonist, pioglitazone *(Wakino et al., 2004)*.

The ability of NSAIDs to bind to PPAR-γ may be due to their characteristic structures consisting of a lipophilic backbone and an acid moiety, most commonly a carboxylate (Figure 6.1). This was supported by a study that demonstrated ibuprofen-induced Rho-inhibition was eradicated when neurons were also treated with PPAR-γ antagonist GW9662 or with PPAR-γ knockdown with siRNA *(Dill et al., 2010)*.

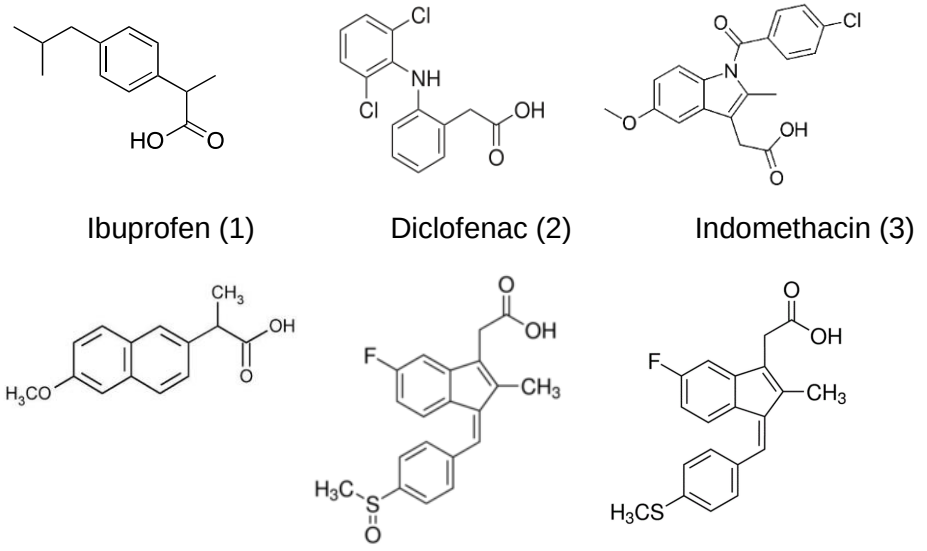

Ibuprofen (1) Diclofenac (2) Indomethacin (3)

Naproxen (4) Sulindac (5) Sulindac sulfide (6)

Figure 6.1: Chemical structure of several NSAIDs.

There are several classes of NSAIDs based upon their chemical structure including thiazinecarboxamides (piroxicam) derivatives of arylacetic acid (indomethacin), aminoarylcarboxylic acid (flufenamic acid), arylpropionic acid (ibuprofen and fenoprofen), and salicylic acid (aspirin) *(Lehmann et al., 1997)*. The different classes of NSAIDs exhibited a spectrum of agonist activity of PPAR-γ. Ibuprofen, fenoprofen and

flufenamic acid exhibiting the greatest effect on PPAR-γ and indomethacin, piroxicam and salicylic acid having little or no effect *(Lehmann et al., 1997)*.

This correlated with more recent studies where ibuprofen, indomethacin and sulindac sulfide demonstrated the ability to reduce levels of activated Rho, whereas, piroxicam, meloxicam and naproxen did not *(Dill et al., 2010, Fu et al., 2007, Wang et al., 2009, Zhou et al., 2003)*. The reduced levels of activated Rho led to an associated increase in axonal growth in neuronal cultures seen with ibuprofen and indomethacin but not with naproxen *(Dill et al., 2010, Fu et al., 2007, Wang et al., 2009)*. Inhibition of COX by ibuprofen is primarily by the S (+)-enantiomer, however, both the S (+) and R (-) enantiomers inhibit Rho-activation *(Wang et al., 2009, Zhou et al., 2003)*. The effect of other NSAIDs on Rho activity have not been reported but a number have shown promising effects on nerve regeneration. For example, diclofenac treatment in a sciatic nerve transection injury resulted in improved functional recovery and faster recovery of regenerated axons *(Mohammadi et al., 2013)*.

Previously, NSAIDs have been mostly studied in the PNS as PPAR-γ agonists however, they seem to work through a different mechanism in the CNS *(Kopp et al., 2012)*. In both systems the pharmacological effects of NSAIDs are still independent of their well-known activity on COX-1 and 2 *(Kopp et al., 2012, Wang et al., 2009)*. As seen with the PNS, ibuprofen and indomethacin both demonstrate positive effects on neurite elongation in cell culture models of the CNS *(Dill et al., 2010, Fu et al., 2007)*, however, this isn't extrapolated into the animal models, as only improvement in myelination and functional recovery is seen *(Sharp et al., 2013, Wang et al., 2009, Xing et al., 2011)*.

NSAIDs also exhibit neuroprotective properties suggesting that they have promise for the treatment of neurodegenerative disease. In a model of Alzheimer's disease, treatment with ibuprofen, indomethacin and sulindac sulfide resulted in lower levels of the amyloid beta peptide 1-42 (Aβ42) which is a major hallmark of the disease *(Lim et al., 2000, Zhou et al., 2003)*. NSAIDs that do not block the Rho/ROCK pathway via PPAR-γ activation were not effective in these models. This suggests that the reduction

of Aβ42 peptide levels may be linked to inhibition of Rho/ROCK and is independent of NSAID mediated inhibition of COX *(Zhou et al., 2003)*.

Considering the evidence presented above, the repositioning of current–approved drugs is likely to be valuable in moving therapies for the treatment of PNI rapidly towards the clinic. Although there have been many advancements made in the identification of targets for pharmacological agents to treat nerve injury, the field is still in its infancy. To date only a few agents have been directly tested in humans for applications related to peripheral nerve function. Ibuprofen and a host of other NSAIDs are routinely used for the treatment of inflammation and pain and already have well-established safety and efficacy profiles *(Chan et al., 2014)*. Therefore, it would be feasible to test such drugs in humans following nerve injury with a low risk of toxic effects. Furthermore, the need for extensive pre-clinical studies can be a drawback in the development of new drugs for treating nerve injuries *(Chan et al., 2014)*, making the repurposing of established drugs an attractive alternative proposition.

To the best of our knowledge ibuprofen and diclofenac are the only NSAIDs that have been studied in PNI models. The relative affinities of a number of NSAIDs for PPAR-γ have been determined and follow the rank order sulindac sulfide > diclofenac > indomethacin > ibuprofen *(Puhl et al., 2015)*. Given the promising results obtained with ibuprofen and diclofenac, this could mean that other NSAIDs could have promising effects on nerve regeneration and may even exceed those already seen. Building upon the understanding of how NSAIDs interact with PPAR-γ will help the development of more effective drugs targeting this receptor following PNI *(Lezana et al., 2016)*.

6.1.4 Metabolism of sulindac

Sulindac is a NSAID indicated for the relief of signs and symptoms of arthritic conditions, including osteoarthritis and rheumatoid arthritis. Sulindac is a pro-drug which undergoes reversible reduction to sulindac sulfide through the action of liver enzymes and colonic bacteria and sulindac sulfone by the irreversible oxidation of the sulfoxide in the liver

(Figure 6.2) *(Lee et al., 2010, Gurpinar et al., 2013)*. In addition to inhibiting COX, sulindac sulfide also inhibits Ras-mediated signal transduction *(Felts et al., 2007)*.

The metabolite, sulindac sulfone (Exisulind), does not inhibit COX, however, it has demonstrated anticancer *in vitro* and *in vivo* activity *(Gurpinar et al., 2013)*. This compound did not receive FDA approval due to hepatotoxicity.

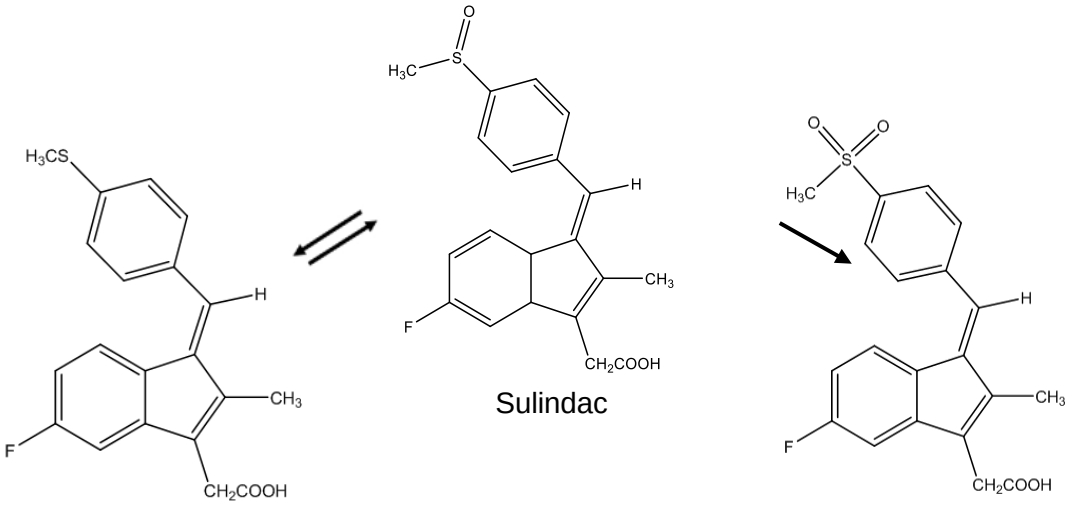

Figure 6.2: The metabolism of the prodrug sulindac to sulindac sulfide and sulindac sulfone *(Lee et al., 2010).*

6.1.5 Bond geometry influences the mechanism of action of sulindac sulfide

The side effects associated with sulindac sulfide mediated COX inhibition would discourage prolonged use in PNI. However, a study by Felts *et al.* (2008) found that inhibition of COX can be removed by modifying the chemical structure of the drug whilst retaining an effect on PPAR-γ *(Felts et al., 2008)*. Sulindac sulfide binds tightly to COX via a rapid reversible interaction of the 2′-methyl group of the indene or indole rings with the hydrophobic pocket in the COX active site *(Walters et al., 2009)*. The removal of this group changes the geometry of the benzylidene double bond; switching the compound from a *Z* to *E* isomer (Figure 6.3). This in turn leads to the eradication of the time-dependent interaction with COX *(Walters et al., 2009)*. When tested 2'-des-methly sulindac sulfide was able to bind to and activate PPAR-dependent transcription but had

no effect on COX inhibition up to concentrations of 250 μM, demonstrating the compounds ability to activate PPAR-γ independent of COX activity *(Felts et al., 2007)*.

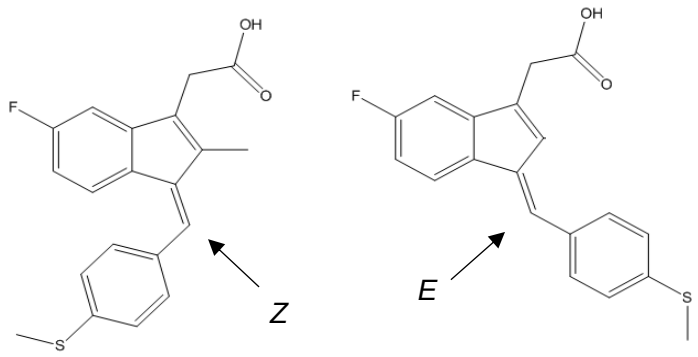

Sulindac sulfide

2'-Des-methyl sulindac sulfide

Figure 6.3: Chemical structures of the Z and E isomers of sulindac sulfide.

The eradication of COX activity should eliminate the gastrointestinal and cardiovascular side effects of sulindac sulfide, thus allowing higher doses to be administered and improving the potential for sulindac sulfide to be used in other clinical indications *(Felts et al., 2008, Walters et al., 2009)*. The altered stereochemistry of sulindac sulfide introduced the possibility of developing novel PPAR-γ agonists *(Felts et al., 2007)*. A study developed a series of novel derivatives as potential agonists PPAR-γ. It was found that optimal affinity was obtained (EC_{50} 0.1 μM) through the addition of nonpolar and aromatic substitutions on the benzylidene ring in addition to retention of the carboxylic acid side chain *(Felts et al., 2008)*. This new finding has opened up new opportunities to develop novel drug therapies for PNI.

6.1.6 Aims of chapter 6

The aim of this chapter was to investigate the effects of selected NSAID's in nerve regeneration in established *in vitro* and *in vivo* models. The study began with an exploration of the correlation between NSAID affinity for PPAR-γ and their regenerative capacity. The second part of the study involved the synthesis of a desmethyl derivative of sulindac sulfide in order to explore its effects in peripheral nerve regeneration.

6.2 Results

6.2.1 Effect of NSAIDs on neurite growth in 3D EngNT co-cultures

3D EngNT co-culture models containing SCL4.1/F7 and PC12 cell lines were used to investigate the capacity of the NSAIDs sulindac sulfide, diclofenac, indomethacin and naproxen to modulate neurite outgrowth. Three of the drugs, namely sulindac sulfide, diclofenac and indomethacin, were found to increase neurite growth at all treatment doses in comparison to the no drug control. Naproxen, however, only results in a small increase in neurite growth at a dose of 200 μM. Furthermore a statistically significant increase was observed with a 100 μM dose of sulindac sulfide and 10 μM diclofenac (Figure 6.4).

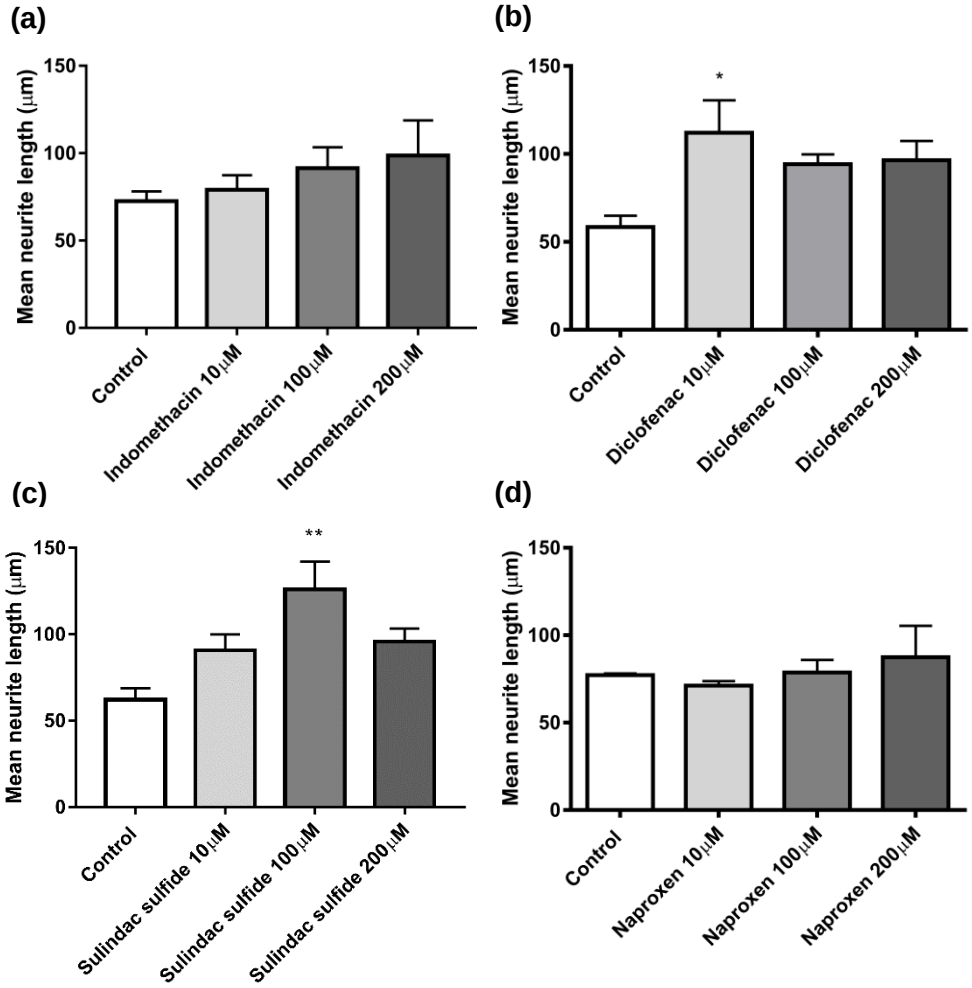

Figure 6.4: The effect of NSAIDs on neurite growth in the 3D EngNT co-culture. *Sulindac sulfide, diclofenac and indomethacin increased neurite growth at all doses in comparison to the control, whereas naproxen gave minimal effect at a dose of 200 μM. A significant increase in growth was seen with 100 μM sulindac sulfide and 10 μM diclofenac. N=6 of EngNT co-culture gels, mean ± SEM for each compound tested. One-way ANOVA with Dunnett's post hoc test, *p < 0.05 and **p < 0.01.*

The increase in neurite length was compared amongst all the NSAIDs tested in the EngNT co-culture model at 100 µM dose, including ibuprofen. A correlation between PPAR-γ affinity of NSAIDs and nerve regeneration capacity was determined. The relative affinities of a number of NSAIDs for PPAR-γ have been determined and follow the rank order sulindac sulfide > diclofenac > indomethacin > ibuprofen *(Puhl et al., 2015)*. The order of neurite length increase followed a similar rank order (Table 6.1). It was also found that a NSAID with no affinity for PPAR-γ showed minimal effect on nerve regeneration. Sulindac sulfide had the greatest effect on nerve regeneration, with a 106% increase in neurite length relative to the no drug control, and therefore this was the most suitable candidate to investigate further.

NSAID	**Affinity for PPAR – γ *(Puhl et al., 2015)***	**Neurite length at 100 µM dose (as a percentage to the control)**
Sulindac sulfide	1.87 µM	106%
Diclofenac	3.70 µM	73%
Ibuprofen	80.6 µM	55.2%
Indomethacin	21.3 µM	19.3%
Naproxen	No affinity	2%

Table 6.1: Correlation between PPAR-γ affinity of several NSAIDs and nerve regeneration capacity. *Both the affinity (Puhl et al., 2015) and neurite length followed a similar rank order with sulindac sulfide having the highest affinity for PPAR-γ and the greatest regenerative capacity. Naproxen had no affinity for PPAR-γ and a corresponding lack of effect on nerve regeneration.*

As sulindac sulfide has the greatest effect on nerve regeneration, further analysis was conducted with sulindac sulfide with treatments ranging from 1 to 100 µM or no drug treatment in the EngNT co-culture model (Figure 6.4).

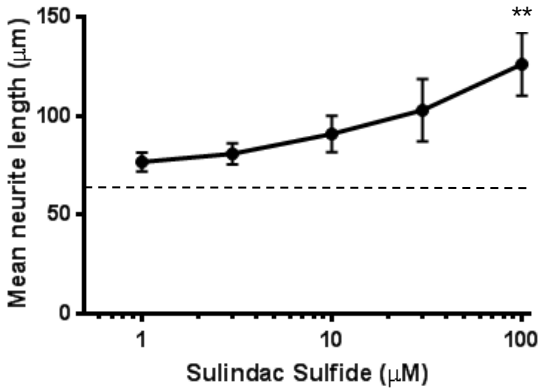

Figure 6.5: Sulindac sulfide increases neurite growth in a dose dependent manner. *Significant increases in neurite length were seen with 100 µM doses of sulindac sulfide, however, all doses increased neurite growth when compared to no drug control (shown by dotted line) after 72 h exposure. N=6, mean ± SEM for each condition One-way ANOVA with Dunnett's post hoc test, **p < 0.01.*

Sulindac sulfide is a metabolite of the parent compound, sulindac, which is known to inhibit COX enzymes. As the NSAID drugs are thought to act via a different mechanism in peripheral nerve regeneration independent of COX inhibition, 3D EngNT co-culture models containing SCL4.1/F7 and PC12 cell lines were used to investigate whether the parent compound, sulindac also had an effect on neurite growth. It was found that sulindac had minimal effect on neurite growth between a dose range of 10 μM and 200 μM (Figure 6.6)

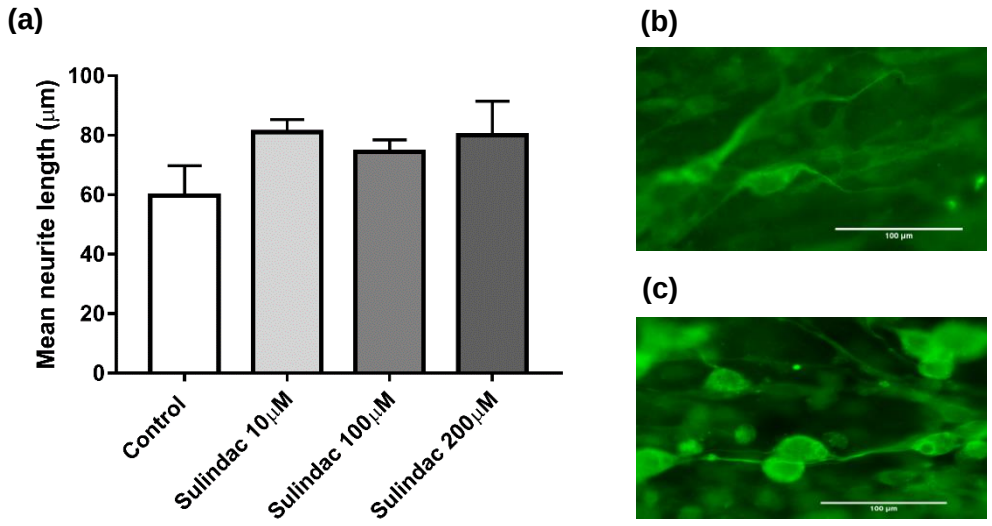

Figure 6.6: Sulindac has minimal effect on neurite growth in a co-culture of SCL4.1/F7 and PC12 cells. *The neurite length was similar to the no-drug treatment control in all cases, after 72 h exposure (a). Fluorescence micrographs of the monolayer cultures show neurite length with (b) no drug treatment, (c) 10 μM sulindac. Cultures were immunostained to detect β-III tubulin (green) Scale bar = 100 μm. N = 6, mean ± SEM for each condition. One-way ANOVA with Dunnett's post-hoc test.*

In summary, sulindac sulfide was found to exert the greatest effect on neurite growth in the *in vitro* co-culture model and so was selected to take forward for evaluation in *in vivo* PNI studies. The crush injury model was selected to screen the effect of sulindac sulfide as the recovery returns to baseline by 4 weeks. This provides a higher through-put model in comparison to the transection model, providing robust and reliable data in a shorter period of time and as consequence also reduces experiment time and cost.

6.2.2 Crush injury model delivering sulindac sulfide through osmotic pumps

6.2.2.1 Quantification of neuronal growth

To quantify and assess neuronal growth rat sciatic nerves were dissected at 28 days post-injury and 10 µm transverse sections were taken to determine axon number. The neurofilament-positive axons present in the proximal and distal stumps were quantified using the protocol outlined in section 4.2.1. Analysis demonstrated a decrease in axon number following surgery but treatment with 11 µg/day sulindac sulfide was found to result in an increase in the number of axons in the distal stump in comparison to no drug treatment (Figure 6.7). Furthermore, the number of axons quantified in the distal stump of the sulindac sulfide group exceeded the axon number in the corresponding proximal stump of the same animal. A dose of 11 µg/day sulindac sulfide was used *in vivo* to match what was used in the *in vitro* model.

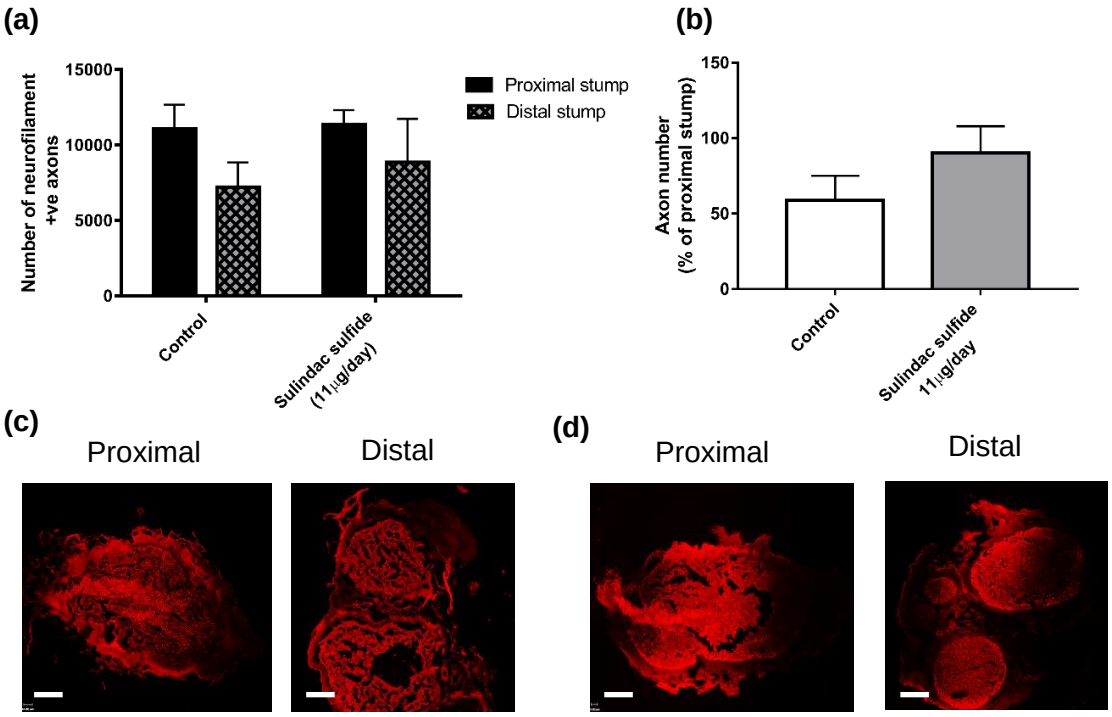

Figure 6.7: Sulindac sulfide increased the number of axons in the distal stump following a crush injury. *The number of axons in the distal stump increases with sulindac sulfide treatment in comparison to no drug treatment (a) the axon counts were also expressed as a percentage of the proximal stump in each animal (b). Micrographs are transverse sections showing neurofilament positive neurites at 5 mm proximal and distal to the injury site in the control group (c) and sulindac sulfide treatment group (d). Scale bar = 100 µm. N=3, data are means ± SEM.*

6.2.2.2 Functional recovery

In addition to histology, the motor and sensory recovery was studied using; muscle weight, static sciatic index, electrophysiology, and von Frey analysis. Sensory recovery was monitored throughout the experiment using von Frey and both groups returned to baseline by 28 days. The animals in the sulindac sulfide treatment group responded to a lower threshold than the control group from day 4 post injury meaning they had a better response to sensation stimuli in their hind paw (Figure 6.8). To evaluate motor recovery the gastrocnemius muscle was harvested and weighed immediately at the 28 day end point. The muscle mass in the treatment group was larger than seen in the control group (Figure 6.9). Lastly, small differences were observed between the groups using SSI, but it was also evident that the SSI was better in the treatment group between day 1 and 11 post injury. Furthermore, the SSI returned to baseline in both in the treatment group which was within 25 days and 28 days in the control group (Figure 6.10).

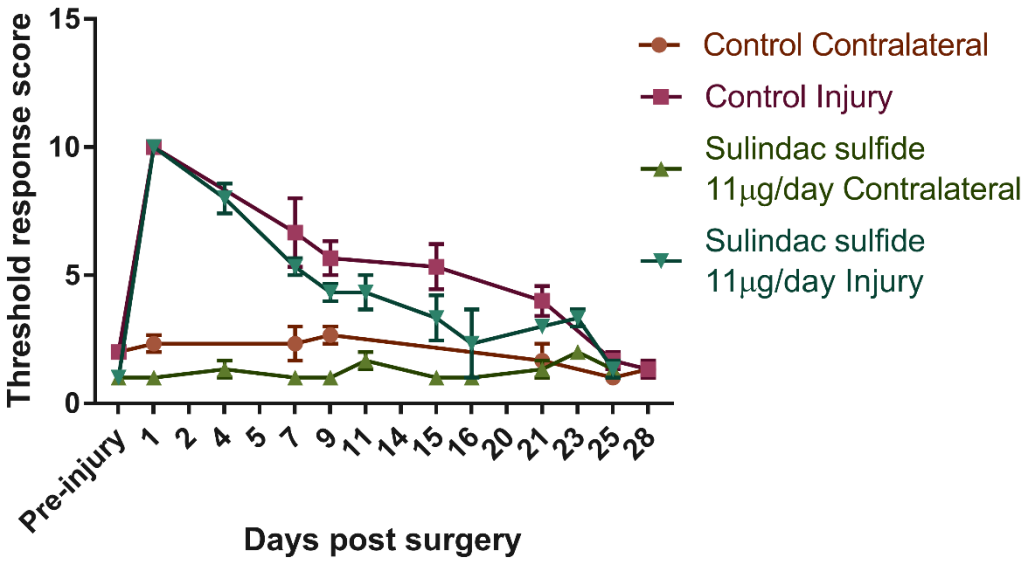

Figure 6.8: Von Frey in a crush injury treated with sulindac sulfide. *Sensory recovery was seen with sulindac sulfide treatment at a dose of 11μg/day in comparison to no drug treatment. N=3, mean ± SEM.*

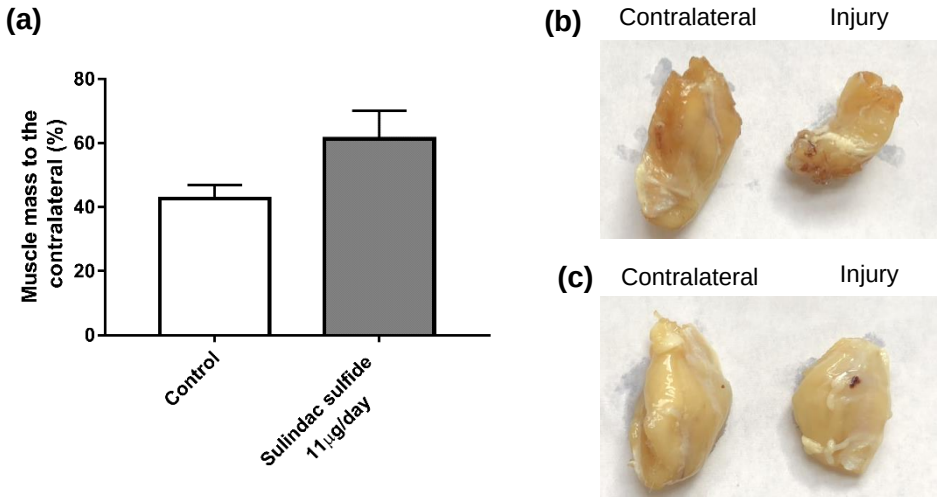

Figure 6.9: Treatment with sulindac sulfide increased the gastrocnemius muscle mass. *Sulindac sulfide increased the mass of the gastrocnemius muscle in the injury side as a % of the contralateral side (a). Images of the harvested gastrocnemius muscle from the contralateral and injured hind leg from the control group (b) and sulindac sulfide treat group (c). N=3, mean ± SEM.*

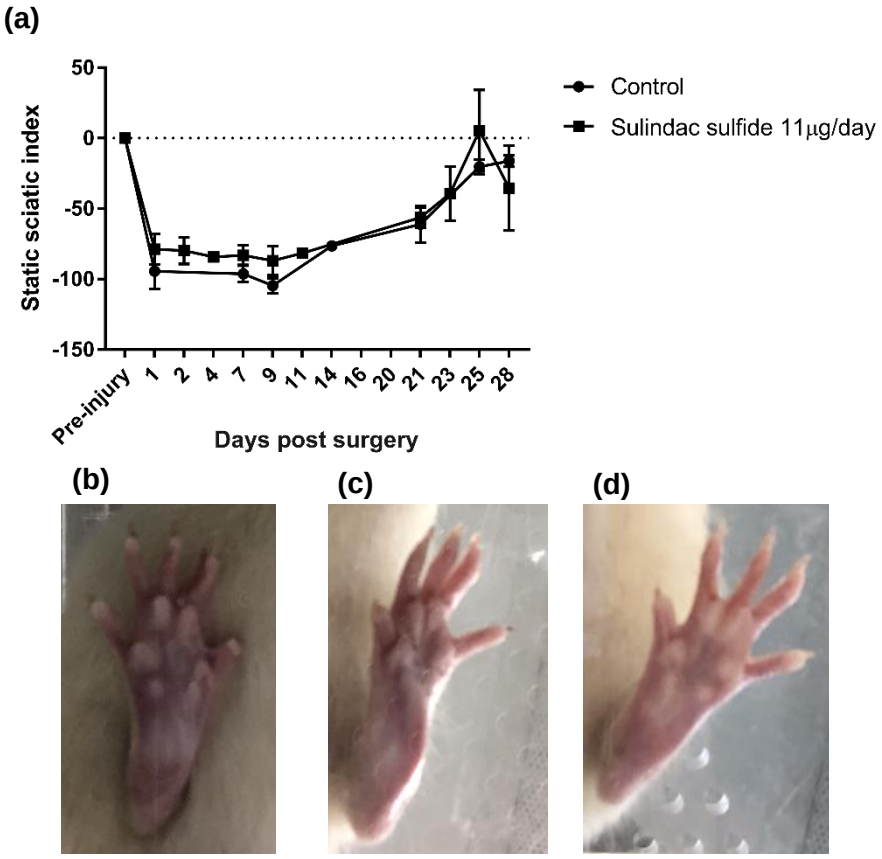

Figure 6.10: SSI in a crush injury treated with sulindac sulfide. *The SSI had improved in the sulindac sulfide treatment group between day 1 and 11 post-injury, but no difference was seen between the groups after 11 days (a). Hind paw images used to conduct SSI quantitation; contralateral (b), control (c) and sulindac sulfide 11 μg/day (d). N=3, means ± SEM.*

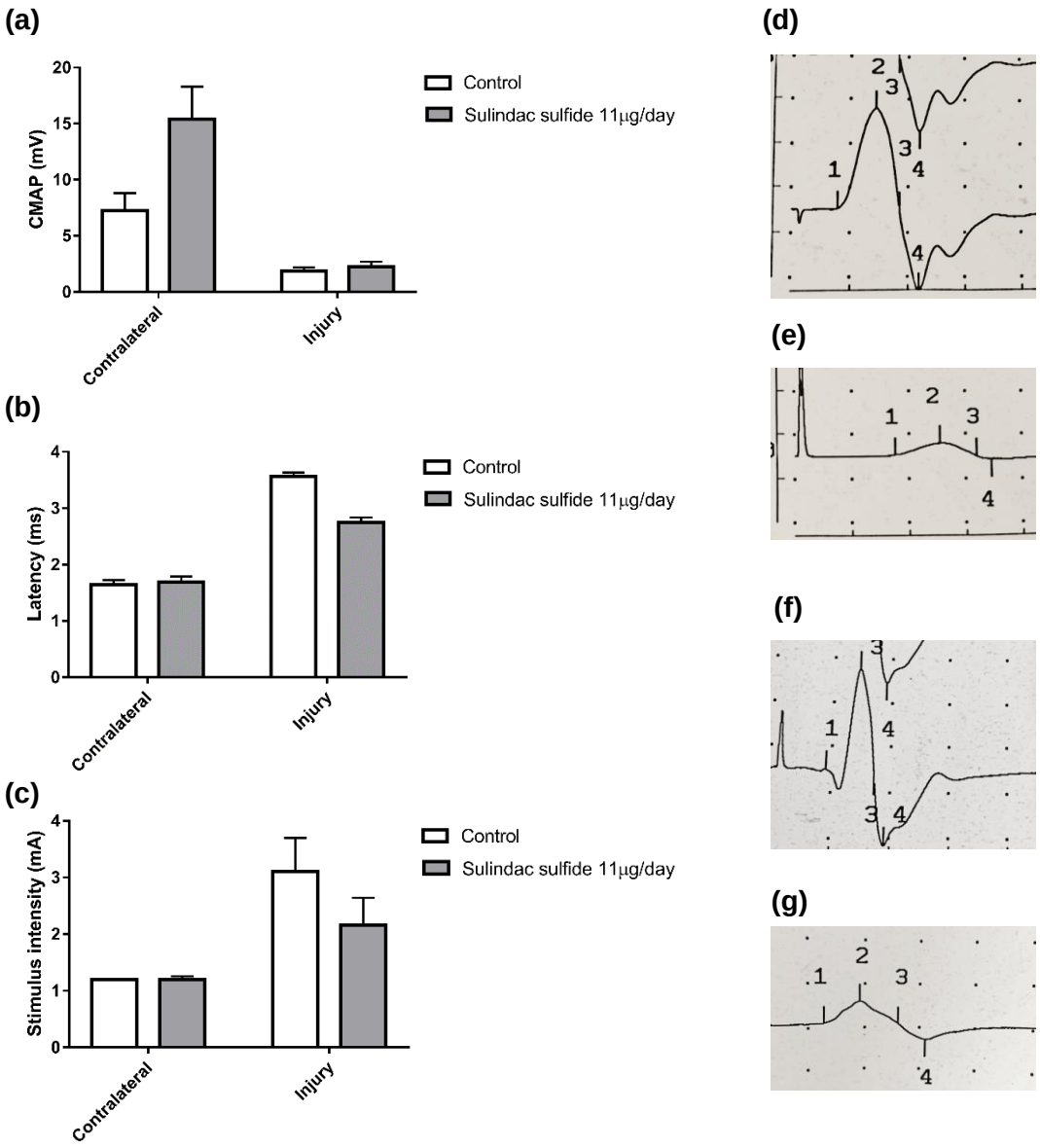

Figure 6.11: Electrophysiological evaluation of sciatic nerve 28 days after a crush injury treated with sulindac sulfide. *The sciatic nerve was stimulated proximal to the repair site and the CMAP was recorded from the gastrocnemius muscle. The CMAP amplitude was slightly larger in the ibuprofen treatment group (a). There was a reduction in latency and the stimulus intensity in the treatment groups (b), (c). The electrophysiological traces for the contralateral (d) and injury (e) gastrocnemius muscle in the control group and the contralateral (f) and injury (g) gastrocnemius muscle in the treatment group. N=3, means ± SEM.*

Electrophysiology was used to investigate the response of the gastrocnemius muscle to electrical stimulation of the proximal nerve. The CMAP was recorded from the non-injured contralateral and injured side in all animals (Figure 6.11). A small difference was seen in CMAP with and without sulindac sulfide treatment after four weeks (Figure 6.11 (a)). A difference was observed in the latency between the two groups with the latency being lower with sulindac sulfide treatment (Figure 6.11 (b)). Furthermore, the

stimulus intensity needed to provoke a response from the muscle on the injured side was lower in the treatment group than the control group (Figure 6.11 (c)).

6.2.2.3 Vasculature

The vascularisation was examined via immunohistochemical staining of transverse sections for RECA-1. Analysis revealed the presence of blood vessels throughout the injured nerves in both the proximal and distal sections, however, there was a higher numbers of blood vessels in the proximal stump. There was no difference in the number of blood vessels between the groups (Figure 6.12 (a)), however, a larger blood vessel diameter was observed in the distal stump of the sulindac sulfide treatment group (Figure 6.12 (b)).

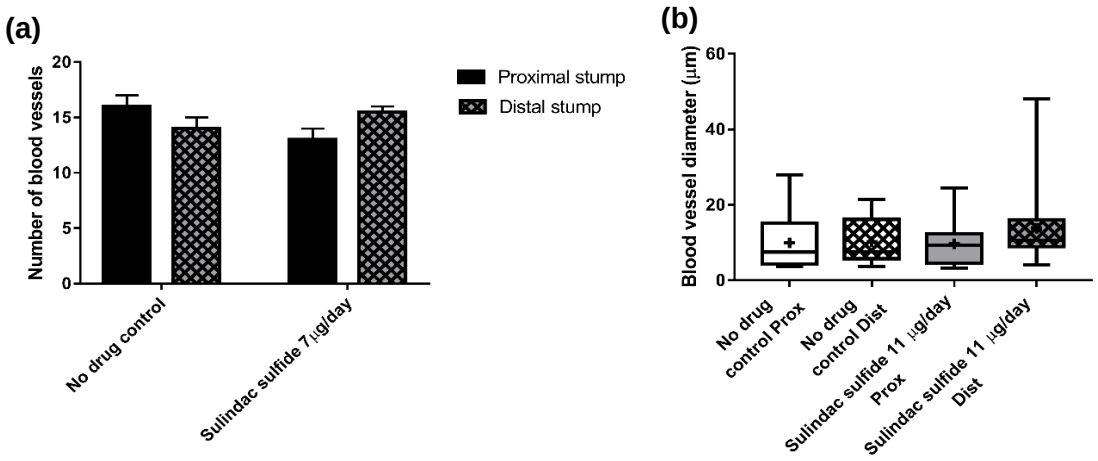

Figure 6.12: Vasculature changes following a crush injury treated with sulindac sulfide. *Quantitative analysis of the number (a) and diameter (b) of blood vessels by RECA-1. N=3, mean ± SEM for each condition. Box plots show the distribution of blood vessel diameter with boxes extending from the max to min, + indicates mean.*

6.2.2.4 Residual drug

At the start of the study there was difficulty loading the osmotic pumps with sulindac sulfide due to its poor solubility. For this reason the osmotic pumps were collected during the tissue harvest at the end point of the study to test for residual drug. The osmotic pumps were washed with 1 mL DMSO and this solution was analysed using UV-Vis spectrophotometry. The results demonstrated that the expected amount of drug (108 µg) remained the osmotic pumps and the animals received the correct dose over the four week period (total dose = 308 µg).

6.2.3 Characterisation of sulindac sulfide-loaded PLGA nanofibres

As a main aim of this body of work was to develop a local delivery system for PNI treatment, sulindac sulfide, was tested in the electrospun PLGA biomaterial platform previously introduced in chapter 5. This provided additional evidence of the robustness of the local delivery system and its applicability to other drug compounds, especially those with challenging properties.

6.2.3.1 Scanning electron microscopy (SEM)

The composition and morphology of the PLGA loaded with sulindac sulfide was analysed using SEM. The nanofibers with a drug to polymer ratio of 1:17.5 were smooth and randomly aligned. This formulation fabricated nanofibres with an average diameter of ~0.8 µm (Figure 6.13 (a), (b)). However, a change in the composition of the nanofibres was observed when they were stored at room temperature for 7 days. The nanofibres lost their smooth structure as the fibres began to amalgamate together and small deposits of drug became visible on the surface (Figure 6.15 (c), (d)).

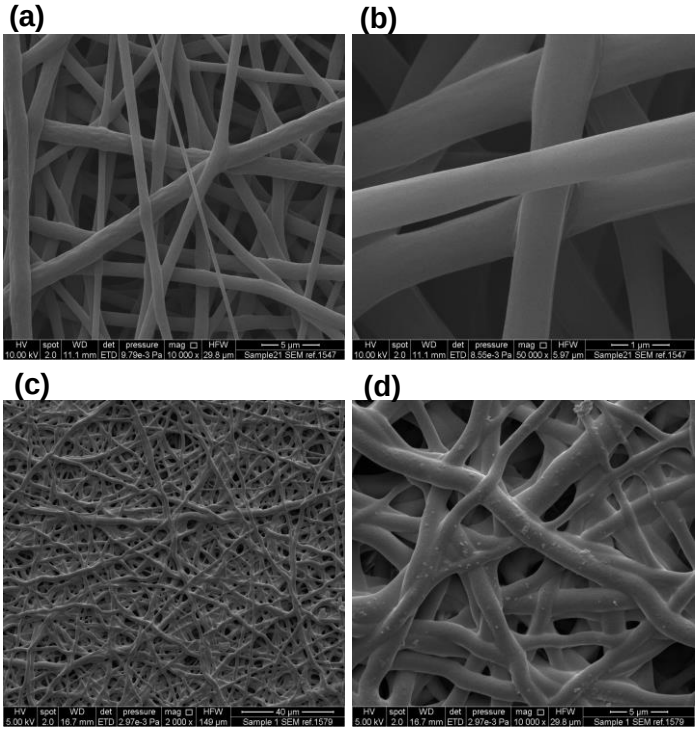

Figure 6.13: SEM images of sulindac sulfide-loaded electrospun PLGA nanofibres. *The nanofibres presented different surface appearances under different storage conditions; (a), (b) at 4 ºC and (c), (d) at 27 ºC for 7 days.*

6.2.3.2 Drug release

In vitro drug release from sulindac sulfide-loaded PLGA nanofibres was measured every hour for 6 h and then every 24 h for 20 days. At each time point a 1 mL sample of drug solution was taken and analysed using UV-Vis spectroscopy (Figure 2.11). The sulindac sulfide-loaded PLGA nanofibres demonstrated first order steady state release with 100% of the drug being released within 20 days (Figure 6.14).

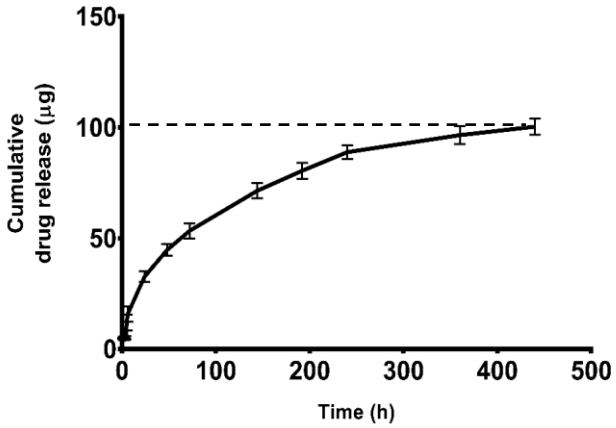

Figure 6.14: Drug release from sulindac sulfide-loaded electrospun PLGA nanofibres. *The initial drug load is shown by the dotted line. N=3, mean ± SEM.*

6.2.4 Crush injury model delivering sulindac sulfide through PLGA nanofibres

Sulindac sulfide-loaded PLGA nanofibres were surgically implanted into a rat sciatic nerve as a cuff around a crush injury. In contrast to the control material, the drug-loaded material exhibited poorer handling properties as it became stiffer at room temperature. The material could not be wrapped compactly around the nerve (Figure 6.15 (a), (b)). At 28 days the composition of the nanofibres had changed. As the material degraded it formed a closer wrap around the nerve. There were no visual abnormalities seen during the harvest including inflammation or change in fascia around the injury site (Figure 6.15 (c)).

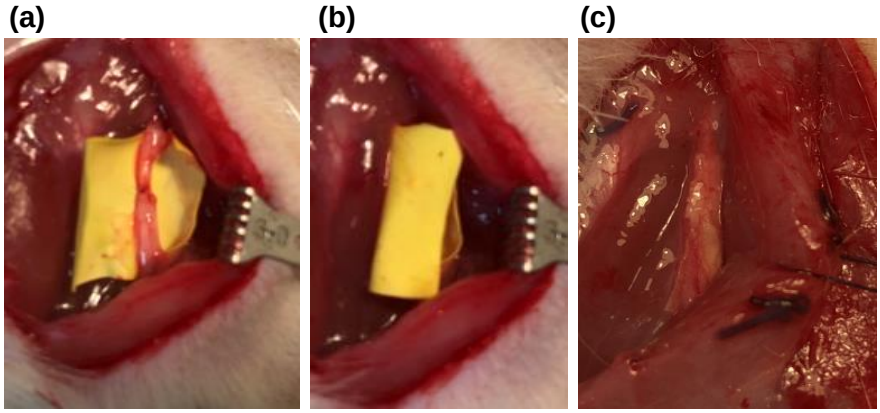

Figure 6.15: Surgical implanting of the sulindac sulfide-loaded PLGA nanofibres. *Surgical implanting (a), (b) and harvest (c).*

6.2.4.1 Quantification of neuronal growth

Rat sciatic nerves were dissected at 28 days post-injury and 10 μm transverse sections were taken to determine axon number. The neurofilament-positive axons present in the proximal and distal stumps were quantified.

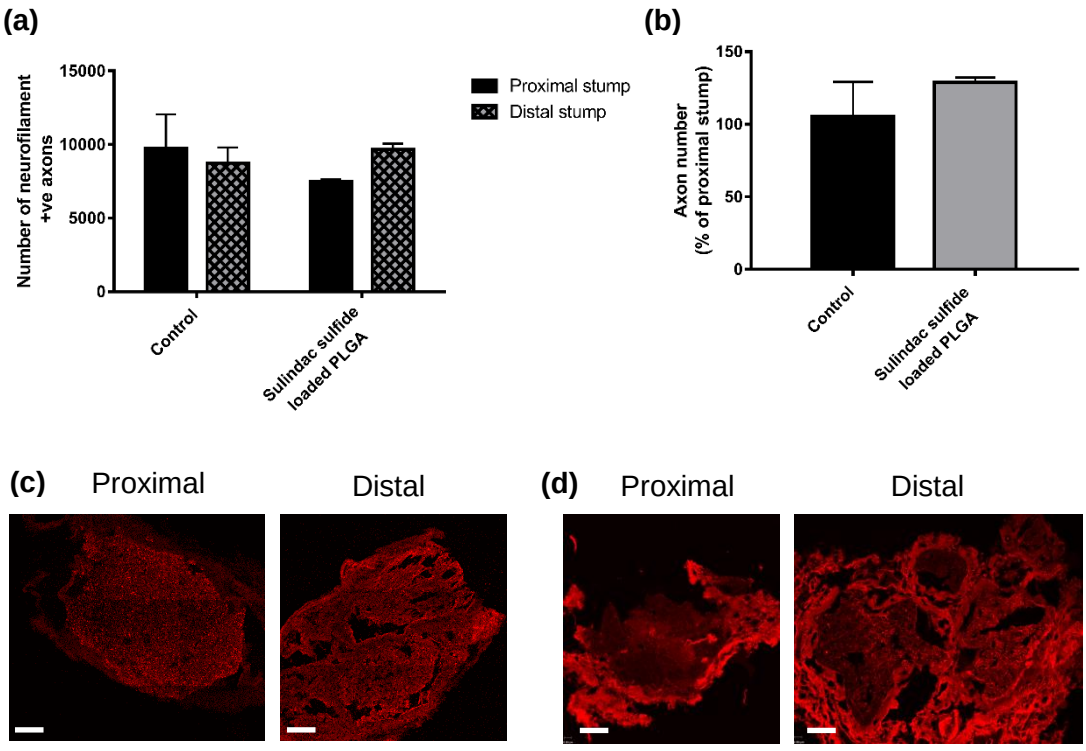

Figure 6.16: Axon number following a crush injury treated with sulindac sulfide-loaded PLGA. *The number of axons in the distal stumps increases with sulindac sulfide treatment in comparison to no drug treatment (a) the axon counts were also expressed as a percentage of the proximal stump in each animal (b). Micrographs are transverse sections showing neurofilament positive neurites at 5 mm proximal and distal to the injury site in the no drug control group (c) and sulindac sulfide treatment group (d). Scale bar = 100 μm. N=3, data are means ± SEM.*

Analysis demonstrated a loss in axon number following surgery but treatment with sulindac sulfide released from PLGA increased the number of axons in the distal stump in comparison to no drug treatment (Figure 6.16). Furthermore, the number of axons quantified in the distal stump of the sulindac sulfide group exceeded the axon number in the corresponding proximal stump of the same nerve.

6.2.4.2 Functional recovery

Motor and sensory recovery was also studied using muscle weight, SSI, electrophysiology, and von Frey analysis. The animals in the treated group demonstrated similar responses to sensory stimulation to the control group. However, the threshold response to von Frey filaments was lower in the treatment group from day 21 post injury (Figure 6.17)

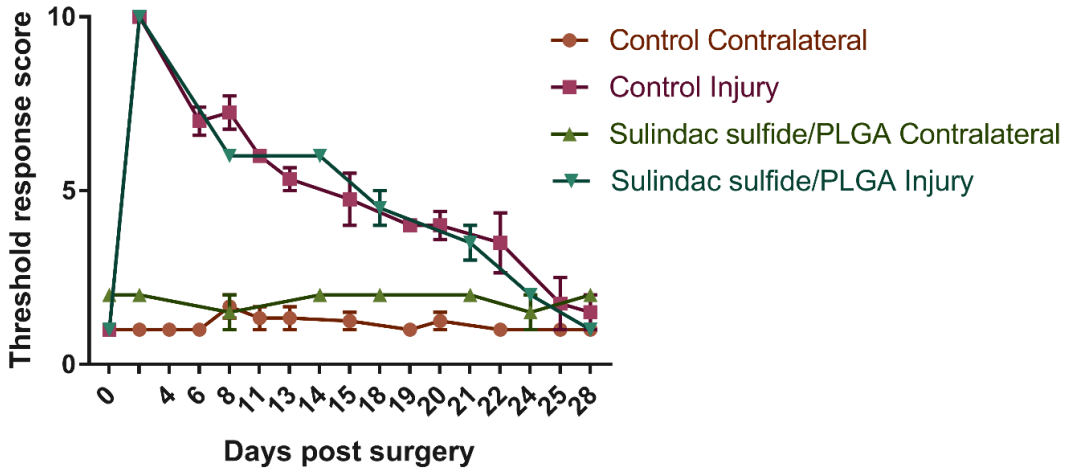

Figure 6.17: Von Frey in a crush injury treated with sulindac sulfide-loaded PLGA nanofibres. *Improved sensory recovery was seen with sulindac sulfide treatment from day 21 post injury. N=3, mean ± SEM.*

The gastrocnemius muscle was also harvested and weighed immediately. There was a no difference in muscle mass between treatment and control group (Figure 6.18). Furthermore, no difference was seen in the SSI between the two groups, however, the SSI in the control group returned back to the baseline by 28 days whereas the treated group did not (Figure 6.19).

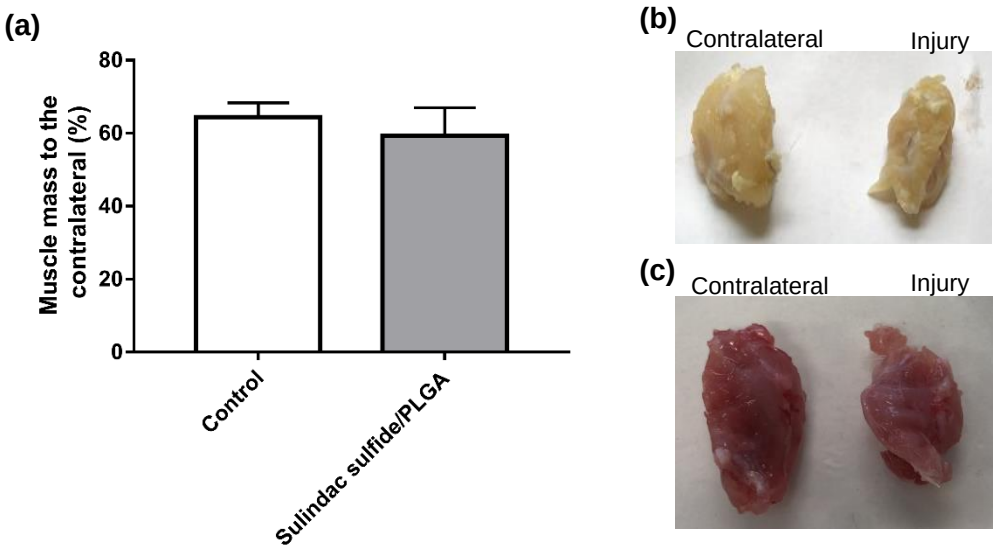

Figure 6.18: Muscle mass in a crush injury treated with sulindac sulfide-loaded PLGA nanofibres. *No difference in muscle mass was seen between the two groups (a). Images of the harvested gastrocnemius muscle from the contralateral and injured hind leg from the group treated with blank PLGA (b) and sulindac sulfide-loaded PLGA (c). N=3 mean ± SEM.*

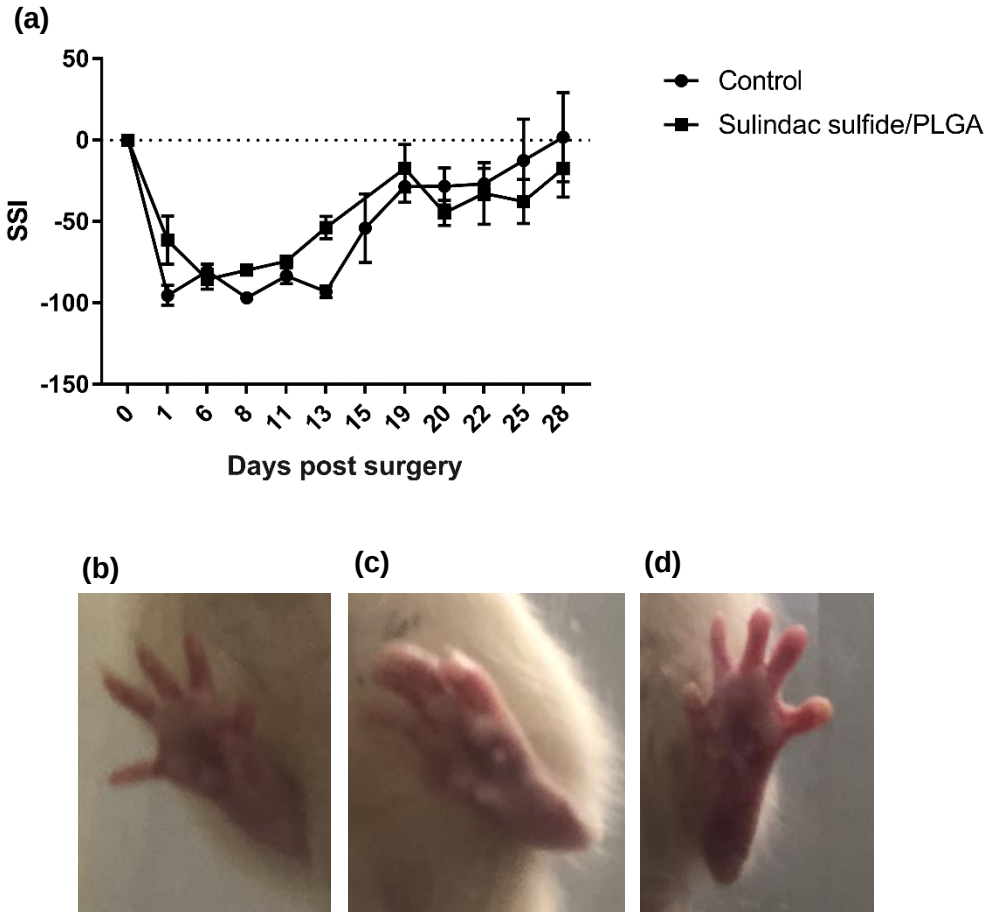

Figure 6.19: SSI in a crush injury treated with sulindac sulfide-loaded PLGA nanofibres. *No difference in the SSI was seen between the groups (a). Hind paw images used to conduct SSI quantification for contralateral (b), control (c) and sulindac sulfide treated (d) groups. N=3, means ± SEM.*

The CMAPs were recorded from the non-injured contralateral and injured side in all animals. No differences were observed in any of the outcome measures between the two groups (Figure 6.20).

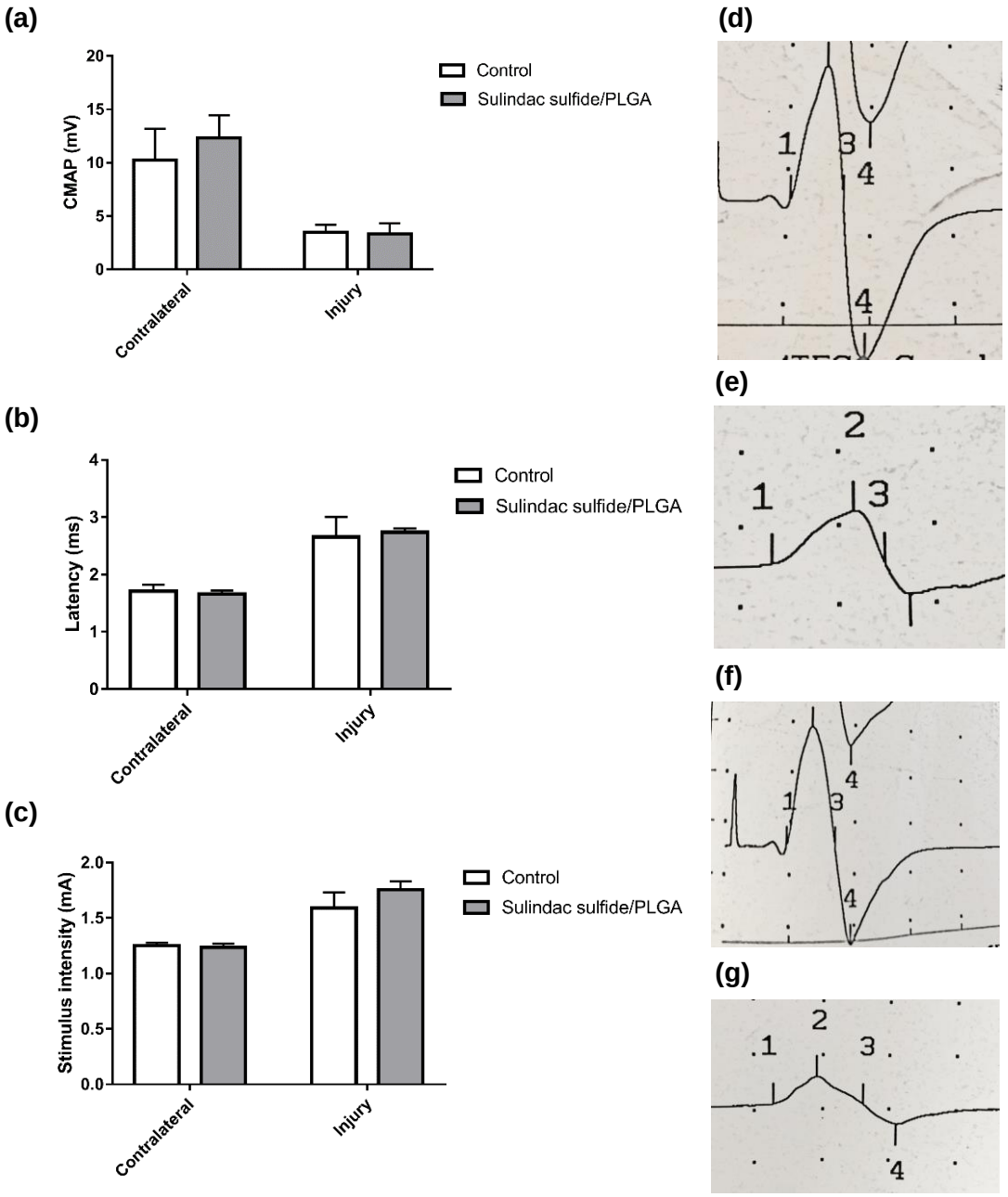

Figure 6.20: Electrophysiological data 28 days after a crush injury treated with sulindac sulfide-loaded PLGA. *The sciatic nerve was stimulated proximal to the repair site and the CMAP was recorded from the gastrocnemius muscle. There were no differences in any of the measures between the two groups (a), (b) and (c). The electrophysiological traces for the contralateral (d) and injury (e) hind paws in the control group and the contralateral (f) and injury (g) hind paws in the treatment group. N=3, means ± SEM.*

6.2.4.3 Vascularisation

Vascularisation was examined via immunohistochemical staining of transverse sections for RECA-1. A difference was observed between the two groups with more blood vessels present in the distal stump of the sulindac sulfide treated group in comparison with the control group (Figure 6.21 (a)). Furthermore, larger blood vessel diameters were found in the sulindac sulfide treatment group (Figure 6.21 (b)).

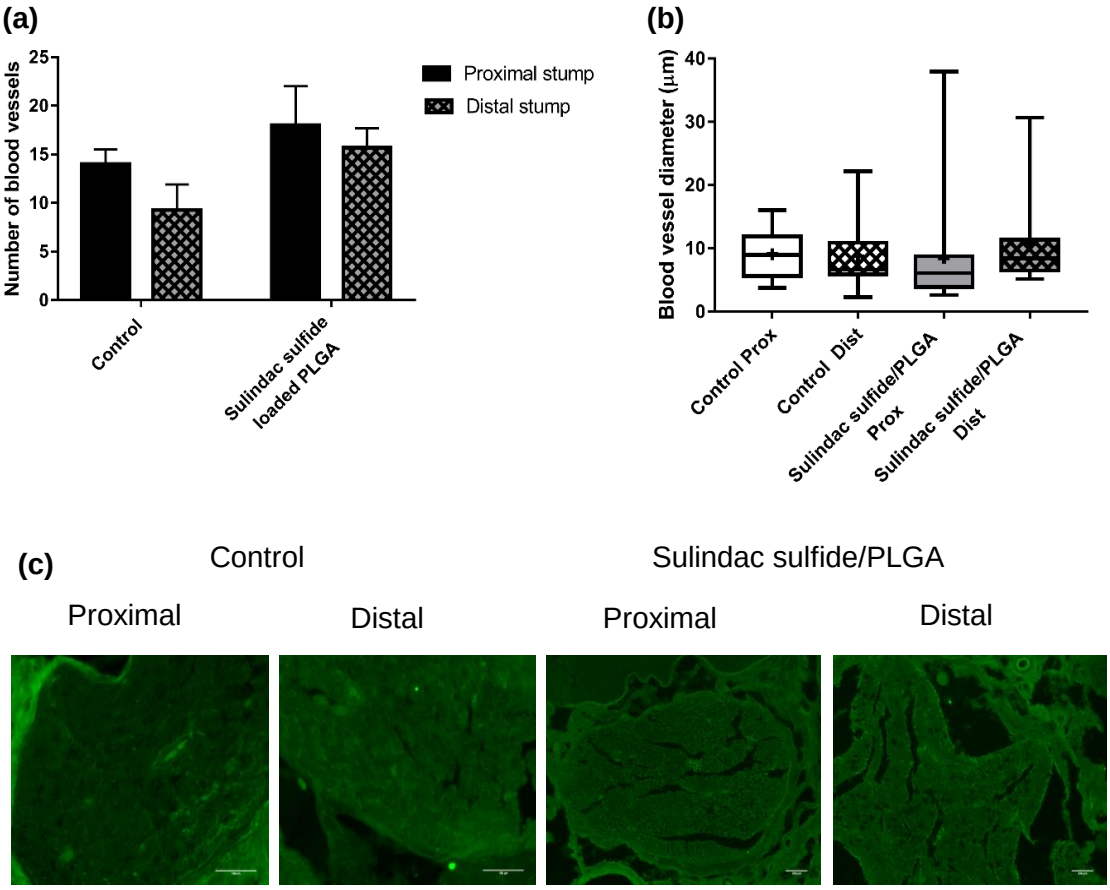

Figure 6.21: Vasculature changes following a crush injury treated with sulindac sulfide-loaded PLGA. *Quantitative analysis of the number (a) and diameter (b) of blood vessels by RECA-1 (green). Immunostained 10 µm transverse sections from the proximal and distal stumps (c). N=3, mean ± SEM for each condition. Box plots show the distribution of blood vessel diameter with boxes extending from the max to min, + indicates mean.*

6.2.5 Synthesis of a sulindac sulfide derivative

The sulindac sulfide derivative, (E)-2-(5-Fluoro-1-(napththalen-1-ylmethylene)-1H-inden-3-yl)-ethanoic acid **(3)** was synthesised using scheme 1. This particular compound was chosen for further studies for regenerative capacity because it demonstrated the greatest affinity (0.1 μM) of all of the derivatives investigated by Felts *et al*., (2008).

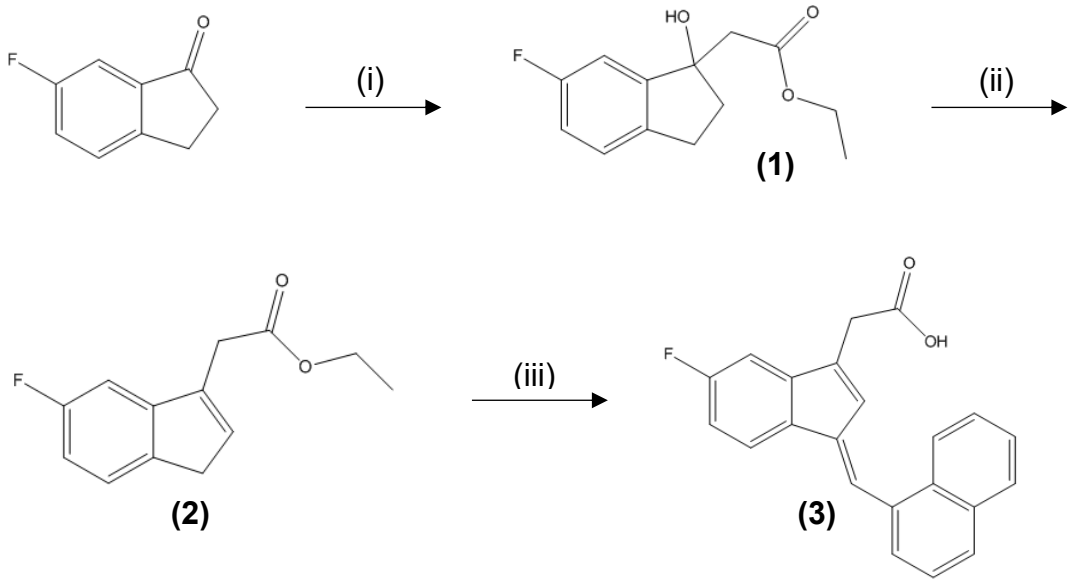

Scheme 1: Synthetic route to compound (3). *Reagents and conditions: (i) Ethyl bromoacetate, activated zinc, Benzene/Ether, reflux 16h (54.3%); (ii) TsOH.H_2O, CaCl2, Toluene, reflux 16h (12.8%); (iii) 1-napthylaldehyde, 1N NaOH, MeOH, reflux, 16h (10%).*

*6.2.5.1 Synthesis of (6-Fluoro-1-hydroxy-indan-1-yl)-acetic acid ethyl ester **(1)***

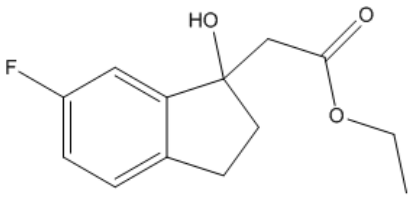

A solution of 5-Fluoroindan-1-one ethyl bromoacetate and activated zinc in benzene and ether was stirred at reflux at 80 °C for ~16 h, after which time the product was purified using a silica gel column chromatography (13:1 hexane:ethyl acetate) furnishing an orange oil (1.87 g, 54.3%). The crude product **(1)** was carried through to the next step.

*6.2.5.2 Synthesis of (6-Fluoro-3H-inden-1-yl)-acetic acid ethyl ester **(2)***

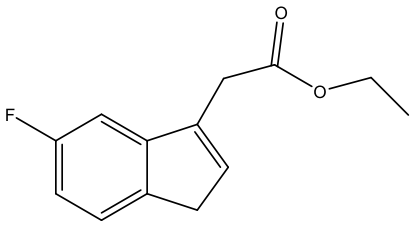

The crude product **(1)** was added to p-Toluenesulfonic acid monohydrate and calcium chloride in Toluene and stirred at reflux overnight (~16 h). After this time the product was purified by column chromatography furnishing a yellow powder **(2)**. However, this purification method furnished a poor yield (~5%), so reverse phase column chromatography was utilised to improve the yield. The product was a yellow powder (240 mg, 12.8%), Rf = 0.43. ^{1}H NMR (500 MHz, CDCl3) δ 7.227-7.189 (m, 1H), 7.09 (dd, J = 2.0. 8.7 Hz, 1H), 6.94-6.90 (m,1H), 6.33-6.31 (m, 1H), 4.10 (q, J = 5.01 Hz, 2H), 3.49 (d, J = 5.01 Hz, 2H), 3.28 (s, 2H), 1.19 (t, J = 5.01 Hz, 3H). LCMS 659 (2M-H), (RT = 4.43, 100%). The data is in agreement with previous literature *(Felts et al., 2007)*.

*6.2.5.3 Synthesis of (E)-2-(5-Fluoro-1-(naphthalene-1-ylmethylene)-1H-inden-3-yl)-ethanoic acid **(3)***

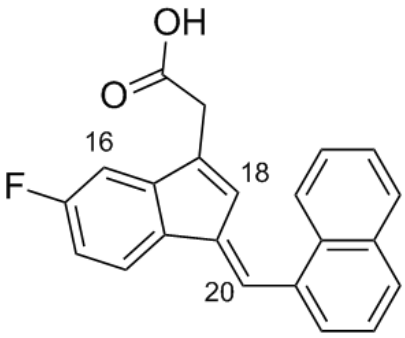

(6-Fluoro-3*H*-inden-1-yl)-acetic acid ethyl ester **(2)** and 1-naphthaldehyde were added in 1 N sodium hydroxide and ethanol were stirred at reflux for 16 h. After this time the product was purified using HPLC furnishing a yellow powder (10 mg, 10 %), Rf = 0.86. ^{1}H NMR (500 MHz, CDCl3) δ 8.14-8.12 (m, 1H, indole C*H*-16), 8.10 (s, 1H, C*H*-20), 7.95-7.91 (m, 2H, indole), 7.66 (d, *J* = 7.10 Hz, 1H), 7.59-7.54 (m, 4H, naphthaldehyde Ar-

C*H*, indole C*H*), 7.32-7.29 (m, 1H, naphthadehyde Ar-C*H*), 7.06 (td *J* = 9.04, 2.25 Hz, 1H, naphthaldehyde Ar-C*H*), 6.83 (s, 1H, C*H*-18), 3.71 (s, 2H). LCMS 659 (2M-H), (RT = 4.46, 100%). HPLC Rt = 55 min, >99% content. The data is in agreement with previous literature *(Felts et al., 2008)*.

*6.2.6 Effect of sulindac sulfide derivative **(3)** on neurite growth in 3D EngNT co-cultures*

3D EngNT co-culture models containing SCL4.1/F7 and PC12 cell lines, were used to investigate the effect of the sulindac sulfide derivative on neurite outgrowth. It was found that the derivative increased neurite growth in a dose dependent manner. Furthermore, the results showed that the derivative elicited an increase in neurite length at lower doses than the other NSAIDs tested in the *in vitro* models previously in chapter 3 and 6 (Figure 6.22)

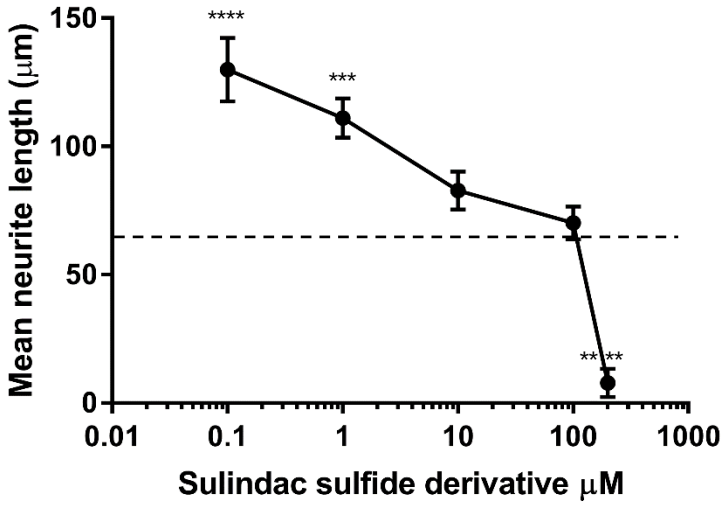

Figure 6.22: The effect of the sulindac sulfide derivative (3) on neurite growth in the 3D EngNT co-culture. *Compound **(3)** increased neurite growth in comparison to the control. A significant increase in growth was seen with 100 μM and 10 μM. N=6 of EngNT co-culture gels, mean ± SEM for each compound tested. One-way ANOVA with Dunnett's post hoc test, *p < 0.05 and **p < 0.01.*

6.3 Discussion

Increased knowledge of signalling pathways has helped promote the development of target-specific treatments for PNI with improved regeneration *(DeGeer and Lamarche-Vane, 2013)*, coupled with a decrease in off-site side effects and opportunities for synergy. In recent years there has been an increase in evidence supporting the Rho/ROCK pathway as a target in peripheral nerve regeneration. The inhibition of the Rho/ROCK pathway has been linked with the activation of PPAR-γ via the upregulation of the SHP-2, providing a platform for pharmacological intervention. This cytosolic PTP dephosphorylates the Rho-GEF Vav. This inactivation suppresses the conversion of inactive GDP-Rho to active GTP-Rho ultimately resulting in the suppression of Rho/ROCK activity *(Wakino et al., 2004)*,

This body of work not only determined that PPAR-γ agonists such as; NSAIDs have an effect on nerve regeneration *in vitro* and *in vivo,* but that there is also a correlation between the PPAR-γ affinity of NSAIDs and their nerve regeneration capacity *in vitro*. Furthermore, it was found that an NSAID with no affinity for PPAR-γ had a minimal effect on nerve regeneration.

6.3.1 NSAID effect on nerve regeneration in vitro

This study utilised the 3D co-culture model containing neurons and Schwann cells developed in chapter 3 to investigate the pro-regenerative effects of NSAIDs in the peripheral nerve. Four NSAIDs; namely diclofenac, sulindac sulfide, indomethacin and naproxen, were tested in addition to the previously studied ibuprofen. All the drugs tested enhanced neurite growth to some extent, with the exception of naproxen which had a minimal effect.

Ibuprofen is the most commonly studied NSAID in PNI and has shown promising effects on nerve regeneration in previous literature and earlier chapters. Ibuprofen promotes neurite growth enhancement in primary neuronal cell cultures in a dose dependent manner *(Dill et al., 2010, Fu et al., 2007, Wang et al., 2009).* This was echoed in this study with ibuprofen eliciting an effect on neurite length, with a 55.2% increase compared

to the no drug control. The effect of ibuprofen was further demonstrated in animal models with an increase in axon number and functional recovery. The findings described in chapter 4 support those reported in previous animal studies in the central and peripheral nervous system, with the promotion of axonal growth following an injury in the CNS *(Fu et al., 2007, Wang et al., 2009)*, and improved functional recovery following a peripheral nerve repair (*Madura et al., 2011*).

Diclofenac is another widely used NSAID available over the counter as an analgesic and anti-inflammatory. Therefore, it has been mostly studied in PNI for its potential to relieve neuropathic pain through inhibition of COX-2. The cyclooxygenase enzymes are upregulated in the injury site following a PNI with increases of COX-1 and COX-2 expression seen in both Schwann cells and macrophages. Diclofenac and other NSAIDs can control neuropathic pain through the modulation of inflammatory and nociceptive pathways *(Kaplan et al., 2018)*. In a neuropathic pain model in the rat tibial nerve, diclofenac suppressed neuropathic pain and elicited anti-allodynic effects following cold and mechanical allodynia tests *(Tamaddonfard et al., 2013)*.

In nerve regeneration diclofenac has been found to have conflicting effects by both improving regeneration but also having harmful effects on developing nerves *(Ayranci et al., 2013, Canan et al., 2008, Colakoglu et al., 2014, Keskin et al., 2015).* Diclofenac is a teratogenic drug as it interrupts axon structure and myelin sheath thickness *(Kaplan et al., 2018).* During the embryonic period the number of nerve fibers and the cross-sectional area of axons in developing sciatic nerves were affected when exposed to diclofenac *(Canan et al., 2008).* Prenatal administration of the drug impairs the sciatic, optic and median nerve in the child. Furthermore, diclofenac has been found to inhibit neuronal stem cell differentiation and reduce proliferation through the apoptotic pathway *(Kaplan et al., 2018)*.

On the other hand, this study demonstrated that diclofenac significantly promoted nerve regeneration in a cell culture model. This echoed what had been seen previously in the literature where beneficial effects had been seen with diclofenac treatment in a transection injury on the rat sciatic nerve. Within 16 weeks diclofenac gave rise to faster

regeneration than no drug treatment suggested by a significant increase in gastrocnemius muscle weight and improved morphometrical indices such as; nerve fibre number and axon diameter *(Mohammadi et al., 2013).*

In this study indomethacin also increased neurite growth (19.3%) in the co-culture model, however, the effect was not as great as that seen with diclofenac (73%). This mirrored the stimulation of neurite growth seen in a DRG neuron culture when treated with indomethacin following exposure to inhibitory substrates *(Fu et al., 2007)*. Furthermore, the same study showed that indomethacin and ibuprofen blocked lysophosphatidic acid-induced Rho A activation in PC12 and DRG neuronal cells *(Fu et al., 2007).* Indomethacin has also demonstrated beneficial effects in CNS injury by reducing cell death of the CNS glial cells, oligodendrocytes, in both *in vitro* and *in vivo* studies. The drug also increased the myelination of axons following a contusion spinal cord injury *(Xing et al., 2011)*.

Sulindac sulfide was also tested in this study and demonstrated the greatest effect on the neurite outgrowth in the co-culture model by increasing the growth by 106%. This is a novel outcome which has not been reported in previous literature, although, inhibition of Rho A by sulindac sulfide had been reported previously *(Zhou et al., 2003).* This suggests that sulindac sulfide has the same mechanism of action of nerve regeneration as the other NSAID with its regenerative capacity linking to the inhibition of the Rho/ROCK pathway.

The final NSAID tested was naproxen which had no effect on neurite growth. Even though the drug had no regenerative properties, no neurotoxic effects were seen. The limited regeneration seen with naproxen indicates that the regenerative properties of NSAIDs may be independent of its activity on COX. This correlates with the study by Fu *et al.* (2007) that found that the effects of ibuprofen via the inhibition of the Rho A pathway are independent of COX action. The different regenerative capacities of the NSAIDs may be a result of their different chemical structures (Figure 6.1). This hypothesis has not been explored in this study but it has previously been suggested that the PPAR-γ binding site cannot accommodate the CCH_3 group *(Xing et al., 2011)*. This study did however

find a correlation between the NSAIDs capacity to improve neurite outgrowth and its affinity for the receptor PPAR-γ introducing a new area for the development of novel compounds for PNI *(Puhl et al., 2015)*.

The list of NSAIDs that have a demonstrated effect in PNI are not limited to the ones tested in this body of work. For example the COX-2 inhibitor, celecoxib, was tested in a sciatic nerve crush injury in rats which resulted in improved functional recovery. Significant improvements were observed in the SFI which was considered to be a result of neuroprotection *(Camara-Lemarroy et al., 2008).* In the same model in mice, acetyl salicylic acid also improved functional recovery seen in the SFI, nociception and gait *(Subbanna et al., 2007)*. In a different injury model involving the transected sciatic nerve being fixed to the adjacent muscle, ketoprofen improved functional recovery and morphometric indices including enhanced regeneration of axons *(Mohammadi et al., 2014)*.

There is some body of evidence that the NSAID class of drugs have great potential to be developed into therapies for PNI. As they are routinely used for inflammation and pain and already have well-established safety and efficacy profiles, the repositioning of these approved drugs is likely to be valuable in moving therapies rapidly towards the clinic *(Chan et al., 2014)*. It would be feasible to test such drugs in humans following nerve injury with a low risk of toxic effects. The need for extensive pre-clinical studies can be a drawback in the development of new drugs for treating nerve injuries *(Chan et al., 2014)*, making the repurposing of established drugs an attractive alternative proposition. Drug discovery and development is expensive and time-consuming with a high risk of failure, as a result more companies and academic researchers are exploring drug repurposing as an alternative *(Padhy and Gupta, 2011)*. This technique employs data mining, bioinformatics and screening platforms to identify drugs that are already used in other clinical indications and reposition them for new applications *(Padhy and Gupta, 2011)*. Many drugs identified with potential to promote nerve regeneration have been the result of this repurposing approach and in particular, agents targeting the Rho pathway

currently used for the treatment of other clinical conditions have already shown benefit in preclinical nerve regeneration studies.

6.3.2 Sulindac sulfide- loaded PLGA characterisation and release

Electrospinning PLGA with sulindac sulfide resulted in smooth, uniform and bead-free nanofibers with a size of ~900nm. The drug release from the PLGA was controlled exhibiting first order release with all the drug released by 20 days, which was longer than the 7 day release seen with ibuprofen (section 5.2.1.3). 30% of drug was released in the first 24 hours indicating that not all the drug was successfully encapsulated within the fibres.

Furthermore, the properties of the nanofibres changed when stored at room temperature. This change in properties may alter the biodegradation of the polymer, which in turn will influence the release and degradation rate of incorporated drug molecules. In previous studies the physical properties of PLGA have been shown to depend upon multiple factors, such as; molecular weight of the polymer, the ratio of lactide to glycolide, exposure to water and storage temperature *(Houchin and Topp, 2009)*. The molecular weight and polydispersity index could affect the ability of the PLGA to be formulated as a drug delivery device and may influence the rate of device degradation and hydrolysis. It was also found that the type of drug encapsulated also effects the release rate *(Siegel et al., 2006)*. The degree of crystallinity of PLGA can influence the mechanical strength, swelling behavior, hydrolysis and biodegradation rate of the polymer. Crystallinity of the polymer is dependent on the type and molar ratio of the individual monomer components in the copolymer chain *(Makadia and Siegel, 2011)*. The crystallinity reduces with the corresponding increase in PLA content which results in quicker degradation rates. A 50:50 ratio of PLA/PGA exhibits the fastest degradation *(Makadia and Siegel, 2011)*.

Further studies of these physical properties of the sulindac sulfide loaded PLGA nanofibers will aid the development and optimisation of a formulation for the local delivery of drugs for PNI from a polymer cuff. Despite the stiff properties, the nanofibres could be

loosely wrapped around the nerve and at the end-point this stiffness had reduced and the material encased the nerve like that observed ibuprofen-loaded nanofibres.

6.3.3 Effect of sulindac sulfide on regeneration in vivo

Regeneration and functional recovery was measured 28 days post injury after sulindac sulfide was delivered locally through either osmotic pumps or drug loaded PLGA nanofibres. Histological analysis demonstrated an increase in axon number in the distal stump in the treatment group at 28 days in comparison with the control group, using both delivery methods. Interestingly, the number of axons in the distal stump exceeded those in the proximal stump in the same animal when the drug was delivered using PLGA, as seen following treatment with ibuprofen-loaded PLGA (section 5.2.3.1). In alignment with the results obtained with ibuprofen treatment in chapter 5 the results with sulindac sulfide suggested that PLGA nanofibres provide additional growth support to the neurons as the number of axons in the distal stump in the PLGA control group at 28 days were higher than those seen in the osmotic pump control group in the crush model. This is supported by the regeneration and functional recovery seen with PLGA based therapies implanted in peripheral nerve models *(Panseri et al., 2008, Subramanian et al., 2012, Nune et al., 2017)*.

There are no previous reports exploring the effect of sulindac sulfide for PNI, however, sulindac sulfide was previously shown to inhibit the activity of Rho in a concentration-dependent manner. The direct effect of sulindac sulfide on Rho activation was explored in SY5YAPP, HEK 293 and PC12 cells and levels of active Rho-GTP were reduced in all of the cell lines tested demonstrating that sulindac sulfide inhibits Rho activation *(Zhou et al., 2003)*.

The electrophysiological results demonstrated no difference in the CMAP following sulindac sulfide treatment by both delivery methods. The latency and stimulus intensity required to acquire a response were both significantly lower in the treatment group delivered by osmotic pumps but not PLGA. This suggests that there may have

been an improvement in target muscle reinnervation with sulindac sulfide treatment, which is similar to what was seen in a previous result with ibuprofen in chapter 5.

These results were consistent with the gastrocnemius muscle mass and the SSI. The muscle mass in the osmotic pump treatment group was higher at ~60 % of the contralateral in comparison to the ~40 % in the no drug treatment group. In all groups the SSI returned to baseline within 28 days. No great differences in SSI were seen between the groups towards the end of the study, however, the SSI was lower in the treatment group in the first 14 days post injury.

Lastly, evaluation of sensory recovery was conducted using von Frey filaments. The treatment group displayed a significantly lower threshold response than the control group from day 4 to 28 post injury when the drug was delivered using osmotic pumps, however, no difference in the threshold response was observed when the drug was delivered from PLGA. Furthermore, sensory function returned to baseline by day 25 in the treatment group but not until day 28 in the control group.

In addition to investigating axon regeneration and functional recovery, this study also explored the vascularisation following injury which demonstrated a higher number of blood vessels and larger diameter in the sulindac sulfide treatment group in comparison with the control group.

6.3.4 Synthesis and screening of sulidac sulfide derivative

The unwanted side effects of sulindac sulfide as a COX inhibitor discourages its prolonged use following a PNI. A study has found that the isomeric chemical structure of sulindac sulfide can be modified to remove its COX inhibitor activity through switching the 2′-methyl group of the indene or indole rings. The removal of this group changes the geometry of the benzylidene double bond; switching the compound from a *Z* to *E* isomer. The acidic side chain was confirmed to be required for PPAR-γ activation so Felts *et al*. (2008) explored the effect of functional group substitutions of the benzylidene ring to improve potency, generating a range of ~29 derivatives with variable affinity for PPAR-γ *(Felts et al., 2008)*. A common feature of known PPAR-γ agonists are large aromatic and

heteroaromatic systems, so naphthyl and biphenyl substitutions were investigated. The attachment of a naphthyl ring at the 1-position yielded a derivative with an EC_{50} of 0.1 μM. In further studies it was confirmed that this derivative binds directly to PPAR-γ as a dose-dependent displacement of a known PPAR-γ agonist, troglitazone, was observed. *(Felts et al., 2008)*. For these reasons this compound was selected for study in this body of work.

In this study compound **(3)** was successfully synthesised with 100% purity, however, a poor yield was obtained. To acquire a better yield of compound **(2)** reverse phase flash column chromatography was used to purify the product instead of the normal phase chromatography column used in the literature. The non-polar properties of the compound resulted in most of the product remaining on the silica column resulting in a yield of ~5%. However, the use of a reverse phase column only increased the yield to 12.8%, therefore, further optimisation of the protocol is needed

A poor yield was also obtained in the final synthesis step, so increasing the reaction time from 2 h to 16 h was considered, however, no improvement in the yield was achieved. Despite the poor yield a high purity (100%) was obtained by using HPLC to purify the product instead of flash chromatography which was used in the literature. Further modifications and optimisation of the protocol need to be investigated to synthesise a higher quantity of the compound for future *in vivo* studies.

Despite the low yield acquired, the pure compound was tested in the co-culture model. The effect of sulindac sulfide derivative was studied in the same 3D co-culture model containing neurons and Schwann cells as the other NSAIDs at the beginning of this chapter. The sulindac sulfide derivative has a significant effect on neurite outgrowth which is a novel finding and has not been reported before. Furthermore, the sulindac sulfide derivative increased neurite growth at lower doses than the other NSAIDs. The optimal dose was 0.1 μM, which elicited an increase of neurite growth by 98.8%. These results show promise that a compound with a greater affinity for PPAR-γ can produce a great effect in neurite outgrowth, however, the effect was lower than the 106% increase

in growth seen with sulindac sufide. To explore whether this effect on outgrowth is also seen in the animals, *in vivo* studies need to be conducted.

In conclusion, the outcomes from this chapter established the effects of select NSAIDs in the *in vitro* and *in vivo* models and identified that there may a significant correlation between the PPAR-γ affinity of a NSAID and their regenerative capacity. Furthermore, the successful synthesis of a desmethyl derivative of sulindac sulfide was achieved and with screening through the *in vivo* co-culture model it was found that the derivative produced a significant effect on regeneration at much lower doses than the other NSAIDs. The work presented here provides evidence that PPAR-γ is a suitable target for drug therapies for PNI and further development in this area could prove to be promising in translating drug therapies for PNI into the clinics.

Chapter 7: Conclusions and future translation

7.1 Overall conclusions

This body of work successfully contributed to the translational research in PNI, by developing drug treatments to improve regeneration and functional recovery. The findings have helped to establish a pipeline that allows the development of small molecules, from the initial identification and synthesis stages all the way through *in vitro* and *in vivo* pre-clinical studies to clinical trials.

In chapter 3 the development of the co-culture model was successful and provided a suitable tool to screen drugs efficiently. This model was validated as the effects seen in this study mimicked those previously demonstrated within the literature *(Dill et al., 2010, Cheng et al., 2008, Joshi et al., 2015)*. As ibuprofen demonstrated the largest effect on neurite growth in the *in vitro* model in chapter 3 it was used to develop *in vivo* models. The research in chapter 4 identified suitable *in vivo* models to screen drugs for PNI and identified outcome measures that allow the robust analysis of regeneration and functional recovery. The objective to find a model that could provide an injury detrimental to function but with a relatively short recovery period was attained through the use of two common experimental injury models; a transection and crush injury. The *in vivo* models proved to be effective to screen drugs as the results found in this study mirrored the beneficial effects of ibuprofen on functional recovery established in previous literature *(Madura et al., 2011)*.

Future work is needed to validate the *in vitro* model and improve its predictive power for *in vivo* studies before advancing widespread adoption in the field and permitting the screening of drugs on a large scale. This would also enable more focused screening and the reduction of the use of animals in research. Moreover, it could open up other avenues for the use of the model such as optimising dosing regimens, as it could provide better estimations of how the drugs act *in vivo*.

Additionally, more in depth analysis should be conducted to determine the effect of drugs on all aspects of nerve repair. The initial outcomes of the drug effect on axonal growth in

chapter 4 were positive but additional work should be done to explore the effect of drugs on cell phenotypes using qPCR and immunocytochemistry. This would advance knowledge of the phenotypic changes of Schwann cells and macrophages following nerve injury and the downstream effects these cell changes have on nerve regeneration, providing us with cell-specific pharmaceutical targets.

Pilot studies using qPCR to explore the changes in Schwann cell phenotype at various time points following a transection injury demonstrated increased expression of Schwann cell biomarkers in the distal stump compared to the proximal stump (Figure 9.2, appendix 2). The upregulation of Krox-20 and Olig-1 in the distal stump over the recovery period could be indicative of more Schwann cells differentiating towards a myelinating phenotype to promote myelination of the regenerated axon. This correlates with the cellular events seen following injury discussed by Fex Svennigsen and Dhalin*, (2013),* in which they show remyelination occurring at ~5 days after injury and continuing as the nerve regenerates and the pattern of gene expression found *in vitro* studies for the significant cellular events that occur following injury *(Jessen and Mirsky, 2015, Arthur-Farraj et al., 2012)*. The findings from this study are not conclusive, however, further investigation of drug effects on cell phenotype could drive drug discovery for PNI. In future work, qPCR could also be used to determine what changes occur in the regeneration associated- genes (RAGs) within the neuronal cell.

In addition, immunohistochemistry was used to determine whether the drug agents are having an impact on the blood vessels surrounding the nerve during regeneration. This study showed that ibuprofen had an impact on angiogenesis in the peripheral nerve, however, further analysis is needed to determine the mechanism of this effect. All of these outcomes together can provide a detailed holistic view of the drug effect on nerve regeneration.

Furthermore, the work conducted in chapter 5 was successful in manufacturing and testing drug-loaded biomaterials as drug delivery systems for the treatment of PNI. Suitable release profiles were obtained and the materials loaded with ibuprofen and tested *in vivo* demonstrated positive effects in nerve regeneration and functional

recovery. The direct comparison of delivery from the drug-loaded biomaterials with the delivery from the osmotic pumps, demonstrated that the systems manufactured in this study were as effective at delivering ibuprofen to the nerve as a well-established experimental tool. Future work will need to further develop and optimise the sustained release from the biomaterials for local delivery. Mathematical modelling will be implemented to aid development and design of a drug delivery device with the correct geometries and drug load to deliver the correct dose over a specific duration. The mathematical model will consists of two phases 1.) Model development and parameterisation and 2.) Model refinement with experimental studies (Figure 7.1).

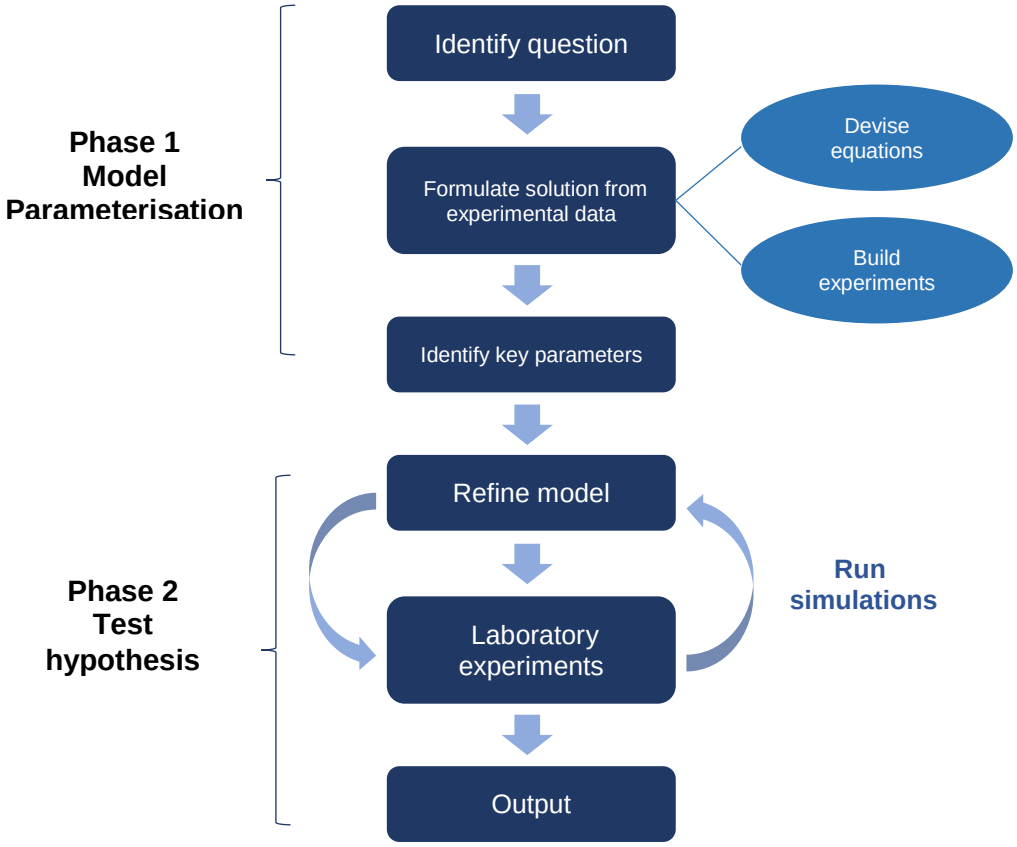

Figure 7.1: Overview of mathematical model concept.

To further progress the field investigations determining the mechanisms by which the drugs are working are needed. One approach which could be conducted for the drugs used in this study is using a Rho A assay to determine the level of Rho-GTPases

following drug treatments and whether the drugs modulate these levels of the Rho-GTPases. Gaining a better understanding of the mechanism by which drugs work for PNI will aid the identification of drugs which could be repurposed for use in this area and the discovery of novel targets and compounds.

With a better understanding of the molecular and cellular targets, more novel compounds can be identified using web-bank informatics. The databases can be used to screen for potential small molecules that have distinctive chemical moieties or affinity for the targets identified in this study. The most promising agents can be taken forward and screened for their pro-regenerative effects using the developed *in vitro* and *in vivo* screening assays.

The work carried out in chapter 6 of this study began to explore the correlation between NSAID affinity for PPAR-γ and their regenerative capacity. Initial studies suggested there was a correlation and so it was hypothesised that drugs with a greater affinity for PPAR-γ would elicit better regenerative effects. The synthesis of a desmethyl derivative of sulindac sulfide with a higher affinity for PPAR-γ than sulindac sulfide elicited a better effect on neurite outgrowth *in vitro* at lower doses than the other NSAIDs tested. Future work should be conducted to explore whether these effects are also seen *in vivo*.

In conclusion, the work presented here has opened up promising new opportunities in the discovery, development and clinical translation of new therapies to treat PNI.

7.2 Future translation

7.2.1 Clinical trial

There is no drug used in the clinic to improve the outcome from PNI, however, the work conducted in this study has started to enhance the clinical translation of drug therapies in this area. Clinical colleagues at the Royal National Orthopaedic Hospital in Stanmore (National referral Centre for Peripheral Nerve Injuries) have access to a relatively large cohort of patients, which has provided us with an opportunity to work with them to help design a clinical trial (IBUPROFLEX) to repurpose ibuprofen for administration following

nerve repair. The study is currently in planning stages with the hope to conduct the trial in 2019.

7.2.2 PNI patient demographic audit

To better inform the clinical trial a patient demographic audit is being undertaken in order to understand the patient populations who are affected by PNI. Having better knowledge of the patients who suffer from a PNI including mechanism of injury, gender, age, occupation *etc*. will help in the recruitment of subjects for the trial and allow us to assign the control and treatment arms across the population more uniformly. It would be of particular interest from this study to know what other long term conditions patients have and the medication they are taking, and gaining knowledge of how this may impact the medication they are prescribed following injury.

In conclusion, the advances in preclinical testing of potential drug therapies, combined with development of clinical trial protocols and relevant outcome measures, provide an exciting opportunity to advance new pharmacological PNI nerve injury treatments into clinical application.

References

AHMED, I., LIU, H. Y., MAMIYA, P. C., PONERY, A. S., BABU, A. N., WEIK, T., SCHINDLER, M. & MEINERS, S. 2006. Three-dimensional nanofibrillar surfaces covalently modified with tenascin-C-derived peptides enhance neuronal growth in vitro. *J Biomed Mater Res A,* 76**,** 851-60.

ALLEN, C., EISENBERG, A., MRSIC, J. & MAYSINGER, D. 2000. PCL-b-PEO micelles as a delivery vehicle for FK506: assessment of a functional recovery of crushed peripheral nerve. *Drug Deliv,* 7**,** 139-45.

ALLODI, I., UDINA, E. & NAVARRO, X. 2012. Specificity of peripheral nerve regeneration: interactions at the axon level. *Prog Neurobiol,* 98**,** 16-37.

AMADO, S., SIMOES, M. J., ARMADA DA SILVA, P. A., LUIS, A. L., SHIROSAKI, Y., LOPES, M. A., SANTOS, J. D., FREGNAN, F., GAMBAROTTA, G., RAIMONDO, S., FORNARO, M., VELOSO, A. P., VAREJAO, A. S., MAURICIO, A. C. & GEUNA, S. 2008. Use of hybrid chitosan membranes and N1E-115 cells for promoting nerve regeneration in an axonotmesis rat model. *Biomaterials,* 29**,** 4409-19.

AMANO, M., NAKAYAMA, M. & KAIBUCHI, K. 2010. Rho-kinase/ROCK: A key regulator of the cytoskeleton and cell polarity. *Cytoskeleton (Hoboken),* 67**,** 545-54.

AMIN, E., DUBEY, B. N., ZHANG, S. C., GREMER, L., DVORSKY, R., MOLL, J. M., TAHA, M. S., NAGEL-STEGER, L., PIEKORZ, R. P., SOMLYO, A. V. & AHMADIAN, M. R. 2013. Rho-kinase: regulation, (dys)function, and inhibition. *Biol Chem,* 394**,** 1399-410.

ANGIUS, D., WANG, H., SPINNER, R. J., GUTIERREZ-COTTO, Y., YASZEMSKI, M. J. & WINDEBANK, A. J. 2012. A systematic review of animal models used to study nerve regeneration in tissue-engineered scaffolds. *Biomaterials,* 33**,** 8034-9.

ARGUIS, M. J., PEREZ, J., MARTINEZ, G., UBRE, M. & GOMAR, C. 2008. Contralateral neuropathic pain following a surgical model of unilateral nerve injury in rats. *Reg Anesth Pain Med,* 33**,** 211-6.

ARMSTRONG, S. J., WIBERG, M., TERENGHI, G. & KINGHAM, P. J. 2007. ECM molecules mediate both Schwann cell proliferation and activation to enhance neurite outgrowth. *Tissue Eng,* 13**,** 2863-70.

AYRANCI, E., ALTUNKAYNAK, B. Z., AKTAS, A., RAGBETLI, M. C. & KAPLAN, S. 2013. Prenatal exposure of diclofenac sodium affects morphology but not axon number of the median nerve of rats. *Folia Neuropathol,* 51**,** 76-86.

BABU, P., BEHL, A., CHAKRAVARTY, B., BHANDARI, P., BHATTI, T. & MAURYA, S. 2008. Entubulation techniques in peripheral nerve repair. *Indian Journal of Neurotrauma,* 5**,** 15-20.

BACKSTROM, E., CHAMBERS, B. J., KRISTENSSON, K. & LJUNGGREN, H. G. 2000. Direct NK cell-mediated lysis of syngenic dorsal root ganglia neurons in vitro. *J Immunol,* 165**,** 4895-900.

BADACHE, A. & DE VRIES, G. H. 1998. Neurofibrosarcoma-derived Schwann cells overexpress platelet-derived growth factor (PDGF) receptors and are induced to proliferate by PDGF BB. *J Cell Physiol,* 177**,** 334-42.

BALDWIN, S. P., KREWSON, C. E. & SALTZMAN, W. M. 1996. PC12 cell aggregation and neurite growth in gels of collagen, laminin and fibronectin. *Int J Dev Neurosci,* 14**,** 351-64.

BALGUDE, A. P., YU, X., SZYMANSKI, A. & BELLAMKONDA, R. V. 2001. Agarose gel stiffness determines rate of DRG neurite extension in 3D cultures. *Biomaterials,* 22**,** 1077-84.

BAPTISTA, A. F., GOMES, J. R., OLIVEIRA, J. T., SANTOS, S. M., VANNIER-SANTOS, M. A. & MARTINEZ, A. M. 2007. A new approach to assess function after sciatic nerve lesion in the mouse - adaptation of the sciatic static index. *J Neurosci Methods,* 161**,** 259-64.

BARR, A. J. 2010. Protein tyrosine phosphatases as drug targets: strategies and challenges of inhibitor development. *Future Med Chem,* 2**,** 1563-76.

BARUT, S., UNLU, Y. A., KARAOGLAN, A., TUNCDEMIR, M., DAGISTANLI, F. K., OZTURK, M. & COLAK, A. 2005. The neuroprotective effects of z-DEVD.fmk, a caspase-3 inhibitor, on traumatic spinal cord injury in rats. *Surg Neurol,* 64**,** 213-20; discussion 220.

BECQ, H., BOSLER, O., GEFFARD, M., ENJALBERT, A. & HERMAN, J. P. 1999. Anatomical and functional reconstruction of the nigrostriatal system in vitro: selective innervation of the striatum by dopaminergic neurons. *J Neurosci Res,* 58**,** 553-66.

BEER, G. M., STEURER, J. & MEYER, V. E. 2001. Standardizing nerve crushes with a non-serrated clamp. *J Reconstr Microsurg,* 17**,** 531-4.

BENITO, C., DAVIS, C. M., GOMEZ-SANCHEZ, J. A., TURMAINE, M., MEIJER, D., POLI, V., MIRSKY, R. & JESSEN, K. R. 2017. STAT3 Controls the Long-Term Survival and Phenotype of Repair Schwann Cells during Nerve Regeneration. *J Neurosci,* 37**,** 4255-4269.

BERVAR, M. 2000. Video analysis of standing--an alternative footprint analysis to assess functional loss following injury to the rat sciatic nerve. *J Neurosci Methods,* 102**,** 109-16.

BEST, T. J. & MACKINNON, S. E. 1994. Peripheral nerve revascularization: a current literature review. *J Reconstr Microsurg,* 10**,** 193-204.

BHANGRA, K. S., BUSUTTIL, F., PHILLIPS, J. B. & RAHIM, A. A. 2016. Using Stem Cells to Grow Artificial Tissue for Peripheral Nerve Repair. *Stem Cells Int,* 2016**,** 7502178.

BHARDWAJ, N. & KUNDU, S. C. 2010. Electrospinning: a fascinating fiber fabrication technique. *Biotechnol Adv,* 28**,** 325-47.

BIAZAR, E., KHORASANI, M. T., MONTAZERI, N., POURSHAMSIAN, K., DALIRI, M., REZAEI TAVIRANI, M., JABARVAND, M., KHOSHZABAN, A., HEIDARI KESHEL, S., JAFARPOUR, M. & ROVIEMIAB, Z. 2010. *Types of neural guides and using nanotechnology for peripheral nerve reconstruction*.

BONTIOTI, E. N., KANJE, M. & DAHLIN, L. B. 2003. Regeneration and functional recovery in the upper extremity of rats after various types of nerve injuries. *J Peripher Nerv Syst,* 8**,** 159-68.

BORKENHAGEN, M., CLEMENCE, J. F., SIGRIST, H. & AEBISCHER, P. 1998. Three-dimensional extracellular matrix engineering in the nervous system. *J Biomed Mater Res,* 40**,** 392-400.

BOZKURT, A., BROOK, G. A., MOELLERS, S., LASSNER, F., SELLHAUS, B., WEIS, J., WOELTJE, M., TANK, J., BECKMANN, C., FUCHS, P., DAMINK, L. O., SCHUGNER, F., HESCHEL, I. & PALLUA, N. 2007. In vitro assessment of axonal growth using dorsal root ganglia explants in a novel three-dimensional collagen matrix. *Tissue Eng,* 13**,** 2971-9.

BRANNON-PEPPAS, L. 1997. Polymers in Controlled Drug Delivery. *MD+DI Qmed.*

BREYER, M. D., LOOK, A. T. & CIFRA, A. 2015. From bench to patient: model systems in drug discovery. *Dis Model Mech,* 8**,** 1171-4.

BRIDGE, P. M., BALL, D. J., MACKINNON, S. E., NAKAO, Y., BRANDT, K., HUNTER, D. A. & HERTL, C. 1994. Nerve crush injuries--a model for axonotmesis. *Exp Neurol,* 127**,** 284-90.

BUSUTTIL, F., RAHIM, A. A. & PHILLIPS, J. B. 2017. Combining Gene and Stem Cell Therapy for Peripheral Nerve Tissue Engineering. *Stem Cells Dev,* 26**,** 231-238.

CAMARA-LEMARROY, C. R., GUZMAN-DE LA GARZA, F. J., BARRERA-ORANDAY, E. A., CABELLO-GARCIA, A. J., GARCIA-TAMEZ, A. & FERNANDEZ-GARZA, N. E. 2008. Celecoxib accelerates functional recovery after sciatic nerve crush in the rat. *J Brachial Plex Peripher Nerve Inj,* 3**,** 25.

CANAN, S., AKTAS, A., ULKAY, M. B., COLAKOGLU, S., RAGBETLI, M. C., AYYILDIZ, M., GEUNA, S. & KAPLAN, S. 2008. Prenatal exposure to a non-steroidal anti-inflammatory drug or saline solution impairs sciatic nerve morphology: a stereological and histological study. *Int J Dev Neurosci,* 26**,** 733-8.

CANTON, I., MCKEAN, R., CHARNLEY, M., BLACKWOOD, K. A., FIORICA, C., RYAN, A. J. & MACNEIL, S. 2010. Development of an Ibuprofen-releasing biodegradable PLA/PGA electrospun scaffold for tissue regeneration. *Biotechnol Bioeng,* 105**,** 396-408.

CAO, Y., WANG, Q., ZHOU, Z., WANG, Y., LIU, Y., JI, Y. & LIU, F. 2012. Changes of peroxisome proliferator-activated receptor-gamma on crushed rat sciatic nerves and differentiated primary Schwann cells. *J Mol Neurosci,* 47**,** 380-8.

CARRIEL, V., GARZON, I., ALAMINOS, M. & CORNELISSEN, M. 2014. Histological assessment in peripheral nerve tissue engineering. *Neural Regen Res,* 9**,** 1657-60.

CARTER, M. & SHIEH, J. 2015. *Cell Culture Techniques,* Academic Press, Elsevier.

CATTIN, A. L., BURDEN, J. J., VAN EMMENIS, L., MACKENZIE, F. E., HOVING, J. J., GARCIA CALAVIA, N., GUO, Y., MCLAUGHLIN, M., ROSENBERG, L. H., QUEREDA, V., JAMECNA, D., NAPOLI, I., PARRINELLO, S., ENVER, T., RUHRBERG, C. & LLOYD, A. C. 2015. Macrophage-Induced Blood Vessels Guide Schwann Cell-Mediated Regeneration of Peripheral Nerves. *Cell,* 162**,** 1127-39.

CHAMBERS, S. M., QI, Y., MICA, Y., LEE, G., ZHANG, X. J., NIU, L., BILSLAND, J., CAO, L., STEVENS, E., WHITING, P., SHI, S. H. & STUDER, L. 2012. Combined small-molecule inhibition accelerates developmental timing and converts human pluripotent stem cells into nociceptors. *Nat Biotechnol,* 30**,** 715-20.

CHAN, C. C., KHODARAHMI, K., LIU, J., SUTHERLAND, D., OSCHIPOK, L. W., STEEVES, J. D. & TETZLAFF, W. 2005. Dose-dependent beneficial and detrimental effects of ROCK inhibitor Y27632 on axonal sprouting and functional recovery after rat spinal cord injury. *Exp Neurol,* 196**,** 352-64.

CHAN, K. M., GORDON, T., ZOCHODNE, D. W. & POWER, H. A. 2014. Improving peripheral nerve regeneration: from molecular mechanisms to potential therapeutic targets. *Exp Neurol,* 261**,** 826-35.

CHANDY, T. & RAO, G. 2002. Preparation of surface-engineered elastin/lamin nerve guide tubes of poly (lactic acid)/ poly (ethylene vinyl acetate). *Journal of bioactive and compatible polymers,* 17**,** 183-194.

CHANG, J., XIE, M., SHAH, V. R., SCHNEIDER, M. D., ENTMAN, M. L., WEI, L. & SCHWARTZ, R. J. 2006. Activation of Rho-associated coiled-coil protein kinase 1 (ROCK-1) by caspase-3 cleavage plays an essential role in cardiac myocyte apoptosis. *Proc Natl Acad Sci U S A,* 103**,** 14495-500.

CHANG, S. H., LEE, H. J., PARK, S., KIM, Y. & JEONG, B. 2018. Fast Degradable Polycaprolactone for Drug Delivery. *Biomacromolecules,* 19**,** 2302-2307.

CHAUHAN, B. C., LEVATTE, T. L., GARNIER, K. L., TREMBLAY, F., PANG, I. H., CLARK, A. F. & ARCHIBALD, M. L. 2006. Semiquantitative optic nerve grading scheme for determining axonal loss in experimental optic neuropathy. *Invest Ophthalmol Vis Sci,* 47**,** 634-40.

CHEN, P., PIAO, X. & BONALDO, P. 2015. Role of macrophages in Wallerian degeneration and axonal regeneration after peripheral nerve injury. *Acta Neuropathol,* 130**,** 605-18.

CHEN, Z. L., YU, W. M. & STRICKLAND, S. 2007. Peripheral regeneration. *Annu Rev Neurosci,* 30**,** 209-33.

CHENG, C., WEBBER, C. A., WANG, J., XU, Y., MARTINEZ, J. A., LIU, W. Q., MCDONALD, D., GUO, G. F., NGUYEN, M. D. & ZOCHODNE, D. W. 2008. Activated RHOA and peripheral axon regeneration. *Exp Neurol,* 212**,** 358-69.

CHIANG, M. C., CHENG, Y. C., CHEN, H. M., LIANG, Y. J. & YEN, C. H. 2014. Rosiglitazone promotes neurite outgrowth and mitochondrial function in N2A cells via PPARgamma pathway. *Mitochondrion,* 14**,** 7-17.

CHUANG-STEIN, C., SANDERS, C. & SNAPINN, S. 2004. An industry survey on current practices in the design and analysis of active control studies. *J Biopharm Stat,* 14**,** 349-58.

CLARKE, J. C., TUFT, B. W., CLINGER, J. D., LEVINE, R., FIGUEROA, L. S., GUYMON, C. A. & HANSEN, M. R. 2011. Micropatterned methacrylate polymers direct spiral ganglion neurite and Schwann cell growth. *Hear Res,* 278**,** 96-105.

CLINICALTRIALS.GOV. 2016. *A Phase I Trial of a Novel Synthetic Polymer Nerve Conduit 'Polynerve' in Participants With Sensory Digital Nerve Injury (UMANC)* [Online]. U.S. National Library of Medicine. Available: https://clinicaltrials.gov/ct2/show/NCT02970864.

COLAK, A., ANTAR, V., KARAOGLAN, A., AKDEMIR, O., SAHAN, E., CELIK, O. & SAGMANLIGIL, A. 2009. Q-VD-OPh, a pancaspase inhibitor, reduces trauma-induced apoptosis and improves the recovery of hind-limb function in rats after spinal cord injury. *Neurocirugia (Astur),* 20**,** 533-40; discussion 540.

COLAKOGLU, S., AKTAS, A., RAIMONDO, S., TURKMEN, A. P., ALTUNKAYNAK, B. Z., ODACI, E., GEUNA, S. & KAPLAN, S. 2014. Effects of prenatal exposure to diclofenac sodium and saline on the optic nerve of 4- and 20-week-old male rats: a stereological and histological study. *Biotech Histochem,* 89**,** 136-44.

DALY, W., YAO, L., ZEUGOLIS, D., WINDEBANK, A. & PANDIT, A. 2012. A biomaterials approach to peripheral nerve regeneration: bridging the peripheral nerve gap and enhancing functional recovery. *J R Soc Interface,* 9**,** 202-21.

DAY, R. M., BOCCACCINI, A. R., MAQUET, V., SHUREY, S., FORBES, A., GABE, S. M. & JEROME, R. 2004. In vivo characterisation of a novel bioresorbable poly(lactide-co-glycolide) tubular foam scaffold for tissue engineering applications. *J Mater Sci Mater Med,* 15**,** 729-34.

DE KONING, P., BRAKKEE, J. H. & GISPEN, W. H. 1986. Methods for producing a reproducible crush in the sciatic and tibial nerve of the rat and rapid and precise testing of return of sensory function. Beneficial effects of melanocortins. *J Neurol Sci,* 74**,** 237-46.

DE LUCA, A. C., FARONI, A. & REID, A. J. 2015. Dorsal root ganglia neurons and differentiated adipose-derived stem cells: an in vitro co-culture model to study peripheral nerve regeneration. *J Vis Exp*.

DEGEER, J. & LAMARCHE-VANE, N. 2013. Rho GTPases in neurodegeneration diseases. *Exp Cell Res,* 319**,** 2384-94.
DENAYER, T., STOHR, T. & ROY, M. V. 2014. Animal models in translational medicine: Validation and prediction. *New Horizons in Translational Medicine,* 2**,** 5-11.
DERGHAM, P., ELLEZAM, B., ESSAGIAN, C., AVEDISSIAN, H., LUBELL, W. D. & MCKERRACHER, L. 2002. Rho signaling pathway targeted to promote spinal cord repair. *J Neurosci,* 22**,** 6570-7.
DERMARDIROSSIAN, C. & BOKOCH, G. M. 2005. GDIs: central regulatory molecules in Rho GTPase activation. *Trends Cell Biol,* 15**,** 356-63.
DEUMENS, R., BOZKURT, A., MEEK, M. F., MARCUS, M. A., JOOSTEN, E. A., WEIS, J. & BROOK, G. A. 2010. Repairing injured peripheral nerves: Bridging the gap. *Prog Neurobiol,* 92**,** 245-76.
DIAO, E., ANDRWWS, A. & DIAO, J. 2004. Animals models pf peripheral nerve injury. *Operative Techniques in Orthopaedics,* 14**,** 153-162.
DILL, J., PATEL, A. R., YANG, X. L., BACHOO, R., POWELL, C. M. & LI, S. 2010. A molecular mechanism for ibuprofen-mediated RhoA inhibition in neurons. *J Neurosci,* 30**,** 963-72.
DING, J., LI, Q. Y., YU, J. Z., WANG, X., SUN, C. H., LU, C. Z. & XIAO, B. G. 2010. Fasudil, a Rho kinase inhibitor, drives mobilization of adult neural stem cells after hypoxia/reoxygenation injury in mice. *Mol Cell Neurosci,* 43**,** 201-8.
DING, T., ZHU, C., YIN, J. B., ZHANG, T., LU, Y. C., REN, J. & LI, Y. Q. 2015. Slow-releasing rapamycin-coated bionic peripheral nerve scaffold promotes the regeneration of rat sciatic nerve after injury. *Life Sci,* 122**,** 92-9.
DONALDSON, K. & HOKE, A. 2014. Studying axonal degeneration and regeneration using in vitro and in vivo model: the translational potential. *Future Neurology,* 9**,** 461-473.
DUAN, W., QUE, L., LV, X., LI, Q., YIN, H. & ZHANG, L. 2012. Tolerance of neurite outgrowth to Rho kinase inhibitors decreased by cyclooxygenase-2 inhibitor. *Neural Regen Res,* 7**,** 2705-12.
DUBEY, N., LETOURNEAU, P. C. & TRANQUILLO, R. T. 1999. Guided neurite elongation and schwann cell invasion into magnetically aligned collagen in simulated peripheral nerve regeneration. *Exp Neurol,* 158**,** 338-50.
DUBREUIL, C. I., WINTON, M. J. & MCKERRACHER, L. 2003. Rho activation patterns after spinal cord injury and the role of activated Rho in apoptosis in the central nervous system. *J Cell Biol,* 162**,** 233-43.
DURRENBERGER, P. F., FACER, P., GRAY, R. A., CHESSELL, I. P., NAYLOR, A., BOUNTRA, C., BANATI, R. B., BIRCH, R. & ANAND, P. 2004. Cyclooxygenase-2 (Cox-2) in injured human nerve and a rat model of nerve injury. *J Peripher Nerv Syst,* 9**,** 15-25.
EAST, E., DE OLIVEIRA, D. B., GOLDING, J. P. & PHILLIPS, J. B. 2010. Alignment of astrocytes increases neuronal growth in three-dimensional collagen gels and is maintained following plastic compression to form a spinal cord repair conduit. *Tissue Eng Part A,* 16**,** 3173-84.
EDOFF, K. & JERREGARD, H. 2002. Effects of IL-1beta, IL-6 or LIF on rat sensory neurons co-cultured with fibroblast-like cells. *J Neurosci Res,* 67**,** 255-63.
ETO, M., SUMI, H., FUJIMURA, H., YOSHIKAWA, H. & SAKODA, S. 2008. Pioglitazone promotes peripheral nerve remyelination after crush injury through CD36 upregulation. *J Peripher Nerv Syst,* 13**,** 242-8.
EVANS, P. J., MACKINNON, S. E., BEST, T. J., WADE, J. A., AWERBUCK, D. C., MAKINO, A. P., HUNTER, D. A. & MIDHA, R. 1995. Regeneration across preserved peripheral nerve grafts. *Muscle Nerve,* 18**,** 1128-38.
FARONI, A., MOBASSERI, S. A., KINGHAM, P. J. & REID, A. J. 2015. Peripheral nerve regeneration: experimental strategies and future perspectives. *Adv Drug Deliv Rev,* 82-83**,** 160-7.
FDA. 2015. *The Drug Development Process* [Online]. FDA U.S. Food and Drug Administration. Available: https://www.fda.gov/forpatients/approvals/drugs/default.htm [Accessed 26/09/2017 2017].
FEDERICI, T., LIU, J. K., TENG, Q., YANG, J. & BOULIS, N. M. 2007. A means for targeting therapeutics to peripheral nervous system neurons with axonal damage. *Neurosurgery,* 60**,** 911-8; discussion 911-8.
FEHLINGS, M. G., KIM, K. D., AARABI, B., RIZZO, M., BOND, L. M., MCKERRACHER, L., VACCARO, A. & OKONKWO, D. O. 2018. Rho Inhibitor VX-210 in Acute Traumatic Subaxial Cervical Spinal Cord Injury: Design of the SPinal Cord Injury Rho INhibition InvestiGation (SPRING) Clinical Trial. *J Neurotrauma*.

FEHLINGS, M. G., THEODORE, N., HARROP, J., MAURAIS, G., KUNTZ, C., SHAFFREY, C. I., KWON, B. K., CHAPMAN, J., YEE, A., TIGHE, A. & MCKERRACHER, L. 2011. A phase I/IIa clinical trial of a recombinant Rho protein antagonist in acute spinal cord injury. *J Neurotrauma,* 28**,** 787-96.

FELTS, A. S., JI, C., STAFFORD, J. B., CREWS, B. C., KINGSLEY, P. J., ROUZER, C. A., WASHINGTON, M. K., SUBBARAMAIAH, K., SIEGEL, B. S., YOUNG, S. M., DANNENBERG, A. J. & MARNETT, L. J. 2007. Desmethyl derivatives of indomethacin and sulindac as probes for cyclooxygenase-dependent biology. *ACS Chem Biol,* 2**,** 479-83.

FELTS, A. S., SIEGEL, B. S., YOUNG, S. M., MOTH, C. W., LYBRAND, T. P., DANNENBERG, A. J., MARNETT, L. J. & SUBBARAMAIAH, K. 2008. Sulindac derivatives that activate the peroxisome proliferator-activated receptor gamma but lack cyclooxygenase inhibition. *J Med Chem,* 51**,** 4911-9.

FENG, X. & YUAN, W. 2015. Dexamethasone enhanced functional recovery after sciatic nerve crush injury in rats. *Biomed Res Int,* 2015**,** 627923.

FENTON, O. S., OLAFSON, K. N., PILLAI, P. S., MITCHELL, M. J. & LANGER, R. 2018. Advances in Biomaterials for Drug Delivery. *Adv Mater***,** e1705328.

FEX SVENNIGSEN, A. & DAHLIN, L. B. 2013. Repair of the Peripheral Nerve-Remyelination that Works. *Brain Sci,* 3**,** 1182-97.

FOURNIER, A. E., TAKIZAWA, B. T. & STRITTMATTER, S. M. 2003. Rho kinase inhibition enhances axonal regeneration in the injured CNS. *J Neurosci,* 23**,** 1416-23.

FU, Q., HUE, J. & LI, S. 2007. Nonsteroidal anti-inflammatory drugs promote axon regeneration via RhoA inhibition. *J Neurosci,* 27**,** 4154-64.

FU, Y. & KAO, W. J. 2010. Drug release kinetics and transport mechanisms of non-degradable and degradable polymeric delivery systems. *Expert Opin Drug Deliv,* 7**,** 429-44.

FUENTES, E. O., LEEMHUIS, J., STARK, G. B. & LANG, E. M. 2008. Rho kinase inhibitors Y27632 and H1152 augment neurite extension in the presence of cultured Schwann cells. *J Brachial Plex Peripher Nerve Inj,* 3**,** 19.

FUJITA, Y. & YAMASHITA, T. 2014. Axon growth inhibition by RhoA/ROCK in the central nervous system. *Front Neurosci,* 8**,** 338.

GAUDET, A. D., POPOVICH, P. G. & RAMER, M. S. 2011. Wallerian degeneration: gaining perspective on inflammatory events after peripheral nerve injury. *J Neuroinflammation,* 8**,** 110.

GENTILE, P., CHIONO, V., CARMAGNOLA, I. & HATTON, P. V. 2014. An overview of poly(lactic-co-glycolic) acid (PLGA)-based biomaterials for bone tissue engineering. *Int J Mol Sci,* 15**,** 3640-59.

GEORGIOU, M., BUNTING, S. C., DAVIES, H. A., LOUGHLIN, A. J., GOLDING, J. P. & PHILLIPS, J. B. 2013. Engineered neural tissue for peripheral nerve repair. *Biomaterials,* 34**,** 7335-43.

GEORGIOU, M., GOLDING, J. P., LOUGHLIN, A. J., KINGHAM, P. J. & PHILLIPS, J. B. 2015. Engineered neural tissue with aligned, differentiated adipose-derived stem cells promotes peripheral nerve regeneration across a critical sized defect in rat sciatic nerve. *Biomaterials,* 37**,** 242-51.

GEUNA, S., RAIMONDO, S., FREGNAN, F., HAASTERT-TALINI, K. & GROTHE, C. 2016. In vitro models for peripheral nerve regeneration. *Eur J Neurosci,* 43**,** 287-96.

GEUNA, S., RAIMONDO, S., RONCHI, G., DI SCIPIO, F., TOS, P., CZAJA, K. & FORNARO, M. 2009. Chapter 3: Histology of the peripheral nerve and changes occurring during nerve regeneration. *Int Rev Neurobiol,* 87**,** 27-46.

GEUNA, S., TOS, P., BATTISTON, B. & GUGLIELMONE, R. 2000. Verification of the two-dimensional disector, a method for the unbiased estimation of density and number of myelinated nerve fibers in peripheral nerves. *Ann Anat,* 182**,** 23-34.

GHONEMI, M. O., RABAH, A. A., SABER, H. M. & RADWAN, W. 2013. Role of Phosphorylated Neurofilament H as a diagnostic and prognostic marker in traumatic brain injury. *The Egyptian Journal of Critical Care Medicine* 1**,** 139-144.

GINGRAS, M., BERGERON, J., DERY, J., DURHAM, H. D. & BERTHOD, F. 2003. In vitro development of a tissue-engineered model of peripheral nerve regeneration to study neurite growth. *FASEB J,* 17**,** 2124-6.

GIRET, S., WONG CHI MAN, M. & CARCEL, C. 2015. Mesoporous-Silica-Functionalized Nanoparticles for Drug Delivery. *Chemistry,* 21**,** 13850-65.

GOMEZ-SANCHEZ, J. A., CARTY, L., IRUARRIZAGA-LEJARRETA, M., PALOMO-IRIGOYEN, M., VARELA-REY, M., GRIFFITH, M., HANTKE, J., MACIAS-CAMARA, N., AZKARGORTA, M., AURREKOETXEA, I., DE JUAN, V. G., JEFFERIES, H. B.,

ASPICHUETA, P., ELORTZA, F., ARANSAY, A. M., MARTINEZ-CHANTAR, M. L., BAAS, F., MATO, J. M., MIRSKY, R., WOODHOO, A. & JESSEN, K. R. 2015. Schwann cell autophagy, myelinophagy, initiates myelin clearance from injured nerves. *J Cell Biol,* 210**,** 153-68.

GOPALAKRISHNAN, S. M., TEUSCH, N., IMHOF, C., BAKKER, M. H., SCHURDAK, M., BURNS, D. J. & WARRIOR, U. 2008. Role of Rho kinase pathway in chondroitin sulfate proteoglycan-mediated inhibition of neurite outgrowth in PC12 cells. *J Neurosci Res,* 86**,** 2214-26.

GREEK, R. 2012. *Animal Models in Drug Development*, IntechOpen.

GREENE, L. A. & TISCHLER, A. S. 1976. Establishment of a noradrenergic clonal line of rat adrenal pheochromocytoma cells which respond to nerve growth factor. *Proc Natl Acad Sci U S A,* 73**,** 2424-8.

GUNTHER, R., SAAL, K. A., SUHR, M., SCHEER, D., KOCH, J. C., BAHR, M., LINGOR, P. & TONGES, L. 2014. The rho kinase inhibitor Y-27632 improves motor performance in male SOD1(G93A) mice. *Front Neurosci,* 8**,** 304.

GURPINAR, E., GRIZZLE, W. E. & PIAZZA, G. A. 2013. COX-Independent Mechanisms of Cancer Chemoprevention by Anti-Inflammatory Drugs. *Front Oncol,* 3**,** 181.

HAASTERT-TALINI, K. 2012. Culture and proliferation of highly purified adult Schwann cells from rat, dog, and man. *Methods Mol Biol,* 846**,** 189-200.

HADLOCK, T. A., HEATON, J., CHENEY, M. & MACKINNON, S. E. 2005. Functional recovery after facial and sciatic nerve crush injury in the rat. *Arch Facial Plast Surg,* 7**,** 17-20.

HALL, S. 2005. The response to injury in the peripheral nervous system. *J Bone Joint Surg Br,* 87**,** 1309-19.

HALL, S. M. 1986. Regeneration in cellular and acellular autografts in the peripheral nervous system. *Neuropathol Appl Neurobiol,* 12**,** 27-46.

HAN, S. W., GREENE, M. E., PITTS, J., WADA, R. K. & SIDELL, N. 2001. Novel expression and function of peroxisome proliferator-activated receptor gamma (PPARgamma) in human neuroblastoma cells. *Clin Cancer Res,* 7**,** 98-104.

HANCOCK, J. F. & HALL, A. 1993. A novel role for RhoGDI as an inhibitor of GAP proteins. *EMBO J,* 12**,** 1915-21.

HART, A. M., TERENGHI, G. & WIBERG, M. 2008. Neuronal death after peripheral nerve injury and experimental strategies for neuroprotection. *Neurol Res,* 30**,** 999-1011.

HAYNES, L. W., RUSHTON, J. A., PERRINS, M. F., DYER, J. K., JONES, R. & HOWELL, R. 1994. Diploid and hyperdiploid rat Schwann cell strains displaying negative autoregulation of growth in vitro and myelin sheath-formation in vivo. *J Neurosci Methods,* 52**,** 119-27.

HENKE, B. R., BLANCHARD, S. G., BRACKEEN, M. F., BROWN, K. K., COBB, J. E., COLLINS, J. L., HARRINGTON, W. W., JR., HASHIM, M. A., HULL-RYDE, E. A., KALDOR, I., KLIEWER, S. A., LAKE, D. H., LEESNITZER, L. M., LEHMANN, J. M., LENHARD, J. M., ORBAND-MILLER, L. A., MILLER, J. F., MOOK, R. A., JR., NOBLE, S. A., OLIVER, W., JR., PARKS, D. J., PLUNKET, K. D., SZEWCZYK, J. R. & WILLSON, T. M. 1998. N-(2-Benzoylphenyl)-L-tyrosine PPARgamma agonists. 1. Discovery of a novel series of potent antihyperglycemic and antihyperlipidemic agents. *J Med Chem,* 41**,** 5020-36.

HERBERT, C. B., NAGASWAMI, C., BITTNER, G. D., HUBBELL, J. A. & WEISEL, J. W. 1998. Effects of fibrin micromorphology on neurite growth from dorsal root ganglia cultured in three-dimensional fibrin gels. *J Biomed Mater Res,* 40**,** 551-9.

HIHI, A. K., MICHALIK, L. & WAHLI, W. 2002. PPARs: transcriptional effectors of fatty acids and their derivatives. *Cell Mol Life Sci,* 59**,** 790-8.

HIRAGA, A., KUWABARA, S., DOYA, H., KANAI, K., FUJITANI, M., TANIGUCHI, J., ARAI, K., MORI, M., HATTORI, T. & YAMASHITA, T. 2006. Rho-kinase inhibition enhances axonal regeneration after peripheral nerve injury. *J Peripher Nerv Syst,* 11**,** 217-24.

HOCKERTZ, S., SCHETTLER, T. & ROGALLA, K. 1992. Effect of acetylsalicylic acid, ascorbate and ibuprofen on the macrophage system. *Arzneimittelforschung,* 42**,** 1062-8.

HODGE, R. G. & RIDLEY, A. J. 2016. Regulating Rho GTPases and their regulators. *Nat Rev Mol Cell Biol,* 17**,** 496-510.

HOKE, A. & BRUSHART, T. 2010. Introduction to special issue: Challenges and opportunities for regeneration in the peripheral nervous system. *Exp Neurol,* 223**,** 1-4.

HOPKINS, A. M., DESIMONE, E., CHWALEK, K. & KAPLAN, D. L. 2015. 3D in vitro modeling of the central nervous system. *Prog Neurobiol,* 125**,** 1-25.

HOU, X. L., CHEN, Y., YIN, H. & DUAN, W. G. 2015. Combination of fasudil and celecoxib promotes the recovery of injured spinal cord in rats better than celecoxib or fasudil alone. *Neural Regen Res,* 10**,** 1836-40.
HOUCHIN, M. & TOPP, E. 2009. Physical properties of PLGA films during polymer degradation. *Journal of Applied Polymer Science,* 114**,** 2848-2854.
HUANG, L., HE, Z., GUO, L. & WANG, H. 2008. Improvement of cognitive deficit and neuronal damage in rats with chronic cerebral ischemia via relative long-term inhibition of rho-kinase. *Cell Mol Neurobiol,* 28**,** 757-68.
HUANG, S., WISZNIEWSKI, L. & CONSTANT, S. 2011. The Use of In Vitro 3D Cell Models in Drug Development for Respiratory Diseases. *In:* KAPETANOVIĆ, I. (ed.) *Drug Discovery and Development.* IntechOpen.
HUNTER, J. G., VAN DELFT, M. F., RACHUBINSKI, R. A. & CAPONE, J. P. 2001. Peroxisome proliferator-activated receptor gamma ligands differentially modulate muscle cell differentiation and MyoD gene expression via peroxisome proliferator-activated receptor gamma -dependent and -independent pathways. *J Biol Chem,* 276**,** 38297-306.
ICHIKAWA, M., YOSHIDA, J., SAITO, K., SAGAWA, H., TOKITA, Y. & WATANABE, M. 2008. Differential effects of two ROCK inhibitors, Fasudil and Y-27632, on optic nerve regeneration in adult cats. *Brain Res,* 1201**,** 23-33.
IKEDA, M. & OKA, Y. 2012. The relationship between nerve conduction velocity and fiber morphology during peripheral nerve regeneration. *Brain Behav,* 2**,** 382-90.
IMADA, M. & SUEOKA, N. 1978. Clonal sublines of rat neurotumor RT4 and cell differentiation. I. Isolation and characterization of cell lines and cell type conversion. *Dev Biol,* 66**,** 97-108.
INSERRA, M. M., YAO, M., MURRAY, R. & TERRIS, D. J. 2000. Peripheral nerve regeneration in interleukin 6-deficient mice. *Arch Otolaryngol Head Neck Surg,* 126**,** 1112-6.
ISAACS, J. 2013. Major peripheral nerve injuries. *Hand Clin,* 29**,** 371-82.
ISAACS, J., MALLU, S. & BATCHELOR, M. 2014. Modification of commercially available image analysis software for semi-automated qualitative analysis of axon regeneration and myelination in the rat sciatic nerve. *J Neurosci Methods,* 233**,** 45-9.
JERREGARD, H. 2001. Sensory neurons influence the expression of cell adhesion factors by cutaneous cells in vitro and in vivo. *J Neurocytol,* 30**,** 327-36.
JESSEN, K. R. & MIRSKY, R. 2016. The repair Schwann cell and its function in regenerating nerves. *J Physiol,* 594**,** 3521-31.
JESSEN, K. R., MIRSKY, R. & SALZER, J. 2008. Introduction. Schwann cell biology. *Glia,* 56**,** 1479-80.
JOHNS, P. 2014. Clinical Neuroscience. Churchill Livingstone.
JOLIVALT, C. G., VU, Y., MIZISIN, L. M., MIZISIN, A. P. & CALCUTT, N. A. 2008. Impaired prosaposin secretion during nerve regeneration in diabetic rats and protection of nerve regeneration by a prosaposin-derived peptide. *J Neuropathol Exp Neurol,* 67**,** 702-10.
JONES, S., EISENBERG, H. M. & JIA, X. 2016. Advances and Future Applications of Augmented Peripheral Nerve Regeneration. *Int J Mol Sci,* 17.
JOSHI, A. R., BOBYLEV, I., ZHANG, G., SHEIKH, K. A. & LEHMANN, H. C. 2015. Inhibition of Rho-kinase differentially affects axon regeneration of peripheral motor and sensory nerves. *Exp Neurol,* 263**,** 28-38.
JUNG, K. M., PARK, K. S., OH, J. H., JUNG, S. Y., YANG, K. H., SONG, Y. S., SON, D. J., PARK, Y. H., YUN, Y. P., LEE, M. K., OH, K. W. & HONG, J. T. 2003. Activation of p38 mitogen-activated protein kinase and activator protein-1 during the promotion of neurite extension of PC-12 cells by 15-deoxy-delta12,14-prostaglandin J2. *Mol Pharmacol,* 63**,** 607-16.
KANJE, M., LUNDBORG, G. & EDSTROM, A. 1988. A new method for studies of the effects of locally applied drugs on peripheral nerve regeneration in vivo. *Brain Res,* 439**,** 116-21.
KANUNGO, I., FATHIMA, N. N., RAO, J. R. & NAIR, B. U. 2013. Influence of PCL on the material properties of collagen based biocomposites and in vitro evaluation of drug release. *Mater Sci Eng C Mater Biol Appl,* 33**,** 4651-9.
KAPADIA, R., YI, J. H. & VEMUGANTI, R. 2008. Mechanisms of anti-inflammatory and neuroprotective actions of PPAR-gamma agonists. *Front Biosci,* 13**,** 1813-26.
KAPLAN, A. A., YURT, K. K., DENIZ, O. G. & ALTUN, G. 2018. Peripheral nerve and diclofenac sodium: Molecular and clinical approaches. *J Chem Neuroanat,* 87**,** 2-11.
KAUNDAL, R. K. & SHARMA, S. S. 2011. GW1929: a nonthiazolidinedione PPARgamma agonist, ameliorates neurological damage in global cerebral ischemic-reperfusion injury through reduction in inflammation and DNA fragmentation. *Behav Brain Res,* 216**,** 606-12.

KEILHOFF, G., WIEGAND, S. & FANSA, H. 2012. Vav deficiency impedes peripheral nerve regeneration in mice. *Restor Neurol Neurosci,* 30**,** 463-79.
KEMP, S. W., CEDERNA, P. S. & MIDHA, R. 2017. Comparative outcome measures in peripheral regeneration studies. *Exp Neurol,* 287**,** 348-357.
KERSTEN, S., DESVERGNE, B. & WAHLI, W. 2000. Roles of PPARs in health and disease. *Nature,* 405**,** 421-4.
KESKIN, I., KAPLAN, S., KALKAN, S., SUTCU, M., ULKAY, M. B. & ESENER, O. B. 2015. Evaluation of neuroprotection by melatonin against adverse effects of prenatal exposure to a nonsteroidal anti-inflammatory drug during peripheral nerve development. *Int J Dev Neurosci,* 41**,** 1-7.
KIM, J. & SHIN, S. C. 2004. Controlled release of atenolol from the ethylene-vinyl acetate matrix. *Int J Pharm,* 273**,** 23-7.
KIMURA, H., FISCHER, W. H. & SCHUBERT, D. 1990. Structure, expression and function of a schwannoma-derived growth factor. *Nature,* 348**,** 257-60.
KITAOKA, Y., SASE, K., TSUKAHARA, C., KOJIMA, K., SHIONO, A., KOGO, J., TOKUDA, N. & TAKAGI, H. 2017. Axonal Protection by Ripasudil, a Rho Kinase Inhibitor, via Modulating Autophagy in TNF-Induced Optic Nerve Degeneration. *Invest Ophthalmol Vis Sci,* 58**,** 5056-5064.
KLESSE, L. J., MEYERS, K. A., MARSHALL, C. J. & PARADA, L. F. 1999. Nerve growth factor induces survival and differentiation through two distinct signaling cascades in PC12 cells. *Oncogene,* 18**,** 2055-68.
KNOBLACH, S. M., ALROY, D. A., NIKOLAEVA, M., CERNAK, I., STOICA, B. A. & FADEN, A. I. 2004. Caspase inhibitor z-DEVD-fmk attenuates calpain and necrotic cell death in vitro and after traumatic brain injury. *J Cereb Blood Flow Metab,* 24**,** 1119-32.
KNOOPS, B., HUBERT, I., HAUW, J. J. & VAN DEN BOSCH DE AGUILAR, P. 1991. Axonal growth and glial migration from co-cultured hippocampal and septal slices into fibrin-fibronectin-containing matrix of peripheral regeneration chambers: a light and electron microscope study. *Brain Res,* 540**,** 183-94.
KNOTT, E. P., ASSI, M. & PEARSE, D. D. 2014. Cyclic AMP signaling: a molecular determinant of peripheral nerve regeneration. *Biomed Res Int,* 2014**,** 651625.
KO, K. R. & FRAMPTON, J. P. 2016. Developments in 3D neural cell culture models: the future of neurotherapeutics testing? *Expert Rev Neurother,* 16**,** 739-41.
KOFRON, C. M., FONG, V. J. & HOFFMAN-KIM, D. 2009. Neurite outgrowth at the interface of 2D and 3D growth environments. *J Neural Eng,* 6**,** 016002.
KOPP, M. A., LIEBSCHER, T., NIEDEGGEN, A., LAUFER, S., BROMMER, B., JUNGEHULSING, G. J., STRITTMATTER, S. M., DIRNAGL, U. & SCHWAB, J. M. 2012. Small-molecule-induced Rho-inhibition: NSAIDs after spinal cord injury. *Cell Tissue Res,* 349**,** 119-32.
KOVACIC, U., SKETELJ, J. & BAJROVIC, F. F. 2003. Sex-related difference in collateral sprouting of nociceptive axons after peripheral nerve injury in the rat. *Exp Neurol,* 184**,** 479-88.
KOVACIC, U., ZELE, T., OSREDKAR, J., SKETELJ, J. & BAJROVIC, F. F. 2004. Sex-related differences in the regeneration of sensory axons and recovery of nociception after peripheral nerve crush in the rat. *Exp Neurol,* 189**,** 94-104.
KRAUS, D., BOYLE, V., LEIBIG, N., STARK, G. B. & PENNA, V. 2015. The Neuro-spheroid--A novel 3D in vitro model for peripheral nerve regeneration. *J Neurosci Methods,* 246**,** 97-105.
KRUSZYNSKA, Y. T., MUKHERJEE, R., JOW, L., DANA, S., PATERNITI, J. R. & OLEFSKY, J. M. 1998. Skeletal muscle peroxisome proliferator- activated receptor-gamma expression in obesity and non- insulin-dependent diabetes mellitus. *J Clin Invest,* 101**,** 543-8.
KUBO, T., YAMAGUCHI, A., IWATA, N. & YAMASHITA, T. 2008. The therapeutic effects of Rho-ROCK inhibitors on CNS disorders. *Ther Clin Risk Manag,* 4**,** 605-15.
KUBO, T. & YAMASHITA, T. 2007. Rho-ROCK inhibitors for the treatment of CNS injury. *Recent Pat CNS Drug Discov,* 2**,** 173-9.
KUFFLER, D. P. 2014. An assessment of current techniques for inducing axon regeneration and neurological recovery following peripheral nerve trauma. *Prog Neurobiol,* 116**,** 1-12.
LABROO, P., HO, S., SANT, H., SHEA, J., GALE, B. K. & AGARWAL, J. 2016. Controlled Delivery of FK506 to Improve Nerve Regeneration. *Shock,* 46**,** 154-9.
LABROO, P., SHEA, J., SANT, H., GALE, B. & AGARWAL, J. 2017. Effect Of combining FK506 and neurotrophins on neurite branching and elongation. *Muscle Nerve,* 55**,** 570-581.

LANGER, R. 2004. Advances in biomaterials, drug delivery and bionanotechnology. *AlChE Journal,* 49**,** 2990-3006.
LANGLEY, G. R., ADCOCK, I. M., BUSQUET, F., CROFTON, K. M., CSERNOK, E., GIESE, C., HEINONEN, T., HERRMANN, K., HOFMANN-APITIUS, M., LANDESMANN, B., MARSHALL, L. J., MCIVOR, E., MUOTRI, A. R., NOOR, F., SCHUTTE, K., SEIDLE, T., VAN DE STOLPE, A., VAN ESCH, H., WILLETT, C. & WOSZCZEK, G. 2017. Towards a 21st-century roadmap for biomedical research and drug discovery: consensus report and recommendations. *Drug Discov Today,* 22**,** 327-339.
LARSEN, J. O. 1998. Stereology of nerve cross sections. *J Neurosci Methods,* 85**,** 107-18.
LECCA, D., NEVIN, D. K., MULAS, G., CASU, M. A., DIANA, A., ROSSI, D., SACCHETTI, G. & CARTA, A. R. 2015. Neuroprotective and anti-inflammatory properties of a novel non-thiazolidinedione PPARgamma agonist in vitro and in MPTP-treated mice. *Neuroscience,* 302**,** 23-35.
LEE, J. K., PAINE, M. F. & BROUWER, K. L. 2010. Sulindac and its metabolites inhibit multiple transport proteins in rat and human hepatocytes. *J Pharmacol Exp Ther,* 334**,** 410-8.
LEE, J. Y., BASHUR, C. A., GOLDSTEIN, A. S. & SCHMIDT, C. E. 2009. Polypyrrole-coated electrospun PLGA nanofibers for neural tissue applications. *Biomaterials,* 30**,** 4325-35.
LEE, M. & GUYURON, B. 2015. Postoperative Neuromas. *In:* TUNNS, R. S., RIZK, E., SHOJA, M. M., BARBARO, N., LOUKAS, M. & SPINNER, R. (eds.) *Nerves and Nerve Injuries.* Academic Press: Elsevier.
LEE, Y. S., BARATTA, J., YU, J., LIN, V. W. & ROBERTSON, R. T. 2002. AFGF promotes axonal growth in rat spinal cord organotypic slice co-cultures. *J Neurotrauma,* 19**,** 357-67.
LEHMANN, J. M., LENHARD, J. M., OLIVER, B. B., RINGOLD, G. M. & KLIEWER, S. A. 1997. Peroxisome proliferator-activated receptors alpha and gamma are activated by indomethacin and other non-steroidal anti-inflammatory drugs. *J Biol Chem,* 272**,** 3406-10.
LESUISSE, C. & MARTIN, L. J. 2002. Long-term culture of mouse cortical neurons as a model for neuronal development, aging, and death. *J Neurobiol,* 51**,** 9-23.
LEZANA, J. P., DAGAN, S. Y., ROBINSON, A., GOLDSTEIN, R. S., FAINZILBER, M., BRONFMAN, F. C. & BRONFMAN, M. 2016. Axonal PPARgamma promotes neuronal regeneration after injury. *Dev Neurobiol,* 76**,** 688-701.
LI, S., WU, H., HU, X. D., TU, C. Q., PEI, F. X., WANG, G. L., LIN, W. & FAN, H. S. 2012. Preparation of electrospun PLGA-silk fibroin nanofibers-based nerve conduits and evaluation in vivo. *Artif Cells Blood Substit Immobil Biotechnol,* 40**,** 171-8.
LI, X. G., LIN, X. J., DU, J. H., XU, S. Z., LOU, X. F. & CHEN, Z. 2016. Combination of methylprednisolone and rosiglitazone promotes recovery of neurological function after spinal cord injury. *Neural Regen Res,* 11**,** 1678-1684.
LIE, M., GROVER, M. & WHITLON, D. S. 2010. Accelerated neurite growth from spiral ganglion neurons exposed to the Rho kinase inhibitor H-1152. *Neuroscience,* 169**,** 855-62.
LILLESAAR, C., ERIKSSON, C. & FRIED, K. 2001. Rat tooth pulp cells elicit neurite growth from trigeminal neurones and express mRNAs for neurotrophic factors in vitro. *Neurosci Lett,* 308**,** 161-4.
LIM, G. P., YANG, F., CHU, T., CHEN, P., BEECH, W., TETER, B., TRAN, T., UBEDA, O., ASHE, K. H., FRAUTSCHY, S. A. & COLE, G. M. 2000. Ibuprofen suppresses plaque pathology and inflammation in a mouse model for Alzheimer's disease. *J Neurosci,* 20**,** 5709-14.
LINGOR, P., TEUSCH, N., SCHWARZ, K., MUELLER, R., MACK, H., BAHR, M. & MUELLER, B. K. 2007. Inhibition of Rho kinase (ROCK) increases neurite outgrowth on chondroitin sulphate proteoglycan in vitro and axonal regeneration in the adult optic nerve in vivo. *J Neurochem,* 103**,** 181-9.
LIU, J. J., WANG, C. Y., WANG, J. G., RUAN, H. J. & FAN, C. Y. 2011. Peripheral nerve regeneration using composite poly(lactic acid-caprolactone)/nerve growth factor conduits prepared by coaxial electrospinning. *J Biomed Mater Res A,* 96**,** 13-20.
LIU, Q., SWISTOWSKI, A. & ZENG, X. 2014. Human neural crest stem cells derived from human pluripotent stem cells. *Methods Mol Biol,* 1210**,** 79-90.
LU, Q., LONGO, F. M., ZHOU, H., MASSA, S. M. & CHEN, Y. H. 2009. Signaling through Rho GTPase pathway as viable drug target. *Curr Med Chem,* 16**,** 1355-65.
LUIS, A. L., RODRIGUES, J. M., GEUNA, S., AMADO, S., SIMOES, M. J., FREGNAN, F., FERREIRA, A. J., VELOSO, A. P., ARMADA-DA-SILVA, P. A., VAREJAO, A. S. & MAURICIO, A. C. 2008. Neural cell transplantation effects on sciatic nerve regeneration after a standardized crush injury in the rat. *Microsurgery,* 28**,** 458-70.

LUNDBORG, G. 2003. Richard P. Bunge memorial lecture. Nerve injury and repair--a challenge to the plastic brain. *J Peripher Nerv Syst,* 8**,** 209-26.
MA, T. C. & WILLIS, D. E. 2015. What makes a RAG regeneration associated? *Front Mol Neurosci,* 8**,** 43.
MADDURI, S., FELDMAN, K., TERVOORT, T., PAPALOIZOS, M. & GANDER, B. 2010. Collagen nerve conduits releasing the neurotrophic factors GDNF and NGF. *J Control Release,* 143**,** 168-74.
MADISON, R. D., ARCHIBALD, S. J. & BRUSHART, T. M. 1996. Reinnervation accuracy of the rat femoral nerve by motor and sensory neurons. *J Neurosci,* 16**,** 5698-703.
MADURA, T., KUBO, T., TANAG, M., MATSUDA, K., TOMITA, K., YANO, K. & HOSOKAWA, K. 2007. The Rho-associated kinase inhibitor fasudil hydrochloride enhances neural regeneration after axotomy in the peripheral nervous system. *Plast Reconstr Surg,* 119**,** 526-35.
MADURA, T., TOMITA, K. & TERENGHI, G. 2011. Ibuprofen improves functional outcome after axotomy and immediate repair in the peripheral nervous system. *J Plast Reconstr Aesthet Surg,* 64**,** 1641-6.
MADURA, T., YAMASHITA, T., KUBO, T., FUJITANI, M., HOSOKAWA, K. & TOHYAMA, M. 2004. Activation of Rho in the injured axons following spinal cord injury. *EMBO Rep,* 5**,** 412-7.
MAKADIA, H. K. & SIEGEL, S. J. 2011. Poly Lactic-co-Glycolic Acid (PLGA) as Biodegradable Controlled Drug Delivery Carrier. *Polymers (Basel),* 3**,** 1377-1397.
MARINA, N., BULL, N. D. & MARTIN, K. R. 2010. A semiautomated targeted sampling method to assess optic nerve axonal loss in a rat model of glaucoma. *Nat Protoc,* 5**,** 1642-51.
MARTENS, W., SANEN, K., GEORGIOU, M., STRUYS, T., BRONCKAERS, A., AMELOOT, M., PHILLIPS, J. & LAMBRICHTS, I. 2014. Human dental pulp stem cells can differentiate into Schwann cells and promote and guide neurite outgrowth in an aligned tissue-engineered collagen construct in vitro. *FASEB J,* 28**,** 1634-43.
MARTINEZ DE ALBORNOZ, P., DELGADO, P. J., FORRIOL, F. & MAFFULLI, N. 2011. Non-surgical therapies for peripheral nerve injury. *Br Med Bull,* 100**,** 73-100.
MARTINEZ, F. O. & GORDON, S. 2014. The M1 and M2 paradigm of macrophage activation: time for reassessment. *F1000Prime Rep,* 6**,** 13.
MARTINS, R. S., SIQUEIRA, M. G., SILVA, C. F. D. & PLESE, J. P. P. 2006. Correlation between parameters of electrophysiological, histomorphometric and sciatic functional index evaluations after rat sciatic nerve repair. *Arq. Neuro-Psiquiatr.,* 64.
MAZZER, P. Y., BARBIERI, C. H., MAZZER, N. & FAZAN, V. P. 2008. Morphologic and morphometric evaluation of experimental acute crush injuries of the sciatic nerve of rats. *J Neurosci Methods,* 173**,** 249-58.
MCGRATH, A. M., NOVIKOVA, L. N., NOVIKOV, L. N. & WIBERG, M. 2010. BD PuraMatrix peptide hydrogel seeded with Schwann cells for peripheral nerve regeneration. *Brain Res Bull,* 83**,** 207-13.
MCKERRACHER, L. & ANDERSON, K. D. 2013. Analysis of recruitment and outcomes in the phase I/IIa Cethrin clinical trial for acute spinal cord injury. *J Neurotrauma,* 30**,** 1795-804.
MCKERRACHER, L. & WINTON, M. J. 2002. Nogo on the go. *Neuron,* 36**,** 345-8.
MENG, Z. X., XU, X. X., ZHENG, W., ZHOU, H. M., LI, L., ZHENG, Y. F. & LOU, X. 2011. Preparation and characterization of electrospun PLGA/gelatin nanofibers as a potential drug delivery system. *Colloids Surf B Biointerfaces,* 84**,** 97-102.
MEZIN, P., TENAUD, C., BOSSON, J. L. & STOEBNER, P. 1994. Morphometric analysis of the peripheral nerve: advantages of the semi-automated interactive method. *J Neurosci Methods,* 51**,** 163-9.
MICHAEL-TITUS, A., REVEST, P. & SHORTLAND, P. 2007. *The Nervous System,* London, Churchill Livingstone.
MILLER, C., JEFTINIJA, S. & MALLAPRAGADA, S. 2001. Micropatterned Schwann cell-seeded biodegradable polymer substrates significantly enhance neurite alignment and outgrowth. *Tissue Eng,* 7**,** 705-15.
MINASE, T., ISHIMA, T., ITOH, K. & HASHIMOTO, K. 2010. Potentiation of nerve growth factor-induced neurite outgrowth by the ROCK inhibitor Y-27632: a possible role of IP(3) receptors. *Eur J Pharmacol,* 648**,** 67-73.
MOHAMMADI, R., AZAD-TIRGAN, M. & AMINI, K. 2013a. Dexamethasone topically accelerates peripheral nerve repair and target organ reinnervation: a transected sciatic nerve model in rat. *Injury,* 44**,** 565-9.

MOHAMMADI, R., HIRSAEE, M. A. & AMINI, K. 2013b. Improvement of functional recovery of transected peripheral nerve by means of artery grafts filled with diclofenac. *Int J Surg,* 11**,** 259-64.
MOHAMMADI, R., MEHRTASH, M., NIKONAM, N., MEHRTASH, M. & AMINI, K. 2014. Ketoprofen combined with artery graft entubulization improves functional recovery of transected peripheral nerves. *J Craniomaxillofac Surg,* 42**,** 2076-81.
MOKARRAM, N., MERCHANT, A., MUKHATYAR, V., PATEL, G. & BELLAMKONDA, R. V. 2012. Effect of modulating macrophage phenotype on peripheral nerve repair. *Biomaterials,* 33**,** 8793-801.
MOLNAR, G., DAGHER, M. C., GEISZT, M., SETTLEMAN, J. & LIGETI, E. 2001. Role of prenylation in the interaction of Rho-family small GTPases with GTPase activating proteins. *Biochemistry,* 40**,** 10542-9.
MORANO, M., WROBEL, S., FREGNAN, F., ZIV-POLAT, O., SHAHAR, A., RATZKA, A., GROTHE, C., GEUNA, S. & HAASTERT-TALINI, K. 2014. Nanotechnology versus stem cell engineering: in vitro comparison of neurite inductive potentials. *Int J Nanomedicine,* 9**,** 5289-306.
MUELLER, B. K., MACK, H. & TEUSCH, N. 2005. Rho kinase, a promising drug target for neurological disorders. *Nat Rev Drug Discov,* 4**,** 387-98.
MUNRO, C. A., SZALAI, J. P., MACKINNON, S. E. & MIDHA, R. 1998. Lack of association between outcome measures of nerve regeneration. *Muscle Nerve,* 21**,** 1095-7.
NAVARRO, X. 2016. Functional evaluation of peripheral nerve regeneration and target reinnervation in animal models: a critical overview. *Eur J Neurosci,* 43**,** 271-86.
NEAL, R. A., THOLPADY, S. S., FOLEY, P. L., SWAMI, N., OGLE, R. C. & BOTCHWEY, E. A. 2012. Alignment and composition of laminin-polycaprolactone nanofiber blends enhance peripheral nerve regeneration. *J Biomed Mater Res A,* 100**,** 406-23.
NICHOLS, C. M., MYCKATYN, T. M., RICKMAN, S. R., FOX, I. K., HADLOCK, T. & MACKINNON, S. E. 2005. Choosing the correct functional assay: a comprehensive assessment of functional tests in the rat. *Behav Brain Res,* 163**,** 143-58.
NISHIJIMA, C., KIMOTO, K. & ARAKAWA, Y. 2001. Survival activity of troglitazone in rat motoneurones. *J Neurochem,* 76**,** 383-90.
NISHIO, Y., KODA, M., KITAJO, K., SETO, M., HATA, K., TANIGUCHI, J., MORIYA, H., FUJITANI, M., KUBO, T. & YAMASHITA, T. 2006. Delayed treatment with Rho-kinase inhibitor does not enhance axonal regeneration or functional recovery after spinal cord injury in rats. *Exp Neurol,* 200**,** 392-7.
NOLTE, R. T., WISELY, G. B., WESTIN, S., COBB, J. E., LAMBERT, M. H., KUROKAWA, R., ROSENFELD, M. G., WILLSON, T. M., GLASS, C. K. & MILBURN, M. V. 1998. Ligand binding and co-activator assembly of the peroxisome proliferator-activated receptor-gamma. *Nature,* 395**,** 137-43.
NUNE, M., SUBRAMANIAN, A., KRISHNAN, U. M., KAIMAL, S. S. & SETHURAMAN, S. 2017. Self-assembling peptide nanostructures on aligned poly(lactide-co-glycolide) nanofibers for the functional regeneration of sciatic nerve. *Nanomedicine (Lond),* 12**,** 219-235.
NUNEZ, G. & DEL PESO, L. 1998. Linking extracellular survival signals and the apoptotic machinery. *Curr Opin Neurobiol,* 8**,** 613-8.
O'ROURKE, C., LEE-REEVES, C., DRAKE, R. A., CAMERON, G. W., LOUGHLIN, A. J. & PHILLIPS, J. B. 2017. Adapting tissue-engineered in vitro CNS models for high-throughput study of neurodegeneration. *J Tissue Eng,* 8**,** 2041731417697920.
OLSON, M. F. 2008. Applications for ROCK kinase inhibition. *Curr Opin Cell Biol,* 20**,** 242-8.
PADHY, B. M. & GUPTA, Y. K. 2011. Drug repositioning: re-investigating existing drugs for new therapeutic indications. *J Postgrad Med,* 57**,** 153-60.
PANAGOPOULOS, G. N., MEGALOIKONOMOS, P. D. & MAVROGENIS, A. F. 2017. The Present and Future for Peripheral Nerve Regeneration. *Orthopedics,* 40**,** e141-e156.
PANSERI, S., CUNHA, C., LOWERY, J., DEL CARRO, U., TARABALLI, F., AMADIO, S., VESCOVI, A. & GELAIN, F. 2008. Electrospun micro- and nanofiber tubes for functional nervous regeneration in sciatic nerve transections. *BMC Biotechnol,* 8**,** 39.
PARK, K. S., LEE, R. D., KANG, S. K., HAN, S. Y., PARK, K. L., YANG, K. H., SONG, Y. S., PARK, H. J., LEE, Y. M., YUN, Y. P., OH, K. W., KIM, D. J., YUN, Y. W., HWANG, S. J., LEE, S. E. & HONG, J. T. 2004. Neuronal differentiation of embryonic midbrain cells by upregulation of peroxisome proliferator-activated receptor-gamma via the JNK-dependent pathway. *Exp Cell Res,* 297**,** 424-33.
PARK, S. W., YI, J. H., MIRANPURI, G., SATRIOTOMO, I., BOWEN, K., RESNICK, D. K. & VEMUGANTI, R. 2007. Thiazolidinedione class of peroxisome proliferator-activated receptor gamma agonists prevents neuronal damage, motor dysfunction, myelin loss,

neuropathic pain, and inflammation after spinal cord injury in adult rats. *J Pharmacol Exp Ther,* 320**,** 1002-12.
PAVIC, R., PAVIC, M. L., TVRDEIC, A., TOT, O. K. & HEFFER, M. 2011. Rat sciatic nerve crush injury and recovery tracked by plantar test and immunohistochemistry analysis. *Coll Antropol,* 35 Suppl 1**,** 93-100.
PFISTER, L. A., ALTHER, E., PAPALOIZOS, M., MERKLE, H. P. & GANDER, B. 2008. Controlled nerve growth factor release from multi-ply alginate/chitosan-based nerve conduits. *Eur J Pharm Biopharm,* 69**,** 563-72.
PHILLIPS, J. B. 2008. Trauma, Repair and Recovery. *In:* PHILLIPS, J. B. (ed.). Oxford: Oxford University Press.
PHILLIPS, J. B. 2014. Monitoring neuron and astrocyte interactions with a 3D cell culture system. *Methods Mol Biol,* 1162**,** 113-24.
PHILLIPS, J. B. & BROWN, R. 2011. Micro-structured materials and mechanical cues in 3D collagen gels. *Methods Mol Biol,* 695**,** 183-96.
PITTIER, R., SAUTHIER, F., HUBBELL, J. A. & HALL, H. 2005. Neurite extension and in vitro myelination within three-dimensional modified fibrin matrices. *J Neurobiol,* 63**,** 1-14.
PRABU, P., DHARMARAJ, N., ARYAL, S., LEE, B. M., RAMESH, V. & KIM, H. Y. 2006. Preparation and drug release activity of scaffolds containing collagen and poly(caprolactone). *J Biomed Mater Res A,* 79**,** 153-8.
PUHL, A. C., MILTON, F. A., CVORO, A., SIEGLAFF, D. H., CAMPOS, J. C., BERNARDES, A., FILGUEIRA, C. S., LINDEMANN, J. L., DENG, T., NEVES, F. A., POLIKARPOV, I. & WEBB, P. 2015. Mechanisms of peroxisome proliferator activated receptor gamma regulation by non-steroidal anti-inflammatory drugs. *Nucl Recept Signal,* 13**,** e004.
QUICK, T. J., SINGH, A. K., FOX, M., SINISI, M. & MACQUILLAN, A. 2016. A quantitative assessment of the functional recovery of flexion of the elbow after nerve transfer in patients with a brachial plexus injury. *Bone Joint J,* 98-B**,** 1517-1520.
QUINTANILLA, R. A., GODOY, J. A., ALFARO, I., CABEZAS, D., VON BERNHARDI, R., BRONFMAN, M. & INESTROSA, N. C. 2013. Thiazolidinediones promote axonal growth through the activation of the JNK pathway. *PLoS One,* 8**,** e65140.
QUINTANILLA, R. A., UTRERAS, E. & CABEZAS-OPAZO, F. A. 2014. Role of PPAR gamma in the Differentiation and Function of Neurons. *PPAR Res,* 2014**,** 768594.
RAFF, M. C., HORNBY-SMITH, A. & BROCKES, J. P. 1978. Cyclic AMP as a mitogenic signal for cultured rat Schwann cells. *Nature,* 273**,** 672-3.
RAIMONDO, S., FORNARO, M., DI SCIPIO, F., RONCHI, G., GIACOBINI-ROBECCHI, M. G. & GEUNA, S. 2009. Chapter 5: Methods and protocols in peripheral nerve regeneration experimental research: part II-morphological techniques. *Int Rev Neurobiol,* 87**,** 81-103.
RAMLI, D., AZIZ, I., MOHAMAD, M., ABDULAHI, D. & SANUSI, J. 2017. The Changes in Rats with Sciatic Nerve Crush Injury Supplemented with Evening Primrose Oil: Behavioural, Morphologic, and Morphometric Analysis. *Evid Based Complement Alternat Med,* 2017**,** 3476407.
RAYNER, M., LARANJEIRA, S., EVANS, R., SHIPLEY, R., HEALY, J. & PHILLIPS, J. 2018. Developing an *in vitro* model to screen drugs for nerve regeneration. *Anatomical Record,* In Press.
REYNAUD, J., CULL, G., WANG, L., FORTUNE, B., GARDINER, S., BURGOYNE, C. F. & CIOFFI, G. A. 2012. Automated quantification of optic nerve axons in primate glaucomatous and normal eyes--method and comparison to semi-automated manual quantification. *Invest Ophthalmol Vis Sci,* 53**,** 2951-9.
RICHARDSON, P. M. 1997. Recovery of biceps function after delayed repair for brachial plexus injury. *J Trauma,* 42**,** 791-2.
RIDLEY, A. J., PATERSON, H. F., NOBLE, M. & LAND, H. 1988. Ras-mediated cell cycle arrest is altered by nuclear oncogenes to induce Schwann cell transformation. *EMBO J,* 7**,** 1635-45.
ROCKWELL, W. B. & EHRLICH, H. P. 1990. Ibuprofen in acute-care therapy. *Ann Surg,* 211**,** 78-83.
ROGLIO, I., BIANCHI, R., GOTTI, S., SCURATI, S., GIATTI, S., PESARESI, M., CARUSO, D., PANZICA, G. C. & MELCANGI, R. C. 2008. Neuroprotective effects of dihydroprogesterone and progesterone in an experimental model of nerve crush injury. *Neuroscience,* 155**,** 673-85.
ROLOFF, F., SCHEIBLICH, H., DEWITZ, C., DEMPEWOLF, S., STERN, M. & BICKER, G. 2015. Enhanced neurite outgrowth of human model (NT2) neurons by small-molecule inhibitors of Rho/ROCK signaling. *PLoS One,* 10**,** e0118536.

ROMERO, E., CUISENAIRE, O., DENEF, J. F., DELBEKE, J., MACQ, B. & VERAART, C. 2000. Automatic morphometry of nerve histological sections. *J Neurosci Methods,* 97**,** 111-22.

RONCHI, G., NICOLINO, S., RAIMONDO, S., TOS, P., BATTISTON, B., PAPALIA, I., VAREJAO, A. S., GIACOBINI-ROBECCHI, M. G., PERROTEAU, I. & GEUNA, S. 2009. Functional and morphological assessment of a standardized crush injury of the rat median nerve. *J Neurosci Methods,* 179**,** 51-7.

RUSCHEWEYH, R. & SANDKUHLER, J. 2001. Bidirectional actions of nociceptin/orphanin FQ on A delta-fibre-evoked responses in rat superficial spinal dorsal horn in vitro. *Neuroscience,* 107**,** 275-81.

RUSSEL, W. M. S. & BURCH, R. L. 1959. *The principles of humane experimental technique,* London, Methuen.

SAGAWA, H., TERASAKI, H., NAKAMURA, M., ICHIKAWA, M., YATA, T., TOKITA, Y. & WATANABE, M. 2007. A novel ROCK inhibitor, Y-39983, promotes regeneration of crushed axons of retinal ganglion cells into the optic nerve of adult cats. *Exp Neurol,* 205**,** 230-40.

SALMORIA, G. V., PAGGI, P. A., CASTRO, F., ROESLER, C. R. M., MOTERLE, D. & KANIS, L. A. 2016. Development of PCL/Ibuprofen tube for pripheral nerve regeneration. *The Second CIRP Conference on Biomanufacturing.*

SANEN, K., MARTENS, W., GEORGIOU, M., AMELOOT, M., LAMBRICHTS, I. & PHILLIPS, J. 2017. Engineered neural tissue with Schwann cell differentiated human dental pulp stem cells: potential for peripheral nerve repair? *J Tissue Eng Regen Med*.

SANTOS, D., GIUDETTI, G., MICERA, S., NAVARRO, X. & DEL VALLE, J. 2016. Focal release of neurotrophic factors by biodegradable microspheres enhance motor and sensory axonal regeneration in vitro and in vivo. *Brain Res,* 1636**,** 93-106.

SAVY, C., MARGULES, S., SOLARI, A., SAINT-JEAN, P. & FARKAS-BARGETON, E. 1988. An image analysis morphometric method for the study of myelinated nerve fibers from mouse trigeminal root. *Anal Quant Cytol Histol,* 10**,** 307-16.

SCHAFERS, M., MARZINIAK, M., SORKIN, L. S., YAKSH, T. L. & SOMMER, C. 2004. Cyclooxygenase inhibition in nerve-injury- and TNF-induced hyperalgesia in the rat. *Exp Neurol,* 185**,** 160-8.

SCHEIB, J. & HOKE, A. 2013. Advances in peripheral nerve regeneration. *Nat Rev Neurol,* 9**,** 668-76.

SCHMANDKE, A., SCHMANDKE, A. & STRITTMATTER, S. M. 2007. ROCK and Rho: biochemistry and neuronal functions of Rho-associated protein kinases. *Neuroscientist,* 13**,** 454-69.

SCHMITT, A. B., BREUER, S., LIMAN, J., BUSS, A., SCHLANGEN, C., PECH, K., HOL, E. M., BROOK, G. A., NOTH, J. & SCHWAIGER, F. W. 2003. Identification of regeneration-associated genes after central and peripheral nerve injury in the adult rat. *BMC Neurosci,* 4**,** 8.

SCHNEIDER, C., LANGER, R., LOVEDAY, D. & HAIR, D. 2017. Applications of ethylene vinyl acetate copolymers (EVA) in drug delivery systems. *J Control Release,* 262**,** 284-295.

SCHOLTZ, J. & WOOLF, C. J. 2002. Can we conquer pain? *Nature Neuroscience,* 5**,** 1062-1067.

SCHUH, C. M., MORTON, T. J., BANERJEE, A., GRASL, C., SCHIMA, H., SCHMIDHAMMER, R., REDL, H. & RUENZLER, D. 2015. Activated Schwann Cell-Like Cells on Aligned Fibrin-Poly(Lactic-Co-Glycolic Acid) Structures: A Novel Construct for Application in Peripheral Nerve Regeneration. *Cells Tissues Organs,* 200**,** 287-99.

SEOK, J., WARREN, H. S., CUENCA, A. G., MINDRINOS, M. N., BAKER, H. V., XU, W., RICHARDS, D. R., MCDONALD-SMITH, G. P., GAO, H., HENNESSY, L., FINNERTY, C. C., LOPEZ, C. M., HONARI, S., MOORE, E. E., MINEI, J. P., CUSCHIERI, J., BANKEY, P. E., JOHNSON, J. L., SPERRY, J., NATHENS, A. B., BILLIAR, T. R., WEST, M. A., JESCHKE, M. G., KLEIN, M. B., GAMELLI, R. L., GIBRAN, N. S., BROWNSTEIN, B. H., MILLER-GRAZIANO, C., CALVANO, S. E., MASON, P. H., COBB, J. P., RAHME, L. G., LOWRY, S. F., MAIER, R. V., MOLDAWER, L. L., HERNDON, D. N., DAVIS, R. W., XIAO, W., TOMPKINS, R. G., INFLAMMATION & HOST RESPONSE TO INJURY, L. S. C. R. P. 2013. Genomic responses in mouse models poorly mimic human inflammatory diseases. *Proc Natl Acad Sci U S A,* 110**,** 3507-12.

SHANG, X., MARCHIONI, F., SIPES, N., EVELYN, C. R., JERABEK-WILLEMSEN, M., DUHR, S., SEIBEL, W., WORTMAN, M. & ZHENG, Y. 2012. Rational design of small molecule inhibitors targeting RhoA subfamily Rho GTPases. *Chem Biol,* 19**,** 699-710.

SHARP, K. G., YEE, K. M., STILES, T. L., AGUILAR, R. M. & STEWARD, O. 2013. A re-assessment of the effects of treatment with a non-steroidal anti-inflammatory (ibuprofen) on promoting axon regeneration via RhoA inhibition after spinal cord injury. *Exp Neurol,* 248**,** 321-37.
SHIN, S. C. & LEE, H. J. 2002. Controlled release of triprolidine using ethylene-vinyl acetate membrane and matrix systems. *Eur J Pharm Biopharm,* 54**,** 201-6.
SI, H. B., ZENG, Y., LU, Y. R., CHENG, J. Q. & SHEN, B. 2017. Control-released basic fibroblast growth factor-loaded poly-lactic-co-glycolic acid microspheres promote sciatic nerve regeneration in rats. *Exp Ther Med,* 13**,** 429-436.
SIEGEL, S. J., KAHN, J. B., METZGER, K., WINEY, K. I., WERNER, K. & DAN, N. 2006. Effect of drug type on the degradation rate of PLGA matrices. *Eur J Pharm Biopharm,* 64**,** 287-93.
SMITH, U. 2001. Pioglitazone: mechanism of action. *Int J Clin Pract Suppl***,** 13-8.
STEINMETZ, K. L. & SPACK, E. G. 2009. The basics of preclinical drug development for neurodegenerative disease indications. *BMC Neurol,* 9 Suppl 1**,** S2.
STEWART, H. J., ECCLESTON, P. A., JESSEN, K. R. & MIRSKY, R. 1991. Interaction between cAMP elevation, identified growth factors, and serum components in regulating Schwann cell growth. *J Neurosci Res,* 30**,** 346-52.
SUBBANNA, P. K., PRASANNA, C. G., GUNALE, B. K. & TYAGI, M. G. 2007. Acetyl salicylic acid augments functional recovery following sciatic nerve crush in mice. *J Brachial Plex Peripher Nerve Inj,* 2**,** 3.
SUBRAMANIAN, A., KRISHNAN, U. M. & SETHURAMAN, S. 2009. Development of biomaterial scaffold for nerve tissue engineering: Biomaterial mediated neural regeneration. *J Biomed Sci,* 16**,** 108.
SUBRAMANIAN, A., KRISHNAN, U. M. & SETHURAMAN, S. 2012. Fabrication, characterization and in vitro evaluation of aligned PLGA-PCL nanofibers for neural regeneration. *Ann Biomed Eng,* 40**,** 2098-110.
SUCKLING, K. 2008. Animal research: too much faith in models clouds judgement. *Nature,* 455**,** 460.
SUN, M., KINGHAM, P. J., REID, A. J., ARMSTRONG, S. J., TERENGHI, G. & DOWNES, S. 2010. In vitro and in vivo testing of novel ultrathin PCL and PCL/PLA blend films as peripheral nerve conduit. *J Biomed Mater Res A,* 93**,** 1470-81.
SUNDERLAND, S. 1951. A classification of peripheral nerve injuries producing loss of function. *Brain,* 74**,** 491-516.
SUNG, J. K., MIAO, L., CALVERT, J. W., HUANG, L., LOUIS HARKEY, H. & ZHANG, J. H. 2003. A possible role of RhoA/Rho-kinase in experimental spinal cord injury in rat. *Brain Res,* 959**,** 29-38.
SUZUKI, K., TANAKA, H., EBARA, M., UTO, K., MATSUOKA, H., NISHIMOTO, S., OKADA, K., MURASE, T. & YOSHIKAWA, H. 2017. Electrospun nanofiber sheets incorporating methylcobalamin promote nerve regeneration and functional recovery in a rat sciatic nerve crush injury model. *Acta Biomater,* 53**,** 250-259.
SUZUKI, Y., SHIBUYA, M., SATOH, S., SUGIMOTO, Y. & TAKAKURA, K. 2007. A postmarketing surveillance study of fasudil treatment after aneurysmal subarachnoid hemorrhage. *Surg Neurol,* 68**,** 126-31; discussion 131-2.
TAJDARAN, K., SHOICHET, M. S., GORDON, T. & BORSCHEL, G. H. 2015. A novel polymeric drug delivery system for localized and sustained release of tacrolimus (FK506). *Biotechnol Bioeng,* 112**,** 1948-53.
TAMADDONFARD, E., SAMADI, F. & EGDAMI, K. 2013. The effects of vitamin B12 and diclofenac and their combination on cold and mechanical allodynia in a neuropathic pain model in rats. *Vet Res Forum,* 4**,** 19-24.
TAMARGO, R. J., ROSSELL, L. A., KOSSOFF, E. H., TYLER, B. M., EWEND, M. G. & ARYANPUR, J. J. 2002. The intracerebral administration of phenytoin using controlled-release polymers reduces experimental seizures in rats. *Epilepsy Res,* 48**,** 145-55.
TAMARGO, R. J., SILLS, A. K., JR., REINHARD, C. S., PINN, M. L., LONG, D. M. & BREM, H. 1991. Interstitial delivery of dexamethasone in the brain for the reduction of peritumoral edema. *J Neurosurg,* 74**,** 956-61.
TANG, B. L. 2003. Inhibitors of neuronal regeneration: mediators and signaling mechanisms. *Neurochem Int,* 42**,** 189-203.
TAO, Y. 2013. Isolation and culture of Schwann cells. *Methods Mol Biol,* 1018**,** 93-104.
TAYLOR, C. A., BRAZA, D., RICE, J. B. & DILLINGHAM, T. 2008. The incidence of peripheral nerve injury in extremity trauma. *Am J Phys Med Rehabil,* 87**,** 381-5.

TEDESCHI, A. 2011. Tuning the orchestra: transcriptional pathways controlling axon regeneration. *Front Mol Neurosci,* 4**,** 60.
TEIXEIRA, L. B., BUHR, K. A., BOWIE, O., DUKE, F. D., NORK, T. M., DUBIELZIG, R. R. & MCLELLAN, G. J. 2014. Quantifying optic nerve axons in a cat glaucoma model by a semi-automated targeted counting method. *Mol Vis,* 20**,** 376-85.
THAI, Q. A., OSHIRO, E. M. & TAMARGO, R. J. 1999. Inhibition of experimental vasospasm in rats with the periadventitial administration of ibuprofen using controlled-release polymers. *Stroke,* 30**,** 140-7.
TODA, K., SMALL, J. A., GODA, S. & QUARLES, R. H. 1994. Biochemical and cellular properties of three immortalized Schwann cell lines expressing different levels of the myelin-associated glycoprotein. *J Neurochem,* 63**,** 1646-57.
TOKUSHIGE, H., WAKI, M., TAKAYAMA, Y. & TANIHARA, H. 2011. Effects of Y-39983, a selective Rho-associated protein kinase inhibitor, on blood flow in optic nerve head in rabbits and axonal regeneration of retinal ganglion cells in rats. *Curr Eye Res,* 36**,** 964-70.
TOS, P., RONCHI, G., PAPALIA, I., SALLEN, V., LEGAGNEUX, J., GEUNA, S. & GIACOBINI-ROBECCHI, M. G. 2009. Chapter 4: Methods and protocols in peripheral nerve regeneration experimental research: part I-experimental models. *Int Rev Neurobiol,* 87**,** 47-79.
TUNG, T. H. 2009. Enhancement of Functional Recovery After Peripheral Nerve Injury With Tacrolimus. July 2009 ed. ClinicalTrials.gov.
VALMIKINATHAN, C. M., DEFRODA, S. & YU, X. 2009. Polycaprolactone and bovine serum albumin based nanofibers for controlled release of nerve growth factor. *Biomacromolecules,* 10**,** 1084-9.
VAN AELST, L. & CLINE, H. T. 2004. Rho GTPases and activity-dependent dendrite development. *Curr Opin Neurobiol,* 14**,** 297-304.
VAREJAO, A. S., CABRITA, A. M., MEEK, M. F., BULAS-CRUZ, J., MELO-PINTO, P., RAIMONDO, S., GEUNA, S. & GIACOBINI-ROBECCHI, M. G. 2004. Functional and morphological assessment of a standardized rat sciatic nerve crush injury with a non-serrated clamp. *J Neurotrauma,* 21**,** 1652-70.
VIKMAN, K. S., BACKSTROM, E., KRISTENSSON, K. & HILL, R. H. 2001. A two-compartment in vitro model for studies of modulation of nociceptive transmission. *J Neurosci Methods,* 105**,** 175-84.
VITA, G., SANTORO, M., TROMBETTA, G., LEONARDI, L. & MESSINA, C. 1992. A computer-assisted automatic method for myelinated nerve fiber morphometry. *Acta Neurol Scand,* 85**,** 18-22.
VLEGGEERT-LANKAMP, C. L. 2007. The role of evaluation methods in the assessment of peripheral nerve regeneration through synthetic conduits: a systematic review. Laboratory investigation. *J Neurosurg,* 107**,** 1168-89.
WADA, K., NAKAJIMA, A., KATAYAMA, K., KUDO, C., SHIBUYA, A., KUBOTA, N., TERAUCHI, Y., TACHIBANA, M., MIYOSHI, H., KAMISAKI, Y., MAYUMI, T., KADOWAKI, T. & BLUMBERG, R. S. 2006. Peroxisome proliferator-activated receptor gamma-mediated regulation of neural stem cell proliferation and differentiation. *J Biol Chem,* 281**,** 12673-81.
WAKINO, S., HAYASHI, K., KANDA, T., TATEMATSU, S., HOMMA, K., YOSHIOKA, K., TAKAMATSU, I. & SARUTA, T. 2004. Peroxisome proliferator-activated receptor gamma ligands inhibit Rho/Rho kinase pathway by inducing protein tyrosine phosphatase SHP-2. *Circ Res,* 95**,** e45-55.
WALTERS, M. J., BLOBAUM, A. L., KINGSLEY, P. J., FELTS, A. S., SULIKOWSKI, G. A. & MARNETT, L. J. 2009. The influence of double bond geometry in the inhibition of cyclooxygenases by sulindac derivatives. *Bioorg Med Chem Lett,* 19**,** 3271-4.
WANG, G., HU, X., LIN, W., DONG, C. & WU, H. 2011. Electrospun PLGA-silk fibroin-collagen nanofibrous scaffolds for nerve tissue engineering. *In Vitro Cell Dev Biol Anim,* 47**,** 234-40.
WANG, H., WU, M., ZHAN, C., MA, E., YANG, M., YANG, X. & LI, Y. 2012. Neurofilament proteins in axonal regeneration and neurodegenerative diseases. *Neural Regen Res,* 7**,** 620-6.
WANG, J., TIAN, L., LUO, B., RAMAKRISHNA, S., KAI, D., LOH, X. J., YANG, I. H., DEEN, G. R. & MO, X. 2018. Engineering PCL/lignin nanofibers as an antioxidant scaffold for the growth of neuron and Schwann cell. *Colloids Surf B Biointerfaces,* 169**,** 356-365.

WANG, X., BUDEL, S., BAUGHMAN, K., GOULD, G., SONG, K. H. & STRITTMATTER, S. M. 2009. Ibuprofen enhances recovery from spinal cord injury by limiting tissue loss and stimulating axonal growth. *J Neurotrauma,* 26**,** 81-95.
WANG, Z., HAN, N., WANG, J., ZHENG, H., PENG, J., KOU, Y., XU, C., AN, S., YIN, X., ZHANG, P. & JIANG, B. 2014. Improved peripheral nerve regeneration with sustained release nerve growth factor microspheres in small gap tubulization. *Am J Transl Res,* 6**,** 413-21.
WATZLAWICK, R., SENA, E. S., DIRNAGL, U., BROMMER, B., KOPP, M. A., MACLEOD, M. R., HOWELLS, D. W. & SCHWAB, J. M. 2014. Effect and reporting bias of RhoA/ROCK-blockade intervention on locomotor recovery after spinal cord injury: a systematic review and meta-analysis. *JAMA Neurol,* 71**,** 91-9.
WEST, C. A., HART, A. M., TERENGHI, G. & WIBERG, M. 2007. Analysis of the dose-response of N-acetylcysteine in the prevention of sensory neuronal loss after peripheral nerve injury. *Acta Neurochir Suppl,* 100**,** 29-31.
WETTSCHURECK, N. & OFFERMANNS, S. 2002. Rho/Rho-kinase mediated signaling in physiology and pathophysiology. *J Mol Med (Berl),* 80**,** 629-38.
WILCZEWSKA, A. Z., NIEMIROWICZ, K., MARKIEWICZ, K. H. & CAR, H. 2012. Nanoparticles as drug delivery systems. *Pharmacol Rep,* 64**,** 1020-37.
WILLERTH, S. M. & SAKIYAMA-ELBERT, S. E. 2007. Approaches to neural tissue engineering using scaffolds for drug delivery. *Adv Drug Deliv Rev,* 59**,** 325-38.
WOOD, M. D. & MACKINNON, S. E. 2015. Pathways regulating modality-specific axonal regeneration in peripheral nerve. *Exp Neurol,* 265**,** 171-5.
WU, R., YAN, Y., YAO, J., LIU, Y., ZHAO, J. & LIU, M. 2015. Calpain 3 Expression Pattern during Gastrocnemius Muscle Atrophy and Regeneration Following Sciatic Nerve Injury in Rats. *Int J Mol Sci,* 16**,** 26927-35.
XIAO, W. D., YU, A. X. & LIU, D. L. 2014. Fasudil hydrochloride could promote axonal growth through inhibiting the activity of ROCK. *Int J Clin Exp Pathol,* 7**,** 5564-8.
XING, B., LI, H., WANG, H., MUKHOPADHYAY, D., FISHER, D., GILPIN, C. J. & LI, S. 2011. RhoA-inhibiting NSAIDs promote axonal myelination after spinal cord injury. *Exp Neurol,* 231**,** 247-60.
XU, W., COX, C. S. & LI, Y. 2011. Induced pluripotent stem cells for peripheral nerve regeneration. *J Stem Cells,* 6**,** 39-49.
XU, Y., LI, J. J., YU, D. G., WILLIAMS, G. R., YANG, J. H. & WANG, X. 2017. Influence of the drug distribution in electrospun gliadin fibers on drug-release behavior. *Eur J Pharm Sci,* 106**,** 422-430.
YAKSH, T. L., DIRIG, D. M., CONWAY, C. M., SVENSSON, C., LUO, Z. D. & ISAKSON, P. C. 2001. The acute antihyperalgesic action of nonsteroidal, anti-inflammatory drugs and release of spinal prostaglandin E2 is mediated by the inhibition of constitutive spinal cyclooxygenase-2 (COX-2) but not COX-1. *J Neurosci,* 21**,** 5847-53.
YAMAGISHI, S., OGASAWARA, S., MIZUKAMI, H., YAJIMA, N., WADA, R., SUGAWARA, A. & YAGIHASHI, S. 2008. Correction of protein kinase C activity and macrophage migration in peripheral nerve by pioglitazone, peroxisome proliferator activated-gamma-ligand, in insulin-deficient diabetic rats. *J Neurochem,* 104**,** 491-9.
YANG, D. P., ZHANG, D. P., MAK, K. S., BONDER, D. E., POMEROY, S. L. & KIM, H. A. 2008. Schwann cell proliferation during Wallerian degeneration is not necessary for regeneration and remyelination of the peripheral nerves: axon-dependent removal of newly generated Schwann cells by apoptosis. *Mol Cell Neurosci,* 38**,** 80-8.
YANG, W. W. & PIERSTORFF, E. 2012. Reservoir-based polymer drug delivery systems. *J Lab Autom,* 17**,** 50-8.
YANG, Z., WANG, J., LIU, X., CHENG, Y., DENG, L. & ZHONG, Y. 2013. Y-39983 downregulates RhoA/Rho-associated kinase expression during its promotion of axonal regeneration. *Oncol Rep,* 29**,** 1140-6.
YGGE, J. 1989. Neuronal loss in lumbar dorsal root ganglia after proximal compared to distal sciatic nerve resection: a quantitative study in the rat. *Brain Res,* 478**,** 193-5.
YIP, P. M., ZHAO, X., MONTGOMERY, A. M. & SIU, C. H. 1998. The Arg-Gly-Asp motif in the cell adhesion molecule L1 promotes neurite outgrowth via interaction with the alphavbeta3 integrin. *Mol Biol Cell,* 9**,** 277-90.
YU, X. & BELLAMKONDA, R. V. 2001. Dorsal root ganglia neurite extension is inhibited by mechanical and chondroitin sulfate-rich interfaces. *J Neurosci Res,* 66**,** 303-10.
ZAREI, K., SCHEETZ, T. E., CHRISTOPHER, M., MILLER, K., HEDBERG-BUENZ, A., TANDON, A., ANDERSON, M. G., FINGERT, J. H. & ABRAMOFF, M. D. 2016.

Automated Axon Counting in Rodent Optic Nerve Sections with AxonJ. *Sci Rep,* 6**,** 26559.
ZHANG, B. 2015. Potential use of ethylene vinyl acetate copolymer excipient in oral controlled release application: A literature review. *Celanese***,** 1-10.
ZHANG, F., LIU, F., YAN, M., JI, H., HU, L., LI, X., QIAN, J., HE, X., ZHANG, L., SHEN, A. & CHENG, C. 2010a. Peroxisome proliferator-activated receptor-gamma agonists suppress iNOS expression induced by LPS in rat primary Schwann cells. *J Neuroimmunol,* 218**,** 36-47.
ZHANG, H., LI, Z., XU, P., WU, R., WANG, L., XIANG, Y. & JIAO, Z. 2011. Synthesis of novel mesoporous silica nanoparticles for loading and release of ibuprofen. *J Control Release,* 152 Suppl 1**,** e38-9.
ZHANG, W., GAO, Y., ZHOU, Y., LIU, J., ZHANG, L., LONG, A., ZHANG, L. & TANG, P. 2015. Localized and sustained delivery of erythropoietin from PLGA microspheres promotes functional recovery and nerve regeneration in peripheral nerve injury. *Biomed Res Int,* 2015**,** 478103.
ZHANG, Y., ZHI, Z., JIANG, T., ZHANG, J., WANG, Z. & WANG, S. 2010b. Spherical mesoporous silica nanoparticles for loading and release of the poorly water-soluble drug telmisartan. *J Control Release,* 145**,** 257-63.
ZHANG, Z., OTTENS, A. K., LARNER, S. F., KOBEISSY, F. H., WILLIAMS, M. L., HAYES, R. L. & WANG, K. K. 2006. Direct Rho-associated kinase inhibition [correction of inhibiton] induces cofilin dephosphorylation and neurite outgrowth in PC-12 cells. *Cell Mol Biol Lett,* 11**,** 12-29.
ZHAO, Y., PATZER, A., HERDEGEN, T., GOHLKE, P. & CULMAN, J. 2006. Activation of cerebral peroxisome proliferator-activated receptors gamma promotes neuroprotection by attenuation of neuronal cyclooxygenase-2 overexpression after focal cerebral ischemia in rats. *FASEB J,* 20**,** 1162-75.
ZHOU, Y., SU, Y., LI, B., LIU, F., RYDER, J. W., WU, X., GONZALEZ-DEWHITT, P. A., GELFANOVA, V., HALE, J. E., MAY, P. C., PAUL, S. M. & NI, B. 2003. Nonsteroidal anti-inflammatory drugs can lower amyloidogenic Abeta42 by inhibiting Rho. *Science,* 302**,** 1215-7.
ZOCHODNE, D. W., GUO, G. F., MAGNOWSKI, B. & BANGASH, M. 2007. Regenerative failure of diabetic nerves bridging transection injuries. *Diabetes Metab Res Rev,* 23**,** 490-6.

Appendix 1

An evaluation of the published literature (Table 8.1) revealed that a more extensive list of drugs and small molecule inhibitors of the Rho/ROCK pathway have been tested in injuries of the CNS in comparison to PNS. However, there is significant overlap and it is likely drugs used to target injuries in the CNS could also be used to improve regeneration in the PNS.

Compound	Clinical indication	Reported target/action	Reference
Rhosin	CNS injury	Rho inhibitor	*(Shang et al., 2012)*
Y16	CNS injury	Rho inhibitor	*(Shang et al., 2013)*
Cethrin(®)/ VX-210	Clinical trial for acute spinal cord injury Phase I/IIa Phase 2b/3	Rho inhibitor	*(Fehlings et al., 2011)* *(Fehlings et al., 2018)*
Fasudil	Optic nerve damage CNS injury Spinal cord injury. Spinal cord injury. Optic nerve injury. CNS injury	ROCK inhibitor	*(Lingor et al., 2007)* *(Ding et al., 2010)* *(Nishio et al., 2006)* *(Sung et al., 2003)* *(Ichikawa et al., 2008)* *(Gopalakrishnan et al., 2008)*

Ripasudil	CNS injury	ROCK Inhibitor	*(Kitaoka et al., 2017)*
Dimethyl-Fasudil (HA-1152)	Optic nerve injury. CNS injury CNS injury CNS injury	ROCK inhibitor	*(Lingor et al., 2007)* *(Minase et al., 2010)* *(Zhang et al., 2006)* *(Gopalakrishnan et al., 2008)*
Y-27632	Optic nerve injury. CNS injury CNS injury Spinal cord injury. CNS injury Spinal cord injury. Spinal cord injury. Spinal cord injury. Optic nerve injury. Optic nerve injury. CNS injury Optic nerve injury.	ROCK Inhibitor	*(Lingor et al., 2007)* *(Gunther et al., 2014)* *(Minase et al., 2010)* *(Fournier et al., 2003)* *(Zhang et al., 2006)* *(Dergham et al., 2002)* *(Chan et al., 2005)* *(Sung et al., 2003)* *(Sagawa et al., 2007)* *(Ichikawa et al., 2008)* *(Gopalakrishnan et al., 2008)* *(Monnier et al., 2003)*
Y-39983	Optic nerve injury. Optic nerve injury. Optic nerve injury.	ROCK Inhibitor	*(Yang et al., 2013)* *(Sagawa et al., 2007)* *(Tokushige et al., 2011)*
Ibuprofen	CNS injury CNS injury Spinal cord injury Spinal cord injury. CNS injury.	PPAR-γ agonist	*(Dill et al., 2010)* *(Fu et al., 2007)* *(Wang et al., 2009)* *(Xing et al., 2011)* *(Sharp et al., 2013)*
Indomethacin	CNS injury. Spinal cord injury.	PPAR- γ agonist	*(Fu et al., 2007)* *(Xing et al., 2011)*

Rosiglitazone	CNS injury. Spinal cord injury.	PPAR- γ agonist	*(Lezana et al., 2016)* *(Park et al., 2007)*
Pioglitazone	Spinal cord injury	PPAR- γ agonist	*(Park et al., 2007)*
AMA0076	Glaucoma.	ROCK inhibitor	*(Van de Velde et al., 2014)*
SAR407899	Renal vascular resistance.	ROCK inhibitor	*(Grisk et al., 2012)*
Statins (Class)	Hypercholesterolemia.	Rho inhibitor	*(Martin et al., 2001)*
Morelloflavona	Cancer.	Rho GTPases inhibitor	*(Pang et al., 2009)*
SLx-2119	Anti-fibrotic.	ROCK inhibitor	*(Boerma et al., 2008)*
Atorvastatin	Anti-fibrotic.	ROCK inhibitor	*(Boerma et al., 2008)*
SB-772077-B	Pulmonary Vasodilator Hypertension	ROCK Inhibitor	*(Dhaliwal et al., 2009)* *(Doe et al., 2007)*
Fasudil and Celecoxib	Spinal cord injury.	ROCK inhibitor COX-2 inhibitor	*(Hou et al., 2015)*
Methylprednisolone and Rosiglitazone	Spinal cord injury	NK-kappa-B PPAR- γ agonist	*(Li et al., 2016)*

Table 8.1: Studies that have explored the effect of drugs and other experimental small molecules targeted the Rho/ROCK pathway in clinical indications other than PNI. *Inclusion criteria included literature that has studied compounds targeting Rho, ROCK and PPAR-gamma directly. The inclusion criteria also only including literature that had studied PPAR-gamma as a target to block or activate the Rho/ROCK pathway and no other signalling pathways. Drugs or small molecules targeting neuropathic pain, inflammation or neurodegenerative diseases were also excluded. Furthermore only novel compounds shown to have effects in other clinical indications which have not yet been studied for any nerve application have been included. Relevant articles were identified and obtained from Pubmed up until 21/01/2018.*

References from table 8.1:

BOERMA, M., FU, Q., WANG, J., LOOSE, D. S., BARTOLOZZI, A., ELLIS, J. L., MCGONIGLE, S., PARADISE, E., SWEETNAM, P., FINK, L. M., VOZENIN-BROTONS, M. C. & HAUER-JENSEN, M. 2008. Comparative gene expression profiling in three primary human cell lines after treatment with a novel inhibitor of Rho kinase or atorvastatin. *Blood Coagul Fibrinolysis,* 19**,** 709-18.

CHAN, C. C., KHODARAHMI, K., LIU, J., SUTHERLAND, D., OSCHIPOK, L. W., STEEVES, J. D. & TETZLAFF, W. 2005. Dose-dependent beneficial and detrimental effects of ROCK inhibitor Y27632 on axonal sprouting and functional recovery after rat spinal cord injury. *Exp Neurol,* 196**,** 352-64.

DERGHAM, P., ELLEZAM, B., ESSAGIAN, C., AVEDISSIAN, H., LUBELL, W. D. & MCKERRACHER, L. 2002. Rho signaling pathway targeted to promote spinal cord repair. *J Neurosci,* 22**,** 6570-7.

DHALIWAL, J. S., BADEJO, A. M., JR., CASEY, D. B., MURTHY, S. N. & KADOWITZ, P. J. 2009. Analysis of pulmonary vasodilator responses to SB-772077-B [4-(7-((3-amino-1-pyrrolidinyl)carbonyl)-1-ethyl-1H-imidazo(4,5-c)pyridin-2-yl)-1 ,2,5-oxadiazol-3-amine], a novel aminofurazan-based Rho kinase inhibitor. *J Pharmacol Exp Ther,* 330**,** 334-41.

DILL, J., PATEL, A. R., YANG, X. L., BACHOO, R., POWELL, C. M. & LI, S. 2010. A molecular mechanism for ibuprofen-mediated RhoA inhibition in neurons. *J Neurosci,* 30**,** 963-72.

DING, J., LI, Q. Y., YU, J. Z., WANG, X., SUN, C. H., LU, C. Z. & XIAO, B. G. 2010. Fasudil, a Rho kinase inhibitor, drives mobilization of adult neural stem cells after hypoxia/reoxygenation injury in mice. *Mol Cell Neurosci,* 43**,** 201-8.

DOE, C., BENTLEY, R., BEHM, D. J., LAFFERTY, R., STAVENGER, R., JUNG, D., BAMFORD, M., PANCHAL, T., GRYGIELKO, E., WRIGHT, L. L., SMITH, G. K., CHEN, Z., WEBB, C., KHANDEKAR, S., YI, T., KIRKPATRICK, R., DUL, E., JOLIVETTE, L., MARINO, J. P., JR., WILLETTE, R., LEE, D. & HU, E. 2007. Novel Rho kinase inhibitors with anti-inflammatory and vasodilatory activities. *J Pharmacol Exp Ther,* 320**,** 89-98.

FEHLINGS, M. G., KIM, K. D., AARABI, B., RIZZO, M., BOND, L. M., MCKERRACHER, L., VACCARO, A. & OKONKWO, D. O. 2018. Rho Inhibitor VX-210 in Acute Traumatic Subaxial Cervical Spinal Cord Injury: Design of the SPinal Cord Injury Rho INhibition InvestiGation (SPRING) Clinical Trial. *J Neurotrauma*.

FEHLINGS, M. G., THEODORE, N., HARROP, J., MAURAIS, G., KUNTZ, C., SHAFFREY, C. I., KWON, B. K., CHAPMAN, J., YEE, A., TIGHE, A. & MCKERRACHER, L. 2011. A phase I/IIa clinical trial of a recombinant Rho protein antagonist in acute spinal cord injury. *J Neurotrauma,* 28**,** 787-96.

FOURNIER, A. E., TAKIZAWA, B. T. & STRITTMATTER, S. M. 2003. Rho kinase inhibition enhances axonal regeneration in the injured CNS. *J Neurosci,* 23**,** 1416-23.

FU, Q., HUE, J. & LI, S. 2007. Nonsteroidal anti-inflammatory drugs promote axon regeneration via RhoA inhibition. *J Neurosci,* 27**,** 4154-64.

GOPALAKRISHNAN, S. M., TEUSCH, N., IMHOF, C., BAKKER, M. H., SCHURDAK, M., BURNS, D. J. & WARRIOR, U. 2008. Role of Rho kinase pathway in chondroitin sulfate proteoglycan-mediated inhibition of neurite outgrowth in PC12 cells. *J Neurosci Res,* 86**,** 2214-26.

GRISK, O., SCHLUTER, T., REIMER, N., ZIMMERMANN, U., KATSARI, E., PLETTENBURG, O., LOHN, M., WOLLERT, H. G. & RETTIG, R. 2012. The Rho kinase inhibitor SAR407899 potently inhibits endothelin-1-induced constriction of renal resistance arteries. *J Hypertens,* 30**,** 980-9.

GUNTHER, R., SAAL, K. A., SUHR, M., SCHEER, D., KOCH, J. C., BAHR, M., LINGOR, P. & TONGES, L. 2014. The rho kinase inhibitor Y-27632 improves motor performance in male SOD1(G93A) mice. *Front Neurosci,* 8**,** 304.

HOU, X. L., CHEN, Y., YIN, H. & DUAN, W. G. 2015. Combination of fasudil and celecoxib promotes the recovery of injured spinal cord in rats better than celecoxib or fasudil alone. *Neural Regen Res,* 10**,** 1836-40.

ICHIKAWA, M., YOSHIDA, J., SAITO, K., SAGAWA, H., TOKITA, Y. & WATANABE, M. 2008. Differential effects of two ROCK inhibitors, Fasudil and Y-27632, on optic nerve regeneration in adult cats. *Brain Res,* 1201**,** 23-33.

KITAOKA, Y., SASE, K., TSUKAHARA, C., KOJIMA, K., SHIONO, A., KOGO, J., TOKUDA, N. & TAKAGI, H. 2017. Axonal Protection by Ripasudil, a Rho Kinase Inhibitor, via Modulating Autophagy in TNF-Induced Optic Nerve Degeneration. *Invest Ophthalmol Vis Sci,* 58**,** 5056-5064.

LEZANA, J. P., DAGAN, S. Y., ROBINSON, A., GOLDSTEIN, R. S., FAINZILBER, M., BRONFMAN, F. C. & BRONFMAN, M. 2016. Axonal PPARgamma promotes neuronal regeneration after injury. *Dev Neurobiol,* 76**,** 688-701.

LI, X. G., LIN, X. J., DU, J. H., XU, S. Z., LOU, X. F. & CHEN, Z. 2016. Combination of methylprednisolone and rosiglitazone promotes recovery of neurological function after spinal cord injury. *Neural Regen Res,* 11**,** 1678-1684.

LINGOR, P., TEUSCH, N., SCHWARZ, K., MUELLER, R., MACK, H., BAHR, M. & MUELLER, B. K. 2007. Inhibition of Rho kinase (ROCK) increases neurite outgrowth on chondroitin sulphate proteoglycan in vitro and axonal regeneration in the adult optic nerve in vivo. *J Neurochem,* 103**,** 181-9.

MARTIN, G., DUEZ, H., BLANQUART, C., BEREZOWSKI, V., POULAIN, P., FRUCHART, J. C., NAJIB-FRUCHART, J., GLINEUR, C. & STAELS, B. 2001. Statin-induced inhibition of the Rho-signaling pathway activates PPARalpha and induces HDL apoA-I. *J Clin Invest,* 107**,** 1423-32.

MINASE, T., ISHIMA, T., ITOH, K. & HASHIMOTO, K. 2010. Potentiation of nerve growth factor-induced neurite outgrowth by the ROCK inhibitor Y-27632: a possible role of IP(3) receptors. *Eur J Pharmacol,* 648**,** 67-73.

MONNIER, P. P., SIERRA, A., SCHWAB, J. M., HENKE-FAHLE, S. & MUELLER, B. K. 2003. The Rho/ROCK pathway mediates neurite growth-inhibitory activity associated with the chondroitin sulfate proteoglycans of the CNS glial scar. *Mol Cell Neurosci,* 22**,** 319-30.

NISHIO, Y., KODA, M., KITAJO, K., SETO, M., HATA, K., TANIGUCHI, J., MORIYA, H., FUJITANI, M., KUBO, T. & YAMASHITA, T. 2006. Delayed treatment with Rho-kinase inhibitor does not enhance axonal regeneration or functional recovery after spinal cord injury in rats. *Exp Neurol,* 200**,** 392-7.

PANG, X., YI, T., YI, Z., CHO, S. G., QU, W., PINKAEW, D., FUJISE, K. & LIU, M. 2009. Morelloflavone, a biflavonoid, inhibits tumor angiogenesis by targeting rho GTPases and extracellular signal-regulated kinase signaling pathways. *Cancer Res,* 69**,** 518-25.

PARK, S. W., YI, J. H., MIRANPURI, G., SATRIOTOMO, I., BOWEN, K., RESNICK, D. K. & VEMUGANTI, R. 2007. Thiazolidinedione class of peroxisome proliferator-activated receptor gamma agonists prevents neuronal damage, motor dysfunction, myelin loss, neuropathic pain, and inflammation after spinal cord injury in adult rats. *J Pharmacol Exp Ther,* 320**,** 1002-12.

SAGAWA, H., TERASAKI, H., NAKAMURA, M., ICHIKAWA, M., YATA, T., TOKITA, Y. & WATANABE, M. 2007. A novel ROCK inhibitor, Y-39983, promotes regeneration of crushed axons of retinal ganglion cells into the optic nerve of adult cats. *Exp Neurol,* 205**,** 230-40.

SHANG, X., MARCHIONI, F., EVELYN, C. R., SIPES, N., ZHOU, X., SEIBEL, W., WORTMAN, M. & ZHENG, Y. 2013. Small-molecule inhibitors targeting G-protein-coupled Rho guanine nucleotide exchange factors. *Proc Natl Acad Sci U S A,* 110**,** 3155-60.

SHANG, X., MARCHIONI, F., SIPES, N., EVELYN, C. R., JERABEK-WILLEMSEN, M., DUHR, S., SEIBEL, W., WORTMAN, M. & ZHENG, Y. 2012. Rational design of small molecule inhibitors targeting RhoA subfamily Rho GTPases. *Chem Biol,* 19**,** 699-710.

SHARP, K. G., YEE, K. M., STILES, T. L., AGUILAR, R. M. & STEWARD, O. 2013. A re-assessment of the effects of treatment with a non-steroidal anti-inflammatory (ibuprofen) on promoting axon regeneration via RhoA inhibition after spinal cord injury. *Exp Neurol,* 248**,** 321-37.

SUNG, J. K., MIAO, L., CALVERT, J. W., HUANG, L., LOUIS HARKEY, H. & ZHANG, J. H. 2003. A possible role of RhoA/Rho-kinase in experimental spinal cord injury in rat. *Brain Res,* 959**,** 29-38.

TOKUSHIGE, H., WAKI, M., TAKAYAMA, Y. & TANIHARA, H. 2011. Effects of Y-39983, a selective Rho-associated protein kinase inhibitor, on blood flow in optic nerve head in rabbits and axonal regeneration of retinal ganglion cells in rats. *Curr Eye Res,* 36**,** 964-70.

VAN DE VELDE, S., VAN BERGEN, T., SIJNAVE, D., HOLLANDERS, K., CASTERMANS, K., DEFERT, O., LEYSEN, D., VANDEWALLE, E., MOONS, L. & STALMANS, I. 2014. AMA0076, a novel, locally acting Rho kinase inhibitor, potently lowers intraocular pressure in New Zealand white rabbits with minimal hyperemia. *Invest Ophthalmol Vis Sci,* 55**,** 1006-16.

WANG, X., BUDEL, S., BAUGHMAN, K., GOULD, G., SONG, K. H. & STRITTMATTER, S. M. 2009. Ibuprofen enhances recovery from spinal cord injury by limiting tissue loss and stimulating axonal growth. *J Neurotrauma,* 26**,** 81-95.

XING, B., LI, H., WANG, H., MUKHOPADHYAY, D., FISHER, D., GILPIN, C. J. & LI, S. 2011. RhoA-inhibiting NSAIDs promote axonal myelination after spinal cord injury. *Exp Neurol,* 231**,** 247-60.

YANG, Z., WANG, J., LIU, X., CHENG, Y., DENG, L. & ZHONG, Y. 2013. Y-39983 downregulates RhoA/Rho-associated kinase expression during its promotion of axonal regeneration. *Oncol Rep,* 29**,** 1140-6.

ZHANG, Z., OTTENS, A. K., LARNER, S. F., KOBEISSY, F. H., WILLIAMS, M. L., HAYES, R. L. & WANG, K. K. 2006. Direct Rho-associated kinase inhibition [correction of inhibiton] induces cofilin dephosphorylation and neurite outgrowth in PC-12 cells. *Cell Mol Biol Lett,* 11**,** 12-29.

Appendix 2

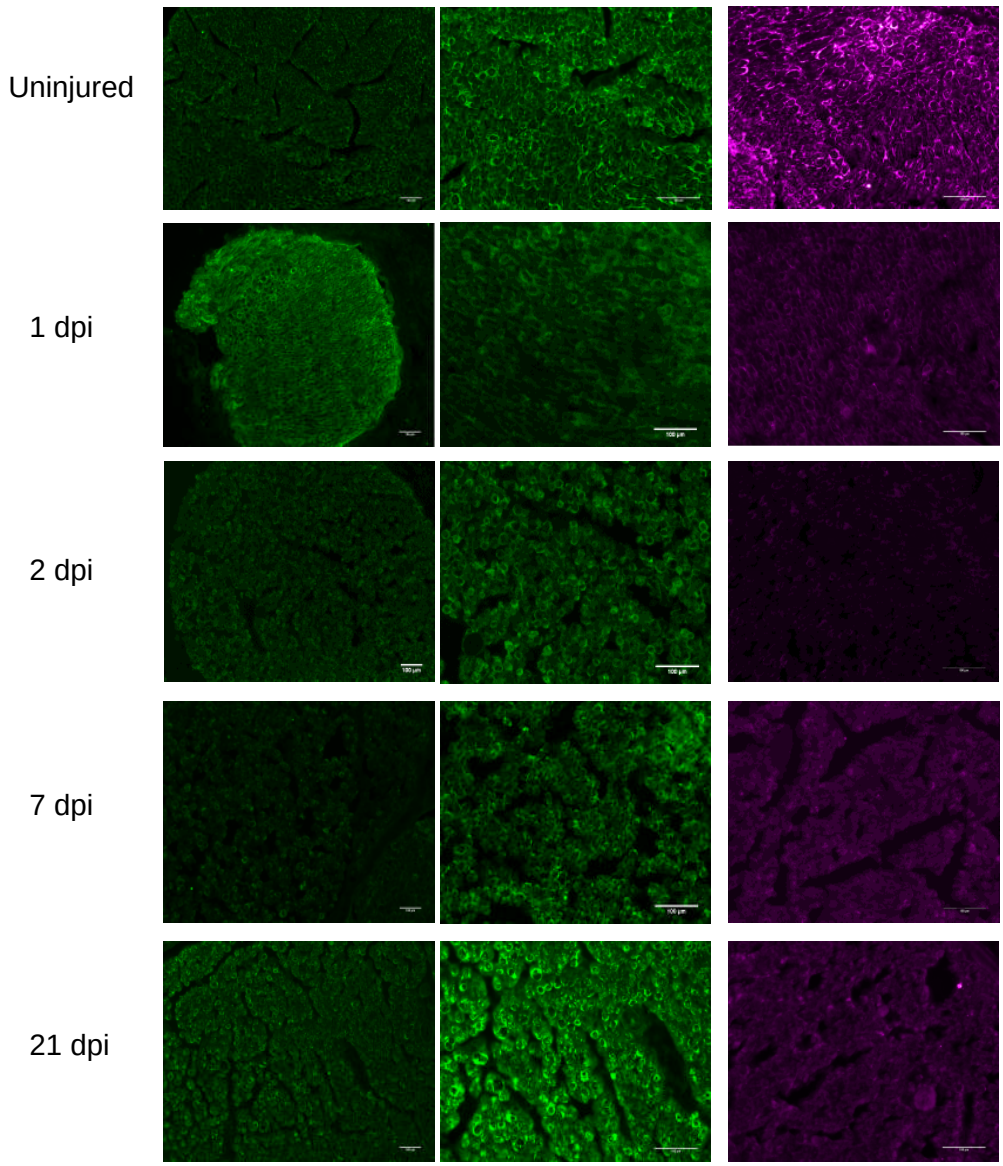

Figure 9.1: Schwann cell presence and phenotype at various time points following a transection injury. *Micrographs are 10 µm transverse sections from the distal stump immunostained Schwann cells with s100 (green) and c-Jun (magenta).*

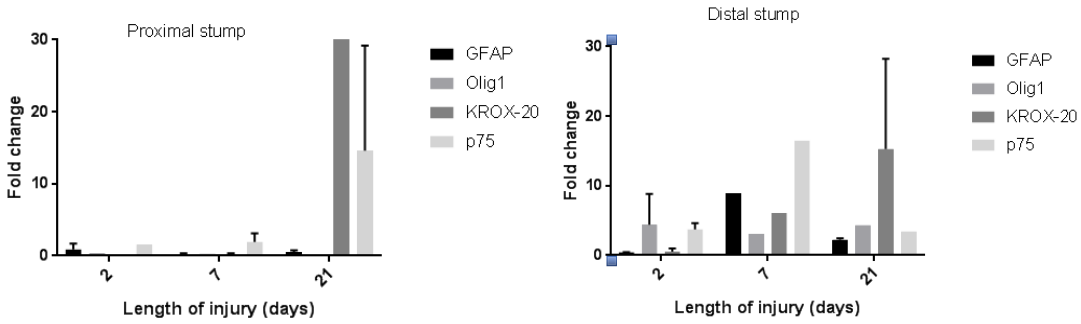

***Figure 9.2:* Fold change of gene expression of Schwann cell phenotype biomarkers following injury in rat sciatic nerve.** *The fold change relates expression of biomarkers to a no injury control. Nerve tissue was analysed from the proximal and distal stump at different time points following primary repair injury (N=1-3, dependent on nerve samples available).*

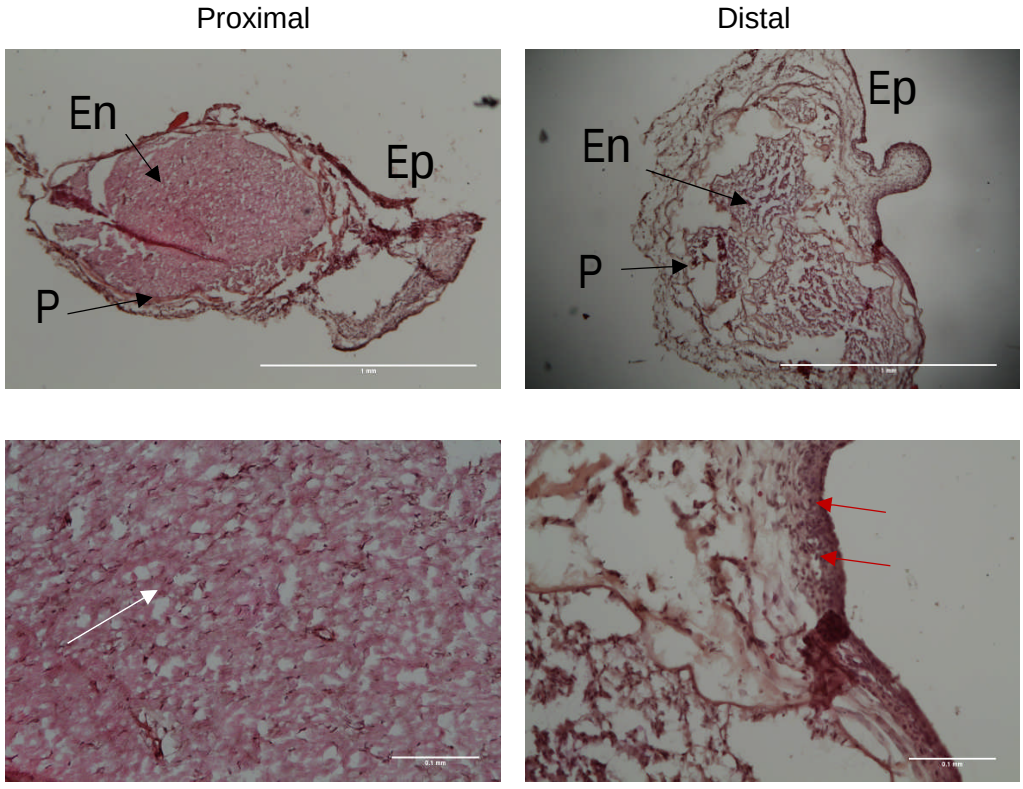

Figure 9.3: Haematoxylin and Eosin staining following the use of osmotic pumps in a transection injury. *Some key characteristics of the nerve tissue are highlighted Ep= epineurium, P =perinerium, En=endoneurium, myelin (white arrow) and monocytes (red arrow).*

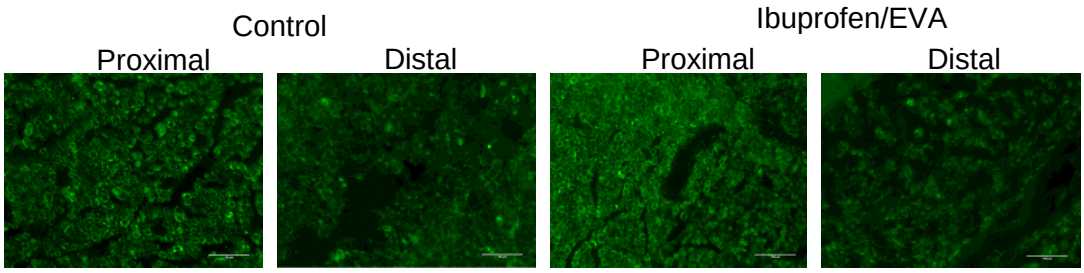

Figure 9.4: Schwann cell presence and morphology following a transection injury treated with ibuprofen-loaded EVA*. Micrographs are 10 µm transverse sections from the proximal and distal stumps immunostained with s100 (green).*

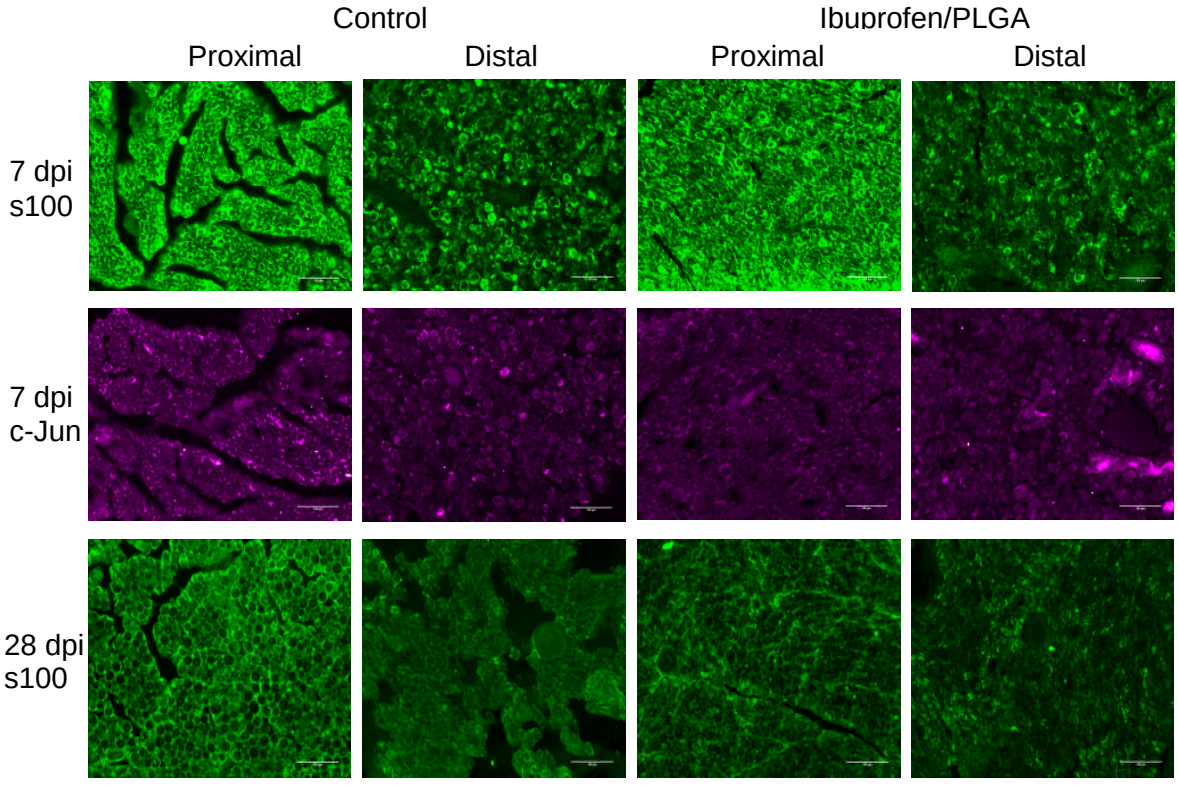

Figure 9.5: Schwann cell presence and morphology following a crush injury treated with ibuprofen-loaded PLGA*. Micrographs are 10 µm transverse sections from the proximal and distal stumps immunostained with s100 (green) and c-Jun (magenta).*

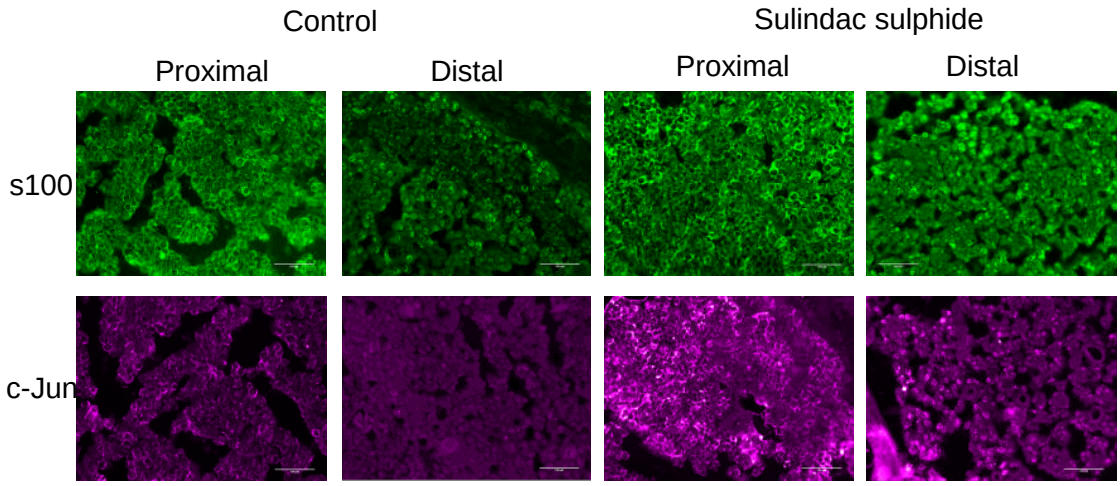

Figure 9.6: Schwann cell presence and morphology following a transection injury treated with sulindac sulfide*. Micrographs are 10 µm transverse sections from the proximal and distal stumps immunostained with s100 (green) and c-Jun (magenta).*

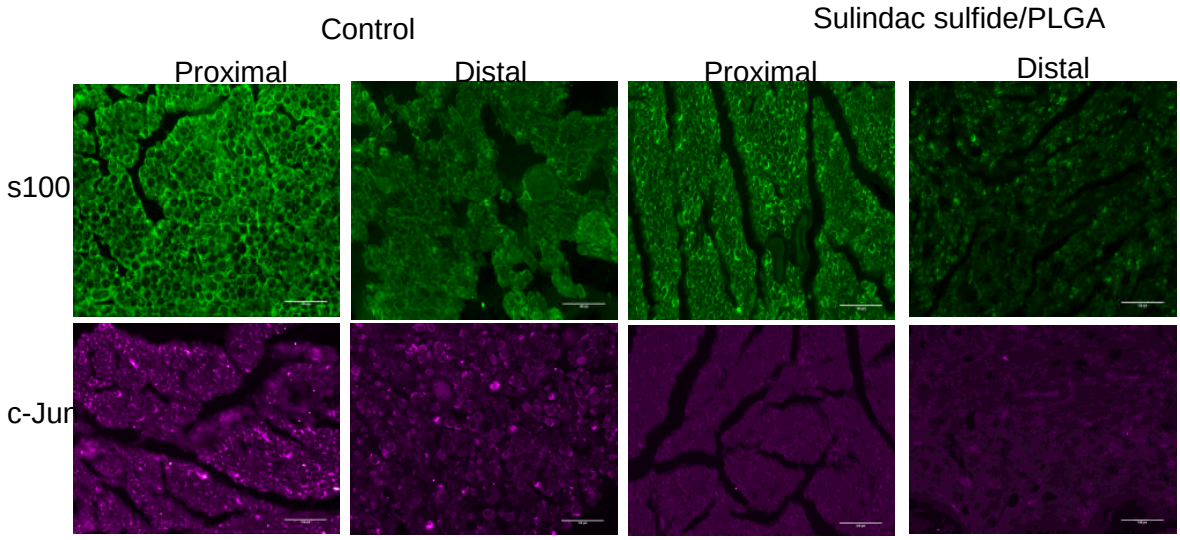

Figure 9.7: Schwann cell presence and morphology following a crush injury treated with sulindac sulfide-loaded PLGA*. Micrographs are 10 µm transverse sections from the proximal and distal stumps immunostained with s100 (green) and c-Jun (magenta).*

Appendix 3

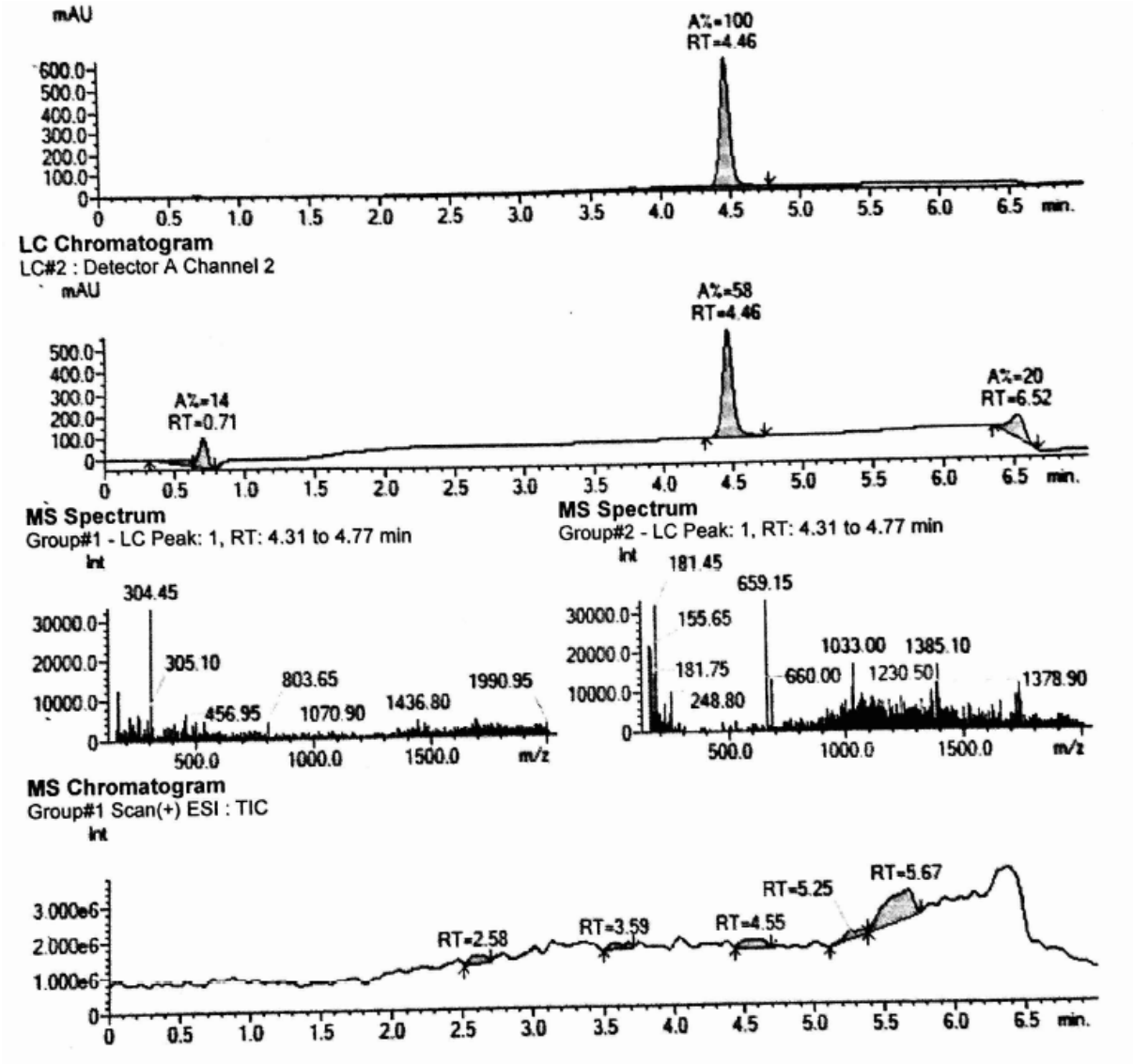

Figure 10.1: LCMS analysis for compound (3).

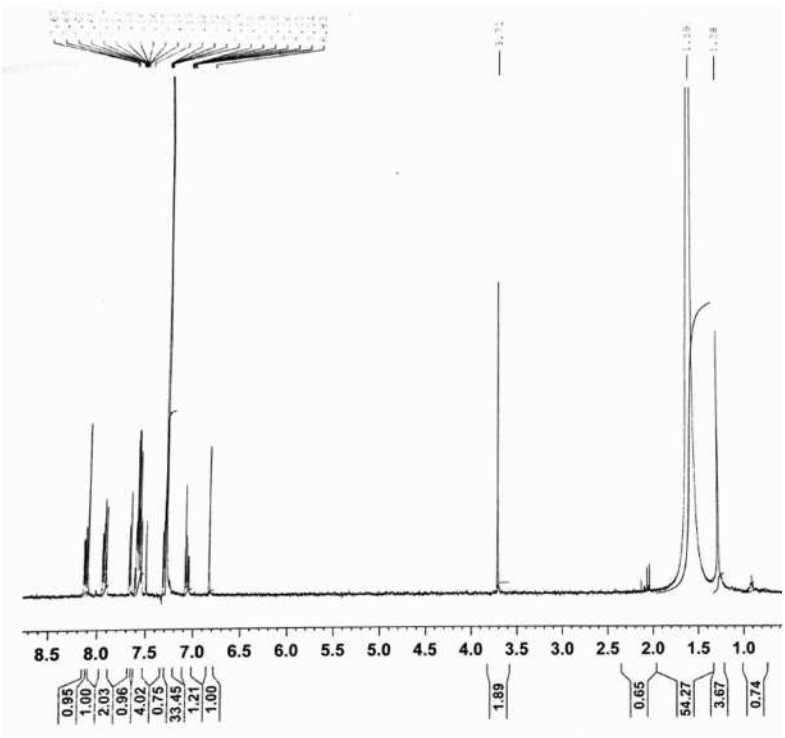

Figure 10.2: 1H NMR spectrum for compound (3).

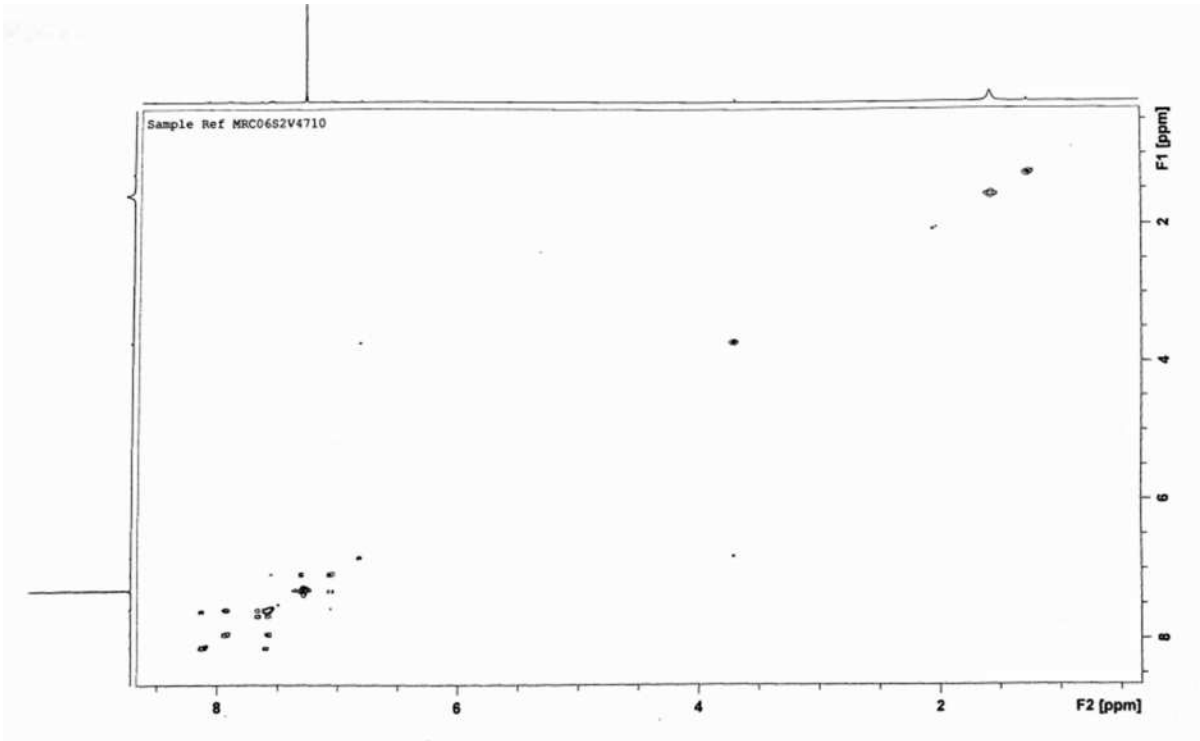

Figure 10.3: COSY spectrum for compound (3).